



LATVIJAS
UNIVERSITĀTE

Promocijas darbs

Rīga 2024

Kristaps Saršūns

CIETO ŠĶĪDUMU
VEIDOŠANĀS UN
FIZIKĀLĶĪMISKO ĪPAŠĪBU
RAKSTUROJUMS PĒC
UZBŪVES LĪDZĪGU
ORGANISKO MOLEKULU
VAIRĀKKOMPONENTU
SISTĒMĀS

Doctoral Thesis

Characterization of Formation and
Physico-Chemical Properties of Solid
Solutions in Multicomponent Systems of
Structurally Similar Organic Molecules



LATVIJAS UNIVERSITĀTE

ĶĪMIJAS FAKULTĀTE

Kristaps Saršūns

CIETO ŠĶĪDUMU VEIDOŠANĀS UN FIZIKĀLĶĪMISKO ĪPAŠĪBU RAKSTUROJUMS PĒC UZBŪVES LĪDZĪGU ORGANISKO MOLEKULU VAIRĀKKOMPONENTU SISTĒMĀS

PROMOCIJAS DARBS

Zinātnes doktora (Ph.D.) zinātniskā grāda iegūšanai
dabaszinātnēs (ķīmijas nozarē)

Apakšnozare: fizikālā ķīmija

Darba vadītāji:

asoc. prof., *Dr. chem.* **Agris Bērziņš**
pētn., *Dr. chem.* **Toms Rēķis**

RĪGA, 2024

Mixed crystal, 'solid solution', is a solid phase with similar behaviour to the liquid solution in which the ratio of two or more components can vary freely without the generation of a new phase.

Jakobs Henriks van't Hofs, 1890

Promocijas darbs izstrādāts Latvijas Universitātes Ķīmijas fakultātes Fizikālās ķīmijas katedrā laika posmā no 2020. gada līdz 2023. gadam.



**LATVIJAS
UNIVERSITĀTE**

Šis darbs ir realizēts ar Eiropas Sociālā fonda granta Nr. 8.2.2.0/20/I/006, SIA “Mikrotikls” doktorantūras stipendijas, ko administrē Latvijas Universitātes Fonds, un Latvijas Zinātnes padomes finansēta projekta Nr. lzp-2018/1-0312, atbalstu.

NACIONĀLAIS
ATTĪSTĪBAS
PLĀNS 2020



EIROPAS SAVIENĪBA
Eiropas Sociālais
fonds

IEGULDĪJUMS TAVĀ NĀKOTNĒ



LATVIJAS UNIVERSITĀTE
FONDS



FLPP
FUNDAMENTĀLO UN
LIETIŠKO PĒTĪJUMU
PROJEKTI

Darbs sastāv no kopsavilkuma latviešu un angļu valodā un no piecām zinātniskajām publikācijām, t. sk. no izstrādes procesā esoša manuskripta.

Darba forma: publikāciju kopa ķīmijas nozarē, fizikālās ķīmijas apakšnozarē.

Darba zinātniskie vadītāji: asoc. prof., *Dr. chem.* **Agris Bērziņš**
pētn., *Dr. chem.* **Toms Rēķis**

Zinātniskais konsultants: vad. pētn., *Dr. chem.* **Artis Kons**

Darba recenzenti:

- 1) prof., *Dr. chem.* **Donāts Erts** (Latvijas Universitāte)
- 2) *Dr. phys.* **Anatolijs Mišņovs** (Latvijas Organiskās sintēzes institūts)
- 3) asoc. prof., *Dr. chem.* **Mihails Arhangeliskis** (Varšavas Universitāte)

Promocijas darba aizstāvēšana notiks 2024. gada 23. janvārī plkst. 14.00 Latvijas Universitātes Ķīmijas nozares promocijas padomes atklātā sēdē Latvijas Universitātes Dabaszinātņu akadēmiskajā centrā Rīgā, Jelgavas ielā 1, 217. auditorijā.

Ar promocijas darbu un tā kopsavilkumu var iepazīties Latvijas Universitātes Bibliotēkā Rīgā, Raiņa bulvārī 19.

Latvijas Universitātes Ķīmijas zinātņu nozares promocijas padomes:

priekšsēdētājs: prof., *Dr. chem.* **Edgars Sūna**

sekretāre: asoc. prof., *Dr. chem.* **Vīta Rudoviča**

Vāka attēli veidoti Wepik.com (AI Image Generator)

© Latvijas Universitāte, 2024
© Kristaps Saršūns, 2024

ISBN 978-9934-36-153-1

ISBN 978-9934-36-154-8 (PDF)

ANOTĀCIJA

Cieto šķīdumu veidošanās un fizikālķīmisko īpašību raksturojums pēc uzbūves līdzīgu organisko molekulu vairākkomponentu sistēmās. Saršūns, K., zinātniskie vadītāji asoc. prof., *Dr. chem.* Bērziņš, A. un pētn., *Dr. chem.* Rēķis, T., zinātniskais konsultants vad. pētn., *Dr. chem.* Kons, A. Zinātnisko publikāciju kopas kopsavilkums fizikālās ķīmijas apakšnozarē, 51 lappuses, 32 attēli, 6 tabulas, 44 literatūras avoti. Latviešu valodā.

Darbā pētīta cieto šķīdumu veidošanās starp vairākām molekulārās struktūras ziņā līdzīgām organiskajām cietvielām: farmaceutiski aktīvajām vielām benperidolu un droperidolu, kas atšķiras ar vienkāršās/divkāršās saites esamību starp diviem oglekļa atomiem, modeļvielām aizvietotām nitrobenzoscābēm, kas atšķiras ar aizvietotāju (halogēna atoms / metilgrupa / hidroksilgrupa) un, ksantonu un tioksantonu, kas atšķiras ar S/O atomu, kā arī luminoforiem tioksantona atvasinājumiem, kas atšķiras ar halogēna atomiem. Katrā no pētītajām sistēmām, veicot vielu maisījumu kristalizāciju dažādās vielu attiecībās, izmantojot pulvera rentgendifraktometriju un no termiskās analīzes datiem konstruētas fāžu diagrammas, noskaidrota vielu šķīdība vienai otrā. Benperidola un droperidola gadījumā papildus izpētīta šo vielu savstarpējā šķīdība nesolvatētās un solvatētās kristāliskajās struktūrās. Noteikts, ka visos gadījumos cieto šķīdumu veidošanos nosaka gan līdzība starp apmaināmo aizvietotāju vai grupu stēriskajām īpašībām un starpmolekulāro mijiedarbību veidošanas spēju, kā arī kristāliskā struktūra, kurā notiek aizvietotāju vai grupu apmaiņa, atšķirīgu starpmolekulāro mijiedarbību dēļ. Ar kvantu ķīmiskajiem aprēķiniem novērtēts, vai cieto šķīdumu veidošanās izraisīta starpmolekulāro mijiedarbību izmaiņu noteikšana ļauj paredzēt cieto šķīdumu veidošanās varbūtību. Noteikts, ka šāda pieeja ir derīga sistēmā benperidols – droperidols, kurā cieto šķīdumu veidošanās saistās ar nelielām molekulārās struktūras izmaiņām, turpretī tā nav izmantojama aizvietotām nitrobenzoscābēm, kurās molekulārās struktūras izmaiņas izraisa būtiskas atšķirības vielu veidotajās strpmolekulārajās mijiedarbībās. Cietajiem šķīdumiem starp tioksantona atvasinājumiem pētītas arī luminiscences īpašības, nosakot, ka dažos no cietajiem šķīdumiem pat neliela sastāva izmaiņas nodrošina būtisku luminiscences īpašību maiņu, turpretī citos būtiskas sastāva izmaiņas minimāli ietekmē luminiscences īpašības.

Atslēgvārdi: *cietais šķīdums, termiskā analīze, rentgendifrakcija, divkomponentu fāžu diagramma, luminiscence, aprēķinu ķīmija*

SATURS / CONTENTS

Apzīmējumu saraksts	8
Ievads	9
Publicētie rezultāti	12
1. Promocijas darba teorētiskie pamati un pētītās sistēmas	15
1.1. Cieto šķīdumu struktūra un termodinamiskais raksturojums	15
1.2. Cieto šķīdumu pētījumi, izmantojot dažādas fizikālās cietfāžu pētīšanas metodes	16
1.3. Pētītās sistēmas	19
2. Eksperimentālā daļa	21
3. Rezultāti un to izvērtējums	23
3.1. Divkomponentu sistēmas ksantons – tioksantons (1) cieto šķīdumu veidošanās	23
3.2. Dažādu aizvietotu nitrobenzoscābju (2) divkomponentu sistēmu cieto šķīdumu veidošanās	27
3.3. Divkomponentu sistēmas benperidols – droperidols (3) cieto šķīdumu veidošanās	32
3.4. Dažādu tioksantona halogēnatvasinājumu (4) divkomponentu sistēmu cieto šķīdumu veidošanās	38
3.4.1. Divkomponentu sistēma, kura satur joda un hlora atvasinājumus	38
3.4.2. Divkomponentu sistēmas, kuras satur joda, hlora, broma un fluora atvasinājumus	44
Secinājumi	49
Pateicības	50

Abbreviations	56
Introduction	57
Results Published	60
1. Research Background	63
1.1. Structural aspects and thermodynamic characterization of solid solutions ..	63
1.2. Investigation of solid solutions using various physical solid state research methods	64
1.3. Objects of Investigation	67
2. Experimental Section	69
3. Results and Discussion	71
3.1. Formation of solid solutions of the xanthone – thioxanthone (1) two-component system	71
3.2. Formation of solid solutions of a substituted nitrobenzoic acids (2) two-component systems	75
3.3. Formation of solid solutions of the beneperidol – droperidol (3) two-component system	80
3.4. Formation of solid solutions of a various thioxanthone halogen derivatives (4) two-component systems	86
3.4.1. In a two-component system containing iodine and chlorine derivatives	86
3.4.2. In two-component systems containing iodine, chlorine, bromine and fluorine derivatives	92
Conclusions	97
Acknowledgements	98
Literatūras saraksts / References	99
Publikācijas / Publications	103
I Solid solutions in xanthone – thioxanthone binary system: how well are similar molecules discriminated in the solid state?	105
II Fine-tuning solid state luminescence properties of organic crystals <i>via</i> solid solution formation: the example of 4-iodothioxanthone – 4-chlorothioxanthone system	115
III Experimental and computational investigation of benperidol and droperidol solid solutions in different crystal structures	123
IV Experimental and computational study of solid solution formed between substituted nitrobenzoic acids	137
V Modulation of physico-chemical properties <i>via</i> solid solution formation of thioxanthone derivatives	153

APZĪMĒJUMU SARAKSTS

ACN	acetonitrils
AEŠH	augsti efektīvā šķīduma hromatogrāfija
^B I (u.c.) / ^B S _{šķīdinātājs} / ^B DH	benperidola polimorfā forma / solvāts / dihidrāts
^D I / ^D S _{šķīdinātājs} / ^D DH	droperidola polimorfā forma / solvāts / dihidrāts
DFT	blīvuma funkcionālā teorija
DH	dihidrāts
DMSO- <i>d</i> ₆	deiterēts dimetilsulfoksīds
DSC	diferenciāli skenējošā kalorimetrija
EtOH	etanols
FAV	farmaceitiski aktīvā viela
<i>F</i> _{hkl}	struktūrfaktors
HMDS	heksametildisiloksāns
KMR	kodolmagnētiskā rezonanse
Me	metilgrupa
MeOH	metanols
NBA	nitrobenzoksābe
PXRD	pulvera rentgendifraktometrija
S _{šķīdinātājs}	solvāts
SCXRD	monokristāla rentgendifraktometrija
SS	cietais šķīdums
TG	termogravimetrija
TX / TXANT	tioksantons
XAN	ksantons
XRD	rentgendifrakcija
¹ H KMR	protonu kodolmagnētiskā rezonanse
I (u.c.) forma	I polimorfā (kristāliskā) forma
Φ	kvantu iznākums
δ	ķīmiskā nobīde

IEVADS

Cietie šķīdumi starp neorganiskajām vielām ir plaši pētītas un labi zināmas cietās fāzes, kurās materiāla uzbūve un īpašības ir atkarīgas no komponentu sastāva. Šādas fāzes un to nodrošinātā īpašību maiņa ir plaši sastopamas tādās materiālu klasēs kā metālu sakausējumos, minerālos, keramikās u.c. Turpretī pētījumu par cieto šķīdumu veidošanos starp organiskajām vielām ir būtiski mazāk¹. Vēl jo vairāk, ir pamatoti uzskatīt, ka cietie šķīdumi starp organiskām vielām un to izveides rezultātā izmainītas fizikālās īpašības līdz šim bieži ir tikuši atstāti bez ievēribas un detalizētas izpētes². Tomēr interese par cieto šķīdumu veidošanos starp organiskajām cietvielām pēdējās desmitgades laikā ir būtiski pieaugusi, uz ko skaidri norāda pieaugums zinātnisko publikāciju skaitā, kas pēta šo parādību, galvenokārt, pārbaudot līdz šim pieņemtās un izsakot jaunas hipotēzes kristālīnženierijas jomā^{3,4}. Papildus tam, cietie šķīdumi paver perspektīvu iespēju materiāla īpašību modulēšanai, mainot komponentu sastāvu nepārtrauktā veidā⁵. Tiesa, vēlamajai īpašībai jābūt pietiekami jutīgai attiecībā pret cietā šķīduma sastāvu⁶.

Kristālīnženierijas pieeja tiek izmantota, lai dizainētu un uzlabotu tādas nozīmīgas kristālu fizikālās un/vai ķīmiskās īpašības kā šķīdību^{7,8}, kušanas temperatūru⁹, nelineārās optiskās¹⁰ un mehāniskās īpašības¹¹. Pakāpeniska īpašību regulēšana var tikt panākta, ķīmiski modificējot molekulas, proti, izmainot kādu no aizvietotajiem molekulārajā struktūrā¹². Tomēr izveidot viennozīmīgu kristālīnženierijas stratēģiju, kas ļautu uzlabot šīs īpašības nepārtrauktā veidā, nav vienkāršs uzdevums. Jau vairākus desmitus gadus atpakaļ Kitaigorodskas darbos^{13,14} ir aprakstīts, ka lielu lomu tajā, vai cietais šķīdums starp konkrētiem savienojumiem spēs veidoties, spēlē līdzība aizvietojamo molekulu izmērā un formā, un cieto šķīdumu veidošanās galvenokārt ir saistīta ar tīru komponentu struktūru līdzību¹⁵ jeb izomorfismu¹⁶. Tomēr kopš šī laika iegūtais kristalogrāfisko datu kopums rāda, ka Kitaigorodskas atrastās likumības nav pilnīgas un ir nepieciešama to pārskatīšana un attīstīšana¹⁷.

Līdz šim cieto šķīdumu veidošanās spēja ir novērota un pētīta starp uzbūves ziņā līdzīgām organiskām molekulām, kuras atšķiras ar F/H atomu¹⁸; aizvietotāju (halogēna atoms un halogēna atoms/metilgrupa)¹⁹; ar S/O atomu²⁰; ar heteroatoma esamību/neesamību aromātiskajā gredzenā²¹, utt. Lai gan, ņemot vērā līdzšinējo pētījumu rezultātus, varētu tikt definēti vispārīgi un empīriski kritēriji, kas ļautu noteikt cieto šķīdumu veidošanās spēju starp strukturāli līdzīgām molekulām, literatūrā ir aprakstīti gadījumi, kuros pat ļoti līdzīgas molekulas tomēr nespēj veidot cietos šķīdumus¹⁷.

Līdz ar to sistemātiskai datu iegūšanai par to, vai strukturāli līdzīgas organiskās molekulas spēj aizvietot viena otru kristāliskajā struktūrā, nodrošinot cieto šķīdumu veidošanos, ir augsta zinātniskā aktualitāte, un ir nepieciešama detalizēta dažādu individuālu sistēmu izpēte, lai identificētu galvenos faktoros, kas ļautu formulēt vispārīgas likumības un modeļus, ar kuru palīdzību varētu paredzēt šādu fāžu veidošanās varbūtību. Šim nolūkam pētījumiem izvēlētas gan ļoti līdzīgas molekulas ksantonu un tioksantonu, kas atšķiras ar S/O atomu, gan aizvietotas nitrobenzoksābes, kas atšķiras ar aizvietotāju (halogēna atoms / metilgrupa / hidroksilgrupa) un starp kurām cieto šķīdumu veidošanās pētīta dažādos vielas izomēros, gan farmaceitiskās vielas benperidols un droperidols, kas atšķiras ar vienkāršās/divkāršās saites esamību starp diviem oglekļa atomiem, starp kurām papildus pētīta cieto šķīdumu veidošanās dažādās šo vielu veidotās nesolvatētās un solvatētās fāzēs.

Jāatzīmē, ka tikai dažos no līdzšinējiem pētījumiem cieto šķīdumu veidošanās ir skaidrota ar kvantu ķīmiskos aprēķinos iegūtām enerģijas izmaiņām, lai gan šādi aprēķini ir viens no veidiem, kas ļautu nonākt līdz minētajām likumībām un modeļiem. Līdz ar to šādi pētījumi veikti gan starp uzbūves ziņā relatīvi atšķirīgākajām aizvietotajām nitrobenzoscābēm, gan relatīvi līdzīgākajiem benperidolu un droperidolu to dažādās kristāliskajās fāzēs.

Papildus tam, līdzšinējos pētījumos ar organiskām vielām pamatā veikta tikai cieto šķīdumu veidošanās identificēšana un kristalogrāfiskā analīze, bet ir maz pētījumu par šādu cieto šķīdumu iespējām izmainīt industriāli nozīmīgas fizikālās īpašības. Līdz ar to pētījumiem papildus izvēlēti tioksantona atvasinājumi, kas atšķiras ar halogēna atomiem un ir istabas temperatūras luminofoori, un kuriem bez cieto šķīdumu veidošanās izpētes veikta arī iegūto fāžu luminiscences īpašību raksturošana.

Promocijas darba mērķis un uzdevumi

Šī pētījuma **mērķis** ir, izmantojot gan eksperimentālos pētījumus, gan kvantu ķīmijas aprēķinus, identificēt galvenos faktorus, kas nodrošina cieto šķīdumu veidošanos starp uzbūves ziņā līdzīgām organiskajām molekulām, kā arī iegūt kristāliskās fāzes ar smalki regulējamām fizikālķīmiskajām īpašībām.

Izvirzīti šādi **uzdevumi**:

- 1) raksturot cieto šķīdumu veidošanās iespējas dažādās divkomponentu sistēmās, balstoties uz informāciju par attiecīgo kristālisko fāžu daudzveidību, un raksturot iegūto cieto šķīdumu struktūras un termodinamisko stabilitāti fāžu diagrammu veidā;
- 2) noskaidrot tioksantonu atvasinājumu veidoto cieto šķīdumu luminiscences īpašības un to maiņu atkarībā no komponentu sastāva, lai iegūtu jaunus materiālus ar smalki regulējamām luminiscences īpašībām;
- 3) veikt kvantu ķīmiskos aprēķinus benperidola un droperidola, kā arī aizvietoto nitrobenzoscābju veidotās cieto šķīdumu modeļu struktūrās, lai noskaidrotu iespēju izmantot starpmolekulāro mijiedarbību enerģijas izmaiņas cieto šķīdumu veidošanās iespējamības novērtēšanai dažādās kristāliskajās struktūrās.

Tēzes

1. Molekulas spēju aizstāt vienai otru dažādās fāzēs nosaka gan līdzība apmaināmo funkcionālo grupu īpašībās un veidotajās raksturīgajās starpmolekulārajās mijiedarbībās, gan arī fāzes kristāliskā struktūra.
2. Cieto šķīdumu veidošanās pieeju ir iespējams izmantot, lai smalki regulētu organisko luminoforu fizikālās īpašības.
3. Starpmolekulāro mijiedarbību enerģijas izmaiņu analīze, modelējot cieto šķīdumu veidošanos, ir izmantojama cieto šķīdumu veidošanās varbūtības noteikšanai starp uzbūves ziņā pietiekoši līdzīgām molekulām.

Zinātniskā novitāte

1. Konstruētas dažādu divkomponentu sistēmu fāžu diagrammas, raksturojot pētīto cieto šķīdumu termodinamisko stabilitāti, kā arī identificējot dažādas šādās sistēmās sastopamās sarežģītības (tai skaitā, iespējamību iegūt cieto šķīdumu polimorfus).
2. Noteikti cieto šķīdumu veidošanos regulējoši faktori starp molekulārās uzbūves ziņā līdzīgām organiskajām vielām (izmainīts kāds no atomiem vai funkcionālajām grupām), kā arī kristāliskās struktūras un tajās pastāvošo starpmolekulāro mijiedarbību loma cieto šķīdumu veidošanās procesā.
3. Iegūti luminiscenti materiāli ar smalki regulējamām luminiscences īpašībām, kas līdz šim organisko molekulu veidotās sistēmās tikpat kā nav pētīti.
4. Iegūti jauni cietie šķīdumi, t. sk. cietie šķīdumi vairākās F-TXANT, gan Cl-TXANT polimorfajās formās šo vielu binārā sistēmā, kas uzrāda atšķirīgas luminiscences īpašības.
5. Analizējot kvantu ķīmisko aprēķinu rezultātus dažādās binārās sistēmās, demonstrēta starpmolekulāro mijiedarbību enerģijas izmaiņu analīzes metode un tās pielietojums cieto šķīdumu veidošanās iespējamības noteikšanai dažādās kristāliskajās struktūrās.

Praktiskā nozīme

1. Izvirzīti jauni priekšlikumi un risinājumi, lai palīdzētu iegūt jaunus materiālus ar modificētām fizikālajām īpašībām, tai skaitā luminiscences īpašībām un kušanas temperatūru, kā arī apzinātas cieto šķīdumu veidošanās likumības starp uzbūves ziņā līdzīgām organiskajām vielām, gūstot izpratni par strukturālajiem un mijiedarbību enerģijas faktoriem.
2. Iegūti jauni optoelektronikas materiāli, balstoties uz zināšanām par savienojumu molekulārajām un kristāliskajām struktūrām, tādējādi demonstrējot iespēju ar kristālīnženieriju veidot pievilcīgus molekulāru kristālu materiālus ar smalki regulējamām (no komponentu sastāva atkarīgām) luminiscences īpašībām.
3. Starpmolekulāro mijiedarbību enerģijas izmaiņu aprēķinos noteiktās informācijas salīdzināšanā ar eksperimentālajiem datiem, iegūta informācija par šādas aprēķinu izmantošanas iespējām cieto šķīdumu veidošanās paredzēšanā, ko tālāk iespējams izmantot, izstrādājot vispārīgu aprēķinu metodiku cieto šķīdumu veidošanās paredzēšanai.

PUBLICĒTIE REZULTĀTI

Zinātniskās publikācijas

1. **Saršūns, K.**, Bērziņš, A., Rekis, T. Solid solutions in xanثone – thioxanthone binary system: how well are similar molecules discriminated in the solid state? *Crystal Growth & Design*[‡], **2020**, 20(12), 7997–8004. DOI: 10.1021/acs.cgd.0c01241 (Web of Science/Scopus, Q2/Q1, IF₂₀₂₀ = **4.076**).

K. Saršūns izstrādāja 75% no eksperimentālā darba apjoma, sniedza ieguldījumu publikācijas rakstīšanā (50%), noformēja pētījuma rezultātus atbilstoši žurnāla prasībām, kā arī sniedza ieguldījumu, sagatavojot atbildes uz recenzentu jautājumiem un aizrādījumiem.

2. **Saršūns, K.**, Ķemere, M., Karziņins, A., Kļimenkovs, I., Bērziņš, A., Sarakovskis, A., Rekis, T. Fine-tuning solid state luminescence properties of organic crystals via solid solution formation: the example of 4-iodothioxanthone – 4-chlorothioxanthone system. *Crystal Growth & Design*, **2022**, 22(8), 4838–4844. DOI: 10.1021/acs.cgd.2c00313 (Web of Science/Scopus, Q1/Q1, IF₂₀₂₂ = **4.010**).

K. Saršūns izstrādāja 75% no eksperimentālā darba apjoma, sniedza ieguldījumu publikācijas rakstīšanā (50%), noformēja pētījuma rezultātus atbilstoši žurnāla prasībām, kā arī sniedza ieguldījumu, sagatavojot atbildes uz recenzentu jautājumiem un aizrādījumiem.

3. **Saršūns, K.**, Bērziņš, A. Experimental and computational investigation of benperidol and droperidol solid solutions in different crystal structures. *Crystal Growth & Design*, **2023**, 23(2), 1133–1144. DOI: 10.1021/acs.cgd.2c01269 (Web of Science/Scopus, Q1/Q1, IF₂₀₂₃ = **4.010**).

K. Saršūns izstrādāja 90% no eksperimentālā darba apjoma, sniedza ieguldījumu publikācijas rakstīšanā (75%), noformēja pētījuma rezultātus atbilstoši žurnāla prasībām, kā arī sniedza ieguldījumu, sagatavojot atbildes uz recenzentu jautājumiem un aizrādījumiem.

4. **Saršūns, K.**, Kons, A., Rekis, T., Bērziņš, A. Experimental and computational study of solid solution formed between substituted nitrobenzoic acids. *Crystal Growth & Design*, **2023**, 23(9), 6609–6622. DOI: 10.1021/acs.cgd.3c00529 (Web of Science/Scopus, Q2/Q1, IF₂₀₂₃ = **4.010**).

K. Saršūns izstrādāja 90% no eksperimentālā darba apjoma, sniedza ieguldījumu publikācijas rakstīšanā (75%), noformēja pētījuma rezultātus atbilstoši žurnāla prasībām, kā arī sniedza ieguldījumu, sagatavojot atbildes uz recenzentu jautājumiem un aizrādījumiem.

5. **Saršūns, K.**, Kons, A., Leduskrastrs, K., Kļimenkovs, I., Bērziņš, A., Rekis, T. Modulation of physico-chemical properties via solid solution formation of thioxanthone derivatives. *Manuskripts izstrādes procesā*.

K. Saršūns izstrādāja 75% no eksperimentālā darba apjoma, sniedza ieguldījumu publikācijas rakstīšanā (60%) un noformēja pētījuma rezultātus atbilstoši žurnāla prasībām.

[‡]Recenzēts žurnāls, kuru izdod American Chemical Society (ISSN: 1528-7505)

Konferences

Šī pētījuma rezultāti prezentēti mutiski trīs starptautiskajās zinātniskajās konferencēs (no tām divas Latvijas Universitātes) un stenda referāta formā trīspadsmit starptautiskajās zinātniskajās konferencēs gan attālināti, gan klātienē.

Divkomponentu sistēma ksantons – tioksantons

- **Saršūns, K.**, Karziņins, A., Leduskrasts, K., Bērziņš, A., Rekis, T. Formation of solid solution in xanthone derivative systems exhibiting luminescence properties. *University of Latvia 79th International Scientific Conference*, 12. februāris, **2021**, Tiešsaiste. (mutiskā prezentācija/ tēžu grāmata)
- **Saršūns, K.**, Karziņins, A., Leduskrasts, K., Bērziņš, A., Rekis, T. Formation of solid solution in xanthone derivative systems exhibiting luminescence properties. *64th International Conference for Students of Physics and Natural Sciences*, 16. - 19. marts, **2021**, Tiešsaiste. (stenda referāts/ tēžu grāmata/ sertifikāts)
- **Saršūns, K.**, Karziņins, A., Leduskrasts, K., Bērziņš, A., Rekis, T. Formation of solid solution in xanthone derivative systems exhibiting luminescence properties. *11th Belgian Crystallography Symposium*, 17. marts, **2021**, Tiešsaiste. (stenda referāts/ tēžu grāmata/ sertifikāts)
- **Saršūns, K.**[§], Karziņins, A., Leduskrasts, K., Bērziņš, A., Rekis, T.[‡]. Modulation of luminescence spectra *via* solid solution formation of xanthone derivatives[§] / Formation of solid solution in xanthone derivative systems exhibiting luminescence properties[‡]. *BCA/BACG Online Joint Spring Meeting*, 29. marts - 1. aprīlis, **2021**, Tiešsaiste. (stenda referāts[§]/mutiskā prezentācija[‡]/ tēžu grāmata^{§, ‡}/ sertifikāts)
§, ‡ – prezentējais.
- **Saršūns, K.**, Bērziņš, A., Rekis, T. Solid solution formation in xanthone – thioxanthone binary system: experimental investigation. *23rd International conference EcoBalt 2023*, 9. - 11. oktobris, **2023**, Tallina, Igaunija. (stenda referāts/ tēžu grāmata/ sertifikāts/ speciālizdevums MDPI žurnālā – *Proceedings*, **2023**, 92(1), 67. DOI: 10.3390/proceedings2023092067)

Dažādu aizvietotu nitrobenzoksābju divkomponentu sistēmas

- **Saršūns, K.**, Bērziņš, A. Computational prediction and experimental confirmation of solid solution formation from different nitrobenzoic acid derivatives and their isomers. *61st International Scientific Conference “Materials Science and Applied Chemistry”*, 23. oktobris, **2020**, Tiešsaiste. (stenda referāts/ tēžu grāmata)
- **Saršūns, K.**, Bērziņš, A. Computational prediction and experimental confirmation of solid solution formation from different nitrobenzoic acid derivatives and their isomers. *2nd International Online Conference on Crystals*, 10. - 20. novembris, **2020**, Tiešsaiste. (stenda referāts/ tēžu grāmata)
- **Saršūns, K.**, Bērziņš, A., Rekis, T. Structural and energetic factors that contributes to solid solution formation between different nitrobenzoic acid derivatives and their isomers. *63rd International Scientific Conference “Materials Science and Applied Chemistry”*, 21. oktobris, **2022**, Tiešsaiste. (stenda referāts/ tēžu grāmata/ sertifikāts)

- **Saršūns, K.**, Kons, A., Reķis, T., Bērziņš, A. Experimental and computational study of solid solution formed between substituted nitrobenzoic acids. *12th Bologna Convention on Crystal Forms*, 10. - 12. septembris, **2023**, Boloņa, Itālija. (stenda referāts/ tēžu grāmata/ sertifikāts)

Divkomponentu sistēma benperidols – droperidols

- **Saršūns, K.**, Bērziņš, A. Experimental and computational investigation of benperidol and droperidol solid solutions in different crystal structures. *26th Congress and General Assembly of the International Union of Crystallography*, 22. - 29. augusts, **2023**, Melburna, Austrālija. (stenda referāts/ tēžu grāmata/ sertifikāts)

Dažādu tioksantona halogēnatvasinājumu divkomponentu sistēmas

- **Saršūns, K.**, Leduskrasts, K., Bērziņš, A., Reķis, T. Formation of solid solution in thioxanthone derivative systems exhibiting luminescence properties. *11th Bologna Convention on Crystal Forms*, 10. - 11. septembris, **2021**, Tiešsaiste. (stenda referāts/ tēžu grāmata/ sertifikāts)
- **Saršūns, K.**, Leduskrasts, K., Bērziņš, A., Reķis, T. Modulation of luminescence spectra *via* solid solution formation of thioxanthone derivatives. *22nd International conference EcoBalt 2021*, 21. - 23. oktobris, **2021**, Tiešsaiste. (mutiskā prezentācija/ tēžu grāmata/ sertifikāts)
- **Saršūns, K.**, Leduskrasts, K., Bērziņš, A., Reķis, T. Modulation of luminescence spectra *via* solid solution formation of thioxanthone derivatives. *62nd International Scientific Conference "Materials Science and Applied Chemistry"*, 22. oktobris, **2021**, Tiešsaiste. (stenda referāts/ tēžu grāmata/ sertifikāts)
- **Saršūns, K.**, Bērziņš, A., Reķis, T. Fine-tuning solid state luminescence properties of molecular crystals *via* solid solution formation. *University of Latvia 80th International Scientific Conference*, 11. februāris, **2022**, Tiešsaiste. (mutiskā prezentācija/ tēžu grāmata)
- **Saršūns, K.**, Leduskrasts, K., Bērziņš, A., Reķis, T. Fine-tuning solid state luminescence properties of molecular crystals *via* solid solution formation. *30th Annual Meeting of the German Crystallographic Society*, 14. - 17. marts, **2022**, Tiešsaiste. (stenda referāts/ tēžu grāmata/ sertifikāts)
- **Saršūns, K.**, Leduskrasts, K., Bērziņš, A., Reķis, T. Fine-tuning solid state luminescence properties of molecular crystals *via* solid solution formation. *17th European Powder Diffraction Conference*, 31. maijs - 3. jūnijs, **2022**, Šibenika, Horvātija. (stenda referāts/ tēžu grāmata/ sertifikāts)

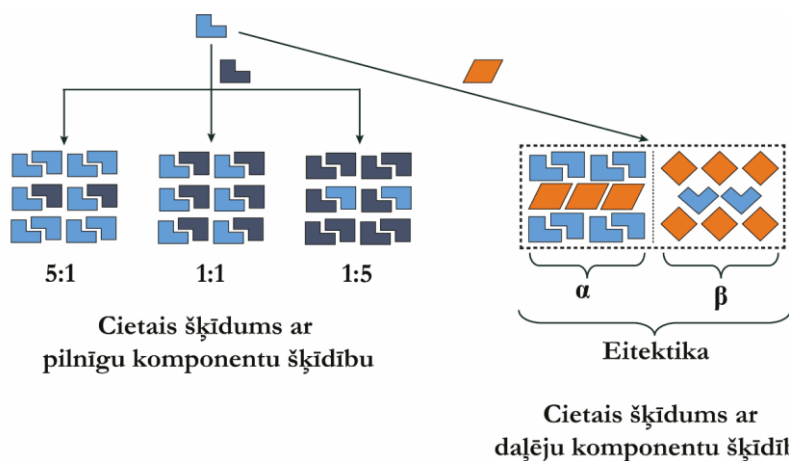
1. PROMOCIJAS DARBA TEORĒTISKIE PAMATI UN PĒTĪTĀS SISTĒMAS

1.1. Cieto šķīdumu struktūra un termodinamiskais raksturojums

Cieto šķīdumu struktūra

Cietie šķīdumi ir kristāliskas fāzes, kas sastāv no vismaz diviem komponentiem noteiktās robežās brīvi maināmā attiecībā. Atkarībā no komponentu šķīdības, cietie šķīdumi tiek iedalīti divos tipos, t. i., pilnīgas komponentu un daļējas komponentu šķīdības cietajos šķīdumos (sk. 1.1. att.):

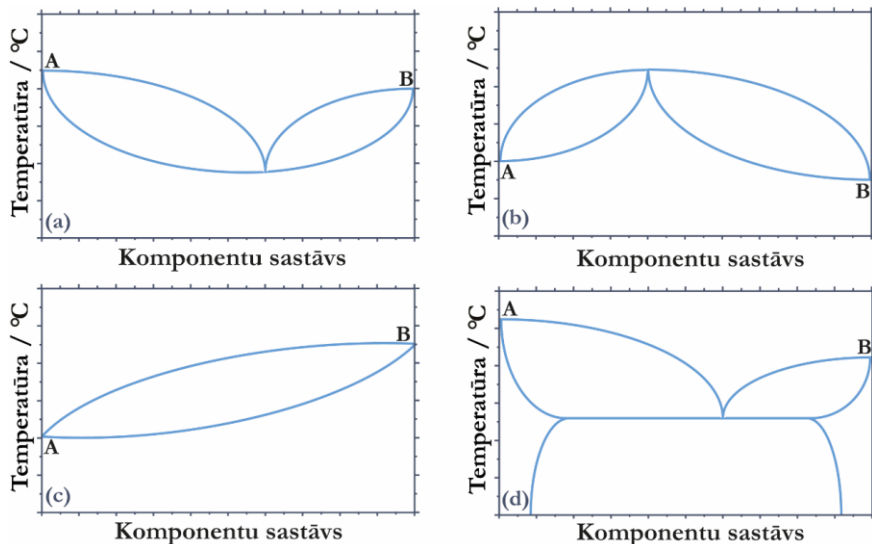
- cietos šķīdumus ar komponentu pilnīgu (neierobežotu) savstarpējo šķīdību novēro, kad vienas vielas molekulas iešķīst otras vielas kristāliskajā struktūrā pilnā koncentrācijas diapazonā;
- cietos šķīdumus ar komponentu daļēju (ierobežotu) savstarpējo šķīdību novēro, kad vienas vielas molekulas var iešķīst otras vielas kristāliskajā struktūrā tikai līdz zināmai koncentrācijai¹.



1.1. att. Cieto šķīdumu veidošanās starp organisku cietvielu molekulām shematiskais attēlojums²².

Cieto šķīdumu termodinamiskais raksturojums

Konstruējot divkomponentu fāžu diagrammas, iespējams noskaidrot cieto šķīdumu veidošanās iespējamību, kā arī tos raksturot, piemēram, nosakot komponentu sajaukšanās attiecību robežas un termodinamisko stabilitāti. 1.2. attēlā redzamas pamata fāžu diagrammas, kurās iesaistīti cietie šķīdumi.



1.2. att. Divkomponentu sistēmu fāžu diagrammas sistēmām ar cieto šķīdumu veidošanos (ar pilnīgu (a) – (c) un daļēju (d) komponentu sajaukšanos).

Literatūrā ziņots par organisko cietvielu spēju sajaukties pilnīgā^{16,23,24} un daļējā kompozīcijas diapazonā^{25–27}. Fāžu diagrammu konkrētam savienojumam definē cietfāžu termodinamiskā daba. Gadījumi (a) un (b) attēlo organisko cietvielu sajaukšanos visā kompozīciju apgabalā, attiecīgi veidojot neideālus cietos šķīdumus ar maksimālo un minimālo kušanas temperatūru kādā noteiktā komponentu attiecībā, bet (c) gadījumā ideālu cieto šķīdumu, kurā kušanas temperatūras maksimums un minimums atbilst tīriem komponentiem. Cietfāzes A un B šajos gadījumos ir izostrukturālas. Savukārt (d) gadījumā ierobežota sajaukšanās skaidrojama ar to, ka pie noteikta sastāva cietā šķīduma struktūra vairs nav termodinamiski stabila, un tā vietā veidojas mehānisks divu fāžu (cieto šķīdumu ar robežgadījuma sastāvu) maisījums. Sajaukšanās apgabala platumu un citas kvantitatīvas fāžu diagrammas īpašības nosaka cietfāžu A un B fizikālķīmiskās īpašības – kušanas entalpijas un kušanas temperatūras.

1.2. Cieto šķīdumu pētījumi, izmantojot dažādas fizikālās cietfāžu pētīšanas metodes

Cieto šķīdumu identifikācijai ir pieejamas daudzas fizikālās cietfāžu pētīšanas metodes un to kombinācijas, no kurām visbiežāk izmantotās ir pulvera rentgendifrakcija (PXRD), diferenciāli skenējošā kalorimetrija (DSC), un komponentu daudzuma noteikšanai – kodolmagnētiskās rezonanses spektroskopija (KMR) un augsti efektīvā šķīduma hromatogrāfija (AESĤ), savukārt, to struktūru detalizētai raksturošanai visbiežāk tiek izmantota monokristāla rentgendifrakcijas (SCXRD) analīze. Šajā darbā tika pētītas arī iegūto cieto šķīdumu cietfāžu luminiscences īpašības, izmantojot fotoluminiscences spektroskopiju. Lai rūpīgi analizētu cietos šķīdumus, ir nepieciešams izmantot dažādas pieejas, jo katra no fizikālajām cietfāžu pētīšanas metodēm sniedz unikālu, bet ierobežotu informāciju par fāzi. Kopsavilkums par fizikālo cietfāžu pētīšanas metožu pielietojumu dažādu cieto šķīdumu raksturlielumu noteikšanā dots 1.1. tabulā.

Fizikālo cietfāžu pētīšanas metožu pielietojums cieto šķīdumu raksturošanai^{1,28}

Pielietojums	Pētīšanas metode						Luminiscences spektroskopija ^b
	SCXRD	PXRD	KMR	AEŠH	DSC	TG	
Kristāliskas fāzes identifikācija	✓	✓			✓	✓	✓
Kristāliskā struktūra	✓	✓ ^a					
Molekulu ģeometrija	✓						
Ūdeņraža saišu mijiedarbības (t. sk. vājās mijiedarbības)	✓		✓				
Termiskā stabilitāte		✓			✓	✓	
Stehiometrijas noteikšana	✓		✓	✓		✓	
Fāžu pārejas		✓			✓	✓	✓
Kušanas temperatūra					✓		
Desolvatācija/-hidratācija					✓	✓	
Luminiscences īpašības							✓

^a – kristāliskās struktūras režģu parametru noteikšana, dažkārt arī struktūras noteikšana;

^b – savienojumiem, kuriem ir novērojama luminiscences parādība.

Cietfāžu luminiscence

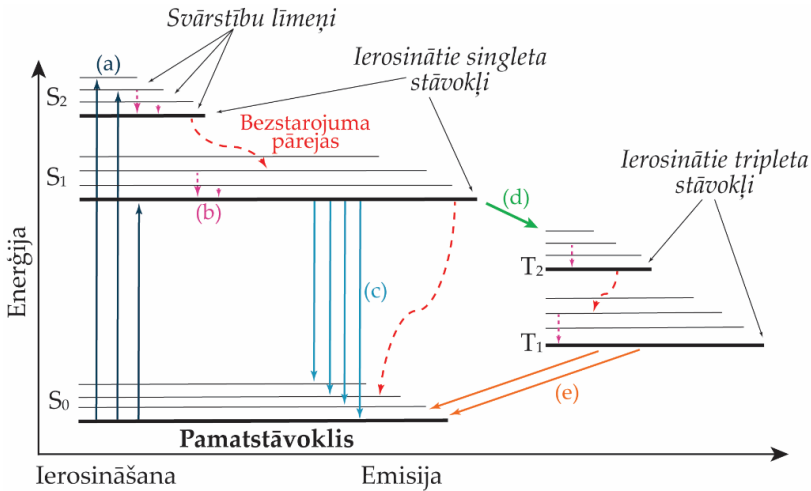
Luminiscence ir fizikāla parādība, kurā novērojama elektromagnētiskā starojuma emisija no ierosināta materiāla. Luminiscences procesā elektroni no ierosināta stāvokļa atgriežas pamatstāvoklī, sākotnēji daļu no enerģijas zaudējot bezstarojuma pārejās un tikai tad izstarojot elektromagnētiskā starojuma kvantu, kura enerģija atbilst enerģijas starpībai starp iesaistītajiem enerģijas līmeņiem (ierosināto līmeni un pamatstāvokli). Ar luminiscenci saistītie procesi parādīti 1.3. attēlā (šādu enerģijas līmeņu shēmu ar izzīmētiem procesiem sauc par Jablonska diagrammu)²⁹.

Apzīmējumi (a) – (e), kas iekļauti 1.3. attēlā raksturo enerģijas pārejas procesus laika skalā:

- (a) absorbcija (10^{-15} s);
- (b) vibrāciju relaksācija (10^{-14} – 10^{-10} s);
- (c) fluorescenci (10^{-9} – 10^{-7} s);
- (d) starpsistēmu pāreja (10^{-8} – 10^{-6} s);
- (e) fosforescenci (10^{-6} – 10 s).

Organisko luminoforu fotofizikālās īpašības visbiežāk raksturo ar fotoluminiscenci. Fotoluminiscences gadījumā elektrona ierosināšana notiek, vielai absorbējot enerģiju elektromagnētiskā starojuma – redzamās gaismas (vai UV) kvanta – formā.

Pēc kvanta absorbēšanas luminofors tiek ierosināts no singleta pamatstāvokļa (S_0) uz ierosinātu singleta stāvokli (S_1 ; procesa apzīmējums (a)) ar secīgu vibrāciju relaksāciju (b) un fluorescenci (c). Fluorescenci ir emisija no ierosinātiem singleta (S_n) stāvokļiem, tās norisei nepieciešami trīs secīgi procesi: (a) → (b) → (c), savukārt, fosforescenci ir emisija no ierosinātiem tripleta (T_n) stāvokļiem, un tā ietver četrus secīgus procesus: (a) → (b) → (d) → (e)^{30,31}.



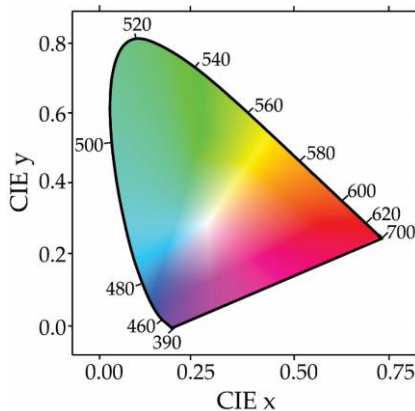
1.3. att. Shematisks ar luminiscenci saistīto procesu attēlojums – Jablonska diagrammas veidā.

Efektīva luminofora būtiskākais rādītājs ir fotoluminiscences kvantu iznākums (Φ). Tas tiek definēts kā emitēto fotonu attiecība pret absorbēto fotonu skaitu un aprēķina pēc vienādojuma (1).

$$\Phi_{\%} = \frac{\Sigma P_E}{\Sigma P_A} \cdot 100, \quad (1)$$

kur $\Phi_{\%}$ – kvantu iznākums, ΣP_E – visu izstaroto fotonu summa, ΣP_A – visu absorbēto fotonu summa³².

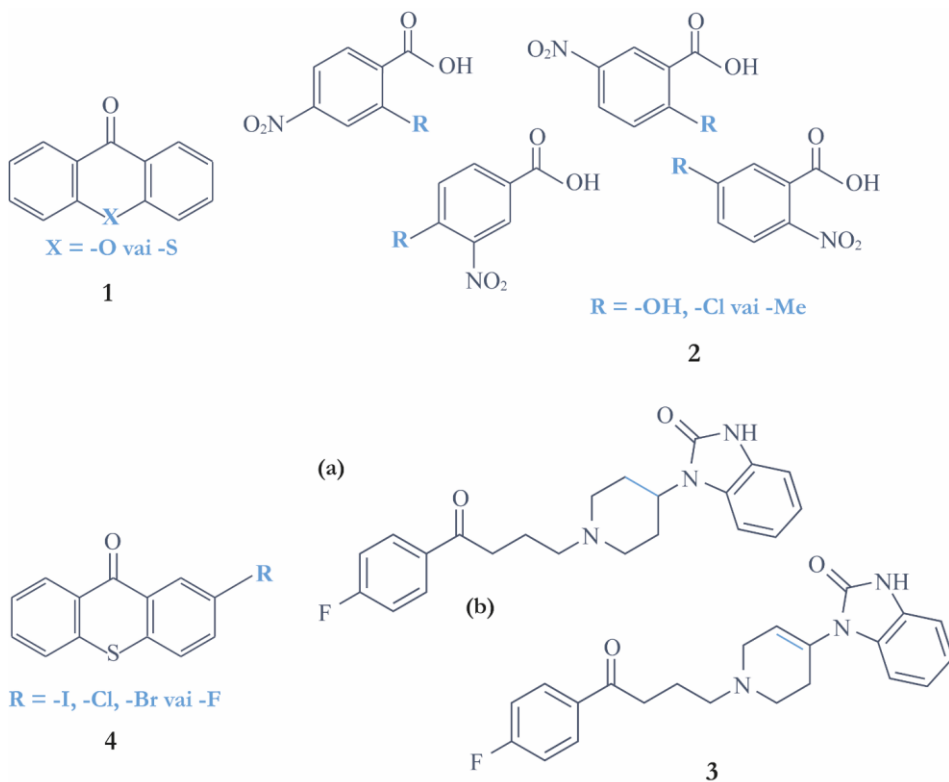
Paraugu izstarotās gaismas (luminiscences) krāsu iespējams raksturot ar krāsu (jeb fotometriskajām) koordinātām. Balstoties uz materiāla luminiscences spektru un cilvēka acs spektrālo jutību, krāsu koordinātas parāda, kādā krāsā novērotājs redz luminiscences gaismu. Visbiežāk gaismas krāsu apraksta, izmantojot CIE 1931 XYZ krāsu telpu (CIE – International Commission on Illumination), kas tika izveidota 1931. gadā. Krāsa tiek raksturota, izmantojot divas koordinātas: x un y (sk. 1.4. att.)³³.



1.4. att. CIE hromatiskuma diagramma (CIE 1931, standarta vizualizācija).

1.3. Pētītās sistēmas

Darba ietvaros pētītas četras savienojumu sistēmas (struktūrformulas dotas 1.5. att.). Pētītas divas sistēmas, kas satur dažādas vienkāršas modeļvielas: **ksantona analogi (1)**, abas molekulas ir aromātiskas un planāras, savstarpēji atšķiras pēc aizvietotāja aromātiskajā gredzenā jeb pēc O un S atoma³⁴, un **aizvietotas nitrobenzoscābes (2)** savstarpēji atšķiras, pirmkārt, pēc aizvietotāja C2, C4 vai C5 pozīcijā un, otrkārt, pēc nitrogrupas novietojuma C2, C3, C4 vai C5 pozīcijā. Informācija par nitrobenzoscābju atvasinājumu un to izomēru cietvielu formu daudzveidību pēta Ķīmijas fakultātes Fizikālās ķīmijas katedrā un ir pieejama zinātniskajā publikācijā³⁵.



1.5. att. Pētīto savienojumu sistēmu struktūrformulas (1 – ksantona analogi; 2 – aizvietotas nitrobenzoscābes; 3 – benperidols (a) un droperidols (b); 4 – tiokantona atvasinājumi).

Pētītas arī farmaceitiski aktīvās vielas (FAV): **benperidols (3a)** (1-({1-[4-(4-fluorfenil)-4-oksobutil]-piperidīn-4-il}-1,3-dihidro-2H-benzimidazol-2-ons) un **droperidols (3b)** (1-({1-[4-(4-fluorfenil)-4-oksobutil]-1,2,3,6-tetrahidro-4-pīridil}-1,3-dihidro-2H-benzimidazol-2-ons), kas ir antipsihotiskas zāļu vielas, kurām ir antidepresanta un antiamnēziju uzlabojošs efekts un kuras savā starpā atšķiras pēc C8–C9 saites jeb 1,2,3,6-tetrahidropīridīna cikla vietā benperidolam ir piperidīna cikls^{36,37}. Droperidola un benperidola cietvielu formu daudzveidība iepriekš plaši pēta Ķīmijas fakultātes Fizikālās ķīmijas katedrā, un ir pieejama zinātniskajās publikācijās^{38–40}, atklājot, ka abas vielas veido vairākas polimorfās formas, hidrātus, etanola, metanola, acetonnitrila, kā arī citu šķīdinātāju solvātus.

Visbeidzot, pētītas modeļvielas, kurām istabas temperatūrā ir novērojama luminiscences parādība⁴¹: **tioksantona atvasinājumi (4)**, to molekulārās struktūras ir līdzīgas un savā starpā atšķiras pēc aizvietotāja C2 pozīcijā.

2. EKSPERIMENTĀLĀ DAĻA

1. Fāžu identifikācijai pulvera rentgendifraktogrammas uzņemtas ar iekārtu *Bruker D8 Advance* ar 1D pozīcijas jutīgo *Lynxeye* detektoru, izmantojot *Bragg–Brentano* ģeometriju un vara anoda ($\text{Cu K}\alpha$) rentgenstaru avotu. Paraugu iepresēja stikla kivetē. Uzņemšanas režīms: $3^\circ - 35^\circ 2\theta$, ātrums $0,2\text{s}/0,02^\circ$ (Latvijas Universitāte, Rīga, Latvija).
2. Pulvera rentgendifraktogrammas struktūras noteikšanai uzņemtas ar iekārtu *Bruker D8 Discover* ar 1D *Lynxeye* detektoru, izmantojot caurstarojošo ģeometriju (lietojot Gobela spoguļus) un vara anoda ($\text{Cu K}\alpha$) rentgenlampu. Paraugu iepresēja borsilikāta stikla kapilārā ar iekšējo diametru $0,5\text{ mm}$ (Hilgenberg glass No. 10), ievietoja goniometriskajā kapilārū turētājā, un uzņemšanas laikā rotēja ar ātrumu 60 apgr./min . Uzņemšanas režīms: $4^\circ - 70^\circ 2\theta$, ātrums $36\text{s}/0,01^\circ$ (Latvijas Universitāte, Rīga, Latvija).
3. Monokristālu rentgendifraktometri izmantoti, lai noteiktu izaudzēto monokristālu kristāliskās struktūras. Paraugšs fiksēts ar eļļu magnētiskā *CryoCap* neilona cilpā un novietots uz goniometra galvas:
 - *Rigaku XtaLAB Synergy-S dualflex* difraktometrs ar *HyPix6000* detektoru un $\text{Cu K}\alpha$ rentgenstaru avotu – $\lambda = 1,54184\text{ \AA}$ (Latvijas Organiskās sintēzes institūts, Rīga, Latvija);
 - *Huber 4 circle kappa* difraktometrs ar *Pilatus CdTe 1M* detektoru un sinhrotrono starojumu – $\lambda = 0,61992\text{ \AA}$ (P24, PETRA III, Deutsches Elektronen-Synchrotron DESY, Hamburga, Vācija);
 - *Arinax MD3* difraktometrs ar *Eiger 16M Hybrid-pixel* detektoru un sinhrotrono starojumu – $\lambda = 0,68879\text{ \AA}$ (BioMAX, MAX IV Synchrotron, Lunda, Zviedrija).
4. Diferenciāli skenējošais kalorimetrs/termogravimetrs *Mettler Toledo TGA/DSC2* izmantots iegūto fāžu raksturošanai un solvātos esošā šķīdinātāja stehiometrijas noteikšanai. Uzņemšanas režīms: $25\text{ }^\circ\text{C} - 240\text{ }^\circ\text{C}$, karsēšanas ātrums $10\text{ }^\circ\text{C}\cdot\text{min}^{-1}$, N_2 atmosfērā (plūsmas ātrums $100 \pm 10\text{ mL}\cdot\text{min}^{-1}$). Paraugu karsēšanu veica vaļējos alumīnija kausiņos ar tilpumu $100\mu\text{L}$ (Latvijas Universitāte, Rīga, Latvija).
5. Diferenciāli skenējošais kalorimetrs *TA Instruments DSC 25* izmantots kušanas un maksimālās temperatūras noteikšanai – divkomponentu sistēmu fāžu diagrammu konstruēšanai. Uzņemšanas režīms: $25\text{ }^\circ\text{C} - 250\text{ }^\circ\text{C}$ (atkarībā no tīra komponenta kušanas temperatūras), karsēšanas ātrums $2 - 5\text{ }^\circ\text{C}\cdot\text{min}^{-1}$, N_2 atmosfērā (plūsmas ātrums $50 \pm 10\text{ mL}\cdot\text{min}^{-1}$). Paraugu karsēšanu veica aiztaisītos alumīnija kausiņos ar tilpumu $70\mu\text{L}$ (Latvijas Universitāte, Rīga, Latvija).
6. Kodolmagnētiskās rezonanses spektroskops *Bruker Fourier 300 MHz* izmantots izvēlētu kristalizācijas produktu saturošo komponentu procentuālā sastāva noteikšanai. Spektus uzņēma, par šķīdinātāju izmantojot dimetilsulfoksīdu (DMSO)- d_6 ($\delta = 2,49\text{ ppm}$), un par iekšējo standartu izmantots HMDS ($\delta = 0,055\text{ ppm}$), pret kuru mērītas ķīmiskās nobīdes (δ) miljondaļās (ppm) (Latvijas Universitāte, Rīga, Latvija).

7. Kristalizācijas produktu luminiscences pētījumi:

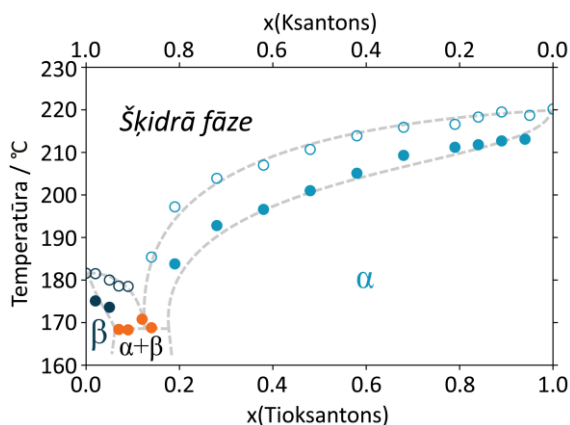
- fotoluminiscences spektri uzņemti, izmantojot spektrofluorimetru *Edinburgh Instruments FS5*, kas aprīkots ar nepārtraukta starojuma CW 150 W ksenona lampu un viena fotona skaitīšanas (SPD) detektoru (Latvijas Organiskās sintēzes institūts, Rīga, Latvija);
- fotoluminiscences kvantu iznākuma mērījumi veikti, lietojot integrējošās sfēras bloku *N-MO1* (papildpiederums *Edinburgh Instruments* fotoluminiscences spektrometram, lietojot tiešās ierosmes metodi), un ierosināšanas-emisijas kartes konstruētas, izmantojot fotoluminiscences spektrometru *Edinburgh Instruments FLS1000*, kas aprīkots ar ozonu ģenerējoša nepārtraukta starojuma CW 450 W ksenona lampu un *High Speed Red Detector* fotoelektronu pavairotāju (Latvijas Universitātes Cietvielu fizikas institūts, Rīga, Latvija).

8. Kristālisko struktūru noteikšanai no pulvera datiem, kristalizācijas produktu kristāliskā režģa parametru noteikšanai un Rietvelda optimizācijai izmantotas datorprogrammas *Topas5* un *Expo2014*, monokristālu rentgendifrakcijas datu integrēšanai izmantota datorprogramma *CrysAlisPro*, struktūras risināšanai un precizēšanai izmantotas datorprogrammas *JANA2006* un *Olex2*, periodiskiem DFT-D aprēķiniem izmantota datorprogrammas *Quantum ESPRESSO* un *CASTEP*, starpmolekulāro mijiedarbību un kristālisko struktūru raksturošanai *CrystalExplorer*, bet molekulu gāzes fāzes aprēķiniem *Gaussian09*.

3. REZULTĀTI UN TO IZVĒRTĒJUMS

3.1. Divkomponentu sistēmas ksantons – tioksantons (1) cieto šķīdumu veidošanās^A

Pētot cieto šķīdumu veidošanos starp strukturāli līdzīgām organiskajām molekulām, kā pirmā izvēlēta sistēma, kas satur divas modeļvielas – ksantonu un tioksantonu. Viens no veidiem, kā izpētīt vai cietais šķīdums spēj veidoties pētāmajā sistēmā, ir izveidot attiecīgās divkomponentu sistēmas kušanas fāžu diagrammu. Šajā gadījumā bināras sistēmas kušanas fāžu diagramma tika konstruēta, lai noskaidrotu, cik labi abas, ļoti līdzīgas molekulas tiek izšķirtas. Tika noskaidrots, ka starp ksantonu un tioksantonu neveidojas cietais šķīdums ar neierobežotu komponentu šķīdību, bet gan divi cietie šķīdumi ar ierobežotu komponentu šķīdību, t. i., tuvu tīram ksantona un tioksantona reģionam (sk. 3.1. att.). Tas norāda to, ka abas stipri līdzīgās molekulas kristāliskajā struktūrā pakojas atšķirīgi. Kā var redzēt pēc fāžu diagrammas, ksantons iešķīst tioksantonā, veidojot cieto šķīdumu (α) plašā komponentu sastāva diapazonā. Kristalizējot tioksantona – ksantona maisījumus ar ksantona saturu $>0 - 80$ mol%, tiek iegūts vienfāzes produkts.



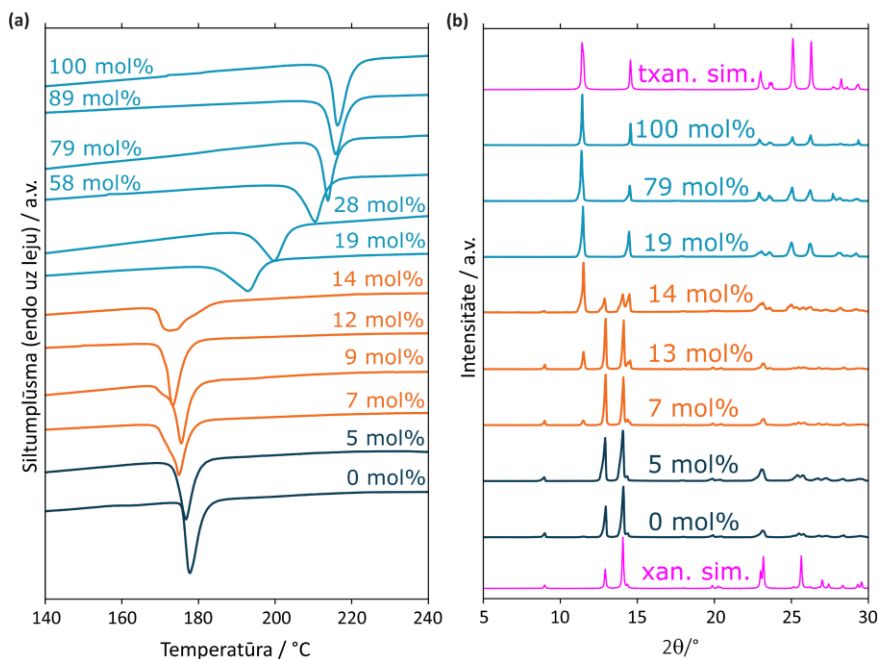
3.1. att. Binārās sistēmas ksantons – tioksantons kušanas fāžu diagramma. Cieto šķīdumu un atbilstošās vienkomponentu fāzes identiskā zilā tonī, fāžu maisījumi oranžā krāsā (pildīti marķieri – soliduss / eitektika; tukši marķieri – likviduss; līnijas attēlotas uzskatāmībai).

Pēc termiskās analīzes rezultātiem (sk. 3.2a. att., iegūtās derivatogrammas), novērojama kušanas endoterma, kas atbilst vienfāzes paraugam. Turklāt, arī skatoties pēc PXRD rezultātiem, minētajā komponentu sastāvā ($>0 - 80$ mol%, ksantona satura), difrakcijas ainas ir ļoti līdzīgas tīra tioksantona paraugam, un netiek novēroti refleksi, kas atbilstu tīra ksantona paraugam (sk. 3.2b. att.). Nelielas refleksu nobīdes un relatīvās intensitātes izmaiņas ir raksturīgas cietajiem šķīdumiem. Termiskās analīzes rezultāti liecina, ka ksantonā var izšķīdināt nelielu tioksantona daudzumu, t. i., šai binārajai sistēmai pastāv otrs cietais šķīdums (β). Piemēram, maisījums, kas satur 5 mol%

^ASaršūns, K., Bērziņš, A., Rekis, T. Solid solutions in xanthone – thioxanthone binary system: how well are similar molecules discriminated in the solid state? *Crystal Growth & Design*, 2020, 20(12), 7997–8004.

tioksantona, kŭst parādot vienu endotermisku signālu (sk. 3.2a. att.) un satur tikai ksantonam raksturīgos difrakcijas refleksus (sk. 3.2b. att.).

Skatoties pēc fāžu diagrammas, ir novērojams salīdzinoši šaurs divfāžu apgabals, kurā atrodas abu komponentu ierobežota sastāva cieto šķīdumu α un β fizikālie maisījumi. Tas ir saistīts ar papildu endotermisko signālu derivatogrammās (3.2a. att., iekrāsotas oranžā krāsā), kas norāda uz eitektisko kušanu. Šajā gadījumā, eitektisko kušanu var novērot kā mazus, bet izteiktus plecus ar kušanas temperatūru ap 169 K (sk. 3.2a. att.). Papildus tam, divu fāžu maisījumu var novērot arī PXRD ainās (sk. 3.2b. att., iekrāsotas oranžā krāsā).

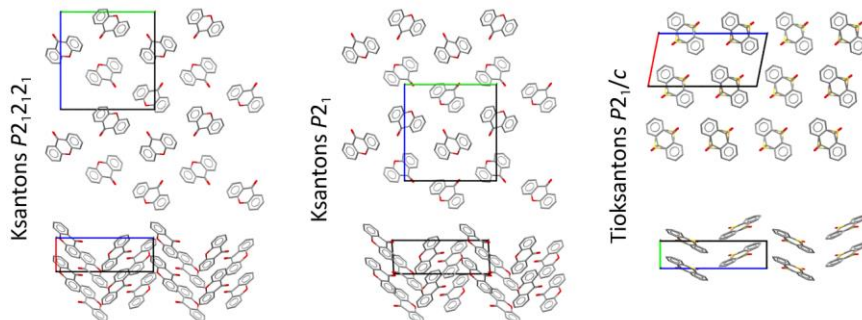


3.2. att. Derivatogrammas (a) un PXRD ainās (b) dažādiem binārās sistēmas ksantons – tioksantons sastāviem. Krāsu apzīmējums ir identisks tam, kas izmantots 3.1. attēlā, no kristāla struktūrām simulētas difrakcijas ainās – purpursarkanā krāsā (sarindotas atkarībā no iesvērtā tioksantona satura).

Šaurs divfāžu apgabals norāda, ka abas molekulas kristāliskajā struktūrā ir diezgan slikti izšķiramas. Komponentu sastāva diapazonos $>0 - 7$ mol% un $20 - <100$ mol% (tioksantons) abas molekulas iekļaujas vienā fāzē, nevis veido atsevišķu ksantona un tioksantona fāžu fizikālu maisījumu. Šķīšanas diapazona atšķirības starp cietajiem šķīdumiem α un β var izskaidrot ar dažādajiem atomu izmēriem – S un O. Cietā šķīdumā α , acīmredzot, ir daudz vairāk iespējams aizstāt tioksantona molekulas ar ksantona molekulām, jo O atoms ir ievērojami mazāks par S atomu, savukārt, cietajam šķīdumam β arvien pieaugošā ksantona molekulu daļa ir jāaizstāj ar relatīvi lielāka S atomu saturošām tioksantona molekulām, lai paplašinātu sastāva diapazonu. Novērotā atšķirība starp cietajiem šķīdumiem liecina, ka, lai gan abas pētītās molekulas ir ļoti līdzīgas un cietajam šķīdumam atbilst liels koncentrāciju diapazons, tomēr dažos ierobežotos sastāvos molekulas pakojas atšķirīgi un ir grūti izšķiramas.

Par ksantona kristālisko struktūru ziņots daudzos pētījumos, kur galvenokārt ir pierādīts, ka šī viela kristalizējas ortorombiskajā telpiskajā grupā $P2_12_12_1$. Šajā pētījumā

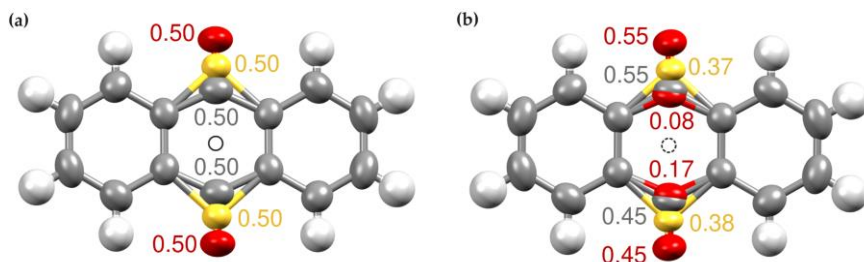
izmantotā tīra ksantona PXRD aina atbilst $P2_12_12_1$ polimorfam. Abi ksantona polimorfi ir ļoti līdzīgi (sk. 3.3. att.), $P2_12_12_1$ polimorfs⁴² kristalizējas ar vienu molekulu asimetriskā vienībā ($Z' = 1$). Otrā, nesēn atklāto polimorfu⁴³, var uzskatīt par pirmā polimorfa monoklīno deformāciju ($\beta \approx 93^\circ$). Tā aprakstīta $P2_12_12_1$ telpiskās grupas apakšgrupā, proti, $P2_1$, un atšķiras ar to, ka tā satur divas molekulas asimetriskajā vienībā ($Z' = 2$), lai kompensētu otrās kārtas vītnes (skrūves) asu zudumu.



3.3. att. Kristālisko struktūru attēlojums divām zināmām ksantona (pa kreisi un pa vidu)^{42,43} polimorfajām formām un tioksantonam (pa labi).

Tioksantona struktūra atrisināta un precizēta monoklīnajā $P2_1/c$ telpiskajā grupā. Šī struktūra nav sakārtota un tādējādi tiek izveidots statistiskais (pseido)inversijas centrs (sk. 3.4a. att.). Savukārt, cietā šķīduma kristālisko struktūru labāk apraksta $P2_1$ telpiskās grupas simetrijas operācijas. Neskatoties uz to, izmantoti simetrijas ierobežojumi atomu pozīcijām un anizotropās nobīdes parametri, kas atbilst $P2_1/c$ telpiskajai grupai. Tomēr, aizņemības faktori komponentiem, kas savstarpēji ir inversi saistīti un nesakārtoti (S un O atomi), tika noteikti, taču faktiski pastāv novirze no ideālas 0,5:0,5 attiecības un līdz ar to no $P2_1/c$ simetrijas. Īpaši attiecībā uz mazāko cietā šķīduma komponentu – ksantona molekulu (sk. 3.4b. att.). Atrisinot ksantona nesakārtotā komponenta – skābekļa atoma aizņemības faktorus, kas ir attiecīgi 0,08 un 0,17, un atbilst 1:2 nevis 1:1 attiecībai, rezultāts ir pretstatā tam, kāda simetrija tiek paredzēta, izvēloties $P2_1/c$ telpisko grupu.

Neskatoties uz ksantona un tioksantona molekulu strukturālo līdzību, kristāliskā stāvoklī tie pakojas atšķirīgi, kas ir saskaņā ar iegūto fāžu diagrammu. Ja abu komponentu struktūras būtu izostrukturālas, veidotos neierobežotas šķīdības cietais šķīdums.



3.4. att. Molekulārā izvietoējuma attēlojums tīra tioksantona (a) un sistēmas tioksantons – ksantons [75 : 25 mol%] cietā šķīduma (b) kristāliskajai struktūrai (ar atvērtu apli apzīmēts statistiskais (pseido)inversijas centrs).

Tioksantona un cietā šķīduma (75 mol% tioksantona) kristāliskās struktūras dati norādīti 3.1. tabulā.

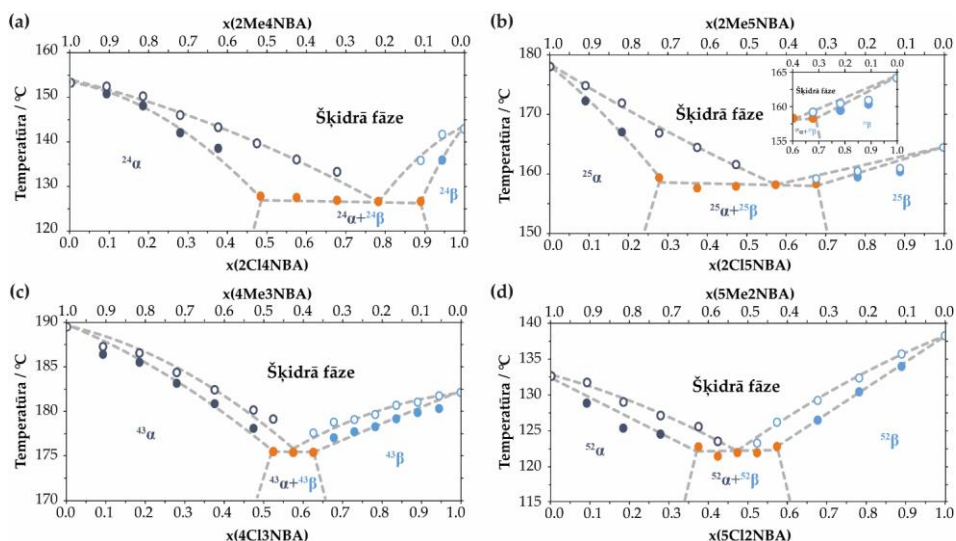
3.1. tabula.

Struktūras risinājuma kristalogrāfiskā informācija (integrētie refleksi: [$F_{hkl}^2 > 3\sigma(F_{hkl}^2)$])

Kristāls	Tioksantons	Tioksantons : Ksantons [75 : 25 mol%]
Kristalogrāfiskie dati		
T / K	301	301
Formula	$C_{13}H_8SO$	$0,75 C_{13}H_8SO \cdot 0,25 C_{13}H_8O_2$
Molmasa / $g \text{ mol}^{-1}$	212,3	208,2
Singonija	Monoklīnā	Monoklīnā
Telpiskā grupa	$P2_1/c$	$P2_1$
$a / \text{Å}$	7,8388(7)	7,8269(4)
$b / \text{Å}$	3,9891(2)	3,9933(2)
$c / \text{Å}$	15,8019(11)	15,7726(7)
$\beta / ^\circ$	101,199(7)	101,525(4)
$V / \text{Å}^3$	484,71(6)	483,02(4)
Z, Z'	2, 0,5	2, 1
$F(000)$	220	217
$\rho_{apr.} / g \text{ cm}^{-3}$	1,4544	1,4316
μ / mm^{-1}	2,661	2,183
Nomērītie refleksi	2455	1907
$[\sin(\theta)/\lambda]_{max} / \text{Å}^{-1}$	0,63	0,63
Unikālie refleksi	1818	1755
Integrētie refleksi	1219	939
$R_{int.}$	0,0294	0,0193
Risinājums		
Risinājuma metode	Pilnās matricas mazāko kvadrātu no F_{hkl}	
Parametru skaits	83	89
R_1 (integrētie)	0,0413	0,0379
wR (visi)	0,0513	0,0550

3.2. Dažādu aizvietotu nitrobenzoscābju (2) divkomponentu sistēmu cieto šķīdumu veidošanās^B

Tika pētīta cieto šķīdumu veidošanās starp uzbūves ziņā līdzīgām modeļvielām – nitrobenzoscābes atvasinājumiem, kas atšķiras tikai pēc aizvietotāja (metilgrupa, hidroksilgrupa vai hlora atoms) un tā novietojuma molekulārajā struktūrā. Izvēlēto savienojumu spēja aizvietot vienam otru, t. i., spēja veidot cieto šķīdumu, pētīta visās iespējamās 12 binārajās sistēmās, pa 3 katram nitrobenzoscābes izomēram. Bināriem maisījumiem, kas satur izvēlētos savienojumus dažādos sastāvos, veikta kristalizācija, un tālāk veikta fāžu identifikācija ar PXRD metodi, kā arī divkomponentu fāžu diagrammas konstruēšana pēc DSC analīzes datiem (sk. 3.5. att.). Papildus tam veikta kristālisko struktūru analīze un kvantu ķīmijas aprēķini, lai racionalizētu un spētu rast risinājumu cieto šķīdumu veidošanās prognozēšanai attiecīgajās kristāliskajās struktūrās.

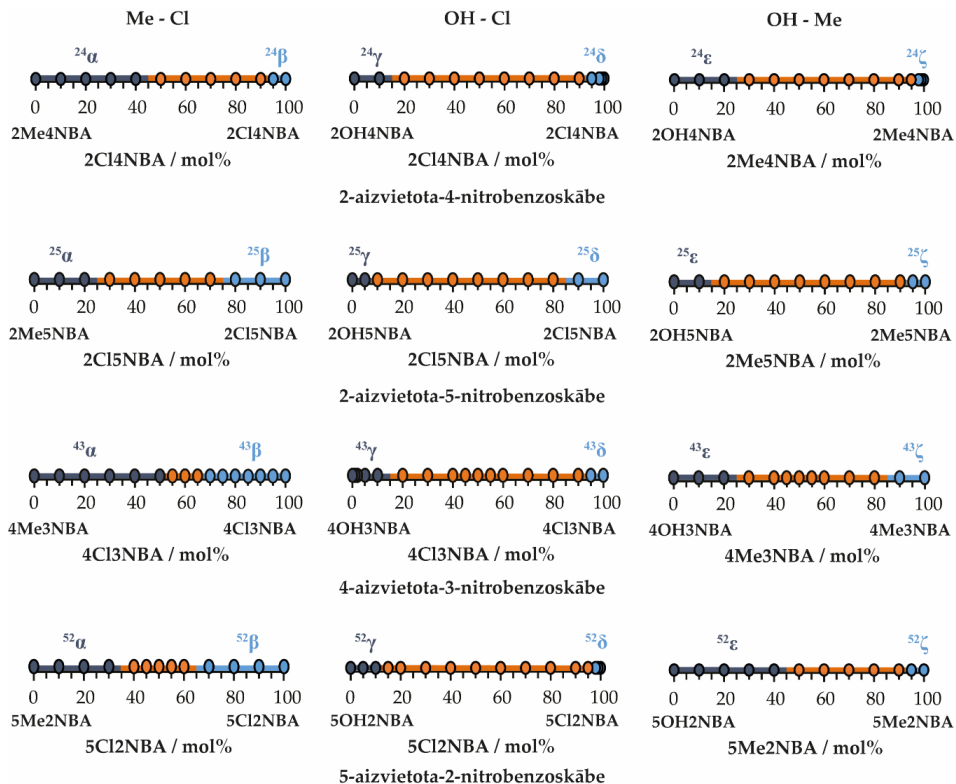


3.5. att. Bināru sistēmu kušanas fāžu diagrammas: 2Me4NBA – 2Cl4NBA (a), 2Me5NBA – 2Cl5NBA (b), 4Me3NBA – 4Cl3NBA (c) un 5Me2NBA – 5Cl2NBA (d). Cietie šķīdumi un atbilstošās vienkomponentu fāzes identiskā zilā tonī, fāžu maisījumi oranžā krāsā (pildīti marķieri – soliduss / eitektika; tukši marķieri – likviduss; līnijas attēlotas uzskatāmībai).

Nevienā no šīm binārajām sistēmām neveidojas cietais šķīdums ar pilnīgu komponentu šķīdību, bet visos gadījumos veidojas divi dažādi cietie šķīdumi (t. i., cietais šķīdums ar daļēju komponentu šķīdību), kas ir tuvu tīru komponentu apgabalam, skatīt 3.5. attēlu. Noskaidrots, ka zināmā mērā visas metilnitrobenzoscābes spēj iešķīst hlornitrobenzoscābes kristāliskajā struktūrā un otrādi. Iegūtie cietie šķīdumi apzīmēti kā α (metilnitrobenzoscābe iešķīdusi hlornitrobenzoscābes kristāliskajā struktūrā) un β (hlornitrobenzoscābe iešķīdusi metilnitrobenzoscābes kristāliskajā struktūrā), indeksi norāda metil / hlora un nitrogrupas novietojumu. Visās fāžu diagrammās ir arī salīdzinoši šaurs divfāžu apgabals, kurā atrodas abi cieto šķīdumu fizikāli maisījumi ar ierobežotu

^BSaršūns, K., Kons, A., Rekis, T., Bērziņš, A. Experimental and computational study of solid solution formed between substituted nitrobenzoic acids. *Crystal Growth & Design*, **2023**, 23(9), 6609–6622.

sastāvu. Tas ir tāpēc, ka aizstātās funkcionālās grupas nav identiska izmēra un neveido identiskas starpmolekulārās mijiedarbības, kā rezultātā šie savienojumi kristāliskajā struktūrā pakojas atšķirīgi un neļauj pilnībā aizstāt molekulas šajās kristāliskajās struktūrās. 3.6. attēlā apkopota informācija par cieto šķīdumu spēju veidoties iepriekš analizētajām metilnitrobenzoscābju un hlornitrobenzoscābju binārajām sistēmām, kā arī pārējās analizētajās binārajās sistēmās, kas satur hidroksil / hlornitrobenzoscābes un hidroksil / metilnitrobenzoscābes.



3.6. att. Fāzes, kas iegūtas dažādos sastāvos veicot aizvietotu nitrobenzoscābju bināro sistēmu maisījumu kristalizācijas pētījumus (krāsu apzīmējums ir identisks tam, kas izmantots 3.5. attēlā).

Rezultāti šajās papildu binārajās sistēmās apstiprina, ka sastāva diapazons, kurā var iegūt cietos šķīdumus, ir atšķirīgs katrā nitrobenzoscābes izomēru pāri, ko izraisa dažādās kristāliskās struktūras. Redzams, ka kristalizējoties sastāviem, kas satur galvenokārt vienu no komponentiem, visās pētītajās binārajās sistēmās tika iegūts cietais šķīdums, kā arī fāžu diagrammās vienmēr novērojams divfāžu apgabals, kas apstiprina šo savienojumu ierobežotu šķīdību savā starpā. Pārējie iegūtie cietie šķīdumi apzīmēti kā ϵ (hidroksilnitrobenzoscābe iešķīdusi metilnitrobenzoscābes kristāliskajā struktūrā), ζ (metilnitrobenzoscābe iešķīdusi hidroksilnitrobenzoscābes kristāliskajā struktūrā), γ (hidroksilnitrobenzoscābe iešķīdusi hlornitrobenzoscābes kristāliskajā struktūrā), un δ (hlornitrobenzoscābe iešķīdusi hidroksilnitrobenzoscābes kristāliskajā struktūrā), indeksi norāda metil / hlora / hidroksil un nitrogrupas novietojumu. Tomēr pēc 3.6. attēla, var spriest, ka ne visas funkcionālās grupas var vienlīdz viegli tikt nomainītas kristāliskajā struktūrā. Iespējama ir tikai hidroksilgrupas saturošu molekulu aizstāšana ar metilgrupu

saturošām molekulām, ciktāl tas ir novērots hloratoma un metilgrupas aizvietošanai, jo metilnitrobenzoscābes šķīdība hidroksinitrobenzoscābē ir no 10 līdz 40 mol%. Visos pārējos trīs aplūkotajos aizvietošanas scenārijos (metilgrupu saturošu molekulu aizstāšana ar hidroksilgrupu saturošām molekulām, hlora atomu saturošas molekulas ar hidroksilgrupu saturošām molekulām vai hidroksilgrupu saturošas molekulas ar hlora atomu saturošām molekulām) šķīdība var tikt sasniegta tikai līdz 10 mol% vai pat 5 mol%. Funkcionālo grupu un to īpašību salīdzinājums liecina, ka tas nav pārsteidzoši, jo hidroksilgrupu un metilgrupu, un hlora atomu un hidroksilgrupu aizstāšana ir saistīta ar lielākām molekulu izmēra izmaiņām, kā arī lielākām atšķirībām molekulu veidotajās starpmolekulārajās mijiedarbībās, salīdzinot ar izmaiņām, kas ieviestas, aizstājot metilgrupu un hlora atomu. Tāpēc paredzams, ka molekulas, kurās šādas funkcionālās grupas ir aizstātas, šķīdība kristāliskajā struktūrā būs zemāka. Lai gan ir nedaudz pārsteidzoši, ka metilgrupu saturošu molekulu šķīdība hidroksilgrupu saturošās molekulās ir diezgan augsta visos izomēros, tas varētu būt tāpēc, ka metilgrupa var darboties kā vāju ūdeņraža saišu donors, un tas varētu ļaut izvairīties no straujas enerģijas palielināšanās kristāliskajā struktūrā, aizstājot šīs funkcionālās grupas.

Papildus eksperimentālajiem pētījumiem, pētītas kristāliskās struktūras, tādējādi mēģinot noskaidrot, vai kristalogrāfiskā analīze un ar molekulu nomaiņu saistītās enerģijas izmaiņu analīze varētu tikt izmantota, lai prognozētu cietā šķīduma veidošanās spēju. Analizēta starpmolekulāro mijiedarbību enerģija eksperimentālajās kristāliskajās struktūrās un struktūrās, kas modelē cieto šķīdumu (*Aizvietota*) un izostrukturālo fāzi ar pilnīgi visu molekulu nomaiņu (*Izostrukturāla*), skatīt 3.2. tabulu.

3.2. tabula.

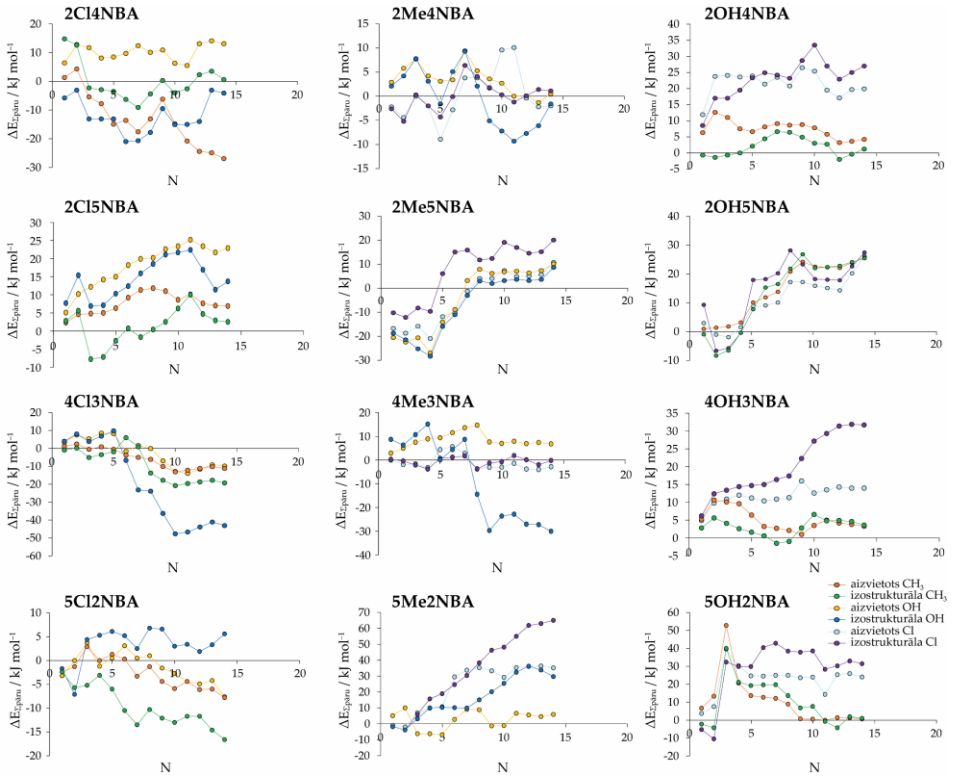
Starpmolekulāro mijiedarbību enerģijas summas (rēķināta programmā *CrystalExplorer*) izmaiņas, aizstājot funkcionālo grupu tuvākajām molekulām (3,80 Å) un molekulu pāriem, kuru atomi atrodas 15 Å rādiusā no centrālās molekulas

Struktūra	2OH4NBA		2Cl4NBA		2Me4NBA	
	-Cl	-CH ₃	-OH	-CH ₃	-OH	-Cl
<i>Izmaiņas E_{Starpm.} tuvākajām molekulām / kJ mol⁻¹</i>						
<i>Aizvietota</i>	+31,4	+16,9	+6,2	+1,9	-2,7	-3,5
<i>Izostrukturāla</i>	+18,3	+2,1	+7,2	+4,3	+12,9	+10,6
<i>Izmaiņas E_{Starpm.} molekulu pāriem 15 Å rādiusā ap centrālo molekulu / kJ mol⁻¹</i>						
<i>Aizvietota</i>	+11,4	+2,9	+4,6	-5,0	+0,9	-0,9
<i>Izostrukturāla</i>	+15,1	+0,9	+0,5	-7,6	-0,4	+0,6
Struktūra	2OH5NBA		2Cl5NBA		2Me5NBA	
	-Cl	-CH ₃	-OH	-CH ₃	-OH	-Cl
<i>Izmaiņas E_{Starpm.} tuvākajām molekulām / kJ mol⁻¹</i>						
<i>Aizvietota</i>	+9,4	+11,0	+8,5	+1,1	+15,4	+12,0
<i>Izostrukturāla</i>	+5,4	+9,1	+11,3	+3,6	+14,4	+17,8
<i>Izmaiņas E_{Starpm.} molekulu pāriem 15 Å rādiusā ap centrālo molekulu / kJ mol⁻¹</i>						
<i>Aizvietota</i>	+12,4	+11,4	+8,8	-2,1	+7,9	+7,6
<i>Izostrukturāla</i>	+13,7	+10,9	+5,3	-2,2	+8,2	+13,0

3.2. tabula. (Turpinājums)

Struktūra	4OH3NBA		4Cl3NBA		4Me3NBA	
	-Cl	-CH ₃	-OH	-CH ₃	-OH	-Cl
	<i>Izmaiņas $E_{Starpm.}$ tuvākajām molekulām / kJ mol⁻¹</i>					
<i>Aizvietota</i>	+14,8	+9,4	-10,0	-9,2	+6,4	+6,1
<i>Izostrukturāla</i>	+18,6	+6,9	-12,8	-19,5	+6,6	+4,4
	<i>Izmaiņas $E_{Starpm.}$ molekulu pāriem 15 Å rādiusā ap centrālo molekulu / kJ mol⁻¹</i>					
<i>Aizvietota</i>	+1,3	-1,1	-6,1	-4,4	-1,3	+3,4
<i>Izostrukturāla</i>	+1,8	-0,7	-23,5	-6,1	-11,8	+6,4
Struktūra	5OH2NBA		5Cl2NBA		5Me2NBA	
	-Cl	-CH ₃	-OH	-CH ₃	-OH	-Cl
	<i>Izmaiņas $E_{Starpm.}$ tuvākajām molekulām / kJ mol⁻¹</i>					
<i>Aizvietota</i>	+2,6	+0,6	-6,1	-4,4	+6,0	+23,9
<i>Izostrukturāla</i>	+0,5	+4,7	-25,6	-14,9	+3,2	+15,7
	<i>Izmaiņas $E_{Starpm.}$ molekulu pāriem 15 Å rādiusā ap centrālo molekulu / kJ mol⁻¹</i>					
<i>Aizvietota</i>	+14,9	+3,0	-5,0	-4,8	+8,2	+19,0
<i>Izostrukturāla</i>	+20,2	+1,9	-21,1	-7,6	-6,7	+34,4

Pirmkārt, novērotās izmaiņas *aizvietotajās* un *izostrukturālajās* struktūrās skaidri parāda, ka katrā no kristāliem starpmolekulāro mijiedarbību un funkcionālās grupas aizvietošanas iespaidā radītās izmaiņas ir atšķirīgas. Neskatoties uz to, 3.2. tabulā norādītās mijiedarbības enerģijas izmaiņas starp molekulām, kas atrodas blakus aizstātajai funkcionālajai grupai, nevar būt tieši saistītas ar eksperimentāli noteikto šķīdības robežu attiecīgajā molekulu pāri, jo attiecīgi ir novērojami gadījumi, kad enerģija kļūst efektīvāka. Otrkārt, līdzīgs secinājums novērots arī tad, kad datorprogrammā *CrystalExplorer* aprēķināta molekulu pāru starpmolekulāro mijiedarbību enerģija tuvākajām molekulām 15 Å rādiusā no centrālās molekulas (*oriģinālajām* un *izostrukturālajām* struktūrām, ko var attiecināt kā kristāliskā režģa enerģijas aproksimāciju). Treškārt, papildu informācija par enerģijas starpībām iegūta, analizējot starpmolekulāro mijiedarbību enerģiju molekulu pāriem, ko veido molekulas, kuras atrodas 3,80 Å rādiusā no centrālās molekulas. Šo molekulu pāru kumulatīvās mijiedarbības enerģijas starpības diagrammas, palielinoties attālumam starp molekulārajiem centriem *aizvietotajās* un *izostrukturālajās* struktūrās un sākotnējā (*oriģinālā*) struktūrā, ir parādītas 3.7. attēlā.



3.7. att. Molekulu pāru kumulatīvās enerģijas izmaiņas, palielinoties attālumam starp centriem – aizvietotajām un izostrukturālajām struktūrām (N = molekulas numurs).

Kopumā var secināt, ka enerģija ir jāsālīdzina ar alternatīvajiem stāvokļiem, kas pieejami dotā sastāva sistēmai, un var būt nepieciešams novērtēt arī termisko un entropijas efektu. Tas labi redzams, salīdzinot enerģijas izmaiņas, kas saistītas ar izvēlēto funkcionālo grupu aizstāšanu visos izomēros, kā, piemēram, metilgrupas aizstāšanu ar hlora atomu, kas kristalizācijas eksperimentos ļāva iegūt cietos šķīdumus ar augstāko sasniegto šķīdību. Gandrīz visu aprēķinu rezultātā ir novērojams enerģijas pieaugums, lai gan, analizējot starpmolekulārās mijiedarbības šajās struktūrās, nevarēja konstatēt nevienu konkrētu cēloni, kas veicinātu enerģijas pieaugumu. Arī, palielinot aplūkojamo molekulu pāru skaitu, starpmolekulāro mijiedarbību enerģijai ir tendence konverģēt līdz rezultātam, kas atspoguļo kopējo enerģiju visiem molekulu pāriem, kuras atrodas 15 Å rādiusā no centrālās molekulas, kā tas parādīts 3.2. tabulā, lai gan dažām struktūrām, lai sasniegtu šo vērtību, kopsummā bija jāiekļauj lielāks molekulu skaits.

3.3. Divkomponentu sistēmas benperidols – droperidols (3) cieto šķīdumu veidošanās^C

Cieto šķīdumu veidošanās starp divām farmaceutiski aktīvām vielām – benperidolu un droperidolu, pētīta gan nesolvatētām, gan solvatētām šo abu savienojumu formām. Lai noskaidrotu vai cietais šķīdums var veidoties starp šīm divām vielām, veikta abu šo vielu maisījumu pārkristalizēšana dažādās vielu attiecībās. Kristalizācijas pētījumi veikti, izmainot apstākļus, lai iegūtu dažādas šo vielu cietfāzes – nesolvatētas (izvēlētos apstākļos benperidolam var iegūt polimorfus **^BI** vai **^BII** un droperidolam polimorfus **^DII**), dihidrātus, kā arī etanola, metanola un acetoniitrila solvātus.

Iegūtie kristalizācijas produkti, kas apkopoti 3.3. tabulā, raksturoti, izmantojot PXRD un DSC/TG analīzi. Kristalizācijas rezultātā vienmēr veidojās fāze vai fāzes ar vēlamu komponentu sastāvu: nesolvatēta fāze vai fāzes (**^BI**, **^BII** un **^DII**) iegūtas kā šķīdinātāju, izmantojot izopropanolu, dihidrāts vai dihidrāti (**^BDH** un **^DDH**) no šķīdinātāju maisījuma acetons/ūdens un attiecīgais solvāts vai solvāti no dažādiem organiskajiem šķīdinātājiem (**^BS_{EiOH}** un **^DS_{EiOH}** no etanola, **^BS_{MeOH}** un **^DS_{MeOH}** no metanola, **^BS_{ACN}** un **^DS_{ACN}** no acetoniitrila). Vairumā gadījumu droperidola un benperidola maisījuma kristalizācijā iegūta tikai viena fāze, kas nozīmē, ka izveidojas cietais šķīdums, kas satur abus komponentus attiecīgajā kristāliskajā struktūrā.

Rezultāti skaidri parāda, ka spēja aizstāt vienu molekulu ar otru ir ļoti atkarīga no kristāliskās struktūras, tostarp pat atšķirīgās spējas pielāgoties citām molekulām, izmantojot izostrukturālo solvātu sēriju **^DS_{EiOH}**, **^DS_{MeOH}** un **^DS_{ACN}**, kā arī **^BS_{EiOH}** un **^BS_{MeOH}**.

3.3. tabula.

**Kristāliskās fāzes, kas iegūtas benperidola un droperidola maisījuma kristalizācijā
vairākām izvēlētām molārām attiecībām***

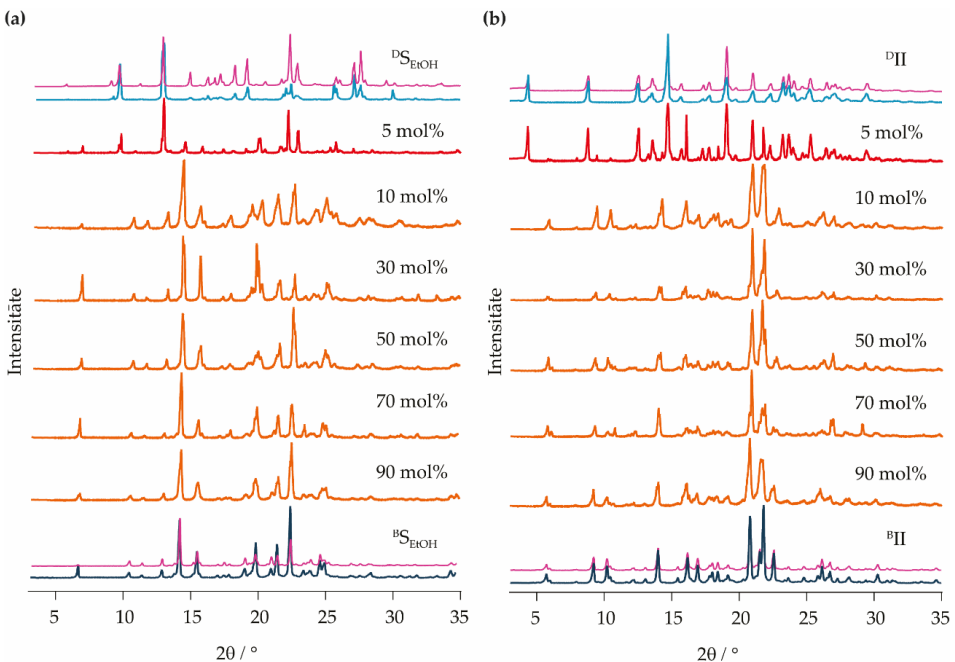
Benperidols / mol%	Iegūtā fāze				
	Nesolvatēta fāze	Etanola solvāts	Metanola solvāts	Acetonitrila solvāts	Dihidrāts
0	^DII	^DS_{EiOH}	^DS_{MeOH}	^DS_{ACN}	^DDH
5	^DII+SS^BII	^DS_{EiOH}+SS^BS_{EiOH}	SS^DS_{MeOH}	SS^DS_{ACN}	SS^DDH
10	SS^BII	SS^BS_{EiOH}	SS^DS_{MeOH}	SS^DS_{ACN}	SS^DDH
20	SS^BII	SS^BS_{EiOH}	SS^DS_{MeOH}+SS^BS_{MeOH}	SS^DS_{ACN}	SS^DDH+SS^BDH
30	SS^BII	SS^BS_{EiOH}	SS^DS_{MeOH}+SS^BS_{MeOH}	SS^DS_{ACN}+SS^BS_{ACN}	SS^DDH+SS^BDH
40	SS^BII	SS^BS_{EiOH}	SS^DS_{MeOH}+SS^BS_{MeOH}	SS^DS_{ACN}+SS^BS_{ACN}	SS^DDH+SS^BDH
50	SS^BII	SS^BS_{EiOH}	SS^BS_{MeOH}	SS^DS_{ACN}+SS^BS_{ACN}	SS^DDH+SS^BDH
60	SS^BII	SS^BS_{EiOH}	SS^BS_{MeOH}	SS^DS_{ACN}+SS^BS_{ACN}	SS^DDH+SS^BDH
70	SS^BII	SS^BS_{EiOH}	SS^BS_{MeOH}	SS^DS_{ACN}+SS^BS_{ACN}	SS^BDH
80	SS^BII	SS^BS_{EiOH}	SS^BS_{MeOH}	SS^BS_{ACN}	SS^BDH

^CSaršūns, K., Bērziņš, A. Experimental and computational investigation of benperidol and droperidol solid solutions in different crystal structures. *Crystal Growth & Design*, **2023**, 23(2), 1133–1144.

90	SS^BII	SS^BS_{EIOH}	SS^BS_{MeOH}	SS^BS_{ACN}	SS^BDH
100	B^I	B^S_{EIOH}	B^S_{MeOH}	B^S_{ACN}	B^DDH

* – **SS** apzīmē cieto šķīdumu attiecīgajai kristāliskajai struktūrai. Tīrās fāzes treknrakstā, bet fāžu maisījumi slīprakstā.

Tas parādās gan kā atšķirīga robeža, līdz kurai ir iespējama molekulu aizstāšana, gan pat pilnīgi atšķirīga vienas molekulas spēja aizstāt otru. Piemēram, nesolvatētajā fāzē **D^{II}** un etanola solvatā **D^S_{EIOH}** netika konstatēta benperidola spēja aizstāt droperidolu, savukārt benperidola aizstāšana ar droperidolu etanola solvatā **B^S_{EIOH}** un nesolvatētajā fāzē **B^{II}** panāka pat līdz komponentu sastāvam, kas bija tuvu pilnīgai aizvietošanai, kad iegūti cietie šķīdumi, kuros 90 mol% benperidola molekulu aizstātas ar otru komponentu. Iegūtās PXRD ainas skatīt 3.8. attēlā. Šie cietie šķīdumi ir attiecīgi apzīmēti kā **SS^BS_{EIOH}** un **SS^BII**.

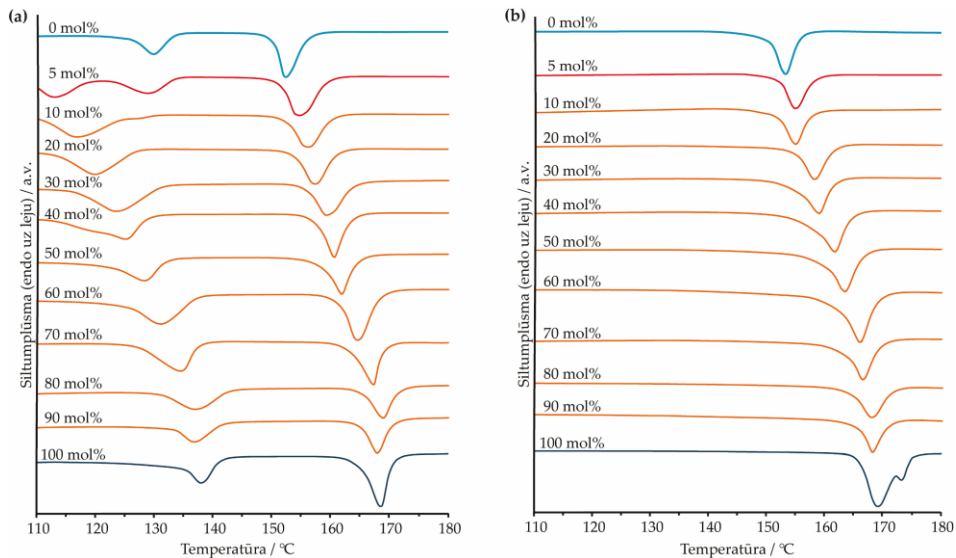


3.8. att. Kristalizācijas produktu PXRD ainas, kristalizējot benperidola un droperidola vielu maisījumus dažādos komponentu sastāvos no etanola (a), iegūstot etanola solvatā fāzi / fāzes, un izopropanola (b), iegūstot nesolvatētu fāzi / fāzes. Cietie šķīdumi oranžā krāsā un atbilstošās vienkomentu fāzes zilā tonī, fāžu maisījumi sarkanā krāsā, un no kristāla struktūrām simulētas difrakcijas ainas – purpursarkanā krāsā (sarindotas atkarībā no iesvērtā benperidola satura).

Papildus tam visi kristalizācijas produkti raksturoti, izmantojot DSC/TG analīzi, un solvatētās fāzes desolvatācijas produktu fāžu identifikācijai izmantoja PXRD metodi, bet fāžu termiskajai raksturošanai DSC/TG analīzi.

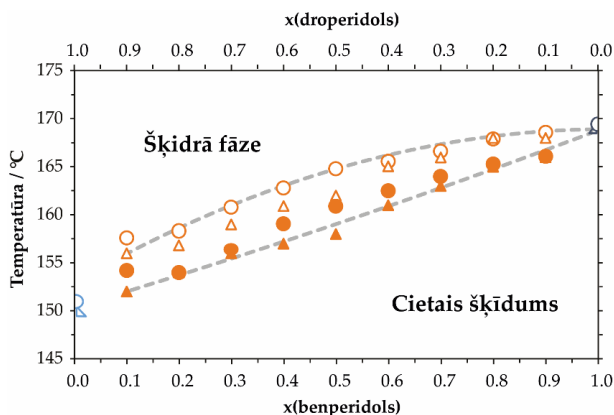
Visu nesolvatēto cieto šķīdumu **SS^BII** paraugu derivatogrammās kušanas endoterma būtībā atbilst vienfāzes paraugam (sk. 3.9b. att.). Praktiski visa komponentu sastāva diapazonā no 90 mol% līdz 10 mol% benperidola kušanas un maksimālā temperatūra

pazeminās monotoni, palielinoties droperidola saturam cietajā šķīdumā, kas atbilst vienas fāzes cietajam šķīdumam. To kušanas temperatūra ir starp benperidola polimorfa B_{II} ($T_{kuš.} = 165\text{ °C}$) un droperidola polimorfa D_{II} ($T_{kuš.} = 151\text{ °C}$) kušanas temperatūru. Pēc šiem datiem konstruēto fāžu diagrammu skatīt 3.10. attēlā. Nobīde no iepriekš minētā novērota pie komponentu sastāva, kad benperidola saturs ir 5 mol%, jo paraugs satur cieto šķīdumu $SS^{B_{II}}$ un droperidola fāzi D_{II} .



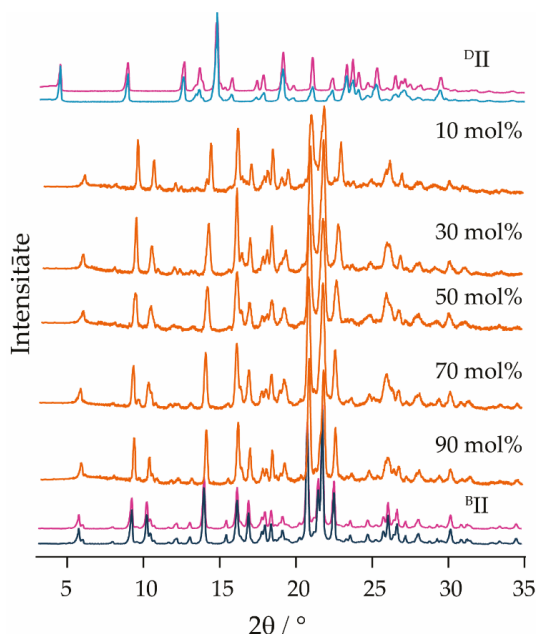
3.9. att. Derivatogrammas solvatētām cietajam šķīdumam $SS^{B_{EtOH}}$ (a), kas iegūts kristalizācijas rezultātā no etanola kopā ar tīru droperidola D_{EtOH} un benperidola etanola solvāta B_{EtOH} fāzi, un nesolvatētām cietajam šķīdumam $SS^{D_{II}}$ (b), kas iegūts kristalizācijas rezultātā no izopropanola kopā ar tīru droperidola D_{II} un benperidola B_{II} fāzi. Krāsu apzīmējums ir identisks tam, kas izmantots 3.8. attēlā (sarindotas atkarībā no iesvērtā benperidola satura).

Solvatētā cietā šķīduma $SS^{B_{EtOH}}$ derivatogrammās (sk. 3.9a. att.) sākotnēji novērojama desolvatācijas temperatūra, no tīra benperidola līdz sastāvam, kas satur 10 mol% benperidola. Desolvatācijas temperatūra monotoni samazinās, palielinoties droperidola saturam cietajā šķīdumā, kas atbilst vienas fāzes cietajam šķīdumam. Turpretī, paraugam, kas satur 5 mol% benperidola, novērojami divi desolvatācijas maksimumi, kas liecina par divu solvatētu fāžu klātbūtni. Līdzīgi, monotona desolvatācijas temperatūras samazināšanās, palielinoties droperidola saturam cietajā šķīdumā, novērota $SS^{B_{MeOH}}$ solvatētajam cietajam šķīdumam, un šī tendence desolvatācijas temperatūrai samazināties, kad palielina aizstājēj komponenta saturu, novērojama citiem solvatētajiem cietajiem šķīdumiem. Turklāt, kušanas temperatūra iegūtajiem $SS^{B_{EtOH}}$ desolvatācijas produktiem un vairumā gadījumu arī no citiem solvatētajiem paraugiem, samazinās monotoni visa komponentu sastāva diapazonā, palielinot droperidola saturu attiecīgajā paraugā. Lai pilnībā izprastu šo sakarību, solvatētie paraugi iegūti kristalizācijas rezultātā, desolvatēti un pēc tam raksturoti.



3.10. att. Daļa no binārās sistēmas benperidols – droperidols kušanas fāžu diagrammas. Apaļie marķieri atbilst paraugu datiem, kas iegūti kristalizācijas rezultātā no izopropanola, trijstūra marķieri atbilst paraugiem, kas iegūti etanola solvāta desolvatācijas rezultātā, un ilustrē sakrītību ar kristalizācijā iegūto paraugu termiskajām īpašībām. Krāsu apzīmējums ir identisks tam, kas izmantots 3.8. un 3.9. attēlā (pildīti marķieri – soliduss; tukši marķieri – likviduss; līnijas attēlotas uzskatāmībai).

Karsējot kristalizācijas eksperimentos iegūtos solvatētos produktus, vienmēr, pirms fizikālas parauga kušanas izveidojas desolvatācijas produkts. Interesanti, ka desolvatācijas produkts nav atkarīgs no desolvatētā parauga fāžu sastāva. Vienīgā solvatētā cietā šķīduma SS^BSe_{IOH} , kas pastāv gandrīz visā komponentu sastāva diapazonā, desolvatācijas produkts vienmēr bija nesolvatēts cietais šķīdums SS^{BII} . Tas atbilst tam, ka tīra benperidola etanola solvāta $^BSe_{IOH}$ galvenais desolvatācijas produkts ir polimorfs BII . Turklāt nesolvatētais cietais šķīdums SS^{BII} iegūts kā vienīgais desolvatācijas produkts arī vairumā no gadījumiem, kad desolvatē pārējo sistēmu paraugus, kas iegūti no metanola, acetonitrila un acetona/ūdens, neatkarīgi no tā, vai paraugā bija cietais šķīdums ar benperidola solvāta struktūru, cietais šķīdums ar droperidola solvāta vai pat to maisījums. To apstiprināja gan desolvatēto paraugu PXRD ainas (sk. 3.11. att., dihidrāta desolvatācijas produktu PXRD ainas), gan to derivatogrammas, kurās kušanas endoterma atbilst viena komponenta fāzei ar kušanas un maksimālo temperatūru, kas ir identiska SS^{BII} komponentu sastāvam.



3.11. att. Dihidrātu paraugu, kas iegūti izmantojot atšķirīgu benperidola un droperidola attiecību kristalizācijas eksperimentos, desolvatācijas produktu PXRD ainas. Cietie šķīdumi oranžā krāsā, atbilstošās vienkomentu fāzes zilā krāsā, fāžu maisījumi sarkanā krāsā, no kristāla struktūrām simulētas difrakcijas ainas – purpursarkanā krāsā (sarindotas atkarībā no iesvērtā benperidola satura).

Ņemot vērā to, ka galvenā uzmanība pievērsta strukturālajiem un enerģētiskajiem aspektiem cieto šķīdumu veidošanā, aizvietojojam daļu no oriģinālajām kristāliskajām struktūrām ar otra komponenta molekulām. Starpmolekulāro mijiedarbību enerģija trim struktūru kopām (*oriģinālā*, *aizvietotā* un *izostrukturālā*) aprēķināta, izmantojot datorprogrammu *Quantum ESPRESSO*. Iegūtie rezultāti apkopoti 3.4. tabulā. Kopumā var secināt, ka vienas molekulas aizvietošana vienmēr ir saistīta ar enerģijas pieaugumu un vismazākā ir ^BII, ^BS_{MeOH}, un ^BS_{EiOH} gadījumā. Tomēr, pilnīgi aizvietojojam visas benperidola molekulas ar droperidola molekulām, tiek nodrošināta efektīvāka starpmolekulārā mijiedarbība lielākajā daļā struktūru ar vislielāko mijiedarbības enerģijas samazināšanos ^BS_{EiOH} gadījumā. Savukārt, tieši pretēji droperidola molekulas aizvietošana ar benperidola molekulām vienmēr noved pie mazāk efektīvām starpmolekulārām mijiedarbībām. Šie rezultāti apstiprina, ka starpmolekulāro mijiedarbību enerģija ir svarīgs faktors, lai noteiktu molekulu aizvietošanās spēju dažādās struktūrās un palīdzētu paredzēt cietā šķīduma eksistenci ^BS_{EiOH} struktūrā. Rezultāti neļauj paredzēt ^BII fāzes veidošanos un ^BS_{ACN} fāzes veidošanos salīdzinoši šaurā koncentrācijas diapazonā.

Starpmolekulāro mijiedarbību enerģija oriģinālajās benperidola un droperidola kristāliskajās struktūrās (kJ uz molu benperidola vai droperidola) un enerģiju izmaiņas, kad tiek aizstāta viena vai visas molekulas vienības elementāršūnā. Struktūrām ar $Z' > 1$ $E_{\text{Starpm.}}$ izmaiņas aizvietotajās struktūrās ir vidējā vērtība no struktūrām, kurās simetriski atšķirīgas molekulas aizvietotas

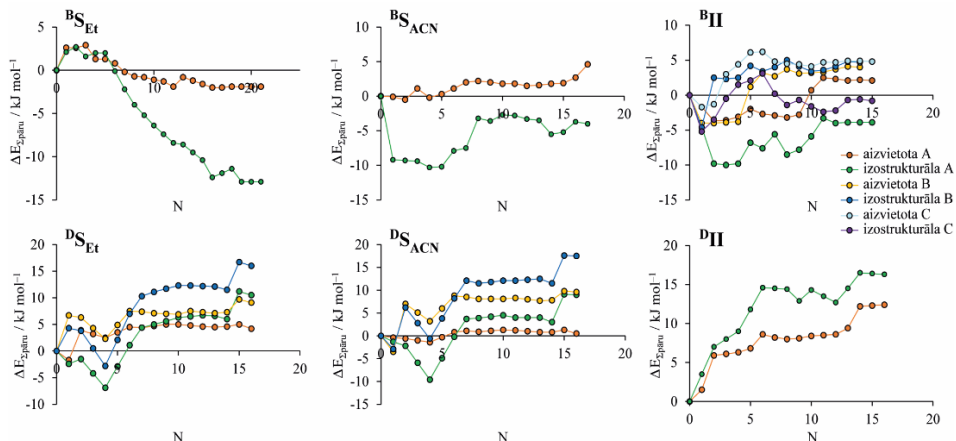
Struktūra	^B II	^B S _{EIOH}	^B S _{MeOH}	^B S _{ACN}	^B DH
<i>E_{Starpm.} benperidola struktūrās / kJ mol⁻¹</i>					
Oriģināla	-244,7	-331,6	-318,2	-288,4	-404,7
<i>Izmaiņas E_{Starpm.} aizvietojot ar droperidola molekulu / kJ mol⁻¹</i>					
Aizvietota	+2,9	+3,6	+3,0	+5,2	+7,8
Izostrukturāla	-0,7	-5,4	-1,8	-3,6	+5,4
Struktūra	^D II	^D S _{EIOH}	^D S _{MeOH}	^D S _{ACN}	^D DH
<i>E_{Starpm.} droperidola struktūrās / kJ mol⁻¹</i>					
Oriģināla	-237,3	-284,4	-281,0	-275,3	-403,5
<i>Izmaiņas E_{Starpm.} aizvietojot ar benperidola molekulu / kJ mol⁻¹</i>					
Aizvietota	+5,4	+5,5	+6,3	+4,4	+4,2
Izostrukturāla	+5,3	+7,4	+8,0	+7,6	+9,6

Lai identificētu to, kā molekulu aizvietošana ietekmē starpmolekulāro mijiedarbību enerģiju, papildus visām trim struktūru kopām izrēķināta pāru starpmolekulārās mijiedarbības enerģija tuvākajām molekulām, kas atrodas apkārt centrālajai molekulai, izmantojot datorprogrammu *CrystalExplorer*. Pirmkārt, novērtēta molekulu aizstāšanas ietekme uz ūdeņraža saišu mijiedarbības stiprumu, otrkārt, novērtēta molekulu aizstāšanas ietekme uz starpmolekulāro mijiedarbības enerģiju molekulu pāriem, kuri veido spēcīgākās dispersijas mijiedarbības (sk. 3.5. tabulu).

Relatīvā vidējā starpmolekulāro mijiedarbību enerģija (kJ mol⁻¹) attiecībā pret oriģinālo struktūru molekulu pāriem, kas veido spēcīgākās dispersijas mijiedarbības

Struktūra	^B II	^B S _{EIOH}	^B S _{MeOH}	^B S _{ACN}	^B DH
Aizvietota	+0,6	-0,7	+0,6	+0,4	+2,1
Izostrukturāla	-0,2	-1,0	-0,1	-0,6	+3,6
Struktūra	^D II	^D S _{EIOH}	^D S _{MeOH}	^D S _{ACN}	^D DH
Aizvietota	+1,5	+0,5	+0,8	+0,4	-0,1
Izostrukturāla	+2,6	+1,9	+1,8	+2,0	0,0

Visbeidzot, sniegts visaptverošāks skatījums uz enerģijas atšķirībām, analizējot starpmolekulāro mijiedarbību enerģiju visiem molekulu pāriem, ko veido molekulas, kuras atrodas 3,80 Å rādiusā no centrālās molekulas. Izmantojot šos rezultātus, aprēķināta molekulu pāru kumulatīvā mijiedarbība enerģija palielinoties distancē starp centroīdiem, un attēlojot to kā izmaiņu starpību *aizvietotajai* un *izostrukturālajai* struktūrai salīdzinājumā pret *oriģinālo* struktūru (sk. 3.12. att.).



3.12. att. Molekulu pāru kumulatīvās enerģijas izmaiņas, palielinoties attālumam starp centroīdiem – aizvietotajām un izostrukturālajām struktūrām (N = molekulas numurs).

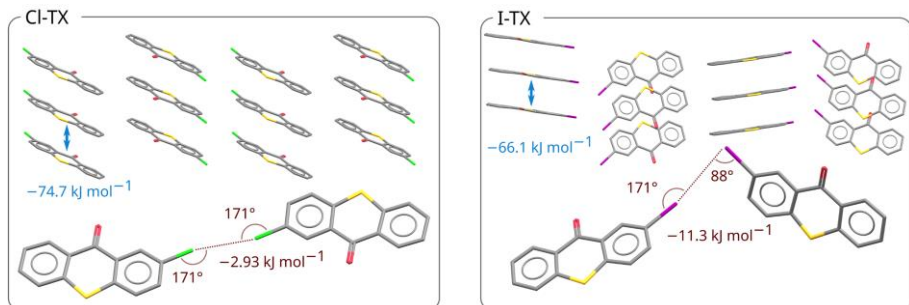
Ņemot vērā aplūkoto struktūru fāžu sastāva atšķirības, starpmolekulāro mijiedarbības enerģiju analīze liecina, ka šajā sistēmā cietie šķīdumi vieglāk veidojas vienkompontu fāzēs, jo eksperimentāli var iegūt cieto šķīdumu pilnā koncentrāciju diapazonā, ja molekulas aizstāšana saglabā tādu pašu starpmolekulāro mijiedarbību efektivitāti kā *oriģinālajā* struktūrā, savukārt, lai cietais šķīdums veidotos pilnā koncentrāciju diapazonā starp solvatētām fāzēm, ir nepieciešamas īpaši izdevīgas starpmolekulārās mijiedarbības, salīdzinot ar *oriģinālo* struktūru.

3.4. Dažādu tioksantona halogēnatvasinājumu (4) divkomponentu sistēmu cieto šķīdumu veidošanās^{D,E}

3.4.1. Divkomponentu sistēma, kura satur joda un hlora atvasinājumus^D

Salīdzinājumā ar savienojumiem no iepriekšējām nodaļām, tioksantona halogēnatvasinājumiem istabas temperatūrā ir novērojama luminiscences parādība. Tomēr, neraugoties uz šo molekulu līdzību, Cl-TX un I-TX molekulu pakojums atšķiras (sk. 3.13. att.)⁴¹.

^DSaršūns, K., Ķemere, M., Karziņš, A., Kļimenkovs, I., Bērziņš, A., Sarakovskis, A., Reķis, T. Fine-tuning solid state luminescence properties of organic crystals *via* solid solution formation: the example of 4-iodothioxanthone – 4-chlorothioxanthone system. *Crystal Growth & Design*, **2022**, 22(8), 4838–4844.

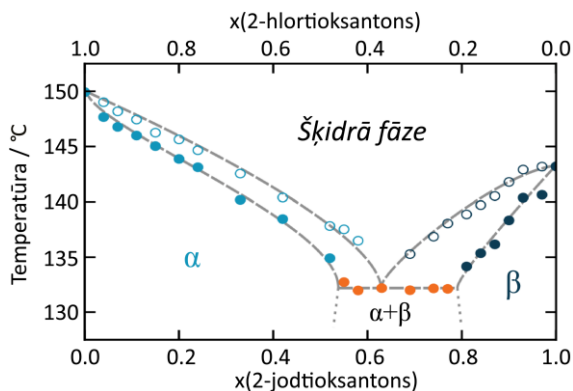


3.13. att. Molekulu pakojuma un ūdeņraža saišu attēlojums CI-TX (pa kreisi) un I-TX (pa labi) struktūrās.

Ņemot vērā, ka abas molekulas ir aromātiskas un planāras, starp molekulām pastāv $\pi \cdots \pi$ starpmolekulārā mijiedarbība. Tomēr ir svarīgi atzīmēt, ka abās struktūrās ir arī cita enerģētiski izdevīga starpmolekulārā mijiedarbība, proti, halogēnsaite. Taču tas bieži tiek ignorēts, analizējot molekulārā līmeņa faktorus, kas ir atbildīgi par luminiscences parādību.

Šī veida starpmolekulārā mijiedarbība ir ļoti specifiska un abos pakojumos⁴⁴ (sk. 3.13. att.) tiek novērota atšķirīga halogēn \cdots halogēn-saišu ģeometrija, kas atbilst efektīvas mijiedarbības kritērijiem. Papildus tam, starpmolekulāro mijiedarbību enerģija rēķināta starp abām halogēnsaišu veidojošajām molekulām, aprēķināta datorprogrammā *Gaussian09*, un attiecīgi tā ir $-2,93 \text{ kJ} \cdot \text{mol}^{-1}$ Cl \cdots Cl saišu pārim un $-11,3 \text{ kJ} \cdot \text{mol}^{-1}$ I \cdots I saišu pārim. Lai gan $\pi \cdots \pi$ starpmolekulārā mijiedarbība abos gadījumos ir ļoti efektīva, halogēnsaiti var uzskatīt par svarīgu ieguldījumu molekulu pakojuma stabilizācijā, īpaši I-TX.

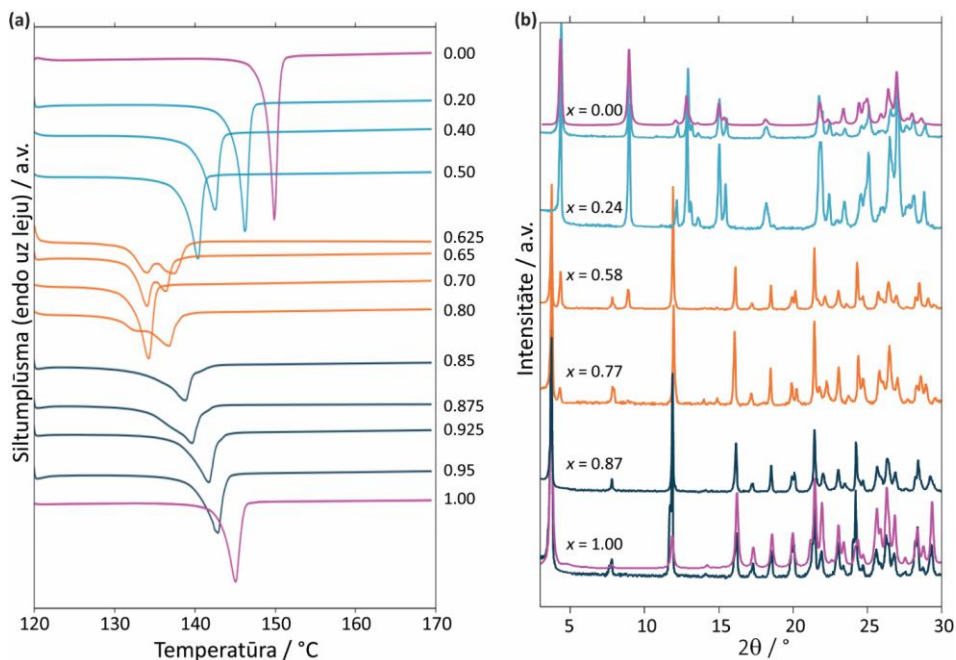
Šajā gadījumā, kušanas fāžu diagramma parāda, ka cietais šķīdums spēj veidoties starp šīm modeļvielām, t. i., veidojot divus cietos šķīdumus ar ierobežotu komponentu šķīdību, pamatojoties uz attiecīgo tīro vielu CI-TX un I-TX struktūrām (sk. 3.14. att.).



3.14. att. Binārās sistēmas CI-TX – I-TX kušanas fāžu diagramma. Cieto šķīdumu un atbilstošās vienkomponentu fāzes identiskā zilā tonī, fāžu maisījumi oranžā krāsā (pildīti marķieri – soliduss / eitektika; tukši marķieri – likviduss; līnijas attēlotas uzskatāmībai).

Cl-TX struktūrā var iešķīst līdz aptuveni 50 mol% I-TX (apzīmēts kā α cietais šķīdums), līdzīgi cietais šķīdums, kura pamatā ir I-TX struktūra, veidojas komponentu sastāvā līdz aptuveni 20 mol% Cl-TX (apzīmēts kā β cietais šķīdums). Atlikušajā sastāva diapazonā termodinamiski stabilākā fāze ir fizikāls maisījums, kas satur abus cietos šķīdumus – gan α , gan β , ar attiecīgajiem ierobežojošajiem sastāviem. Derivatogrammas, kas izmantotas fāžu diagrammas konstruēšanai, skatīt 3.15a. attēlu.

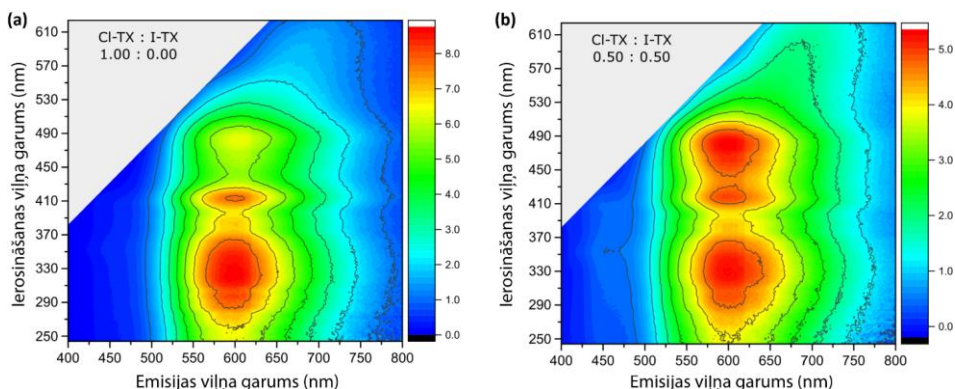
Kad tīra savienojuma kristāliskajā struktūrā ievieto pretējo komponentu, tas noved pie nesakārtotas fāzes veidošanās (proti, cietā šķīduma), un līdz ar to tiek izraisītas nelielas strukturālas izmaiņas, piemēram, kristāliskā režģa parametru novirzes. Šos efektus var redzēt pēc PXRD ainām (sk. 3.15b. att. dažādiem paraugiem). Refleksu pozīcijas un intensitāte atšķiras viena un tā paša cietā šķīduma dažādu komponentu sastāva paraugos. Komponentu sastāvā, kurā veidojas divfāžu maisījums, var novērot abu cieto šķīdumu raksturīgos refleksus.



3.15. att. Derivatogrammas (a) un PXRD ainas (b) dažādiem binārās sistēmas Cl-TX – I-TX sastāviem. Krāsu apzīmējums ir identisks tam, kas izmantots 3.14. attēlā, no kristāla struktūrām simulētas difrakcijas ainas – purpursarkanā krāsā (sarindotas atkarībā no iesvērtā I-TX satura).

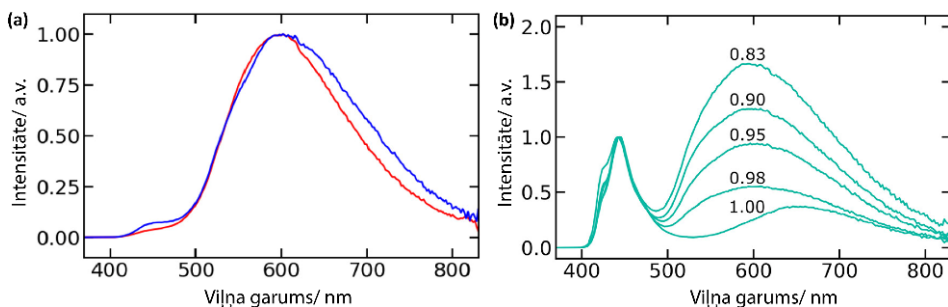
α cietā šķīduma pamatā ir Cl-TX struktūra, tīra Cl-TX luminiscences spektra joslas maksimums novērojams aptuveni pie 600 nm. Šīs joslas ierosmes spektrs satur trīs maksimumus pie 330 nm, 420 nm, 490 nm un nelielu plecu pie aptuveni 390 nm (sk. 3.16a. att.). Tas atbilst literatūrā ziņotajiem rezultātiem par Cl-TX pulveru luminiscences īpašībām, kurā galvenā josla attiecināta uz fosforescenci, savukārt, vājās intensitātes plecs pie aptuveni 450 nm attiecināts uz fluorescenci⁴¹. α cietajā šķīdumā apmēram pusi no Cl-TX molekulām var apmainīt ar I-TX molekulām, lai gan pieejamais komponentu sastāva diapazons ir plašs, luminiscences ierosināšanas-emisijas kartes mainās diezgan nenozīmīgi. Luminiscences joslai pie 600 nm Cl-TX : I-TX kartē ir redzams sarkans

nobīdīts plecs pie sastāva 0,50 : 0,50 (sk. 3.16b. att.). Turklāt ierosmes maksimums pie 490 nm ir tikpat intensīvs kā maksimums pie 330 nm un 420 nm.



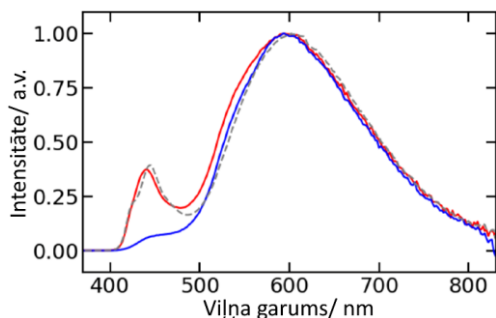
3.16. att. Istabas temperatūras luminiscences ierosināšanas-emisijas kartes α cietajam šķīdumam divos dažādos sastāvos (a) un (b).

Visbeidzot, fluorescences josla pie 450 nm ir daudz izteiktāka (sk. 3.17a. att.). Dati liecina, ka šajā konkrētajā gadījumā halogēna atoma tipam nav būtiskas ietekmes uz fotoluminiscences mehānismu. Acīmredzot, nelielā atšķirība abu molekulu elektroniskajā struktūrā un starpplakņu attāluma izmaiņas kristāliskajā stāvoklī, kas rodas, kad daļa no sākotnējām CI-TX molekulām apmainās ar I-TX molekulām, neizraisa būtiskas luminiscences spektrālo īpašību izmaiņas. Savukārt, pretējā gadījumā, kad I-TX molekulas apmainās ar CI-TX molekulām, tiek ieviestas jaunas emisijas joslas ar maksimumiem zemākos viļņu garumos. Emisijas spektros pie $\lambda_{ieros.} = 330$ nm, kas parādīti 3.17b. attēlā, to var novērot vēl skaidrāk. Turpmāka I-TX aizstāšana ar CI-TX izraisa relatīvās intensitātes izmaiņas starp fluorescences un fosforescences joslām.



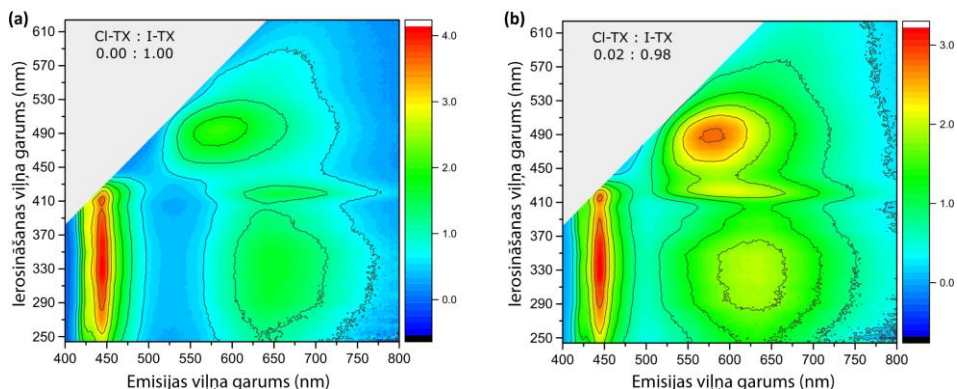
3.17. att. Istabas temperatūras fotoluminiscences spektri ($\lambda_{ieros.} = 330$ nm) α cietajam šķīdumam (a) divās dažādās CI-TX : I-TX attiecībās: 1,00 : 0,00 (sarkanā); 0,50 : 0,50 (zilā) un β cietajam šķīdumam (b) piecās dažādās CI-TX : I-TX attiecībās.

Svarīgi atzīmēt, ka cieto šķīdumu fotoluminiscences spektri būtiski atšķiras no tīro fāžu fizikālo maisījumu fotoluminiscences spektriem tādās pašās attiecībās (sk. 3.18. att.).

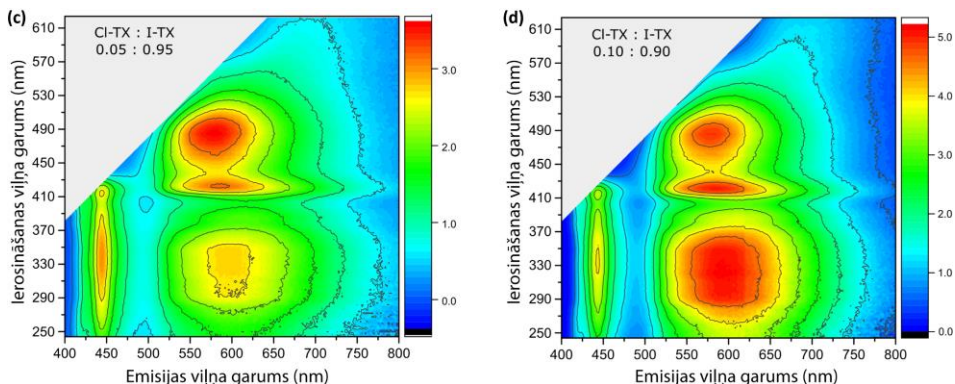


3.18. att. Istabas temperatūras fotoluminiscences spektri ($\lambda_{\text{ieros.}} = 330 \text{ nm}$): 1) 0,40 : 0,60 (I-TX : Cl-TX) mehāniskam maisījumam (sarkanā); 2) lineāra kombinācija starp I-TX un Cl-TX spektriem mērogā 0,40 : 0,60 (raustītā pelēkā); 3) 0,40 : 0,60 (I-TX : Cl-TX) cietais šķīdums (zilā).

β cietā šķīduma pamatā ir I-TX struktūra un tas pastāv ievērojami šaurākā komponentu sastāva diapazonā nekā α cietais šķīdums. Tikai līdz aptuveni 20 mol% I-TX molekulu var tikt apmainītas ar Cl-TX molekulām līdz tiek sasniegta šķīdības robeža. Tomēr šajā gadījumā pat daži mol% pretējā komponenta būtiski ietekmē luminiscences spektrālās īpašības. 3.19a. attēlā ir attēlota tīra pulverveida formā esošā I-TX luminiscences ierosināšanas-emisijas karte. Tajā ir novērojama intensīva josla ar maksimumu pie 445 nm, kas attiecināma uz fluorescenci⁴¹. Tīra I-TX fosforescences joslas ir vājas, taču tās mainās, kad kristāliskajā struktūrā tiek ievietotas Cl-TX molekulas. Tikai 2 mol% Cl-TX būtiski maina kartes raksturlielumus (sk. 3.19. att. (b) – (d)).

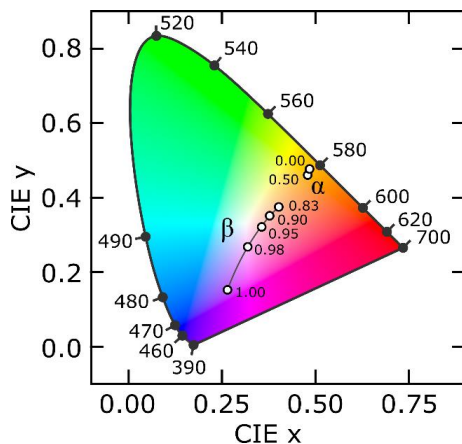


3.19. att. Istabas temperatūras luminiscences ierosināšanas-emisijas kartes β cietajam šķīdumam divos dažādos sastāvos (a) – (d).



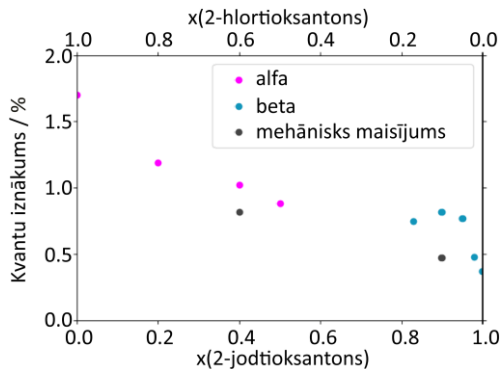
3.19. att. (Turpinājums).

Ņemot vērā, izteikto fosforescences efektu, ko izraisa CI-TX saturs pieaugums I-TX matricā, ir saistīts ar halogēna saiti, t. i., šī saite tieši ir atbildīga par fosforescences mehānismu β cietajā šķīdumā. Spektrālo joslu relatīvās intensitātes izmaiņu dēļ pastāv luminiscences krāsas variācijas, kas attēlotas CIE hromatiskuma diagrammā (sk. 3.20. att.) vairākām β (un α) cieto šķīdumu kompozīcijām.



3.20. att. CIE hromatiskuma diagramma dažādu sastāvu β un α cietajiem šķīdumiem, atliktie punkti iegūti no emisijas spektriem pie $\lambda_{\text{ieros.}} = 330 \text{ nm}$ (istabas temperatūrā).

α cietajam šķīdumam luminiscences krāsa gandrīz neatšķiras pat tad, ja puse no oriģinālajām CI-TX molekulām tiek apmainīta ar I-TX molekulām kristāliskajā struktūrā. Taču β cietā šķīduma gadījumā – tas ir pretēji, jo luminiscences krāsojums ir stipri atkarīgs no komponentu sastāva. CI-TX saturs robežās no tīra līdz 17 mol% CIE hromatiskuma diagrammā ir novērojamas lielas atšķirības, no tā var secināt, ka luminiscences krāsu var smalki regulēt, mainot cietā šķīduma komponentu sastāvu.



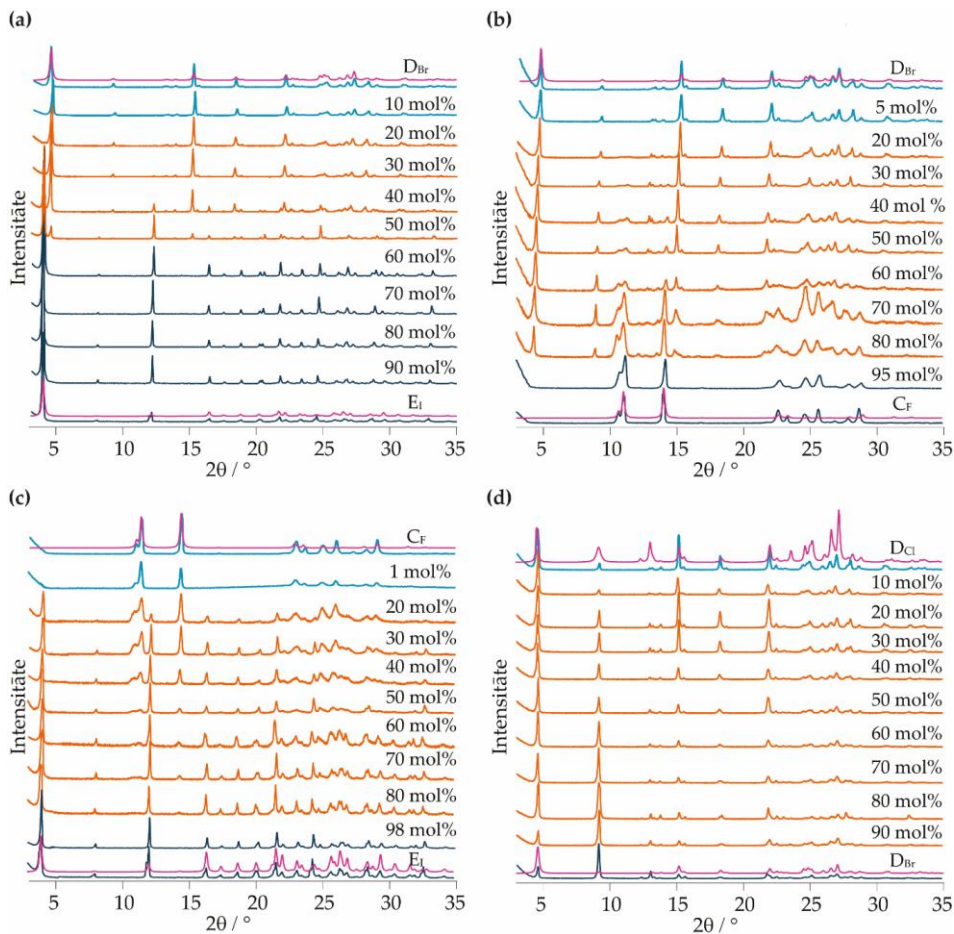
3.21. att. Absolūtie fotoluminiscences kvantu iznākumi Cl-TX – I-TX cietajiem šķīdumiem un mehāniskiem maisījumiem.

Absolūtā fotoluminiscences kvantu iznākuma (Φ) atkarība no cietā šķīduma sastāva attēlota 3.21. attēlā. Tīram Cl-TX kvantu iznākums ir 1,7 %, tas samazinās līdz 0,88 %, kad tiek sasniegts komponentu sastāvs 0,50 : 0,50 (I-TX – Cl-TX). β cietajam šķīdumam kvantu iznākums palielinās, palielinoties Cl-TX saturam, no 0,37 % līdz ~ 0,80 %.

3.4.2. Divkomponentu sistēmas, kuras satur joda, hlora, broma un fluora atvasinājumus^E

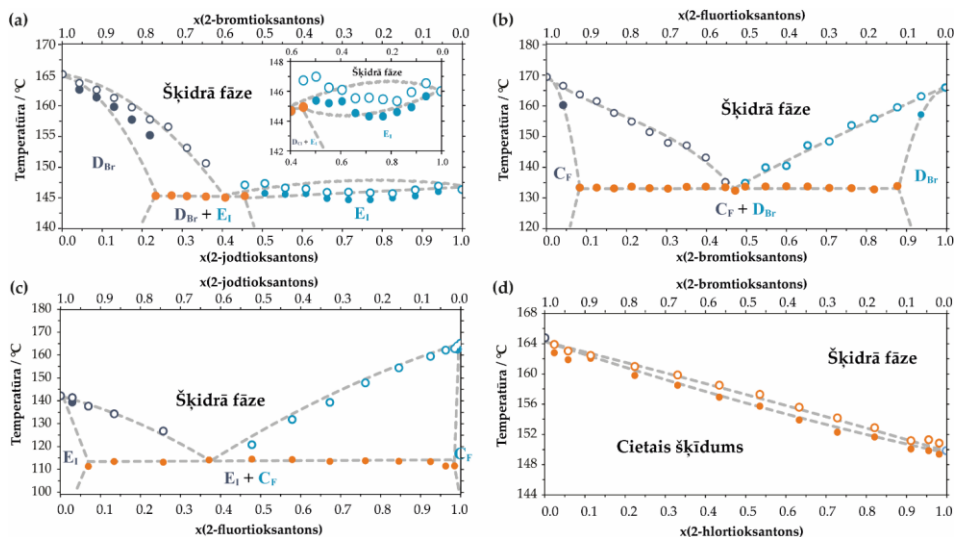
Kā ziņots iepriekšējā sadaļā, kur binārajā sistēmā, kas satur jodtioksantonu un hlortioksantonu, iegūti cietie šķīdumi, kuru luminiscences krāsu var smalki regulēt, mainot komponentu sastāvu, šajā pētījumā tika nolemts pārbaudīt, vai starp citiem tioksantona halogēnatvasinājumiem, t. i., abiem jau nosauktajiem savienojumiem, kā arī bromtioksantonu un fluortioksantonu, veidojas cietie šķīdumi ar smalki regulējamām īpašībām. Zināmi vairāki šo savienojumu polimorfī, kuru struktūras zināmas pēc literatūras datiem⁴¹: hlortioksantons I (*P-1*) **D**_{Cl}, bromtioksantons I (*P-1*) **D**_{Br} un jodtioksantons I (*P2₁2₁2₁*) **E**_I, struktūras noteiktas šī pētījuma ietvaros no: monokristāla datiem – fluortioksantons I (*P2₁/n*) **A**_F, II (*P2₁2₁2₁*) **B**_F, III (*Pc*) **C**_F un hlortioksantons III (*Pna2₁*) **F**_{Cl}, pulvera rentgendifrakcijas datiem – hlortioksantons II (*P2₁2₁2₁*) **E**_{Cl}. Kā secināts no PXRD analīzes rezultātiem (sk. 3.22. att.), Br-TXANT (I forma) un Cl-TXANT (I forma) ir savstarpēji izostrukturālas – 3.22d. attēlā, un to kristāli ir izomorfi⁴¹. Cietais šķīdums ar pilnīgu komponentu šķīdību veidojas starp Br-TXANT un Cl-TXANT molekulām, bet citos gadījumos tā vietā veidojas divi dažādi cietie šķīdumi, kas ir tuvu tīru komponentu apgabalam (sk. 3.23. attēlu).

^ESaršūns, K., Kons, A., Leduskrasts, K., Kļimenkovs, I., Bērziņš, A., Reķis, T. Modulation of physico-chemical properties *via* solid solution formation of thioxanthone derivatives. *Manuskripts izstrādes procesā*.



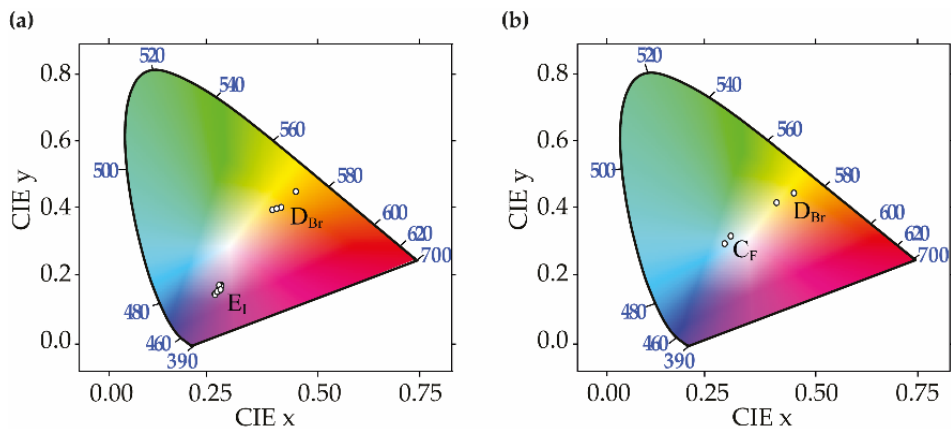
3.22. att. Kristalizācijas produktu PXRD ainas, kas iegūtas, kristalizējot dažādus tioksantona atvasinājumu vielu maisījumus: I-TXANT – Br-TXANT (a), F-TXANT – Br-TXANT (b), I-TXANT – F-TXANT (c) un Br-TXANT – Cl-TXANT (d), dažādos komponentu sastāvos no acetonitrila. Cieto šķīdumu un atbilstošās vienkomponentu fāzes identiskā zilā tonī, fāžu maisījumi oranžā krāsā, un no kristāla struktūram simulētas difrakcijas ainas – purpursarkanā krāsā (sarindotas atkarībā no iesvērtā I-TXANT (a) un (c), F-TXANT (b) un Br-TXANT (d) saturā).

Šaurs divfāžu apgabals norāda, ka abu molekulu atšķirība kristāliskajā struktūrā nav īpaši efektīva – 3.23a. attēlā, sastāva diapazonos $>0 - 20$ mol% un $50 - <100$ mol% (2-jodtioksantons), 3.23b. attēlā, sastāva diapazonos $>0 - 5$ mol% un $90 - <100$ mol% (2-bromtioksantons), 3.23c. attēlā, sastāva diapazonā no 0 līdz 5 mol% un $98 - <100$ mol% (2-fluortioksantons) – un tās ir diezgan slikti izšķiramas, izņemot starp 2-bromtioksantonu un 2-hlortioksantonu, 3.23d. attēlā, kuru savstarpējā šķīdība ir neierobežota visā sastāva diapazonā ($0 - 100$ mol%).

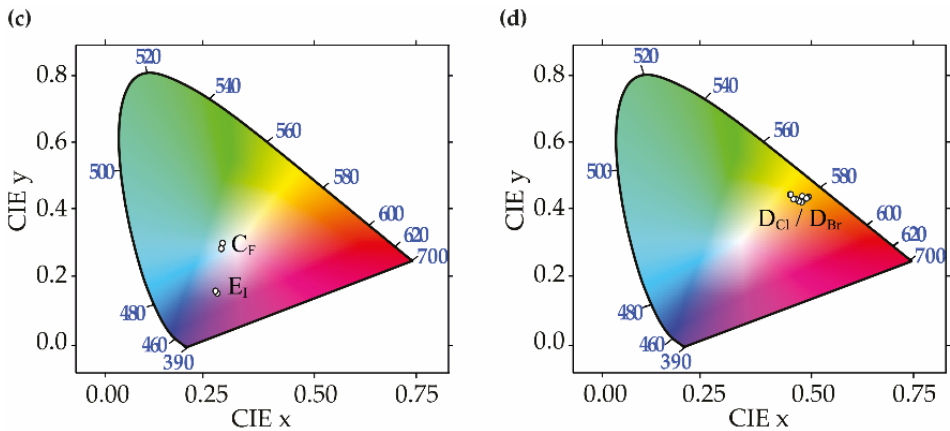


3.23. att. Bināru sistēmu kušanas fāžu diagrammas: I-TXANT – Br-TXANT (a), F-TXANT – Br-TXANT (b), I-TXANT – F-TXANT (c) un Br-TXANT – Cl-TXANT (d). Krāsu apzīmējums ir identisks tam, kas izmantots 3.22. attēlā (pildīti marķieri – soliduss / eitektika; tukši marķieri – likviduss; līnijas attēlotas uzskatāmībai).

Skaidri redzams, ka sastāva diapazons, kurā var iegūt šos cietos šķīdumus, ir atšķirīgs katrā tioksantona atvasinājumu pāri. Vislielākā šķīdība līdz vairāk nekā 50 mol% tika novērota I-TXANT – Br-TXANT sistēmā, bet zemākā (mazāk nekā 5 mol%) F-TXANT – Br-TXANT sistēmā. 3.24. attēlā CIE hromatiskuma diagramma ir attēlota vairākām cieto šķīdumu kompozīcijām dažādās binārās sistēmās.



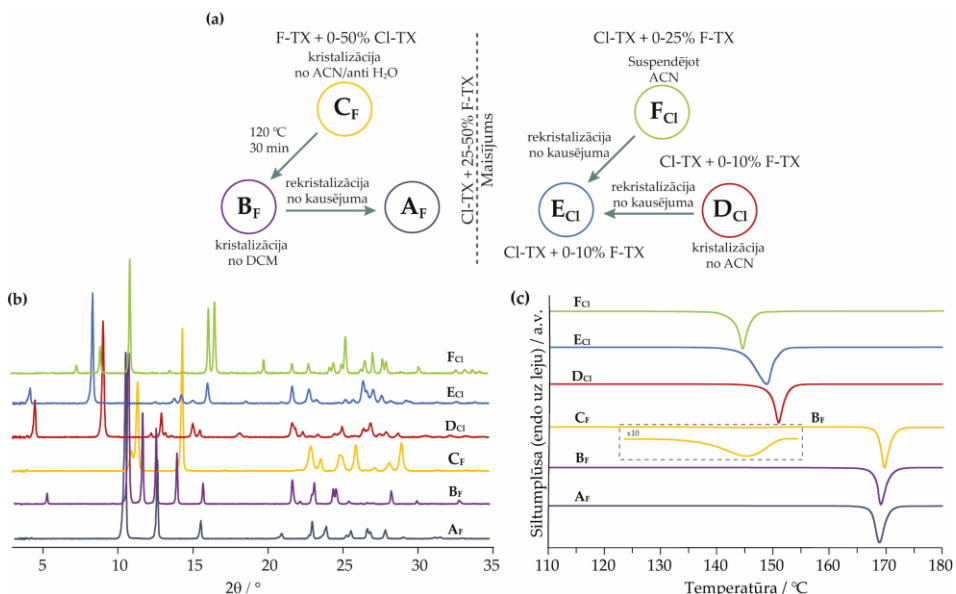
3.24. att. CIE hromatiskuma diagrammas dažādu sastāvu cietajiem šķīdumiem, atliktie punkti iegūti no emisijas spektriem pie $\lambda_{\text{ieros.}} = 330 \text{ nm}$ (istabas temperatūrā): I-TXANT – Br-TXANT (a), F-TXANT – Br-TXANT (b), I-TXANT – F-TXANT (c) un Br-TXANT – Cl-TXANT (d).



3.24. att. (Turpinājums).

Skatoties pēc CIE hromatiskuma diagrammām, luminiscences krāsā ir minimālas izmaiņas neatkarīgi no komponentu sastāva izmaiņām. Pat cietā šķīduma E_I gadījumā luminiscences krāsa lielākoties paliek nemainīga, pat ja puse no sākotnējām I-TXANT molekulām tiek aizstātas ar Br-TXANT molekulām kristāliskajā struktūrā.

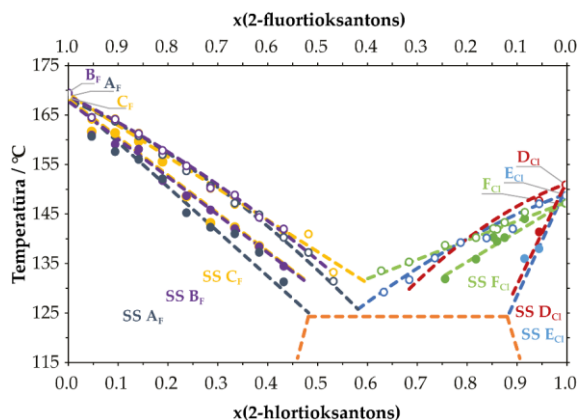
Salīdzinot ar citām šeit aprakstītajām tioksantona atvasinājumu binārajām sistēmām, F-TXANT – Cl-TXANT ir visatšķirīgākā, jo abas vielas var veidot trīs polimorfās formas, shematisku formu iegūšanu un fāžu pārejas skatīt 3.25. attēlā.



3.25. att. Shematisks F-TXANT un Cl-TXANT formu iegūšanas un fāžu pāreju attēlojums (a), difraktogrammas (b), un derivatogrammas, $10^\circ\text{C}\cdot\text{min}^{-1}$ (c).

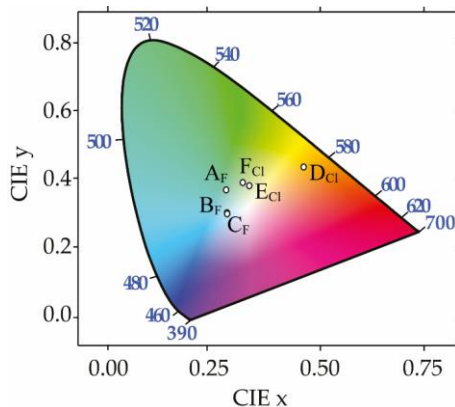
Pētot nesolvatēto F-TXANT un Cl-TXANT polimorfās formas, tika atklāta sarežģīta cieto šķīdumu sistēma. F-TXANT un Cl-TXANT veido trīs dažādas cieto šķīdumu sistēmas ar daļēju komponentu šķīdību. Kušanas fāžu diagramma, kurā raksturotas

nesolvatētas fāzes, parādīta 3.26. attēlā., kur attiecīgi var novērot, ka F-TXANT un Cl-TXANT veido sešu dažādu cieto šķīdumu eitektiskās sistēmas.



3.26. att. Kušanas fāžu diagramma F-TXANT un Cl-TXANT polimorfēm un to cietajiem šķīdumiem (pildīti marķieri – soliduss; tukši marķieri – likviduss; līnijas attēlotas uzskatāmībai).

F-TXANT un Cl-TXANT polimorfo formu CIE hromatiskuma diagramma attēlota 3.27. attēlā.



3.27. att. CIE hromatiskuma diagramma F-TXANT un Cl-TXANT polimorfajām formām, atliekie punkti iegūti no emisijas spektriem pie $\lambda_{ieros.} = 330$ nm (istabas temperatūrā).

Salīdzinot šīs divkomponentu sistēmas ar iepriekšējā nodaļā analizēto I-TXANT – Cl-TXANT, luminiscences krāsojums tik ļoti nemainās, taču galvenā atziņa, kas tika noskaidrota – luminiscences krāsojumu var mainīt ne tikai, mainot komponentu sastāvu cietajā šķīdumā, bet arī starp polimorfajām formām, kā tas ir F-TXANT un Cl-TXANT gadījumā.

SECINĀJUMI

1. Pētītie savienojumi veido cietos šķīdumus gan ar ierobežotu, gan neierobežotu komponentu šķīdību, ko pierāda iegūtās fāžu diagrammas. Cieto šķīdumu veidošanās benperidola – droperidola sistēmā pierāda, ka vienas molekulas spēja aizstāt otru dažādās fāzēs ir būtiski atkarīga no fāzes kristāliskās struktūras, to veidošanās aizvietotajās nitrobenzoscābēs skaidri rāda gan atkarību no apmaināmo funkcionālo grupu īpašībām un tām raksturīgajām starpmolekulārajām mijiedarbībām, gan kristāliskās struktūras, savukārt cieto šķīdumu veidošanās ksantona – tioksantona sistēmā un tioksantonu analogu gadījumā uzrāda atkarību no molekulu pakojuma.
2. Divkomponentu sistēmas benperidols – droperidols solvatēto kristalizācijas produktu desolvatācijā veidojas stabils cietais šķīdums ar benperidola II polimorfās formas kristālisko struktūru gan gadījumā, ja tiek desolvatēts cietais šķīdums benperidola solvātu struktūrā, gan cietais šķīdums droperidola solvātu struktūrā, gan pat šādu cieto šķīdumu maisījums.
3. Organisko kristālu materiālu fizikālo īpašību uzlabošanai var izmantot cieto šķīdumu veidošanās pieeju. Novērots, ka luminiscences īpašību atkarību no sastāva var sagaidīt, ja tiek ietekmētas starpmolekulārās mijiedarbības, kas ir atbildīgas par luminiscenci, ko īpaši ietekmē cieto šķīdumu veidošanās process. Demonstrētā pieeja parāda, ka pretstatā vienfāzes materiāliem, kuros īpašības var regulēt tikai pārtrauktā veidā, izmantojot cietos šķīdumus, luminiscences raksturlielumus ir iespējams mainīt nepārtrauktā veidā.
4. Pierādīts, ka benperidola – droperidola divkomponentu sistēmās starpmolekulāro mijiedarbības enerģiju izmaiņu analīze, modelējot cieto šķīdumu veidošanos, ļauj izskaidrot cieto šķīdumu veidošanās spēju dažādās struktūrās. Lai nesolvatētajās struktūrās veidotos cietais šķīdums plašā koncentrāciju diapazonā ir jāsauglabā mijiedarbības efektivitāte, savukārt cieto šķīdumu veidošanās plašā koncentrāciju diapazonā solvatētajās struktūrās ir iespējama, ja starpmolekulārās mijiedarbības kļūst nedaudz efektīvākas.
5. Novērots, ka aizvietoto nitrobenzoscābju divkomponentu sistēmās, starpmolekulāro mijiedarbību enerģijas izmaiņu analīze, modelējot cieto šķīdumu veidošanos, nav piemērota cieto šķīdumu veidošanās novērtēšanai, jo neiekļauj termiskos un entropijas efektus. Tas skaidrojams ar to, ka atšķirībā no benperidola – droperidola divkomponentu sistēmām, aizvietoto nitrobenzoscābju divkomponentu sistēmās cieto šķīdumu veidošanās saistīta ar būtiskākām ķīmiskās struktūras un līdz ar to starpmolekulāro mijiedarbību izmaiņām.

PATEICĪBAS

Izsaku pateicību Latvijas Universitātes fondam (administrētās SIA “Mikrotīkls” stipendijas doktorantūras studentiem eksakto un medicīnas zinātņu jomā) un Eiropas Sociālajam fondam (grants “*Latvijas Universitātes doktorantūras kapacitātes stiprināšana jaunā doktorantūras modeļa ietvarā*”, granta Nr. 8.2.2.0/20/I/006) mani ļoti būtiski finansiāli atbalstīja praktiski visā doktorantūras garumā. Esmu pagodināts un pateicīgs, ka esmu bijis šīs stipendijas un granta saņēmējs. Kā arī Latvijas Zinātnes padomei (projekts “*Farmaceutisko vairākkomponentu fāžu kristālinženierija efektīvākam kristālisko formu dizainam*”, projekta Nr. Izp-2018/1-0312) par finansiālo atbalstu.

Es vēlos izteikt vislielāko atzinību maniem zinātniskajiem vadītājiem – asociētajam profesoram *Dr. chem.* Agrim Bērziņam par sniegtajiem vērtīgajiem un konstruktīvajiem padomiem šī darba plānošanas un izstrādes gaitā, kā arī par veltīto laiku, un pētniekam *Dr. chem.* Tomam Rēķim par iespēju projekta (“*Structural studies of 4-iodothioxanthone solid solutions exhibiting modulated solid state luminescence properties*”) ietvaros doties mērīt monokristālus uz P24, PETRA III, Deutsches Elektronen-Synchrotron DESY (Hamburga, Vācija) un sniegtajiem noderīgajiem padomiem promocijas darba izstrādes gaitā, kā arī par veltīto laiku.

Vēlos pateikties Fizikālās ķīmijas katedras kolēģiem – šī darba zinātniskajam konsultantam vadošajam pētniekam *Dr. chem.* Artim Konam par sniegtajiem ieteikumiem un ieguldījumu mana promocijas darba tapšanā, *MSc. chem.* Anitai Kalniņai par promocijas darba teksta rediģēšanu, kā arī profesoram *Dr. chem.* Andrim Actiņam par noderīgajiem padomiem. Papildus tam Organiskās ķīmijas katedras kolēģiem – docentam *Dr. chem.* Igoram Kļimenkovam par darbā izmantoto organisko cietvielu sintēzi un pētniekam *MSc. chem.* Rihardam Klūgam par ¹H-KMR spektru uzņemšanu.

Liels paldies Latvijas Organiskās sintēzes institūta pētniecei *Dr. chem.* Kristīnei Krūklei-Bērziņai par monokristālu rentgendifrakcijas mērījumiem un par iespēju projekta (“*Application of cyclodextrin metal-organic frameworks as potential carriers of active pharmaceutical ingredients*”) ietvaros doties noteikt izaudzēto monokristālu kristāliskās struktūras BioMAX, MAX IV Synchrotron (Lunda, Zviedrija), kā arī pētniekam *Dr. chem.* Kasparam Leduskrastam par fotoluminiscences spektru uzņemšanu. Papildus tam Latvijas Universitātes Cietvielu fizikas institūta profesoram *Dr. phys.* Anatolijam Šarakovskim un pētniecei *Ph.D. phys.* Meldrai Ķemerei par luminiscences kvantu iznākuma pētījumu veikšanu un analīzi.

Nobeigumā vēlos izteikt pateicību saviem draugiem par laika pavadīšanu ar mani, kā arī īpašu vislielāko pateicību savai ģimenei – mammai Ilzei Saršūnai, tētim Edgaram Saršūnam un brālim Tomam Saršūnam par ikdienas atbalstu, motivēšanu, ticību maniem spēkiem un par to, ka nemitīgi lepojas ar mani.



**UNIVERSITY
OF LATVIA**

FACULTY OF CHEMISTRY

Kristaps Saršūns

**CHARACTERIZATION OF FORMATION AND PHYSICO-
CHEMICAL PROPERTIES OF SOLID SOLUTIONS IN
MULTICOMPONENT SYSTEMS OF STRUCTURALLY
SIMILAR ORGANIC MOLECULES**

DOCTORAL THESIS

Submitted for the degree of Doctor of Science (Ph.D.)
in Natural Sciences (in the field of Chemistry)

Subfield of Physical Chemistry

Supervisors:

Assoc. Prof., *Dr. chem.* **Agris Bērziņš**
Rsch., *Dr. chem.* **Toms Rēķis**

RIGA, 2024

Mixed crystal, 'solid solution', is a solid phase with similar behaviour to the liquid solution in which the ratio of two or more components can vary freely without the generation of a new phase.

Jacobus Henricus van 't Hoff, 1890

The Doctoral Thesis was carried out at the Chair of Physical Chemistry, Faculty of Chemistry, University of Latvia, Riga, Latvia from 2020 to 2023.



**UNIVERSITY
OF LATVIA**

This work was supported by the European Social Fund grant No. 8.2.2.0/20/I/006, MikroTik Ltd. doctoral scholarship administered by the University of Latvia Foundation, and Latvian Council of Science project No. Izp-2018/1-0312.

NATIONAL
DEVELOPMENT
PLAN 2020



EUROPEAN UNION
European Social
Fund



UNIVERSITY OF LATVIA/
FOUNDATION



FLPP
FUNDAMENTAL AND
APPLIED RESEARCH
PROJECTS

INVESTING IN YOUR FUTURE

The Thesis contains the Summary in Latvian and English, five scientific articles, incl. a manuscript in process of development.

Form of the Thesis: collection of scientific articles in Chemistry, Physical Chemistry.

Supervisors: Assoc. Prof., *Dr. chem.* **Agris Bērziņš**

Rsch., *Dr. chem.* **Toms Rēķis**

Scientific advisor: Sr. Rsch., *Dr. chem.* **Artis Kōns**

Reviewers:

- 1) Prof., *Dr. chem.* **Donāts Erts** (University of Latvia)
- 2) *Dr. phys.* **Anatolijs Mišņovs** (Latvian Institute of Organic Synthesis)
- 3) Assoc. Prof., *Dr. chem.* **Mihails Arhangelskis** (University of Warsaw)

The Thesis will be defended in a public session of the Promotional Committee of Chemistry, University of Latvia at 14.00 on January 23, 2024 at the University of Latvia, Academic Center for Natural Sciences, Jelgavas iela 1, Riga, room 217.

The Thesis and its summary are available at the Library of the University of Latvia, Raiņa bulvāris 19, Riga.

University of Latvia Promotional Committee of Chemistry:

Chairman: Prof., *Dr. chem.* **Edgars Sūna**

Secretary: Assoc. Prof., *Dr. chem.* **Vita Rudoviča**

Front cover images created by Wepik.com (AI Image Generator)

© University of Latvia, 2024

© Kristaps Saršūns, 2024

ISBN 978-9934-36-153-1

ISBN 978-9934-36-154-8 (PDF)

ABSTRACT

Characterization of formation and physico-chemical properties of solid solutions in multicomponent systems of structurally similar organic molecules. Saršūns, K., supervisors Assoc. Prof., *Dr. chem.* Bērziņš, A. and Rsch., *Dr. chem.* Rēķis, T., scientific advisor Sr. Rsch., *Dr. chem.* Kons, A. Summary of the collection of scientific articles in the subfield of physical chemistry, 51 pages, 32 figures, 6 tables, 44 literature references. In English.

This work presents a study of the formation of solid solutions between several organic solids with similar molecular structures: active pharmaceutical ingredients benperidol and droperidol, which differ by the presence of a single/double bond between two carbon atoms, model substances substituted nitrobenzoic acids, which differ by the substituent (halogen atom / methyl group / hydroxyl group), and xanthone and thioxanthone differing by S/O atom, as well as luminophores thioxanthone derivatives differing by halogen atoms. In each of the studied systems, mixtures of substances with different component ratios were crystallized, and powder X-ray diffractometry and construction of phase diagrams from thermal analysis data were used to determine the solubility of substances in each other. In the case of benperidol and droperidol, the mutual solubility of these substances in non-solvated and solvated crystalline structures was additionally investigated. It was determined that in all of the cases, the formation of solid solutions is determined by both the similarity between the steric properties of the exchanged substituents or groups and their ability to form intermolecular interactions, as well as because of the different intermolecular interactions the crystalline structure in which the substituents or groups are exchanged. Quantum chemical calculations were used to assess whether the evaluation of changes in intermolecular interactions caused by the formation of solid solutions can be used to predict the probability of the formation of solid solutions. It was determined that this approach works in the system benperidol – droperidol, in which the formation of solid solutions is associated with small changes in the molecular structure, whereas it is not applicable to substituted nitrobenzoic acids, in which changes in the molecular structure cause significant differences in the intermolecular interactions formed by the substances. The luminescence properties of solid solutions among thioxanthone derivatives were also studied, by determining that in some of the solid solutions even a small change in composition ensures a significant change in luminescence properties, whereas in others, significant changes in composition have only a slight effect on the luminescence properties.

Keywords: *solid solution, thermal analysis, X-ray diffraction, binary phase diagram, luminescence, computational chemistry*

ABBREVIATIONS

ACN	acetonitrile
API	active pharmaceutical ingredient
^B I (etc.) / ^B S _{solvent} / ^B DH	benperidol polymorph form / solvate / dihydrate
^D I / ^D S _{solvent} / ^D DH	droperidol polymorph form / solvate / dihydrate
DFT	density functional theory
DH	dihydrate
DMSO- <i>d</i> ₆	deuterated dimethyl sulfoxide
DSC	differential scanning calorimetry
EtOH	ethanol
<i>F</i> _{hkl}	structure factor
HMDS	hexamethyldisilazane
HPLC	high-performance liquid chromatography
Me	methyl group
MeOH	methanol
NBA	nitrobenzoic acid
NMR	nuclear magnetic resonance
PXRD	powder X-ray diffraction
S _{solvate}	solvate
SCXRD	single crystal X-ray diffraction
SS	solid solution
TG	thermogravimetry
TX / TXANT	thioxanthone
XAN	xanthone
XRD	X-ray diffraction
¹ H NMR	proton nuclear magnetic resonance
I (etc.) form	I polymorph (crystalline) form
Φ	quantum yield
δ	chemical shift

INTRODUCTION

Solid solutions among inorganic substances are widely studied and well-known solid phases for which the structure and properties of the material are dependent on the component ratio. Such phases and the change of properties they provide are widely found in such material classes as metal alloys, minerals, ceramics, etc. On the contrary, solid solutions formed between organic compounds are researched notably less often¹. Moreover, it is reasonable to believe that solid solutions between organic substances and the associated change of the physical properties have so far often been left without attention and detailed study². However, the interest in the formation of solid solutions between organic solids has significantly increased during the last decade, which is clearly indicated by the increase in the number of scientific publications investigating this phenomenon, mainly by testing previously accepted and expressing new hypotheses in the field of crystal engineering^{3,4}. Additionally, solid solutions open the opportunity to modulate material properties by changing the composition of components in a continuous manner⁵. The desired property, however, should be reasonably sensitive to the composition of the solid solution⁶.

Crystal engineering approaches have been used to design and tune important physical and/or chemical properties of crystals, such as solubility^{7,8}, melting point⁹, nonlinear optical¹⁰, and mechanical properties¹¹. Modulation of the properties in a stepwise fashion can be achieved by chemically modifying the constituent molecules, for example, by changing one of the substituents in the molecular structure¹². However, establishing an unambiguous crystal engineering strategy that would allow continuous tuning of any property of a crystalline material is not a straightforward task. Already several decades ago, Kitaigorodsky's works^{13,14} described that a big role in determining whether a solid solution will form between the particular compounds is played by the similarity of the size and shape of the replaceable molecules, and the formation of solid solutions is mainly related to two concepts – structural mimicry¹⁵ and crystal isomorphism¹⁶. However, the large amount of crystallographic data obtained since then shows that Kitaigorodsky's rules are not complete and require revision and development¹⁷.

Solid solutions have been discovered and studied for multicomponent systems of structurally similar organic molecules, where molecules differ by F/H atoms¹⁸; by halogen (and halogen/methyl) substituents¹⁹; by S/O atoms²⁰; by presence/absence of a heteroatom in aromatic systems²¹, etc. Although taking into account the results of the research so far, general and empirical criteria could be defined that would allow determining the ability to form solid solutions between structurally similar molecules, the literature describes cases in which even very similar molecules do not mix in the solid state¹⁷.

Therefore, the systematic acquisition of data on whether structurally similar organic molecules are able to replace each other in the crystalline structure, ensuring the formation of solid solutions, has a high scientific relevance, and detailed studies of various individual systems are necessary to identify the main factors that would allow the formulation of general laws and models to predict the probability of formation of such phases. For this purpose, both very similar molecules xanthone and thioxanthone, which differ by the S/O atom, and substituted nitrobenzoic acids, which differ by the substituent (halogen atom / methyl group / hydroxyl group) and between which the formation of solid solutions was studied in different isomers of the substance, were chosen for this research. Pharmaceutical substances benperidol and droperidol, which differ in the existence of a single/double bond between two carbon atoms, and in which the formation of solid

solutions in the various non-solvated and solvated phases formed by these substances were additionally studied.

It should be noted that only in some of the published studies the formation of solid solutions has been investigated by determining the energy changes using quantum chemical calculations, although such calculations are one of the ways that would allow to arrive at the above-mentioned laws and models. Therefore, such studies have been included as part of this work in the investigation of solid solution formation both between the structurally relatively different substituted nitrobenzoic acids, and between the relatively similar benperidol and droperidol in their different crystalline phases.

In addition, in the previous studies of organic substances mostly only the identification and crystallographic analysis of the formation of solid solutions have been carried out, and there are a limited number of studies of the possibility of such solid solutions to change the industrially important physical properties. Therefore, thioxanthone derivatives, which differ in halogen atoms and are room temperature luminophores, were additionally selected for research and besides studying the formation of solid solutions also characterizing the luminescence properties of the obtained phases.

The purpose and tasks of the doctoral thesis

The **aim** of this research is to use both experimental studies and quantum chemistry calculations for the identification of the main factors that ensure the formation of solid solutions between structurally similar organic molecules, as well as to obtain crystalline phases with fine-tuned physico-chemical properties.

Accordingly, the **tasks** set to address this issue were:

- 1) to characterize the possibilities of the formation of solid solutions in different two-component systems, by considering information about the diversity of the respective crystalline phases, and describe the structure and thermodynamic stability of the obtained solid solutions in the form of phase diagrams;
- 2) to characterize the luminescence properties of solid solutions formed by thioxanthone derivatives and the dependence of these properties on the composition of the components aimed to obtain new materials with finely adjustable luminescence properties;
- 3) to perform quantum chemical calculations in the structures of solid solution models formed by benperidol and droperidol, as well as substituted nitrobenzoic acids aimed to clarify the possibility of using the energy changes of intermolecular interactions for the evaluation of the possibility of solid solution formation in different crystalline structures.

Theses

1. The ability of molecules to replace each other in different phases is determined by both the similarity in the properties of the exchanged functional groups and their formed characteristic intermolecular interactions, as well as the crystal structure of the phase.
2. The solid solution formation approach can be used to fine-tune the physical properties of organic luminophores.
3. The analysis of energy changes of intermolecular interactions by modelling the formation of solid solutions can be used to determine the probability of the formation of solid solutions between structurally sufficiently similar molecules.

Scientific Novelty

1. Melt phase diagrams of various two-component systems have been construed, illustrating the thermodynamic stability of the studied solid solutions, as well as showing the potentially complicated nature of such systems (including the possibility of the formation of polymorphic solid solutions).
2. The factors regulating the formation of solid solutions between organic substances with similar molecular structures (changing one of the atoms or functional groups), as well as the role of the crystal structure having characteristic intermolecular interactions in the formation of the solid solution, have been determined.
3. New luminescent materials with fine-tunable luminescence properties have been obtained. There are a very limited number of previous studies of such materials in systems made of organic compounds.
4. New solid solutions, including solid solutions in several polymorphic forms of both F-TXANT and Cl-TXANT, show different luminescence properties that have been obtained in the binary system of these substances.
5. By analysing the results of quantum chemical calculations in various binary systems, the method of intermolecular interaction energy change evaluation and its application for determining the possibility of the formation of solid solutions in various crystal structures is demonstrated.

Practical Significance

1. New insights and explanations have been provided to help obtain new materials with modified physical properties, including luminescence properties and melting temperature, as well as laws of the formation of solid solutions between structurally similar organic substances have been identified, gaining an understanding of structural and interaction energy factors.
2. New optoelectronic materials have been obtained based on the knowledge of the molecular and crystal structures of compounds, thus demonstrating the ability to use crystal engineering for obtaining molecular crystal materials with fine-tunable component-composition dependent luminescent properties.
3. In the comparison of the information determined in the calculations of intermolecular interaction energy changes with the experimental data, information about the possibilities of using such a calculation approach in predicting the formation of solid solutions was obtained, and this can be further used by developing a general computational chemistry methodology for predicting the formation of solid solutions.

RESULTS PUBLISHED

Publications

1. **Saršūns, K.**, Bērziņš, A., Reķis, T. Solid solutions in xanثone – thioxanthone binary system: how well are similar molecules discriminated in the solid state? *Crystal Growth & Design*[‡], **2020**, 20(12), 7997-8004. DOI: 10.1021/acs.cgd.0c01241 (Web of Science/Scopus, Q2/Q1, IF₂₀₂₀ = **4.076**)

K.Saršūns carried out 75% of the experimental work, contributed to writing the article (50%), prepared the experimental results according to the journal guidelines, as well as contributed to answering the questions and remarks given by the reviewers.

2. **Saršūns, K.**, Ķemere, M., Karziņins, A., Kļimenkovs, I., Bērziņš, A., Sarakovskis, A., Reķis, T. Fine-tuning solid state luminescence properties of organic crystals via solid solution formation: the example of 4-iodothioxanthone – 4-chlorothioxanthone system. *Crystal Growth & Design*, **2022**, 22(8), 4838–4844. DOI: 10.1021/acs.cgd.2c00313 (Web of Science/Scopus, Q1/Q1, IF₂₀₂₂ = **4.010**).

K.Saršūns carried out 75% of the experimental work, contributed to writing the article (50%), prepared the experimental results according to the journal guidelines, as well as contributed to answering the questions and remarks given by the reviewers.

3. **Saršūns, K.**, Bērziņš, A. Experimental and computational investigation of benperidol and droperidol solid solutions in different crystal structures. *Crystal Growth & Design*, **2023**, 23(2), 1133–1144. DOI: 10.1021/acs.cgd.2c01269 (Web of Science/Scopus, Q1/Q1, IF₂₀₂₃ = **4.010**).

K.Saršūns carried out 90% of the experimental work, contributed to writing the article (75%), prepared the experimental results according to the journal guidelines, as well as contributed to answering the questions and remarks given by the reviewers.

4. **Saršūns, K.**, Kons, A., Reķis, T., Bērziņš, A. Experimental and computational study of solid solution formed between substituted nitrobenzoic acids. *Crystal Growth & Design*, **2023**, 23(9), 6609–6622. DOI: 10.1021/acs.cgd.3c00529 (Web of Science/Scopus, Q2/Q1, IF₂₀₂₃ = **4.010**).

K.Saršūns carried out 90% of the experimental work, contributed to writing the article (75%), prepared the experimental results according to the journal guidelines, as well as contributed to answering the questions and remarks given by the reviewers.

5. **Saršūns, K.**, Kons, A., Leduskrasts, K., Kļimenkovs, I., Bērziņš, A., Reķis, T. Modulation of physico-chemical properties via solid solution formation of thioxanthone derivatives. *Manuscript in process of development*.

K.Saršūns carried out 75% of the experimental work, contributed to writing the article (60%) and prepared the experimental results according to the journal guidelines.

[‡]Peer-reviewed journal published by the American Chemical Society (ISSN: 1528-7505)

Conferences

The results of this study were presented orally at three international scientific conferences (two of them at the University of Latvia) and in the form of a poster presentation at thirteen international scientific conferences, both remotely and in person.

Xanthone – thioxanthone two-component system

- **Saršūns, K.**, Karziņins, A., Leduskrasts, K., Bērziņš, A., Rekis, T. Formation of solid solution in xanthone derivative systems exhibiting luminescence properties. *University of Latvia 79th International Scientific Conference*, February 12, **2021**, Online. (oral presentation/ in book of abstracts)
- **Saršūns, K.**, Karziņins, A., Leduskrasts, K., Bērziņš, A., Rekis, T. Formation of solid solution in xanthone derivative systems exhibiting luminescence properties. *64th International Conference for Students of Physics and Natural Sciences*, March 16-19, **2021**, Online. (poster/ in book of abstracts/ certificate)
- **Saršūns, K.**, Karziņins, A., Leduskrasts, K., Bērziņš, A., Rekis, T. Formation of solid solution in xanthone derivative systems exhibiting luminescence properties. *11th Belgian Crystallography Symposium*, March 17, **2021**, Online. (poster/ in book of abstracts/ certificate)
- **Saršūns, K.**[§], Karziņins, A., Leduskrasts, K., Bērziņš, A., Rekis, T.[‡]. Modulation of luminescence spectra *via* solid solution formation of xanthone derivatives[§] / Formation of solid solution in xanthone derivative systems exhibiting luminescence properties[‡]. *BCA/BACG Online Joint Spring Meeting*, March 29 - April 1, **2021**, Online. (poster[§]/oral presentation[‡]/ in book of abstracts^{§, ‡}/ certificate)
§, ‡ – presenter.
- **Saršūns, K.**, Bērziņš, A., Rekis, T. Solid solution formation in xanthone – thioxanthone binary system: experimental investigation. *23rd International conference EcoBalt 2023*, October 9-11, **2023**, Tallinn, Estonia. (poster/ in book of abstracts/ certificate/ special issue in MDPI journal – *Proceedings*, **2023**, 92(1), 67. DOI: 10.3390/proceedings2023092067)

Substituted nitrobenzoic acids two-component systems

- **Saršūns, K.**, Bērziņš, A. Computational prediction and experimental confirmation of Solid Solution formation from different nitrobenzoic acid derivatives and their isomers. *61st International Scientific Conference “Materials Science and Applied Chemistry”*, October 23, **2020**, Online. (poster/ in book of abstracts)
- **Saršūns, K.**, Bērziņš, A. Computational prediction and experimental confirmation of Solid Solution formation from different nitrobenzoic acid derivatives and their isomers. *2nd International Online Conference on Crystals*, November 10-20, **2020**, Online. (poster/ in book of abstracts)
- **Saršūns, K.**, Bērziņš, A., Rekis, T. Structural and energetic factors that contributes to solid solution formation between different nitrobenzoic acid derivatives and their isomers. *63rd International Scientific Conference “Materials Science and Applied Chemistry”*, October 21, **2022**, Online. (poster/ in book of abstracts/ certificate)

- **Saršūns, K.**, Kons, A., Reķis, T., Bērziņš, A. Experimental and computational study of solid solution formed between substituted nitrobenzoic acids. *12th Bologna Convention on Crystal Forms*, September 10-12, **2023**, Bologna, Italy. (poster/ in book of abstracts/ certificate)

Benperidol – droperidol two-component system

- **Saršūns, K.**, Bērziņš, A. Experimental and computational investigation of benperidol and droperidol solid solutions in different crystal structures. *26th Congress and General Assembly of the International Union of Crystallography*, August 22-29, **2023**, Melbourne, Australia. (poster/ in book of abstracts/ certificate)

Various thioxanthone halogen derivatives two-component systems

- **Saršūns, K.**, Leduskrasts, K., Bērziņš, A., Reķis, T. Formation of solid solution in thioxanthone derivative systems exhibiting luminescence properties. *11th Bologna Convention on Crystal Forms*, September 10-11, **2021**, Online. (poster/ in book of abstracts/ certificate)
- **Saršūns, K.**, Leduskrasts, K., Bērziņš, A., Reķis, T. Modulation of luminescence spectra *via* solid solution formation of thioxanthone derivatives. *22nd International conference EcoBalt 2021*, October 21-23, **2021**, Online. (oral presentation/ in book of abstracts/ certificate)
- **Saršūns, K.**, Leduskrasts, K., Bērziņš, A., Reķis, T. Modulation of luminescence spectra *via* solid solution formation of thioxanthone derivatives. *62nd International Scientific Conference “Materials Science and Applied Chemistry“*, October 22, **2021**, Online. (poster/ in book of abstracts/ certificate)
- **Saršūns, K.**, Bērziņš, A., Reķis, T. Fine-tuning solid state luminescence properties of molecular crystals *via* solid solution formation. *University of Latvia 80th International Scientific Conference*, February 11, **2022**, Online. (oral presentation/ in book of abstracts)
- **Saršūns, K.**, Leduskrasts, K., Bērziņš, A., Reķis, T. Fine-tuning solid state luminescence properties of molecular crystals *via* solid solution formation. *30th Annual Meeting of the German Crystallographic Society*, March 14-17, **2022**, Online. (poster/ in book of abstracts/ certificate)
- **Saršūns, K.**, Leduskrasts, K., Bērziņš, A., Reķis, T. Fine-tuning solid state luminescence properties of molecular crystals *via* solid solution formation. *17th European Powder Diffraction Conference*, May 31 - June 3, **2022**, Šibenik, Croatia. (poster/ in book of abstracts/ certificate)

1. RESEARCH BACKGROUND

1.1. Structural aspects and thermodynamic characterization of solid solutions

Structural aspects of solid solutions

Solid solutions are crystalline phases consisting of at least two components in a freely variable composition within certain limits. Depending on the miscibility of the components, solid solutions are divided into two types, i.e., solid solutions of unlimited solubility of components and limited solubility of components (see Figure 1.1.):

- in solid solutions with unlimited solubility (continuous), mutual solubility of components is observed when molecules of one substance dissolve in another substance crystal structure in the full concentration range;
- in solid solutions with limited solubility (discontinuous), mutual solubility of components is observed when molecules of one substance dissolve in another substance crystal structure only up to a certain concentration¹.

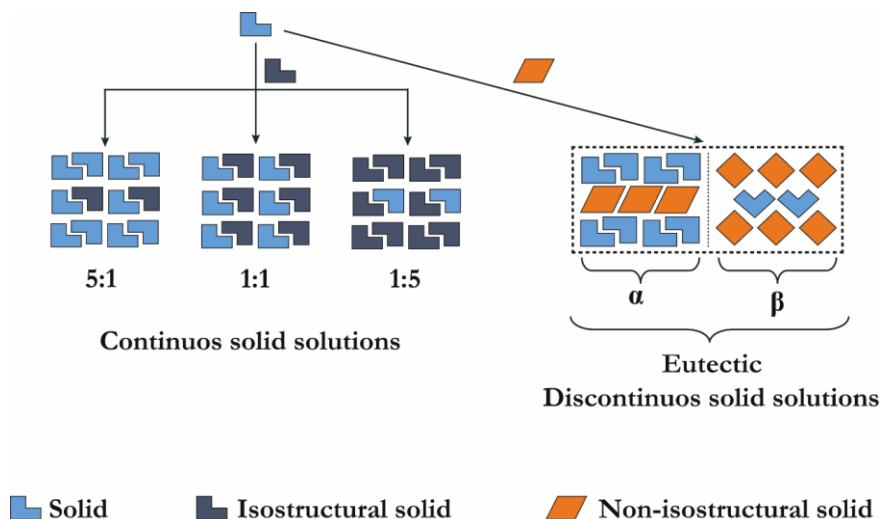


Figure 1.1. Graphical representation of the solid solution formation from two solid organic molecules²².

Thermodynamic characterization of solid solutions

Construction of a melt phase diagram of binary systems reveals the formation of solid solutions as well as allows to characterize them by, e.g., assessing miscibility limits and thermodynamic stability. Figure 1.2. shows principal types of phase diagrams involving solid solutions.

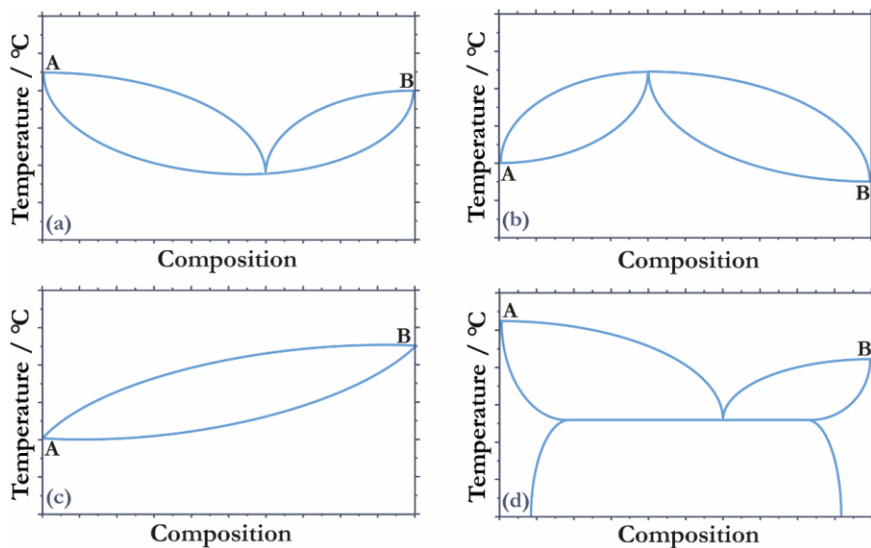


Figure 1.2. Melt phase diagrams of binary systems involving solid solution formation (with full (a) – (c) and partial (d) miscibility in solid state).

Miscibility of organic solids to mix in complete^{16,23,24} and partial composition range^{25–27} have been reported for particular compounds. The phase diagram obtained for a certain compound is governed by the thermodynamics of the respective solid phases. Cases (a) and (b) represent miscibility in the whole composition range for non-ideal solid solutions with maximum and minimum melting temperatures in a given ratio of components, while case (c) represents an ideal solid solution in which the maximum and minimum melting points correspond to pure components. The solid phases A and B in those cases are isostructural. For case (d), however, limited miscibility arises because the solid solution at a certain composition is no longer thermodynamically stable, and a mixture of two phases with the limiting compositions forms instead. The miscibility region width and other quantitative phase diagram properties are determined by properties of the solid phases A and B, namely the enthalpies of melting and melting temperatures.

1.2. Investigation of solid solutions using various physical solid state research methods

Many physical solid state research methods can be used for the identification of solid solutions of which powder X-ray diffraction (PXRD), and thermal analysis (DSC) are the most commonly used, and for determining the quantity of components – nuclear magnetic resonance spectroscopy (NMR) and high-performance liquid chromatography (HPLC), whereas for detailed characterization of their structures most often single crystal X-ray diffraction (SCXRD) analysis is used. In this work, the solid state luminescence properties of the resulting solid solutions were also investigated using photoluminescence spectroscopy. To provide a complete and detailed analysis of solid solutions, it is necessary to use various approaches because each of the physical solid state research methods provides unique but limited information about the phase. A summary of the application of physical solid state research methods in determining the characteristics of various solid solutions is given in Table 1.1.

Table 1.1.

Summary of physical solid state research methods to characterize solid solutions^{1,28}

Application	Research method						Luminescence spectroscopy ^b
	SCXRD	PXRD	NMR	HPLC	DSC	TG	
Identification of crystalline phase	✓	✓			✓	✓	✓
Crystal structure	✓	✓ ^a					
Geometric information on molecules	✓						
Hydrogen bonding interactions (incl. weak interactions)	✓		✓				
Thermal stability		✓			✓	✓	
Stoichiometry	✓		✓	✓		✓	
Phase transformation		✓			✓	✓	✓
Melting point					✓		
De-solvation/-hydration					✓	✓	
Luminescence properties							✓

^a – determination of crystal structure lattice parameters, sometimes also structure determination;

^b – compounds that exhibit a luminescence phenomenon.

Solid state luminescence

Luminescence is a physical phenomenon in which the emission of electromagnetic radiation from an excited material is observed. In the process of luminescence, electrons from an excited state return to the ground state, initially losing part of the energy in non-radiative processes, and only then emitting a quantum of electromagnetic radiation whose energy corresponds to the energy difference between the involved energy levels (excited level and ground state). The processes related to luminescence are shown in Figure 1.3. (such a scheme of energy levels with marked processes is called a Jablonski diagram)²⁹.

Designations (a) – (e), which are included in in the Figure 1.3., describes the energy transition processes in the time scale:

- (a) absorption (10^{-15} s);
- (b) vibrational relaxation ($10^{-14} - 10^{-10}$ s);
- (c) fluorescence ($10^{-9} - 10^{-7}$ s);
- (d) intersystem crossing ($10^{-8} - 10^{-6}$ s);
- (e) phosphorescence ($10^{-6} - 10$ s).

The photophysical properties of organic luminophores are most often characterized by photoluminescence. In the case of photoluminescence, electron excitation occurs when the substance absorbs energy in the form of electromagnetic radiation – a quantum of visible light (or UV).

After quantum absorption, the luminophore is excited from the singlet ground state (S_0) to an excited singlet state (S_1 ; process designation (a)) with sequential vibrational relaxation (b) and fluorescence (c). Fluorescence is emission from excited singlet states (S_n), and it requires three sequential processes: (a) \rightarrow (b) \rightarrow (c), while phosphorescence is emission from excited triplet states (T_n), and involves four sequential processes: (a) \rightarrow (b) \rightarrow (d) \rightarrow (e)^{30,31}.

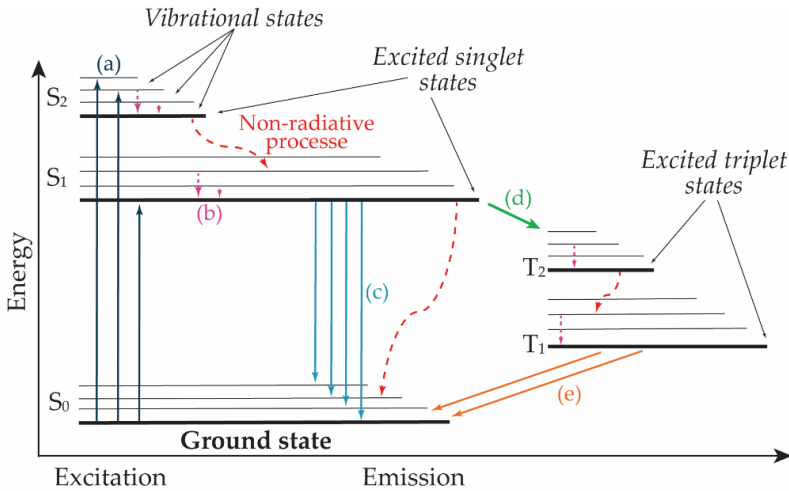


Figure 1.3. Schematic representation of processes related to luminescence - in the form of a Jablonski diagram.

The most important indicator of an efficient lumiphore is the photoluminescence quantum yield (Φ). It is defined as the ratio of photons emitted to the number of photons absorbed and is calculated from equation (1).

$$\Phi_{\%} = \frac{\Sigma P_E}{\Sigma P_A} \cdot 100, \quad (1)$$

where $\Phi_{\%}$ – quantum yield, ΣP_E – the sum of all emitted photons, ΣP_A – the sum of all absorbed photons³².

The colour of the emitted light (luminescence) of the samples can be characterized by colour (or photometric) coordinates. Based on the luminescence spectrum of the material and the spectral sensitivity of the human eye, the colour coordinates show what colour the observer sees in the luminescence. Most often, the colour of light is described using the CIE 1931 XYZ colour space (CIE – *International Commission on Illumination*), which was created in 1931. Colour is described using two coordinates: x and y (see Figure 1.4.)³³.

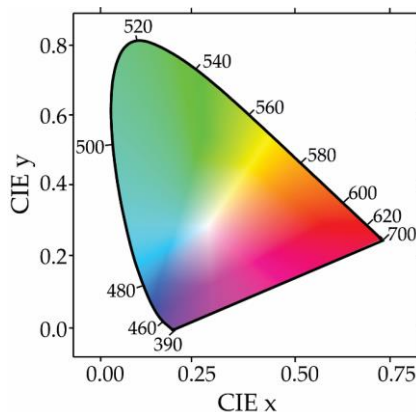


Figure 1.4. CIE chromaticity diagram (CIE 1931, standard observer).

1.3. Objects of Investigation

In total, four systems of compounds were studied (chemical structures are given in Figure 1.5.). Two systems containing different simple model compounds: **xanthone analogues (1)** both molecules are rigid, aromatic and differ only by S/O atoms³⁴, and **substituted nitrobenzoic acids (2)**, they differ from each other, firstly, by the substituent at the C2, C4 or C5 position and, secondly, by the position of the nitro group at the C2, C3, C4 or C5 position. The diversity of nitrobenzoic acid derivatives and their isomers solid forms have been extensively studied and the information has been available as published data within the Department of Physical Chemistry, Faculty of Chemistry³⁵.

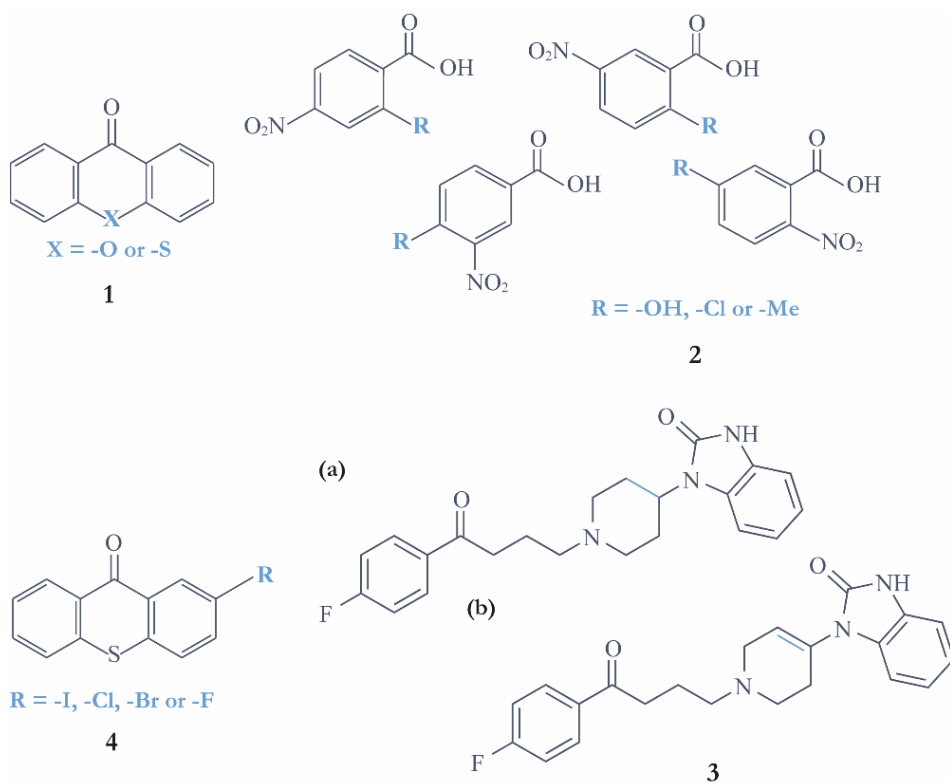


Figure 1.5. Molecular structures of systems of the compounds studied (1 – xanthone analogues; 2 – substituted nitrobenzoic acids; 3 – benperidol (a) and droperidol (b); 4 – thioxanthone derivatives).

A system containing active pharmaceutical ingredients (API): **benperidol (3a)** (1-{1-[4-(4-fluorophenyl)-4-oxobutyl]piperidin-4-yl}-1,3-dihydro-2H-benzimidazol-2-one) and **droperidol (3b)** (1-{1-[4-(4-fluoro-phenyl)-4-oxobutyl]-1,2,3,6-tetrahydro-4-pyridyl}-1,3-dihydro-2H-benzimidazol-2-one), which are antipsychotic drugs that may have antidepressant and anti-amnesic enhancement effects, both compounds are very similar, and the difference is in the C8–C9 bond, which is saturated in benperidol and therefore is part of a piperidine moiety, whereas unsaturated and a part of a 1,2,3,6-tetrahydropyridine moiety in droperidol^{36,37}. The solid forms of benperidol and droperidol have been studied in the Department of Physical Chemistry, Faculty of Chemistry^{38–40} by

discovering that both substances form several polymorphic forms, hydrates, solvates with ethanol, methanol, acetonitrile, and other solvents.

Finally, model compounds, which are room-temperature luminophores demonstrating different luminescence properties⁴¹: **thioxanthone derivatives (4)**, they have a chemically similar structures and differ from each other by the substituent at the C2 position.

2. EXPERIMENTAL SECTION

1. Routine PXRD measurements were performed with a *Bruker D8 Advance* diffractometer using an X-ray tube with copper radiation (Cu K α) with *Bragg–Brentano* geometry and a *LynxEye* position-sensitive detector. The sample was placed in a glass sample holder for PXRD pattern collection. The patterns were recorded from 3° to 35° on the 2 θ scale, using a scan speed of 0.2 s/0.02° (University of Latvia, Riga, Latvia).
2. PXRD data for crystal structure determination were recorded on a *Bruker D8 Discover* diffractometer using an X-ray tube with copper radiation (Cu K α) and a *LynxEye (1D)* detector in transmission mode (incident beam path was equipped with a Göbel Mirror). The sample was loaded into borosilicate glass capillaries of 0.5 mm outer diameter (Hilgenberg glass No. 10). A capillary spinner (60 rpm) and upper and lower knife edges were used. The diffraction patterns were recorded on the 2 θ scale from 4° to 70° at a 0.01° step size using a scan speed of 36 s per step (University of Latvia, Riga, Latvia).
3. SCXRD data were collected on a selected diffractometer. A single crystal was fixed with oil in a nylon loop of a magnetic CryoCap and set on a goniometer head:
 - *Rigaku XtaLAB Synergy-S dualflex* diffractometer equipped with a HyPix6000 detector and microfocused sealed X-ray tube with Cu K α radiation – $\lambda = 1.54184 \text{ \AA}$ (Latvian Institute of Organic Synthesis, Riga, Latvia);
 - *Huber 4 circle kappa* diffractometer equipped with a Pilatus CdTe 1M detector and an X-ray tube with synchrotron radiation – $\lambda = 0.61992 \text{ \AA}$ (P24, PETRA III, Deutsches Elektronen-Synchrotron DESY, Hamburg, Germany);
 - *Arinax MD3* diffractometer equipped with Eiger 16M Hybrid-pixel detector and an X-ray tube with synchrotron radiation – $\lambda = 0.68879 \text{ \AA}$ (BioMAX, MAX IV Synchrotron, Lund, Sweden).
4. DSC/TGA analyses of polymorph and pseudopolymorph forms were performed with a *Mettler Toledo TGA/DSC2* instrument. Heating of samples from 25 °C to 240 °C was performed at a heating rate of 10 °C·min⁻¹ under a N₂ flow (flow rate was 100 ± 10 mL·min⁻¹). Open 100 μ L aluminium pans were used (University of Latvia, Latvia).
5. DSC analyses of crystallization products were performed with a *TA DSC 25 Instrument*. Heating of samples from 25 °C to 250 °C (depending on the melting temperature of pure components) was performed at a heating rate of 2 – 5 °C·min⁻¹ under a N₂ flow (flow rate was 100 ± 10 mL·min⁻¹). A 70 μ L aluminium crucibles were used, and the crucibles were crimped (University of Latvia, Riga, Latvia).
6. ¹H-NMR spectra of pure compounds and most of the crystallization products dissolved in a dimethyl sulfoxide (DMSO)-*d*₆ ($\delta = 2.49$ ppm) were recorded at a nominal temperature of 300 K with a *Bruker Fourier 300 MHz* spectrometer. Chemical shifts (δ) were found in parts per million (ppm) using the residual solvent HMDS ($\delta = 0.055$ ppm) peak as an internal reference (University of Latvia, Riga, Latvia).

7. Photoluminescence measurements:

- photoluminescence spectra of the crystallization products were recorded using an *F55* spectrofluorometer from *Edinburgh Instruments* equipped with a 150 W continuous xenon lamp and single-photon counting detector (Latvian Institute of Organic Synthesis, Riga, Latvia);
 - absolute photoluminescence quantum yield (APLQY) measurements were performed with an Integrating Sphere Assembly *N-M01* (an accessory to *Edinburgh Instruments* luminescence spectrometer, using direct excitation method), and excitation-emission luminescence maps were obtained using an *Edinburgh Instruments* photoluminescence spectrometer *FLS1000* equipped with a ozone generating 450 W continuous xenon lamp and a *High Speed Red Detector* photomultiplier (Institute of Solid State Physics, Riga, Latvia).
8. Structure solution from powder data, crystallization product lattice parameters determination, and Rietveld refinement were performed using software's *Topas5* and *Expo2014*, single crystal X-ray diffraction data were integrated using *CrysAlisPro* software, structure solutions and refinements were performed with the software's *JANA2006* and *Olex2*, for periodical DFT-D calculations using software's *Quantum ESPRESSO* and *CASTEP*, *CrystalExplorer* for characterization of intermolecular interactions and crystalline structures, but *Gaussian09* for molecular gas phase calculations.

3. RESULTS AND DISCUSSION

3.1. Formation of solid solutions of the xanthone – thioxanthone (1) two-component system^A

Through the studies of solid solution formation between structurally similar organic molecules, a system which contains two model compounds – xanthone and thioxanthone, was examined. The most elegant way to explore possible solid solution formation is to construct a binary melt phase diagram of the desired system. A binary melt phase diagram was constructed to explore how well both highly similar molecules are discriminated in the solid state. It was revealed that there is no single continuous solid solution, but two solid solutions form instead, i.e., near pure xanthone and near pure thioxanthone region (see Figure 3.1.). This is an indication that both highly similar molecules pack differently in the solid state. As can be seen in the phase diagram, xanthone dissolves in thioxanthone forming a solid solution (α) in a large composition range. Crystallizing thioxanthone – xanthone mixtures with xanthone content $>0 - 80$ mol% single phases were obtained.

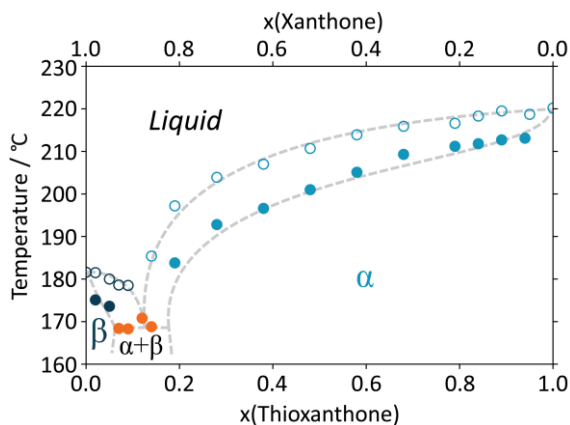


Figure 3.1. Melt phase diagram of xanthone – thioxanthone binary system. Solid solutions and the corresponding single-component phases are in identical shades of blue, and phase mixtures are in orange (closed points represent – solidus / eutectic; open symbols indicate – liquidus; lines are present as guides for the eyes).

The DSC measurements showed a single endothermic signal for each measured composition (see Figure 3.2a). Furthermore, PXRD patterns of the mixtures in the said composition range ($>0 - 80$ mol%, xanthone content) are very similar to that of pure thioxanthone and do not contain the characteristic peaks of pure xanthone phase (see Figure 3.2b). The slight peak shifts and relative intensity variations are typical for solid solutions. The DSC measurements suggest that a small amount of thioxanthone can be dissolved in xanthone, i.e., another solid solution (β) exists for this binary system. For example, a mixture containing 5 mol% thioxanthone melts exhibiting a single

^ASaršūns, K., Bērziņš, A., Rekis, T. Solid solutions in xanthone – thioxanthone binary system: how well are similar molecules discriminated in the solid state? *Crystal Growth & Design*, **2020**, *20*(12), 7997–8004.

endothermic signal (see Figure 3.2a) and only contains the diffraction peaks characteristic to xanthone (see Figure 3.2b).

There is a relatively narrow biphasic region in the phase diagram where physical (different ratio) mixtures of both limiting-composition solid solutions α and β are present. This is associated with an additional endothermic signal in the DSC curves indicating for the eutectic melting. In this case, the eutectic melting signals can be observed as small but pronounced shoulders with an onset of around 169 K (see Figure 3.2a). The mixture of two phases can also be noted in the PXRD patterns (see Figure 3.2b).

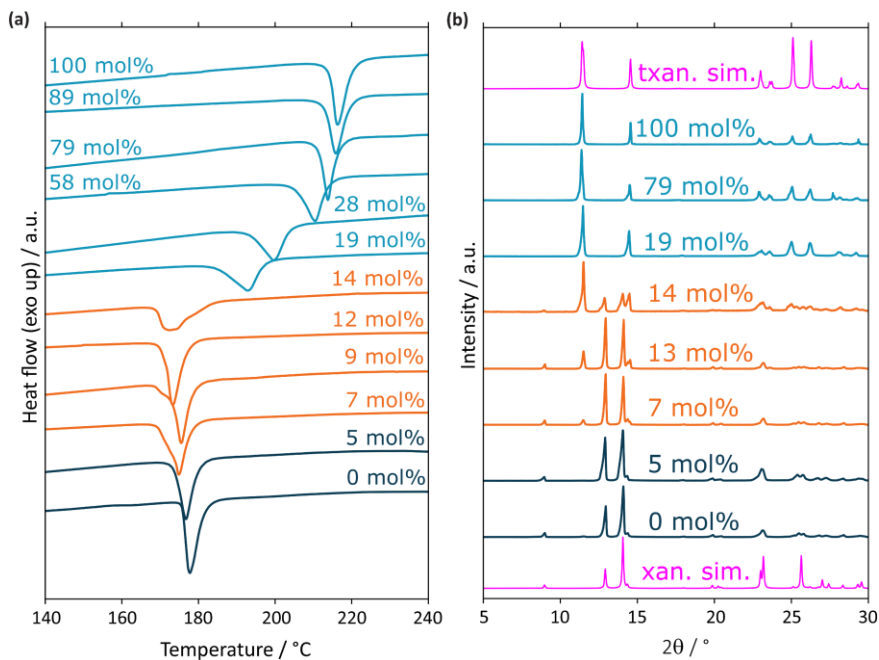


Figure 3.2. DSC curves (a) and PXRD patterns (b) of selected xanthone – thioxanthone compositions. The colour coding is identical to that used in Figure 3.1., the patterns simulated from the crystal structure data of pure components are shown in magenta (the indicated percentage refers to thioxanthone content).

The narrow biphasic region indicates that both molecules are discriminated in the solid state rather poorly. In composition ranges $>0 - 7$ mol% and $20 - <100$ mol% (thioxanthone), both kinds of molecules are incorporated in a single phase rather than a physical mixture of separate xanthone and thioxanthone phases forms. The large miscibility range difference between solid solutions α and β could be explained by the different sizes of S and O atoms. In solid solution α , it is apparently much more feasible to substitute the thioxanthone molecules by xanthone molecules because the O atom is considerably smaller than the S atom. Whereas for solid solution β , an ever-increasing fraction of xanthone molecules needs to be replaced by the large S atom-containing thioxanthone molecules to extend the composition range. Observed behaviour indicates that even though both studied molecules are highly similar and a large part of the composition range corresponds to solid solutions, at some limiting compositions the molecules are discriminated in the solid state as different building blocks.

The structure of xanthone has been reported in numerous studies, where mostly the compound has been shown to crystallize in the orthorhombic space group $P2_12_12_1$. The

PXRD patterns of the xanthone phases correspond to the $P2_12_12_1$ polymorph. Both xanthone polymorphs are very similar (see Figure 3.3.). The $P2_12_12_1$ polymorph⁴² crystallizes with a single molecule in the asymmetric unit ($Z' = 1$). The second polymorph discovered recently⁴³ can be considered as a monoclinic distortion ($\beta \approx 93^\circ$) of the first one. It is described in a subgroup of $P2_12_12_1$, namely, $P2_1$ with $Z' = 2$ to compensate for the loss of the two-fold screw axes.

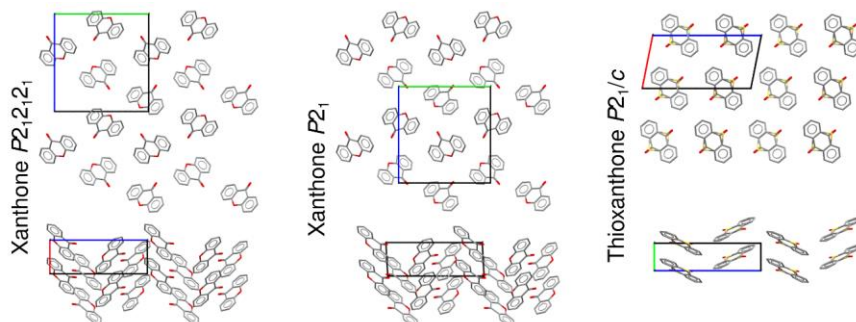


Figure 3.3. Crystal structure representations of the two known polymorphs of xanthone (left and middle)^{42,43} and that of thioxanthone (right).

The structure of thioxanthone has been solved and refined in the monoclinic space group $P2_1/c$. For this structure, disorder is present and thus a statistical (pseudo)inversion centre is created (see Figure 3.4a). The structure of the solid solution phase could be better described in $P2_1$. Nevertheless, the symmetry constraints for the atomic positions and the anisotropic displacement parameters corresponding to $P2_1/c$ were actually used. However, the occupancy for the inversely related disorder components was refined. It was found that a slight deviation from 0.5:0.5 occupancy ratio (and thus from the $P2_1/c$ symmetry) is, in fact, present. Especially concerning the minor solid solution component – xanthone molecule (see Figure 3.4b). The refined xanthone disorder component oxygen atom occupancies are 0.08 and 0.17, which is 1:2 as opposed to 1:1 that would be implied by the symmetry when choosing space group $P2_1/c$.

In spite of the great structural similarity of the xanthone and thioxanthone molecules, they pack differently in the crystalline state. This is in accordance with the obtained phase diagram. Were the structures of both components isostructural, a single continuous solid solution in the whole composition range would exist instead.

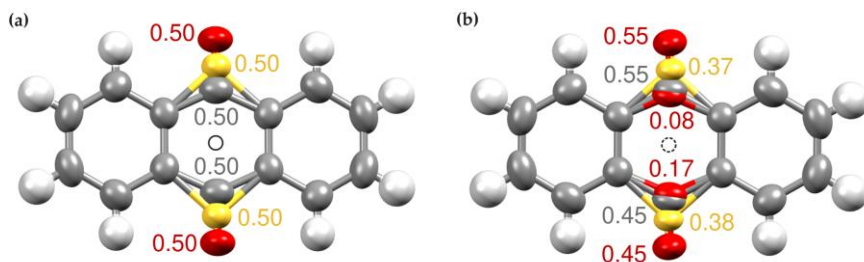


Figure 3.4. Molecular site representations of pure thioxanthone (a) and thioxanthone – xanthone [75 : 25 mol%] solid solution (b) crystal structures (the statistical (pseudo)inversion centre is denoted with an open circle).

Crystallographic data of the thioxanthone crystal and the crystal representing the solid solution (75 mol% thioxanthone) are given in Table 3.1.

Table 3.1.

Crystallographic data of the structure refinements (obs. reflections: [$F_{hkl}^2 > 3\sigma(F_{hkl}^2)$])

Crystal	Thioxanthone	Thioxanthone : Xanthone [75 : 25 mol%]
Crystal data		
<i>T</i> / K	301	301
Formula	C ₁₃ H ₈ SO	0.75 C ₁₃ H ₈ SO · 0.25 C ₁₃ H ₈ O ₂
Formula weight / g mol ⁻¹	212.3	208.2
Crystal system	Monoclinic	Monoclinic
Space group	<i>P</i> 2 ₁ / <i>c</i>	<i>P</i> 2 ₁
<i>a</i> / Å	7.8388(7)	7.8269(4)
<i>b</i> / Å	3.9891(2)	3.9933(2)
<i>c</i> / Å	15.8019(11)	15.7726(7)
β / °	101.199(7)	101.525(4)
<i>V</i> / Å ³	484.71(6)	483.02(4)
<i>Z</i> , <i>Z</i> '	2, 0.5	2, 1
<i>F</i> (000)	220	217
ρ_{calc} / g cm ⁻³	1.4544	1.4316
μ / mm ⁻¹	2.661	2.183
Meas. refl.	2455	1907
$[\sin(\theta)/\lambda]_{max}$ / Å ⁻¹	0.63	0.63
Unique refl.	1818	1755
Obs. refl.	1219	939
<i>R</i> _{int}	0.0294	0.0193
Refinement		
Refinement method	Full-matrix least-squares of <i>F</i> _{hkl}	
No. of parameters	83	89
<i>R</i> ₁ (obs.)	0.0413	0.0379
<i>wR</i> ₂ (all)	0.0513	0.0550

3.2. Formation of solid solutions of a substituted nitrobenzoic acids (2) two-component systems^B

The formation of solid solutions in binary systems formed by two nitrobenzoic acid derivatives of identical scaffolds differing only by the substituent (methyl group, hydroxyl group, or chlorine atom). The formation of solid solutions, i.e., the ability of compounds to replace each other in their pure-state crystal structures, was explored in all of the possible 12 binary systems (3 for each nitrobenzoic acid isomer). Binary mixtures containing different amounts of the selected compounds were crystallized and the solid solution formation was assessed by measuring the phase composition of the crystallization products using PXRD and constructing the two-component phase diagrams based on DSC measurements (see Figure 3.5.). Besides this, we also investigated the capability of computational calculations and crystal structure analysis to rationalize and predict the solid solution formation in the respective systems.

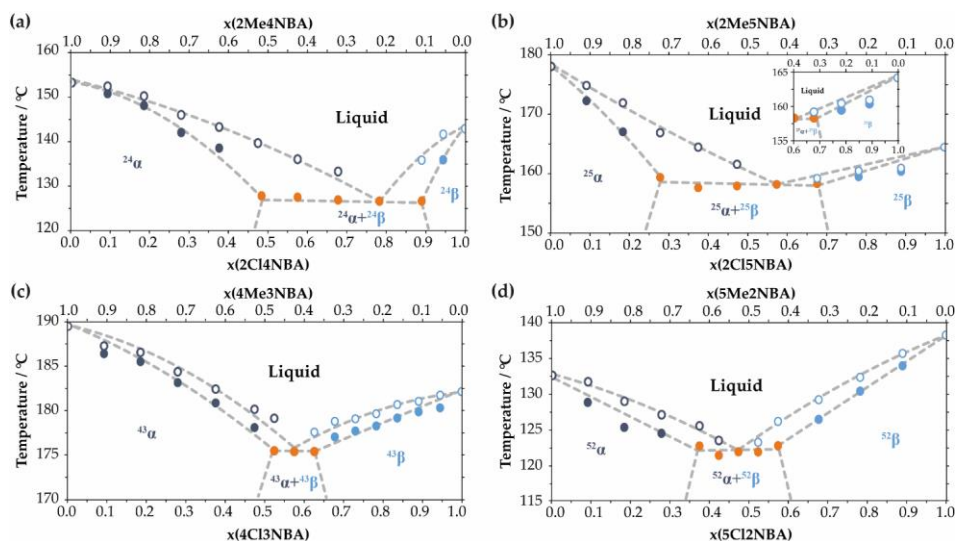


Figure 3.5. Melt phase diagrams of the binary systems: 2Me4NBA – 2Cl4NBA (a), 2Me5NBA – 2Cl5NBA (b), 4Me3NBA – 4Cl3NBA (c) and 5Me2NBA – 5Cl2NBA (d). Solid solutions and the corresponding single-component phases are in identical shades of blue, and phase mixtures are in orange (closed points represent – solidus / eutectic; open symbols indicate – liquidus; lines are present as guides for the eyes).

A continuous solid solution in all of the composition ranges does not form in any of these binary systems, but in all of the cases two different solid solutions close to the pure component region form instead, see Figure 3.5. Therefore, to some extent, all the methylnitrobenzoic acids dissolve in chloronitrobenzoic acids and *vice-versa*. These solid solutions are designated as α (methylnitrobenzoic acids with dissolved chloronitrobenzoic acids) and β (chloronitrobenzoic acids with dissolved methylnitrobenzoic acids), with indices in superscript indicating the position of methyl / chloro and nitro group. In all of the phase diagrams, there is a biphasic region where physical mixtures of both solid

^BSaršūns, K., Kons, A., Rekis, T., Bērziņš, A. Experimental and computational study of solid solution formed between substituted nitrobenzoic acids. *Crystal Growth & Design*, **2023**, 23(9), 6609–6622.

solutions with limiting compositions are present. This is clearly because the replaced functional groups are not of identical size and does not form identical intermolecular interactions, which results in these compounds to pack differently in the solid state and prevent full replacement of the molecules in these crystal structures. Summarized information on the ability of solid solutions to form in the previously analysed binary systems of methylnitrobenzoic acids and chloronitrobenzoic acids, as well as in the other analysed binary systems containing hydroxyl / chloronitrobenzoic acids and hydroxyl / methylnitrobenzoic acids is given in Figure 3.6.

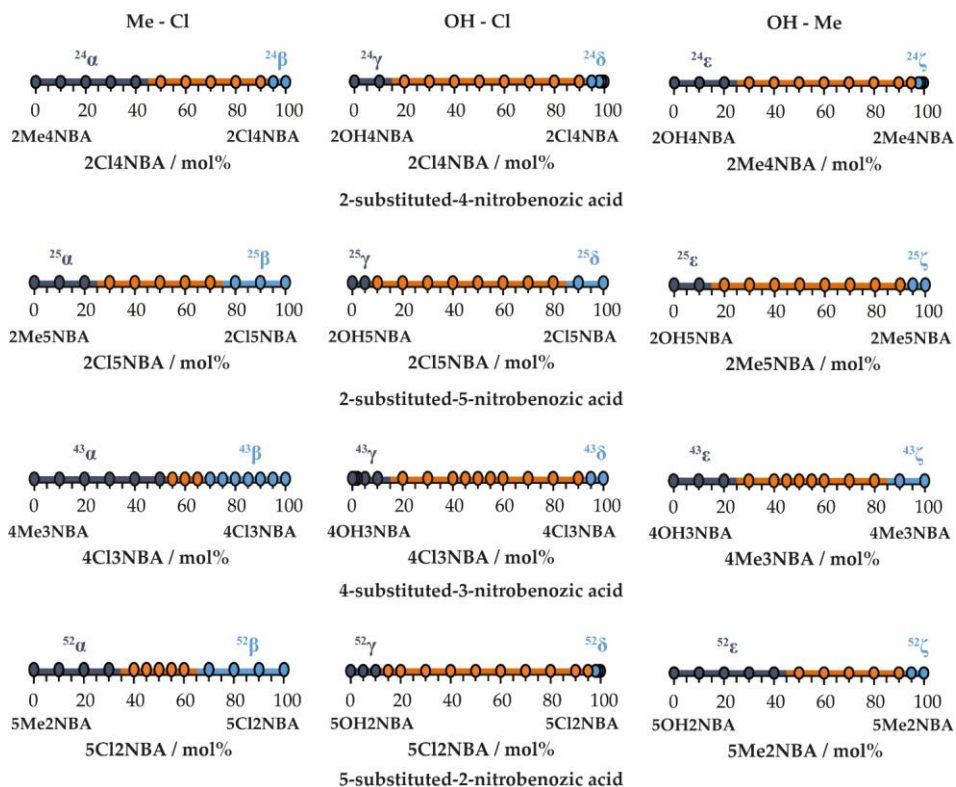


Figure 3.6. Phases obtained in the crystallization of binary mixtures of various substituted nitrobenzoic acids for several tested molar ratios (the colour coding is identical to that used in Figure 3.5.).

The findings in these additional binary systems confirm that the composition range in which the solid solutions can be obtained is different in each pair of nitrobenzoic acid isomers, again likely caused by the different crystal structures. It can be seen that in the crystallization of compositions containing primarily one of the components, a solid solution was obtained in all of the explored binary systems, and there was also always a biphasic region, confirming the limited solubility of these compounds in each other. The obtained solid solutions are designated as γ (hydroxynitrobenzoic acids with dissolved chloronitrobenzoic acids), δ (chloronitrobenzoic acids with dissolved hydroxynitrobenzoic acids), ϵ (hydroxynitrobenzoic acids with dissolved methylnitrobenzoic acids), and ζ (methylnitrobenzoic acids with dissolved hydroxynitrobenzoic acids), with indices in superscripts indicating position of the methyl / chloro / hydroxyl and nitro group. However, additional consideration of these systems

clearly demonstrates that not all of the functional groups can be equally easily replaced in the solid state. From Figure 3.6, it can be concluded that replacing methyl group-containing molecules by chloro-containing molecules (and *vice-versa*) can be done to approximately the same extent as replacing hydroxyl group-containing molecules by the methyl group-containing molecules (from around 10 to 40 mol%). Replacing hydroxyl group-containing molecules by the respective methyl group-containing molecules is only achievable up to around 10 mol%. The same holds for the binary systems with chloro-containing and hydroxyl group-containing molecules where no more than 10 mol% of the opposite component can be incorporated in any of the eight partial solid solutions. The comparison of the functional groups and their properties show that this is not surprising, as replacement of hydroxyl / methyl groups and chloro / hydroxyl group are associated with a larger change in the molecule size, as well as larger differences in the intermolecular interactions possibly formed by the molecules, if compared to changes introduced by replacement of methyl group and Cl. It is somewhat not obvious that the solubility of methyl group-containing molecules in hydroxyl group-containing molecules would be high in all of the systems. However, this could be because the methyl group can act as a donor of weak hydrogen bonds, and this could allow avoiding steep energy increase of the crystal structure by replacing these functional groups.

The crystal structures were investigated and tried to find whether crystallographic analysis and computational analysis of the energy associated with the molecule replacement could provide rationalization of the solid solution formation and in general could be used to predict the solid solution formation capability. Intermolecular interaction energy in the experimental crystal structures and the structures modelling solid solution (*Substituted*) and fully isostructural phase with complete molecule replacement (*Isostructural*) were analysed (see Table 3.2.).

Table 3.2.

Change of the sum of pairwise intermolecular interaction energy calculated in *CrystalExplorer* by the replacement of the functional group for the closest molecules (3.80 Å) to the replaced functional group and for the molecule pairs for which there are atoms within a 15 Å radius from the central molecule

Structure	2OH4NBA		2Cl4NBA		2Me4NBA	
	-Cl	-CH ₃	-OH	-CH ₃	-OH	-Cl
	<i>Change of E_{inter} for the closest molecules / kJ mol⁻¹</i>					
<i>Substituted</i>	+31.4	+16.9	+6.2	+1.9	-2.7	-3.5
<i>Isostructural</i>	+18.3	+2.1	+7.2	+4.3	+12.9	+10.6
	<i>Change of the sum of E_{inter} for the molecules within a 15 Å radius / kJ mol⁻¹</i>					
<i>Substituted</i>	+11.4	+2.9	+4.6	-5.0	+0.9	-0.9
<i>Isostructural</i>	+15.1	+0.9	+0.5	-7.6	-0.4	+0.6
Structure	2OH5NBA		2Cl5NBA		2Me5NBA	
	-Cl	-CH ₃	-OH	-CH ₃	-OH	-Cl
	<i>Change of E_{inter} for the closest molecules / kJ mol⁻¹</i>					
<i>Substituted</i>	+9.4	+11.0	+8.5	+1.1	+15.4	+12.0
<i>Isostructural</i>	+5.4	+9.1	+11.3	+3.6	+14.4	+17.8
	<i>Change of the sum of E_{inter} for the molecules within a 15 Å radius / kJ mol⁻¹</i>					
<i>Substituted</i>	+12.4	+11.4	+8.8	-2.1	+7.9	+7.6
<i>Isostructural</i>	+13.7	+10.9	+5.3	-2.2	+8.2	+13.0

Table 3.2. (Continued)

Structure	4OH3NBA		4Cl3NBA		4Me3NBA	
	-Cl	-CH ₃	-OH	-CH ₃	-OH	-Cl
	<i>Change of E_{Inter} for the closest molecules / kJ mol⁻¹</i>					
<i>Substituted</i>	+14.8	+9.4	-10.0	-9.2	+6.4	+6.1
<i>Isostructural</i>	+18.6	+6.9	-12.8	-19.5	+6.6	+4.4
	<i>Change of the sum of E_{Inter} for the molecules within a 15 Å radius / kJ mol⁻¹</i>					
<i>Substituted</i>	+1.3	-1.1	-6.1	-4.4	-1.3	+3.4
<i>Isostructural</i>	+1.8	-0.7	-23.5	-6.1	-11.8	+6.4
Structure	5OH2NBA		5Cl2NBA		5Me2NBA	
	-Cl	-CH ₃	-OH	-CH ₃	-OH	-Cl
	<i>Change of E_{Inter} for the closest molecules / kJ mol⁻¹</i>					
<i>Substituted</i>	+2.6	+0.6	-6.1	-4.4	+6.0	+23.9
<i>Isostructural</i>	+0.5	+4.7	-25.6	-14.9	+3.2	+15.7
	<i>Change of the sum of E_{Inter} for the molecules within a 15 Å radius / kJ mol⁻¹</i>					
<i>Substituted</i>	+14.9	+3.0	-5.0	-4.8	+8.2	+19.0
<i>Isostructural</i>	+20.2	+1.9	-21.1	-7.6	-6.7	+34.4

Firstly, evaluation of the weak intermolecular interactions formed by the group being replaced and the changes observed by the replacement in *substituted* and *isostructural* structures clearly demonstrated that in each of the crystals, the interactions formed and the changes occurring by the functional group replacement are different. Nevertheless, the change in the sum of the interactions between molecules adjacent to the replaced functional group is given in Table 3.2., could not be directly linked to the experimentally determined solubility limit in the respective molecule pair, as there were cases where the energy became more efficient. Secondly, a similar conclusion was observed also when the sum of the pairwise intermolecular interaction energies for the closest molecules within a 15 Å radius from the central molecule was calculated in *CrystalExplorer* (for *original* and *isostructural* structures being an approximation of lattice energy). Thirdly, additional views on the energy differences were obtained by analysing the interaction energy for molecule pairs formed by molecules for which there are atoms within a 3.80 Å radius from the central molecule. The plots of the difference of cumulative interaction energy from these molecule pairs with increasing distance between molecular centroids in *substituted* and *isostructural* structures and that in the *original* structure are given in Figure 3.7.

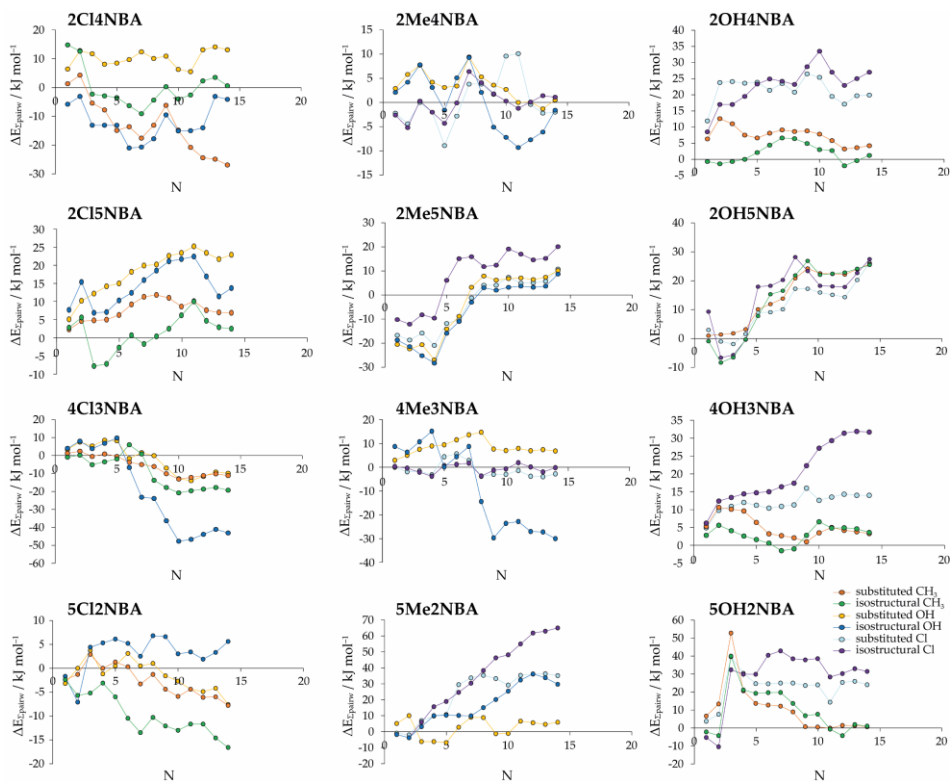


Figure 3.7. Difference in the cumulative interaction energy from the molecule pairs with increasing distance between molecular centroids between substituted and isostructural structures and that of the original structure plotted by increasing distance (N = molecule number).

In general, the energy should be compared with the alternative states available to the system of the given composition and may require an evaluation of the thermal and entropy effects. This is well demonstrated by comparison of the energy change associated with replacement of selected functional groups in all the isomers, as the replacement of the methyl group with Cl, which in the crystallization experiments allowed to obtain solid solutions with the highest achieved dissolution, in almost all the cases was calculated to be associated with energy increase, although no one particular cause could be detected in the analyses of intermolecular interactions in these structures and also, overall, by increasing the number of molecule pairs considered, the energy tends to converge to the result representing the total energy of all molecule pairs for which there are atoms within a 15 Å radius from the central molecule, as shown in Table 3.2., although for some of the structures larger number of molecules appeared to be necessary to be included in the summation to approach this value.

3.3. Formation of solid solutions of the benperidol – droperidol (3) two-component system^C

The formation of solid solutions between two active pharmaceutical ingredients, benperidol and droperidol has been explored by comparing the formation of solid solutions in non-solvated forms as well as in several solvates of these compounds. To evaluate the formation of a solid solution between droperidol and benperidol in different phases, crystallization from a solution of mixtures of both compounds in different ratios was carried out. Several different crystallization conditions to obtain different solid phases – non-solvated forms (in the selected conditions polymorphs **B^I** or **B^{II}** could be obtained for benperidol and polymorph **D^{II}** for droperidol), dihydrates as well as ethanol, methanol, and acetonitrile solvates.

The solid products obtained in the crystallization, summarized in Table 3.3., were characterized by PXRD and DSC/TG. The employed crystallization procedure always resulted in the formation of the phase or phases with the desired composition, as non-solvated phase or phases (**B^I**, **B^{II}**, and **D^{II}**) were obtained from isopropanol, dihydrate or dihydrates (**B^{DH}** and **D^{DH}**) from acetone/water and the respective solvate or solvates from the organic solvents (**B^{SEtOH}** and **D^{SEtOH}** from ethanol, **B^{SMeOH}** and **D^{SMeOH}** from methanol and **B^{SACN}** and **D^{SACN}** from acetonitrile). In most of the cases crystallization of a mixture of droperidol and benperidol produced only a single phase, meaning that a solid solution containing both components in the respective crystal structure formed.

The results clearly show that the ability of replacing one molecule with the other strongly depends on the crystal structure, including even different capability to accommodate the other molecules by the isostructural solvate series **D^{SEtOH}**, **D^{SMeOH}** and **D^{SACN}** and by **B^{SEtOH}** and **B^{SMeOH}**.

Table 3.3.

Phases obtained in crystallization of a mixture of benperidol and droperidol for several selected molar ratios*

Benperidol / mol%	Obtained phase				
	Nonsolvate	Ethanol solvate	Methanol solvate	Acetonitrile solvate	Dihydrate
0	D^{II}	D^{SEtOH}	D^{SMeOH}	D^{SACN}	D^{DH}
5	D^{II}+SS^{B^{II}}	D^{SEtOH}+SS^{B^{II}}	SS^{D^{II}}	SS^{D^{II}}	SS^{D^{II}}
10	SS^{B^{II}}	SS^{B^{II}}	SS^{B^{II}}	SS^{B^{II}}	SS^{B^{II}}
20	SS^{B^{II}}	SS^{B^{II}}	SS^{D^{II}}	SS^{B^{II}}	SS^{D^{II}}
30	SS^{B^{II}}	SS^{B^{II}}	SS^{D^{II}}	SS^{D^{II}}	SS^{D^{II}}
40	SS^{B^{II}}	SS^{B^{II}}	SS^{D^{II}}	SS^{D^{II}}	SS^{D^{II}}
50	SS^{B^{II}}	SS^{B^{II}}	SS^{B^{II}}	SS^{D^{II}}	SS^{D^{II}}
60	SS^{B^{II}}	SS^{B^{II}}	SS^{B^{II}}	SS^{D^{II}}	SS^{D^{II}}
70	SS^{B^{II}}	SS^{B^{II}}	SS^{B^{II}}	SS^{D^{II}}	SS^{B^{II}}
80	SS^{B^{II}}	SS^{B^{II}}	SS^{B^{II}}	SS^{B^{II}}	SS^{B^{II}}

^CSaršūns, K., Bērziņš, A. Experimental and computational investigation of benperidol and droperidol solid solutions in different crystal structures. *Crystal Growth & Design*, 2023, 23(2), 1133–1144.

Table 3.3. (Continued)

90	SS^{BII}	SS^{BS_{EIOH}}	SS^{BS_{MeOH}}	SS^{BS_{ACN}}	SS^{BDH}
100	B^I	B^{SEIOH}	B^{SMeOH}	B^{SACN}	B^{DH}

* – **SS** designates a solid solution with a crystal structure of the respective phase. Pure phases are in bold, and phase mixtures are in italic.

This appears both as a different limit up to which the replacement is possible as well as even a completely different ability of one molecule to replace the other. For example, no ability of benperidol to replace droperidol was detected in the non-solvated phase **DII** and the ethanol solvate **B^{SEIOH}**, whereas the replacement of benperidol with droperidol in ethanol solvate **B^{SEIOH}** and non-solvated phase **B^{II}** was achieved even up to a state close to a complete substitution, as solid solutions where 90 mol% of the benperidol molecules were replaced were obtained, see PXRD patterns in Figure 3.8. These solid solutions are designated as **SS^{BS_{EIOH}}** and **SS^{BII}**, respectively.

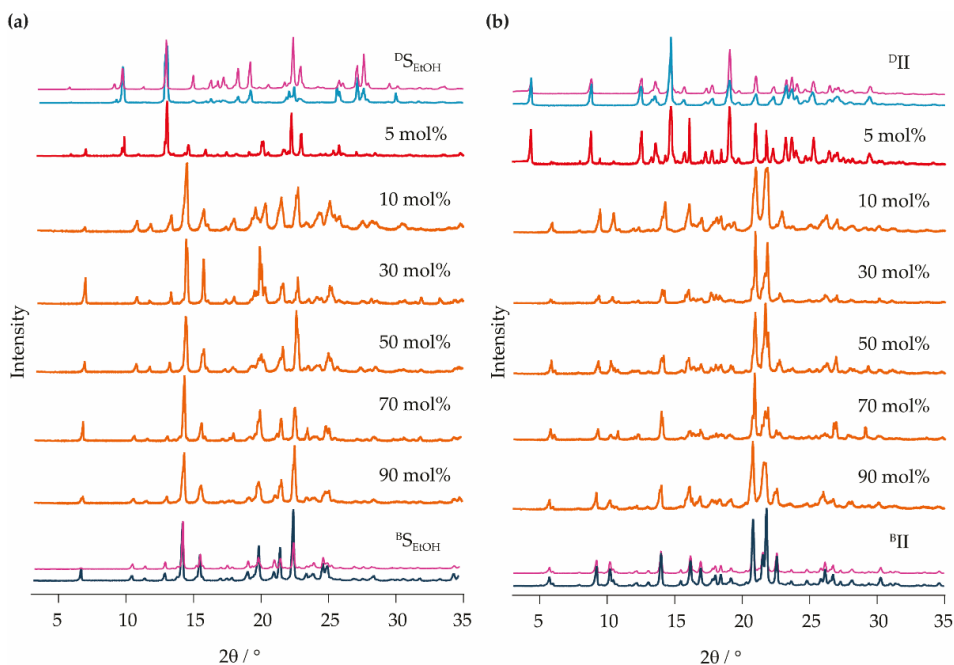


Figure 3.8. PXRD patterns of crystallization products when different ratios of benperidol and droperidol were crystallized from ethanol (a), by obtaining the ethanol solvate phase / phases and isopropanol (b), by obtaining non-solvated phase / phases. Solid solutions are in orange, the corresponding single-component phases are in blue, phase mixtures are in red, and the patterns simulated from the crystal structure data of pure components are shown in magenta (labels show the weighted molar fraction of benperidol used in the crystallization).

All of the samples obtained in the crystallization were additionally characterized by DSC/TG analysis and solvated phases were desolvated, the obtained desolvation products were characterized using PXRD for phase identification and DSC/TG analysis for thermal characterization.

In all the DSC curves of non-solvated solid solution SS^{BII} samples the melting endotherm is consistent with an essentially monophasic sample (see Figure 3.9b). Across the composition range from 90 mol% down to 10 mol% benperidol, the onset and the peak temperature decrease monotonically as the amount of droperidol in the solid solution increases, consistent with the presence of a single solid solution phase in these samples, with the melting point between that of benperidol polymorph BII ($T_{melt} = 165\text{ }^{\circ}\text{C}$) and droperidol polymorph DII ($T_{melt} = 151\text{ }^{\circ}\text{C}$), see the phase diagram constructed from these data in Figure 3.10. A discontinuity in the melting behaviour is observed for 5 mol% benperidol, as the sample contains a mixture of solid solution SS^{BII} and droperidol phase DII .

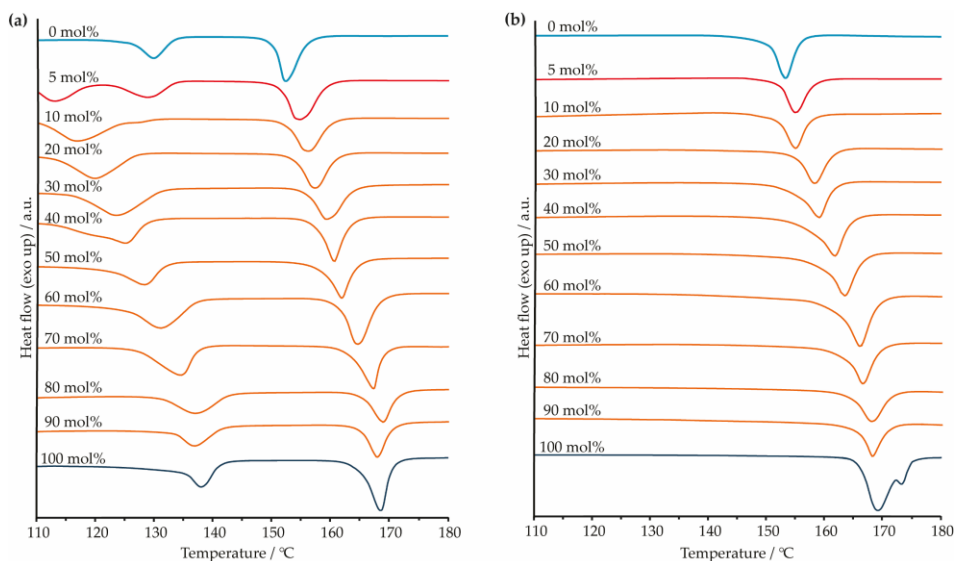


Figure 3.9. DSC curves for the solvated solid solution $SS^{B_{EtOH}}$ (a), obtained in the crystallization from ethanol along with DSC curves of droperidol ethanol solvate D_{EtOH} and benperidol ethanol solvate B_{EtOH} and the non-solvated solid solution SS^{BII} (b), obtained in the crystallization from isopropanol, along with DSC curves of droperidol DII and benperidol BII . The colour coding is identical to that used in Figure 3.8. (labels show the weighted molar fraction of benperidol used in the crystallization).

The DSC curves of the solvated solid solution $SS^{B_{EtOH}}$ (see Figure 3.9a) showed that a single desolvation peak is present across the composition range starting from pure benperidol to 10 mol% benperidol, and the desolvation temperature decreases monotonically as the amount of droperidol in the solid solution increases, consistent with the presence of a single solid solution phase in these samples. In contrast, two desolvation peaks are present for the sample with 5 mol% benperidol, which agrees with the presence of two solvated phases. A similar monotonic decrease of the desolvation temperature by increasing the amount of droperidol in the solid solution was observed also for the solvated solid solution $SS^{B_{MeOH}}$, and a tendency for the desolvation temperature to decrease by increasing the amount of the compound replacing the original compound was observed also for other solvated solid solutions. Besides, the melting peak of the obtained desolvation product of $SS^{B_{EtOH}}$ and in most cases also that obtained from the other solvated samples decreased monotonically over the whole composition range by increasing the amount of droperidol in the sample. To fully understand this monotonic

decrease over the whole composition range, solvated samples obtained in the crystallization were desolvated and characterized.

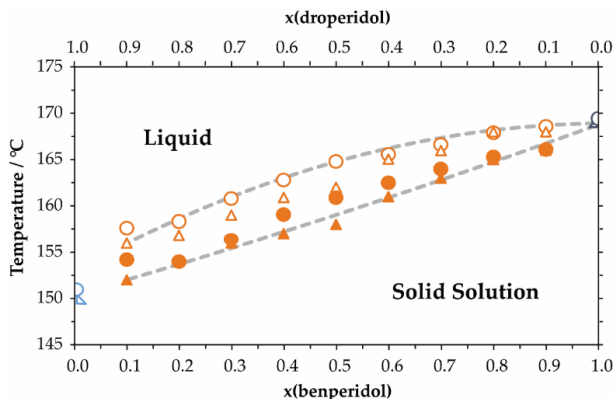


Figure 3.10. Part of a melt-phase diagram of benperidol – droperidol binary system. The circles correspond to data from samples obtained in the crystallization from isopropanol, and the triangles correspond to the data measured for samples obtained in the desolvation of ethanol solvate samples and illustrate the agreement with the thermal characteristics of samples obtained in the crystallization. The colour coding is identical to that used in Figure 3.8. and 3.9. (closed points represent – solidus; open symbols indicate – liquidus; lines are present as guides for the eyes).

By heating the solvated samples obtained in the crystallization experiments a desolvated product always formed prior to the physical melting of the sample. Interestingly, the desolvation product is not dependent on the phase composition of the solvated sample being desolvated. The desolvation product of the only solvated solid solution existing in nearly the whole composition range, $SS^B S_{EtOH}$, always was the non-solvated solid solution $SS^B II$. This is consistent with the main desolvation product of pure benperidol ethanol solvate $B S_{EtOH}$ being polymorph $B II$. Moreover, the non-solvated solid solution $SS^B II$ was obtained as the only desolvation product also by desolvating almost all the samples obtained from methanol, acetonitrile, and acetone/water regardless of whether the sample contained solid solution having the structure of the original benperidol solvate, a solid solution having the structure of the original droperidol solvate or even the mixture thereof. This was confirmed both by the PXRD patterns (see Figure 3.11. for PXRD patterns recorded for the desolvation products of dihydrate samples) of the desolvated samples as well as by their DSC curves in which the melting endotherm was consistent with an essentially monophasic sample with the melting onset and peak temperatures matching that of $SS^B II$ having identical component composition.

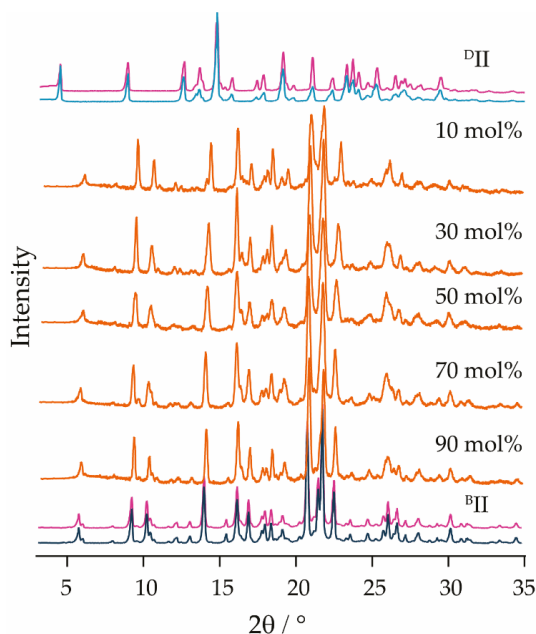


Figure 3.11. PXRD patterns of desolvation products of dihydrate samples obtained using different ratios of benperidol and droperidol in the crystallization Solid solutions in orange, the corresponding single-component phases are in blue, and the patterns simulated from the crystal structure data of pure components are shown in magenta (labels show the weighted molar fraction of benperidol used in the crystallization).

Furthermore, the main focus was on the evaluation of structural and energy-related aspects for the formation of solid solutions by replacing part of the original molecules in the crystal structure with the molecules of the second compound. Intermolecular interaction energy for three sets (*original*, *substituted*, and *isostructural*) of structures was calculated using *Quantum ESPRESSO*. The obtained data are presented in Table 3.4. Overall, the replacement of one of the molecules is always associated with an energy increase, which is the smallest for $^{\text{B}}\text{II}$, $^{\text{B}}\text{S}_{\text{MeOH}}$, and $^{\text{B}}\text{S}_{\text{EtOH}}$. However, full replacement of all the benperidol molecules with droperidol results in more efficient interactions in most of the structures, with the highest decrease of interaction energy calculated for $^{\text{B}}\text{S}_{\text{EtOH}}$. In contrast, the replacement of droperidol molecules with benperidol always results in less efficient interactions. These results confirm that the interaction energy is an important factor in determining the molecule replacement capability in different structures and predict the existence of a solid solution in $^{\text{B}}\text{S}_{\text{EtOH}}$ structure, although the facile formation of $^{\text{B}}\text{II}$ and the relatively narrow concentration range for $^{\text{B}}\text{S}_{\text{ACN}}$ is not predicted by these results.

Table 3.4.

Intermolecular interaction energy in original benperidol and droperidol crystal structures (in kJ per mole of benperidol or droperidol) and energy change when one or all molecules in the unit cell are replaced. For structures with $Z' > 1$ the change of E_{inter} in substituted structures is the average value from structures where the symmetry different molecules were replaced

Structure	^B II	^B S _{EtOH}	^B S _{MeOH}	^B S _{ACN}	^B DH
<i>E_{inter} of benperidol structures / kJ mol⁻¹</i>					
<i>Original</i>	-244.7	-331.6	-318.2	-288.4	-404.7
<i>Change of E_{inter} by insertion of droperidol / kJ mol⁻¹</i>					
<i>Substituted</i>	+2.9	+3.6	+3.0	+5.2	+7.8
<i>Isostructural</i>	-0.7	-5.4	-1.8	-3.6	+5.4
Structure	^D II	^D S _{EtOH}	^D S _{MeOH}	^D S _{ACN}	^D DH
<i>E_{inter} of droperidol structures / kJ mol⁻¹</i>					
<i>Original</i>	-237.3	-284.4	-281.0	-275.3	-403.5
<i>Change of E_{inter} by insertion of benperidol / kJ mol⁻¹</i>					
<i>Substituted</i>	+5.4	+5.5	+6.3	+4.4	+4.2
<i>Isostructural</i>	+5.3	+7.4	+8.0	+7.6	+9.6

To identify the cause of the observed change of intermolecular interaction energy by molecule replacement also calculated pairwise intermolecular interaction energies for the closest molecules for all three sets of structures in *CrystalExplorer*. Firstly, the effect of molecule replacement on the hydrogen bond interaction strength was evaluated. Secondly, the effect of molecule replacement on the interaction energy for molecule pairs forming the strongest dispersion interactions was evaluated (see Table 3.5.).

Table 3.5.

The relative average intermolecular interaction energy (in kJ mol⁻¹) with respect to that in the original structures for molecule pairs forming the strongest dispersion interactions

Structure	^B II	^B S _{EtOH}	^B S _{MeOH}	^B S _{ACN}	^B DH
<i>Substituted</i>	+0.6	-0.7	+0.6	+0.4	+2.1
<i>Isostructural</i>	-0.2	-1.0	-0.1	-0.6	+3.6
Structure	^D II	^D S _{EtOH}	^D S _{MeOH}	^D S _{ACN}	^D DH
<i>Substituted</i>	+1.5	+0.5	+0.8	+0.4	-0.1
<i>Isostructural</i>	+2.6	+1.9	+1.8	+2.0	0.0

Finally, a more comprehensive view of the energy differences was presented by analysing the interaction energy for all molecule pairs formed by molecules for which atoms within a 3.80 Å radius from the central molecule are present. Using these values, cumulative interaction energy was calculated from the molecule pairs with increasing distance between molecular centroids and plotted the difference between this energy in *substituted* and *isostructural* structures and that in the *original* structure. Selected plots are given in Figure 3.12.

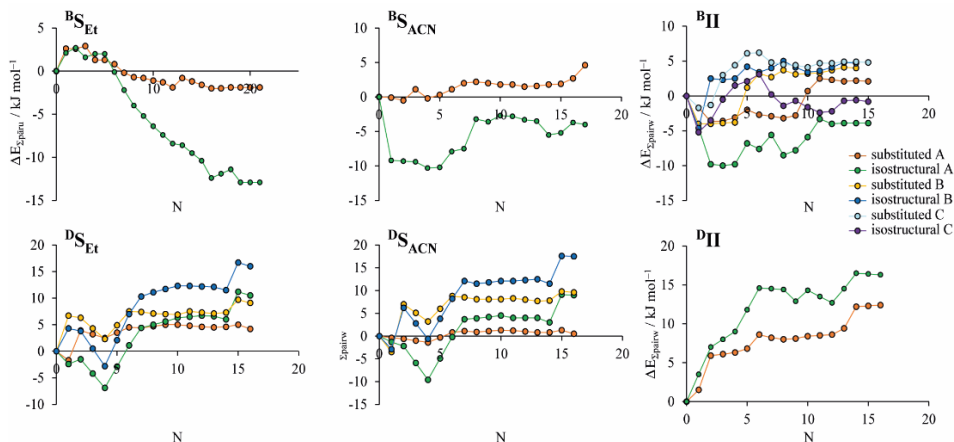


Figure 3.12. Difference in the cumulative energy of the molecule pairs with increasing distance between molecular centroids between substituted and isostructural structures and that in the original structure plotted by increasing distance (N = molecule number).

Taking into account the differences in phase composition between the considered structures, the analysis of the intermolecular interaction energies suggests that in this system solid solutions are more easily formed in single component phases, as a solid solution over a wide composition range can experimentally be obtained if the molecule replacement maintains the same interaction efficiency as in the *original* structure, whereas for solvated phases formation of solid solution over a wide composition range requires notably favourable interactions if compared to the *original* structure.

3.4. Formation of solid solutions of a various thioxanthone halogen derivatives (4) two-component systems^{D,E}

3.4.1. In a two-component system containing iodine and chlorine derivatives^D

In comparison to compounds from the previous sections, halogenated thioxanthenes are organic luminophores at room temperature. However, in spite of molecule similarity, Cl-TX and I-TX have different molecular packings (see Figure 3.13.)⁴¹

^DSaršūns, K., Ķemere, M., Karziņins, A., Kļimenkovs, I., Bērziņš, A., Sarakovskis, A., Rekis, T. Fine-tuning solid state luminescence properties of organic crystals *via* solid solution formation: the example of 4-iodothioxanthone – 4-chlorothioxanthone system. *Crystal Growth & Design*, **2022**, 22(8), 4838–4844.

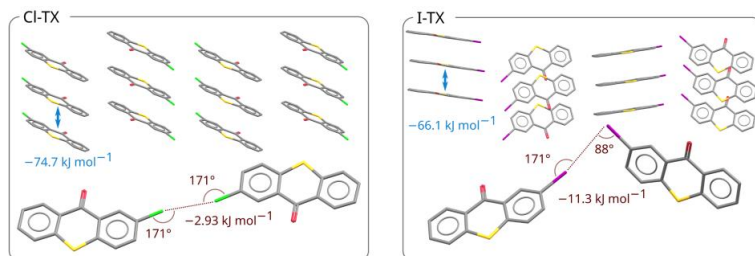


Figure 3.13. Representation of the molecular packing and respective halogen bonding in Cl-TX (left) and I-TX (right).

Considering that both molecules are aromatic and flat, there are $\pi \cdots \pi$ interactions present between the stacked molecules. It is important to note that in both structures also another energetically favourable interaction is present, namely, the halogen bonding. Furthermore, it is often neglected when analysing molecular-level factors responsible for luminescence effects.

This type of interaction is highly directional and both packings display different geometry of halogen \cdots halogen-site contacts corresponding to criteria for efficient interactions in each case⁴⁴ (see Figure 3.13.). Also, interaction energy was calculated between the respective halogen-bonded molecules, computed in *Gaussian09*, and it is $-2.93 \text{ kJ}\cdot\text{mol}^{-1}$ and $-11.3 \text{ kJ}\cdot\text{mol}^{-1}$ for the Cl \cdots Cl bonded and I \cdots I bonded pairs, respectively. While the $\pi \cdots \pi$ interactions are very efficient in both cases, the halogen bonding can be considered an important contribution into the stabilization of the crystal packing, especially for I-TX.

In this case, a melt phase diagram shows that solid state miscibility is present for this system, i.e., there are two limited-solubility solid solutions formed based on the structures of pure Cl-TX and I-TX phases, respectively (see Figure 3.14.).

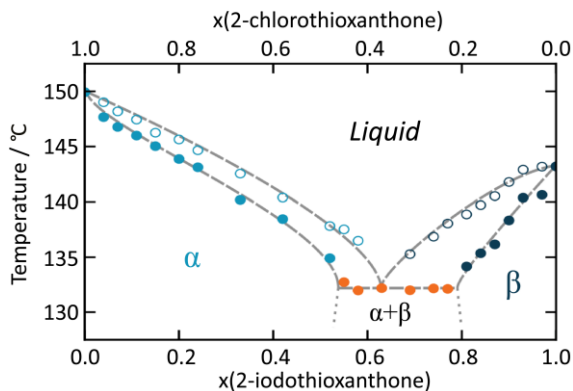


Figure 3.14. Melt phase diagram of Cl-TX – I-TX binary system. Solid solutions and the corresponding single-component phases are in identical shades of blue, and phase mixtures are in orange (closed points represent – solidus / eutectic; open symbols indicate – liquidus; lines are present as guides for the eyes).

The structure of Cl-TX can accommodate up to around 50 mol% of I-TX (solid solution α). Similarly, a solid solution that is based on the I-TX structure forms for compositions with up to around 20 mol% of Cl-TX (solid solution β). In the remaining composition range, a thermodynamically stable system is a physical mixture of both solid solutions α and β with the respective limiting compositions. In Figure 3.15a, DSC curves based on which the binary melt phase diagram was construed are depicted.

When the opposite component is introduced in the crystal structure of a pure compound, it intrinsically leads to a disordered phase (hence the name solid solution) and consequently some minor structural changes are induced, *e.g.*, deviations of the lattice parameters. These effects are reflected in the PXRD patterns (see Figure 3.15b for selected samples). Peak positions and intensities vary in different composition samples of the same solid solution. For the compositions covering the biphasic region the characteristic peaks of both solid solutions can be observed.

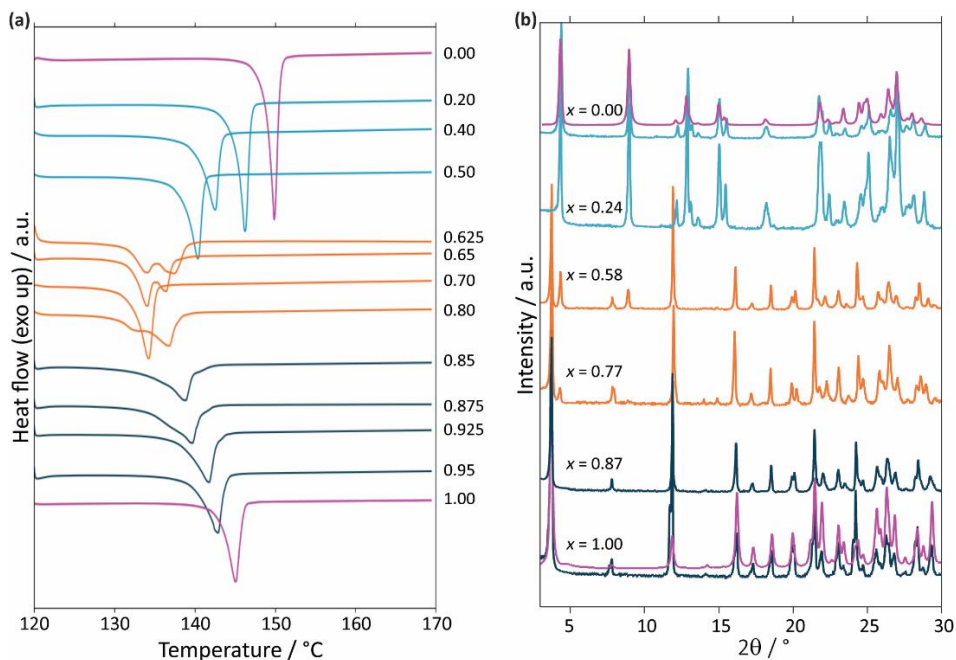


Figure 3.15. DSC curves (a) and PXRD patterns (b) of selected Cl-TX – I-TX composition samples. The colour coding is identical to that used in Figure 3.14., the patterns simulated from the crystal structure data of pure components are shown in magenta (the indicated mole fraction refers to I-TX).

Solid solution α is based on the Cl-TX structure, the luminescence spectrum of pure Cl-TX represents a band with a maximum intensity of around 600 nm. The excitation spectrum for this band contains three maxima at 330 nm, 420 nm, 490 nm, and a small shoulder at around 390 nm (see Figure 3.16a). This is consistent with the reported results on the luminescence properties of Cl-TX powders. There, the main band was attributed to phosphorescence, while the weak intensity shoulder at around 450 nm was attributed to fluorescence⁴¹. In solid solution α as many as around half of the Cl-TX molecules can be exchanged by I-TX. Although the accessible composition range is wide, the excitation-emission maps change rather insignificantly. For the luminescence band at 600 nm, there is a red-shifted shoulder present in the map of Cl-TX : I-TX composition of 0.50 : 0.50

(see Figure 3.16b). Furthermore, the excitation maximum at 490 nm is equally intense as the maximum at 330 nm and 420 nm.

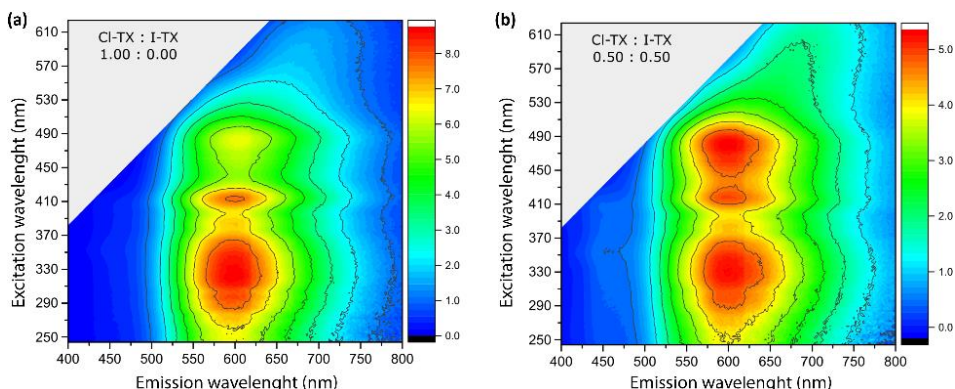


Figure 3.16. Room temperature excitation-emission luminescence maps of solid solution α at two compositions (a) and (b).

Finally, the fluorescence band at 450 nm is much more pronounced (see Figure 3.17a). The data show that in this particular case, the halogen atom type has no major influence on the photoluminescence mechanism. Apparently, the minor difference in the electronic structure of both molecules and interplanar spacing variation in the crystalline state induced when part of the original Cl-TX molecules are exchanged by I-TX molecules do not result in a significant alteration of the luminescence spectral characteristics. New emission bands are introduced with maxima at lower wavelengths. In the emission spectra at $\lambda_{\text{ex}} = 330$ nm given in Figure 3.17b, this can be observed even more clearly. Further replacement of I-TX by Cl-TX induces changes in the relative intensity between the fluorescence and phosphorescence bands.

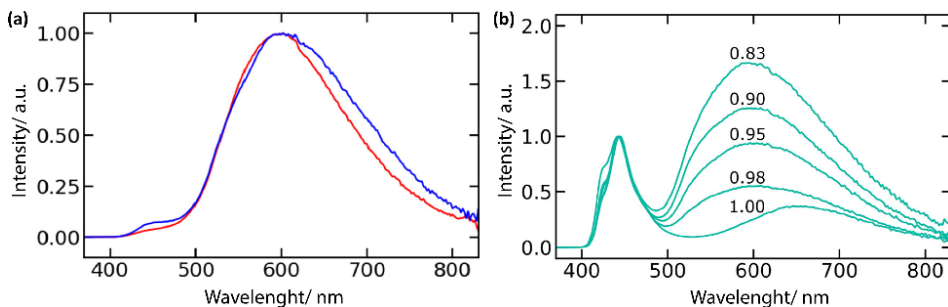


Figure 3.17. Room temperature photoluminescence spectra ($\lambda_{\text{ex}} = 330$ nm) of solid solution α (a) at two Cl-TX : I-TX compositions: 1.00 : 0.00 (red); 0.50 : 0.50 (blue), and solid solution β (b) at five Cl-TX : I-TX ratios.

It is important to note that the solid solution spectra are significantly different from those of the physical mixtures of pure phases in the same ratios (see Figure 3.18.).

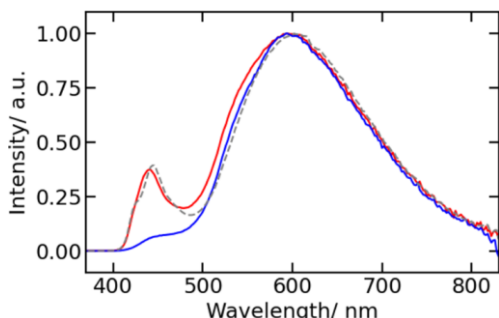


Figure 3.18. Room temperature photoluminescence spectra ($\lambda_{\text{ex}} = 330 \text{ nm}$) of: 1) 0.40 : 0.60 (I-TX : Cl-TX) mechanical mixture (red); 2) linear combination of I-TX and Cl-TX spectra scaled 0.40 : 0.60 (dashed grey); 3) 0.40 : 0.60 (I-TX : Cl-TX) solid solution (blue).

Solid solution β is based on the I-TX structure and it exists in a considerably narrower composition range than solid solution α . Only up to around 20 mol% of the I-TX molecules can be exchanged by Cl-TX, until the solubility limit is reached. However, in this case, even a few mol% of the opposite component has a major effect on the luminescence spectral properties. In Figure 3.19a, an excitation-emission luminescence map of pure I-TX in powdered form is depicted. It features an intense band with a maximum at 445 nm that was attributed to fluorescence⁴¹. The phosphorescence bands of pure I-TX are weak, but they change when Cl-TX molecules are introduced in the crystal structure. Only 2 mol% of Cl-TX significantly changes the map characteristics (see Figure 3.19. (b) – (d)).

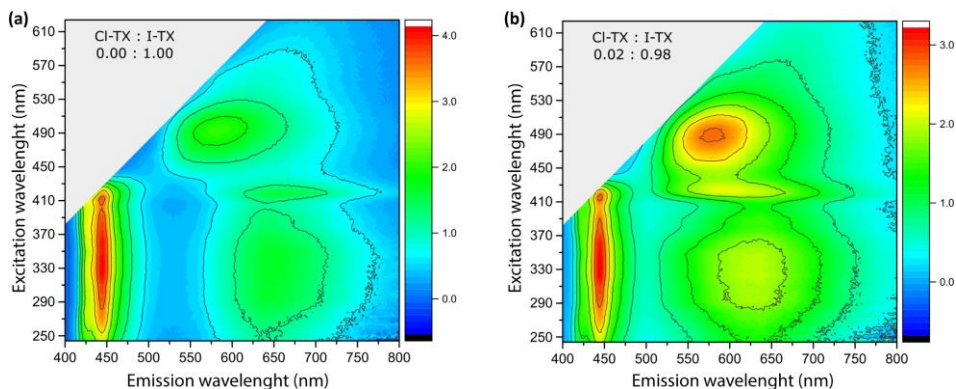


Figure 3.19. Room temperature excitation-emission luminescence maps of solid solution β at four compositions (a) – (d).

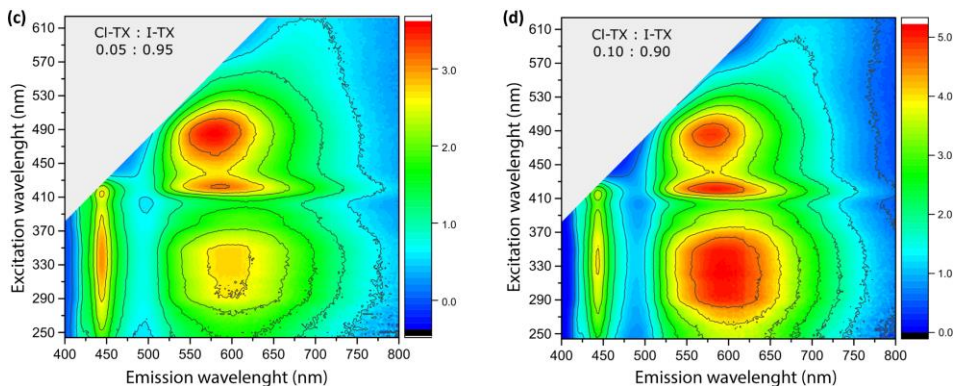


Figure 3.19. (Continued).

Taking this into account, the pronounced phosphorescence effect caused by the increase of CI-TX content in the I-TX matrix is related to the halogen bonding, i.e., this bonding is directly responsible for the phosphorescence mechanism in solid solution β . Due to relative intensity changes of the spectral bands, there is a variation of the luminescence colour. In Figure 3.20, a CIE chromaticity diagram is depicted for several solid solutions β (and α) compositions.

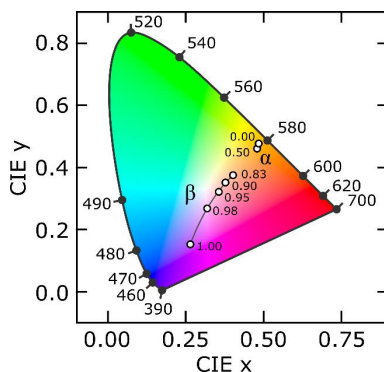


Figure 3.20. CIE chromaticity diagram of several compositions of β and α solid solutions calculated from emission spectra excited at $\lambda_{\text{ex}} = 330$ nm (room temperature).

For solid solution α there is almost no difference in the luminescence colour even if half of the original CI-TX molecules are exchanged by I-TX molecules in the crystal structure. Meanwhile, the colour has a strong composition dependence in solid solution β . Within 17 mol% of CI-TX content, there is a large variation across the CIE space. The luminescence colour can therefore be finely tuned by varying the solid solution composition.

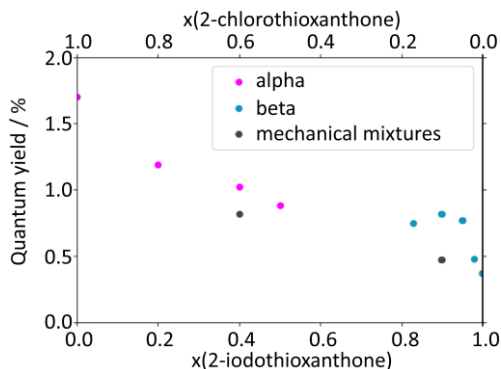


Figure 3.21. Absolute photoluminescence quantum yields of Cl-TX – I-TX solid solutions and mechanical mixtures.

The absolute photoluminescence quantum yield (Φ) dependence on the solid solution composition is depicted in Figure 3.21. For pure Cl-TX, the quantum yield is 1.7 %. It decreases to 0.88 % as the 0.50 : 0.50 (I-TX – Cl-TX) composition is reached. For solid solution β , the quantum yield increases with increasing Cl-TX content from 0.37 % to ~0.80 %.

3.4.2. In two-component systems containing iodine, chlorine, bromine and fluorine derivatives^E

As reported in the previous section, where solid solutions with fine-tunable photoluminescence have been obtained in binary systems which contain iodothioxanthone and chlorothioxanthone molecules, it was decided to check whether other thioxanthone derivatives, i.e., both named compounds with bromothioxanthone and fluorothioxanthone, can also form solid solutions with fine-tunable properties. There are several polymorphs of pure compounds, the structures of which are known from literature data⁴¹: chlorothioxanthone I (*P-1*) **D**_{Cl}, bromothioxanthone I (*P-1*) **D**_{Br}, and iodothioxanthone I (*P2₁2₁2₁*) **E**_I, the structures were determined within the scope of this study from: single-crystal diffraction data – fluorothioxanthone I (*P2₁/n*) **A**_F, II (*P2₁2₁2₁*) **B**_F, III (*Pc*) **C**_F and chlorothioxanthone III (*Pna2₁*) **F**_{Cl}, powder X-ray diffraction data – chlorothioxanthone II (*P2₁2₁2₁*) **E**_{Cl}. As concluded from the results of PXRD analysis (see Figure 3.22.), the Br-TXANT (I form) molecule is isostructural with Cl-TXANT (I form) – Figure 3.22d, and their crystals are isomorphous⁴¹. A continuous solid solution in all the composition ranges forms between Br-TXANT and Cl-TXANT molecules, but in other cases two different solid solutions close to the pure component region form instead (see Figure 3.23.).

^ESaršūns, K., Kons, A., Leduskrasts, K., Kļimenkovs, I., Bērziņš, A., Rekis, T. Modulation of physico-chemical properties via solid solution formation of thioxanthone derivatives. *Manuscript in process of development*.

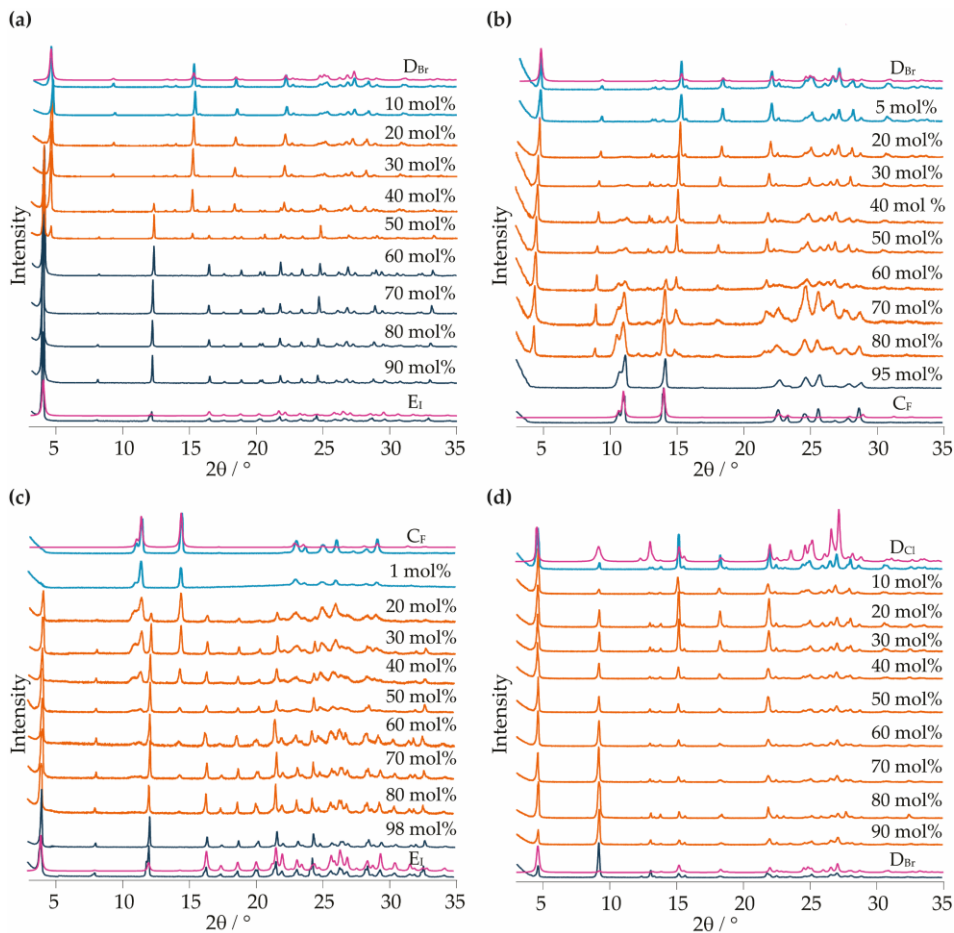


Figure 3.22. PXRD patterns of crystallization products obtained in crystallization of different ratios of thioxanthone derivatives: (a) I-TXANT – Br-TXANT, (b) F-TXANT – Br-TXANT, (c) I-TXANT – F-TXANT and (d) Br-TXANT – Cl-TXANT from acetonitrile. PXRD patterns of solid solutions and the corresponding single component phases are in identical shades of blue, phase mixtures are in orange, and the patterns simulated from the crystal structure data of pure components are shown in magenta (the indicated mole fraction refers to I-TXANT (a) and (c), F-TXANT (b) and Br-TXANT (d)).

The narrow biphasic region implies that the solid-state distinction of both molecules is not particularly effective – Figure 3.23a, in composition ranges $>0 - 20$ mol% and $50 - <100$ mol% (2-iodothioxanthone), Figure 3.23b, in composition ranges $>0 - 5$ mol% and $90 - <100$ mol% (2-bromothioxanthone), Figure 3.23c, in composition ranges $0 - <5$ mol% and $98 - <100$ mol% (2-fluorothioxanthone) – and they are discriminated in the solid state rather poorly, except for 2-bromothioxanthone and 2-chlorothioxanthone, Figure 3.23d, where the solubility of substances is unlimited in whole composition range ($0 - 100$ mol%).

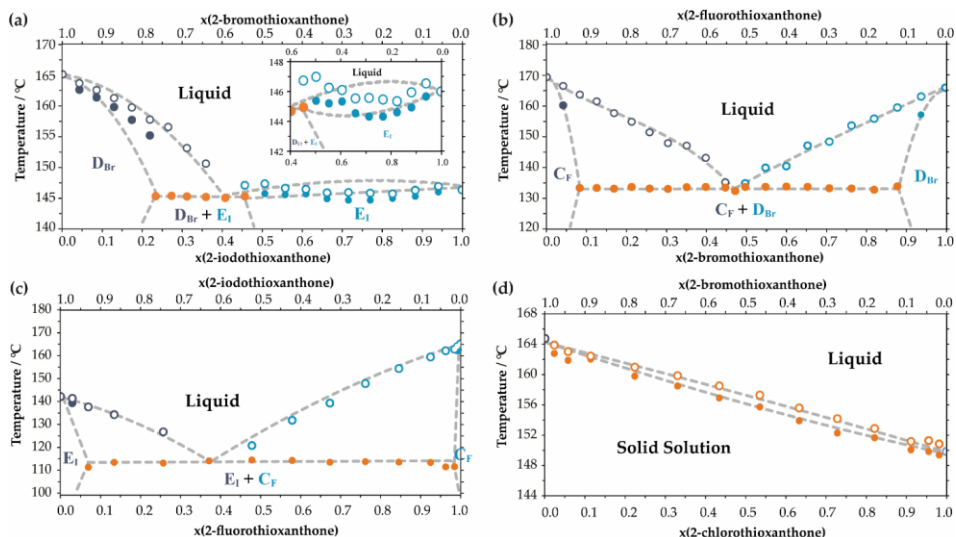


Figure 3.23. Melt phase diagrams of binary systems: I-TXANT – Br-TXANT (a), F-TXANT – Br-TXANT (b), I-TXANT – F-TXANT (c) and Br-TXANT – Cl-TXANT (d). The colour coding is identical to that used in Figure 3.22. (closed points represent – solidus / eutectic; open symbols indicate – liquidus; lines are present as guides for the eyes).

It can clearly be seen that the composition range in which these solid solutions can be obtained is different in each pair of thioxanthone derivatives. The highest solubility up to more than 50 mol% was observed for I-TXANT in Br-TXANT, whereas the lowest (less than 5 mol%) for F-TXANT in Br-TXANT. In Figure 3.24., a CIE chromaticity diagram is depicted for several solid solutions compositions in various binary systems.

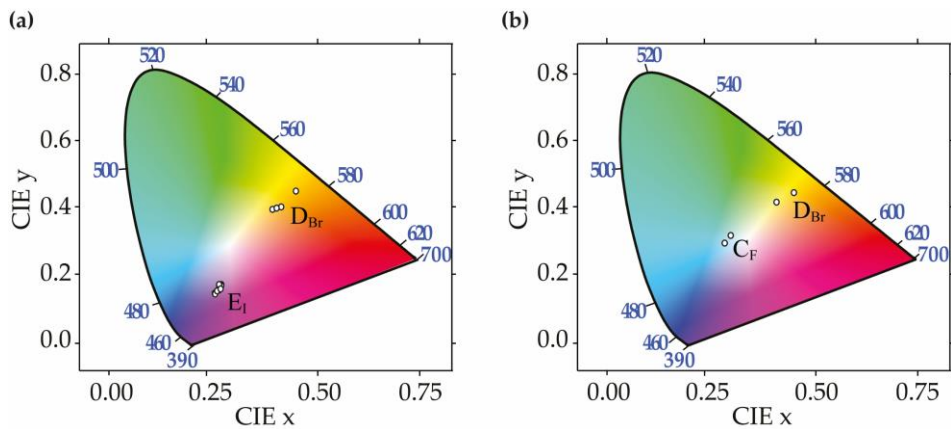


Figure 3.24. CIE chromaticity diagrams of several compositions of solid solutions from emission spectra excited at $\lambda_{ex} = 330$ nm (room temperature): I-TXANT – Br-TXANT (a), F-TXANT – Br-TXANT (b), I-TXANT – F-TXANT (c) and Br-TXANT – Cl-TXANT (d).

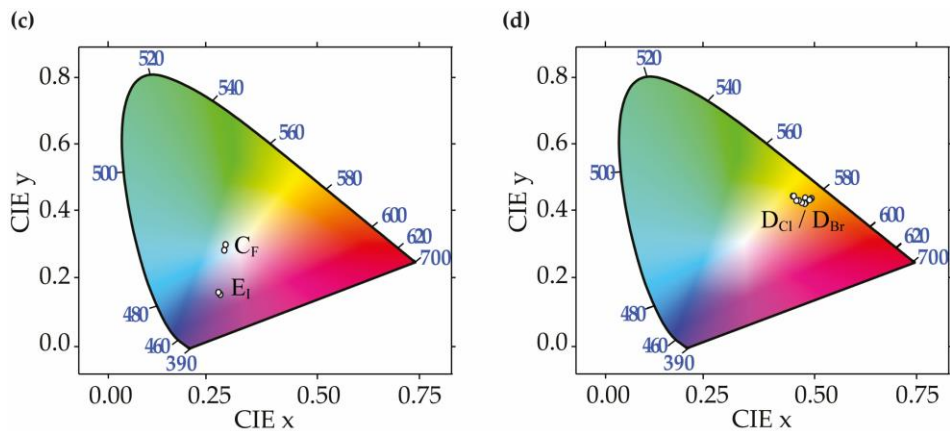


Figure 3.24. (Continued).

According to the CIE diagrams, there is minimal alteration in the colour of luminescence regardless of the variations in component composition. Even in the case of a solid solution E_I , the luminescence colour remains largely unchanged, even if half of the original I-TXANT molecules are replaced by Br-TXANT molecules within the crystal structure.

In comparison to other described thioxanthone derivative binary systems, F-TXANT – Cl-TXANT is the most different because both of these substances can exist in three polymorphic forms, Figure 3.25. shows a flowchart illustrating the different polymorphs discovered, their preparation, and observed phase transitions.

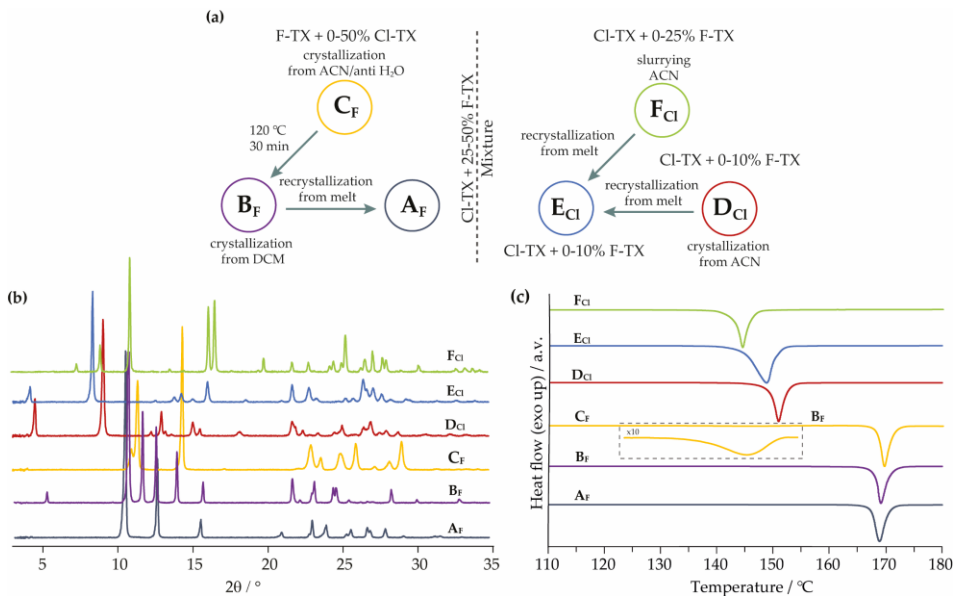


Figure 3.25. Preparation and phase transformations of F-TXANT and Cl-TXANT forms (a), PXRD patterns (b), and DSC curves, $10\text{ }^\circ\text{C}\cdot\text{min}^{-1}$ (c).

Polymorph forms of both compounds were studied to show the existence of a complicated solid solution system. F-TXANT and Cl-TXANT form three different discontinuous solid solutions systems. The melt phase diagram characterizing non-solvated phases is given in Figure 3.26., where it can be observed that F-TXANT and Cl-TXANT form eutectic systems of six different solid solutions, respectively.

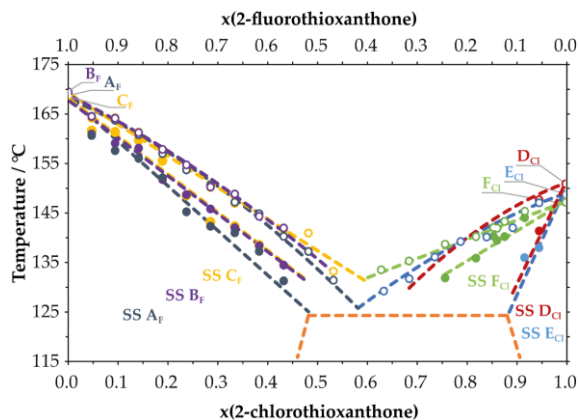


Figure 3.26. Melt phase diagram of F-TXANT and Cl-TXANT polymorphs and their solid solutions (closed points represent – solidus; open symbols indicate – liquidus; lines are present as guides for the eyes).

In Figure 3.27., a CIE chromaticity diagram is depicted for polymorph forms of F-TXANT and Cl-TXANT.

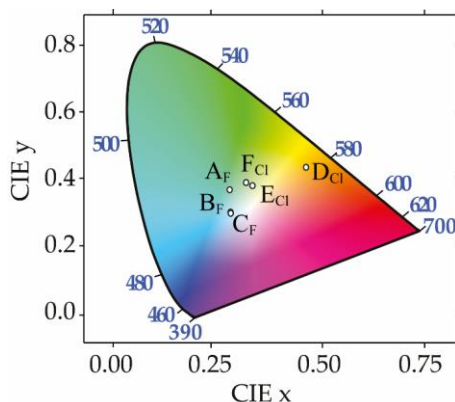


Figure 3.27. CIE chromaticity diagrams of polymorph forms of F-TXANT and Cl-TXANT from emission spectra excited at $\lambda_{ex} = 330$ nm (room temperature).

When comparing these two-component systems with the I-TXANT – Cl-TXANT analysed in the previous chapter, the luminescence colouring does not change as much, but the main insight that was clarified – the luminescence colouring can be changed not only by changing the composition of the components in the solid solution but also between polymorphic forms, as it is the case for F-TXANT and Cl-TXANT.

CONCLUSIONS

1. The formation of solid solutions in the benperidol – droperidol system proves that the ability of one molecule to replace another in different phases significantly depends on the crystal structure of the phase, their formation in substituted nitrobenzoic acids clearly shows both the dependence on the properties of the exchangeable functional groups and their characteristic intermolecular interactions and the crystal structure, while the solid formation of solutions in the xanthone – thioxanthone system and between the thioxanthone analogues shows a dependence on the molecular packing.
2. In the desolvation of the solvated crystallization products of the two-component system benperidol – droperidol, a stable solid solution with the crystal structure of benperidol polymorph form II is formed, regardless of whether a solid solution in the structure of benperidol solvates, a solid solution in the structure of droperidol solvates, or even a mixture of these solid solutions is being desolvated.
3. The solid solution formation approach can be used to improve the physical properties of organic crystal materials. It has been observed that the compositional dependence of the luminescence properties can be expected if the intermolecular interactions responsible for the luminescence are notably affected during the formation of solid solutions. The demonstrated approach shows that, in contrast to single-phase materials, where properties can be tuned only in a discontinuous manner, using solid solutions it is possible to change the luminescence characteristics in a continuous fashion.
4. It has been proven that the analysis of changes in intermolecular interaction energies in the two-component systems of benperidol – droperidol by modelling the formation of solid solutions allows to explain the ability of solid solutions formation in different structures. In order to form a solid solution in non-solvated structures over a wide range of concentrations, the efficiency of interactions must be maintained, while the formation of solid solutions over a wide range of concentrations in solvated structures is possible if the intermolecular interactions become slightly more efficient.
5. It was observed that in two-component systems of substituted nitrobenzoic acids, the analysis of energy changes of intermolecular interactions by modelling the formation of solid solutions is not a suitable tool for evaluating the formation of solid solutions, probably because this approach does not include thermal and entropy effects. This is explained by the fact that, unlike benperidol – droperidol two-component systems, the formation of solid solutions in the two-component systems of substituted nitrobenzoic acids is associated with more significant changes in the chemical structure and, therefore, intermolecular interactions.

ACKNOWLEDGEMENTS

I express my gratitude to the University of Latvia Foundation (MikroTik Ltd. doctoral scholarship in the field of natural and medical sciences), and the European Social Fund (grant “*Strengthening of the capacity of doctoral studies at the University of Latvia within the framework of the new doctoral model*”, grant No. 8.2.2.0/20/I/006) provided vital financial support for the most of my duration of the doctoral studies. I am honoured and grateful to have been the recipient of this scholarship and grant. As well as the Latvian Council of Science (project “*Crystal engineering of pharmaceutical multicomponent phases for more efficient crystalline phase design*”, project No. lzp-2018/1-0312) for financial support.

I would like to express my greatest appreciation to my supervisors – associate professor *Dr. chem.* Agris Bērziņš for his valuable and constructive suggestions during the planning and development of this thesis, as well as his willingness to give time so generously, has been very much appreciated, and researcher *Dr. chem.* Toms Rēķis for the opportunity to go to P24, PETRA III, Deutsches Elektronen-Synchrotron DESY (Hamburg, Germany) to measure monocrystals as part of the project (“*Structural studies of 4-iodothioxanthone solid solutions exhibiting modulated solid state luminescence properties*”) and helpful advice during the development of this thesis, as well as his willingness to give time so generously, has been very much appreciated.

I would like to thank the colleagues of the Department of Physical Chemistry – the scientific consultant of this work, the leading researcher *Dr. chem.* Artis Kons for his suggestions and contribution to the creation of my doctoral thesis, *MSc. chem.* Anita Kalniņa for editing the doctoral thesis text, as well as professor *Dr. chem.* Andris Actiņš for the useful advice. In addition to that, the colleagues of the Department of Organic Chemistry – docent *Dr. chem.* Igors Kļimenkovs for the synthesis of organic solids used in this work and researcher *MSc. chem.* Rihards Klūga for ¹H-NMR spectra measurements.

Many thanks to Latvian Institute of Organic Synthesis researcher *Dr. chem.* Kristīne Krūkle-Bērziņa for the collection of the single crystal X-ray diffraction data and for the opportunity to go to BioMAX, MAX IV Synchrotron (Lund, Sweden) to determine the crystal structures of the grown monocrystals as part of the project (“*Application of cyclodextrin metal-organic frameworks as potential carriers of active pharmaceutical ingredients*”), as well as researcher *Dr. chem.* Kaspars Leduskrasts for recording photoluminescence spectra. In addition, Institute of Solid State Physics, University of Latvia, professor *Dr. phys.* Anatolijs Šarakovskis and researcher *Ph.D. phys.* Meldra Ķemere for performing and analysing the absolute photoluminescence quantum yield.

Finally, I would like to express my gratitude to my friends for spending time with me, as well as my special greatest gratitude to my family – mother Ilze Saršūna, father Edgars Saršūns and brother Toms Saršūns for their daily support, motivation, belief in my abilities and for always being proud of me.

LITERATŪRAS SARAKSTS / REFERENCES

1. Lusi, M. A Rough Guide to Molecular Solid Solutions: Design, Synthesis and Characterization of Mixed Crystals. *CrystEngComm*, **2018**, 20(44), 7042–7052.
2. Hill, A.; Kras, W.; Theodosiou, F.; Wanat, M.; Lee, D.; Cruz-Cabeza, A. J. Polymorphic Solid Solutions in Molecular Crystals: Tips, Tricks, and Switches. *J. Am. Chem. Soc.*, **2023**, 145(37), 20562–20577.
3. Case, D. H.; Srirambhatla, V. K.; Guo, R.; Watson, R. E.; Price, L. S.; Polyzois, H.; Cockcroft, J. K.; Florence, A. J.; Tocher, D. A.; Price, S. L. Successful Computationally Directed Templating of Metastable Pharmaceutical Polymorphs. *Cryst. Growth Des.*, **2018**, 18(9), 5322–5331.
4. Braga, D. Crystal Engineering, Where from? Where To? *Chem. Commun.*, **2003**, 3(22), 2751–2754.
5. D'Agostino, S.; Fornasari, L.; Grepioni, F.; Braga, D.; Rossi, F.; Chierotti, M. R.; Gobetto, R. Precessional Motion in Crystalline Solid Solutions of Ionic Rotors. *Chem. Eur. J.*, **2018**, 24(56), 15059–15066.
6. Lusi, M.; Vitorica-Yrezabal, I. J.; Zaworotko, M. J. Expanding the Scope of Molecular Mixed Crystals Enabled by Three Component Solid Solutions. *Cryst. Growth Des.*, **2015**, 15(8), 4098–4103.
7. Blagden, N.; de Matas, M.; Gavan, P. T.; York, P. Crystal Engineering of Active Pharmaceutical Ingredients to Improve Solubility and Dissolution Rates. *Adv. Drug Deliv. Rev.*, **2007**, 59(7), 617–630.
8. Spoletti, E.; Verma, V.; Cappuccino, C.; Lusi, M. Solid Solution Polymorphs afford two High-Soluble Co-Drug Forms of Tolbutamide and Chlorpropamide. *Chem. Commun.*, **2023**, 59(96), 14321–14324.
9. Perlovich, G. Melting Points of One- and Two-Component Molecular Crystals as Effective Characteristics for Rational Design of Pharmaceutical Systems. *Acta Crystallogr. B. Struct. Sci. Cryst. Eng. Mater.*, **2020**, 76(4), 696–706.
10. Garain, S.; Ansari, S. N.; Kongasseri, A. A.; Chandra Garain, B.; Pati, S. K.; George, S. J. Room Temperature Charge-Transfer Phosphorescence from Organic Donor-Acceptor Co-Crystals. *Chem. Sci.*, **2022**, 13(34), 10011–10019.
11. Saha, S.; Mishra, M. K.; Reddy, C. M.; Desiraju, G. R. From Molecules to Interactions to Crystal Engineering: Mechanical Properties of Organic Solids. *Acc. Chem. Res.*, **2018**, 51(11), 2957–2967.
12. Bolton, O.; Lee, K.; Kim, H. J.; Lin, K. Y.; Kim, J. Activating Efficient Phosphorescence from Purely Organic Materials by Crystal Design. *Nat. Chem.*, **2011**, 3(3), 205–210.
13. Kitaigorodskii, A. I. Molecular Crystals and Molecules. *Acad. Press. New York*, **1973**, 570.
14. Kitaigorodskii, A. I. Conditions of Formation of Substitutional Organic Solid Solutions. In *Mixed Crystals*. Springer-Berlin, **1984**, 200–216.
15. Braga, D.; Desiraju, G. R.; Miller, J. S.; Orpen, A. G.; Price, S. L. Innovation in Crystal Engineering. *CrystEngComm*, **2002**, 4(83), 500–509.
16. Romasanta, A. K. S.; Braga, D.; Duarte, M. T.; Grepioni, F. How Similar Is Similar? Exploring the Binary and Ternary Solid Solution Landscapes of p-Methyl/Chloro/Bromo-Benzyl Alcohols. *CrystEngComm*, **2017**, 19(4), 653–660.

17. Corpinot, M. K.; Bučar, D. K. A Practical Guide to the Design of Molecular Crystals. *Cryst. Growth Des.*, **2019**, *19*(2), 1426–1453.
18. Chakraborty, S.; Desiraju, G. R. C-H...F Hydrogen Bonds in Solid Solutions of Benzoic Acid and 4-Fluorobenzoic Acid. *Cryst. Growth Des.*, **2018**, *18*(6), 3607–3615.
19. Bučar, D. K.; Sen, A.; Mariappan, S. V. S.; MacGillivray, L. R. A [2+2] Cross-Photodimerisation of Photostable Olefins via a Three-Component Cocrystal Solid Solution. *Chem. Commun.*, **2012**, *48*(12), 1790–1792.
20. Shemchuk, O.; Braga, D.; Grepioni, F. Alloying Barbituric and Thiobarbituric Acids: From Solid Solutions to a Highly Stable Keto Co-Crystal Form. *Chem. Commun.*, **2016**, *52*(79), 11815–11818.
21. Schur, E.; Nauha, E.; Lusi, M.; Bernstein, J. Kitaigorodsky Revisited: Polymorphism and Mixed Crystals of Acridine/Phenazine. *Chem. Eur. J.*, **2015**, *21*(4), 1735–1742.
22. Cherukuvada, S.; Nangia, A. Eutectics as Improved Pharmaceutical Materials: Design, Properties and Characterization. *Chem. Commun.*, **2014**, *50*(8), 906–923.
23. Fayzullin, R. R.; Zakharychev, D. V.; Gubaidullin, A. T.; Antonovich, O. A.; Krivolapov, D. B.; Bredikhina, Z. A.; Bredikhin, A. A. Intricate Phase Behavior and Crystal Structure Features of Chiral Para-Methoxyphenyl Glycerol Ether Forming Continuous and Partial Solid Solutions. *Cryst. Growth Des.*, **2017**, *17*(1), 271–283.
24. Fonseca, J. D. C.; Tenorio Clavijo, J. C.; Alvarez, N.; Ellena, J.; Ayala, A. P. Novel Solid Solution of the Antiretroviral Drugs Lamivudine and Emtricitabine. *Cryst. Growth Des.*, **2018**, *18*(6), 3441–3448.
25. D'Agostino, S.; Fornasari, L.; Braga, D. Binary and Ternary Solid Solutions of Ionic Plastic Crystals, and Modulation of Plastic Phase Transitions. *Cryst. Growth Des.*, **2019**, *19*(11), 6266–6273.
26. Wojnarowska, Z.; Smolka, W.; Zotova, J.; Knapik-Kowalczyk, J.; Sherif, A.; Tajber, L.; Paluch, M. The Effect of Electrostatic Interactions on the Formation of Pharmaceutical Eutectics. *Phys. Chem. Chem. Phys.*, **2018**, *20*(43), 27361–27367.
27. Braun, D. E.; Kahlenberg, V.; Griesser, U. J. Experimental and Computational Hydrate Screening: Cytosine, 5-Flucytosine, and Their Solid Solution. *Cryst. Growth Des.*, **2017**, *17*(8), 4347–4364.
28. Lusi, M. Engineering Crystal Properties through Solid Solutions. *Cryst. Growth Des.*, **2018**, *18*(6), 3704–3712.
29. Jaffe, H. H.; Miller, A. L. The Fates of Electronic Excitation Energy. *J. Chem. Educ.*, **1966**, *43*(9), 469.
30. Blasse, G.; Grabmaier, B. C. Luminescent Materials. *Springer-Berlin*, **1994**, 333.
31. Kitai, A. H. Solid State Luminescence. *Springer-Dordrecht*, **1993**, 386.
32. Vij, D. R. Handbook of Applied Solid State Spectroscopy. *Springer-Berlin*, **2006**, 742.
33. Fairchild, M. D. Color Appearance Models. *Wiley*, **2013**, 450.
34. Corpinot, M. K.; Guo, R.; Tocher, D. A.; Buanz, A. B. M.; Gaisford, S.; Price, S. L.; Bučar, D. K. Are Oxygen and Sulfur Atoms Structurally Equivalent in Organic Crystals? *Cryst. Growth Des.*, **2017**, *17*(2), 827–833.

35. Bērziņš, A.; Kons, A.; Saršūns, K.; Belyakov, S.; Actiņš, A. On the Rationalization of Formation of Solvates: Experimental and Computational Study of Solid Forms of Several Nitrobenzoic Acid Derivatives. *Cryst. Growth Des.*, **2020**, *20*(9), 5767–5784.
36. Vardanyan, R. Piperidine-Based Drug Discovery. *Elsevier*, **2017**, 358.
37. Aronson, J. K. Side Effects of Drugs Annual. *Elsevier*, **2003**, 662.
38. Bērziņš, A.; Skarbulis, E.; Reķis, T.; Actiņš, A. On the Formation of Droperidol Solvates: Characterization of Structure and Properties. *Cryst. Growth Des.*, **2014**, *14*(5), 2654–2664.
39. Bērziņš, A.; Skarbulis, E.; Actiņš, A. Structural Characterization and Rationalization of Formation, Stability, and Transformations of Benperidol Solvates. *Cryst. Growth Des.*, **2015**, *15*(5), 2337–2351.
40. Bērziņš, A.; Actiņš, A. Why Do Chemically Similar Pharmaceutical Molecules Crystallize in Different Structures: A Case of Droperidol and Benperidol. *Cryst. Growth Des.*, **2016**, *16*(3), 1643–1653.
41. Wen, Y.; Liu, H.; Zhang, S.; Gao, Y.; Yan, Y.; Yang, B. One-Dimensional π - π Stacking Induces Highly Efficient Pure Organic Room-Temperature Phosphorescence and Ternary-Emission Single-Molecule White Light. *J. Mater. Chem. C*, **2019**, *7*(40), 12502–12508.
42. Tang, J.; Zhao, S.; Wei, Y.; Quan, Z.; Huo, C. CBr₄ Promoted Intramolecular Aerobic Oxidative Dehydrogenative Arylation of Aldehydes: Application in the Synthesis of Xanthenes and Fluorenones. *Org. Biomol. Chem.*, **2017**, *15*(7), 1589–1592.
43. Trapp, N.; Vastakaite, G.; Wennemers, H. CCDC 1906607: Experimental Crystal Structure Determination. *CSD Commun.*, **2019**.
44. Bui, T. T. T.; Dahaoui, S.; Lecomte, C.; Desiraju, G. R.; Espinosa, E. The Nature of Halogen...Halogen Interactions: A Model Derived from Experimental Charge-Density Analysis. *Angew. Chemie Int. Ed.*, **2009**, *48*(21), 3838–3841.

PUBLIKĀCIJAS / PUBLICATIONS

I

Saršūns, K., Bērziņš, A., Rekis, T.

**SOLID SOLUTIONS IN XANTHONE – THIOXANTHONE
BINARY SYSTEM: HOW WELL ARE SIMILAR
MOLECULES DISCRIMINATED IN THE SOLID STATE?**

Crystal Growth & Design, **2020**, 20(12), 7997–8004

Reprinted with permission from American Chemical Society (ACS).

Copyright © 2020, American Chemical Society



Solid Solutions in the Xanthone–Thioxanthone Binary System: How Well Are Similar Molecules Discriminated in the Solid State?

Kristaps Sarūns, Agris Bērziņš, and Toms Reķis*

Cite This: *Cryst. Growth Des.* 2020, 20, 7997–8004

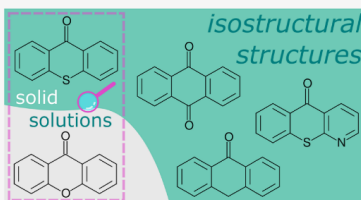
Read Online

ACCESS |

Metrics & More

Article Recommendations

ABSTRACT: The binary system of xanthone–thioxanthone has been explored, showing that two solid solutions (formed based on xanthone and thioxanthone parent structures, respectively) exist for this system. One of the solid solutions shows miscibility of both molecules in a large composition range (>0–80 mol % of xanthone). The structure of thioxanthone has been redetermined to reveal a special case of nonmerohedral twinning in the crystals. Such a twinning feature has apparently been the reason for incorrect crystal structure determination previously. A structure of thioxanthone:xanthone (75:25 mol %) solid solution is also presented. Several similar molecules to the title compounds have been found in the Cambridge Structural Database and shown to crystallize in structures isostructural to that of thioxanthone. The different packing of pure xanthone is thus an exception among the explored compounds.



INTRODUCTION

Solid solutions are multicomponent phases for which the component ratios can be varied in continuum. Therefore, they hold a potential for tuning molecular crystal material properties in a smooth fashion.^{1,2} The question, however, is whether the response of a wanted property is sensitive enough to the varying component ratio. The properties may include nonlinear optical properties, solid-state luminescence and phosphorescence properties, and mechanical properties, like elasticity, to name some. Recently, purely molecular solid solutions have been explored for modulating charge transfer and optical bandgap for possible semiconductor applications.³

This crystal engineering approach is clearly a promising one; however, it does not seem to have gained sufficient attention since more frequently one-component systems or multicomponent systems, like solvates, salts, and cocrystals, are studied. Modulation of the properties (in a stepwise fashion) is then achieved by chemically modifying the constituent molecules, for example, by changing substituents.^{4–7}

Engineering molecular solid solutions is not a straightforward task. The pioneering work on these phases was done by Kitaigorodskii around half a century ago.^{8,9} Generally, it is the similarity of molecule size and shape that play a role in determining whether a solid solution between the particular components will form. Equally important are the resulting intermolecular interactions in the crystal structure. For example, as we have shown in our recent work—solid solutions may form when a similarly shaped molecule that does not disrupt the hydrogen bonding network in the crystal structure or can participate in this bonding equally well is introduced in the system.¹⁰ Solid solutions have been discovered and studied

for multicomponent systems of the following: enantiomers;^{11–17} diastereomers;^{13,18–21} molecules differing by single/double bonds between two carbon atoms;^{22,23} molecules differing by halogen (and halogen/methyl) substituents;^{24–28} molecules differing by S/O atoms;^{29,30} molecules differing by F/H atoms;³¹ aromatic systems differing by presence/absence of a heteroatom;^{32–34} molecules differing by methyl/ethyl substituents.³⁵ Nevertheless, up to date, only somewhat rough and empirical guidelines could be established to define the criteria for solid solution formation, and there are cases when even very similar molecules do not mix in the solid state.³⁶ At the same time, solid solutions have been found to form between molecules that do not display a good fit of their shapes, sizes and electron distribution.^{37–39} Detailed studies on individual systems are therefore necessary to explore possible formation of solid solutions in order to accumulate more knowledge and eventually to be able to generalize the concepts.

We report here a study of xanthone–thioxanthone binary system. We show that xanthone and thioxanthone despite being similar molecules pack differently in the solid state. Nevertheless, solid solutions in a large composition range can be obtained; i.e., up to some limit xanthone can be

Received: September 8, 2020

Revised: October 19, 2020

Published: November 10, 2020



accommodated in the thioxanthone parent structure and *vice versa*. We also demonstrate that a few molecules found in the Cambridge Structural Database that are structurally similar (in terms of their molecular structures) to the studied compounds crystallize in structures isostructural to that of thioxanthone. This leads to a question as to why does xanthone fall out of this pattern.

EXPERIMENTAL SECTION

Materials. Xanthone (99%), thioxanthone (>98%), and acetonitrile (99.8%) were obtained from commercial sources and used without further purification.

Construction of Binary Melt Phase Diagram. Different ratio compositions of xanthone and thioxanthone (a total mass of 0.15 g) were prepared using an analytical balance. The mechanical mixtures of the solids were then completely dissolved in 10–25 mL of acetonitrile at 70°. The clear solutions were cooled and the solvent was allowed to evaporate completely. The solid products were ground in a mortar ensuring complete homogenization. Amounts of around 10 mg were loaded in closed-type aluminum pans for DSC analysis. The analysis were carried out on a DSC25 (TA Instruments) instrument using a heating rate of 10 K min⁻¹. For the construction of the solidus and liquidus lines the peak onset and offset temperatures were used, respectively.

Collection of PXRD Patterns. The remaining samples of the prepared xanthone–thioxanthone compositions were placed in glass sample holders for PXRD pattern collection. A D8 Advance (BRUKER) instrument (Bragg–Brentano θ – θ geometry) was used equipped with a LynxEye position sensitive detector (BRUKER). Copper radiation (Cu K α) at a wavelength of 1.54180 Å was used. The tube voltage and current were set to 40 kV and 40 mA. The divergence slit was set at 0.6 mm, and the antiscattering slit was set at 8.0 mm. The diffraction pattern was recorded using a scanning speed of 1 s/0.02° from 3° to 35° on a 2θ scale.

Single Crystals. Single crystals of pure thioxanthone and a few thioxanthone–xanthone mixtures were grown from acetonitrile solutions with slow evaporation. Single crystals of a suitable quality (one of the pure thioxanthone batch and one of the thioxanthone–xanthone batch) were selected for SCXRD analysis.

Collection of SCXRD Data. The data were collected at 301 K on an XtaLAB Synergy-S dualflex diffractometer (RIGAKU Oxford Diffraction) equipped with a HyPix6000 detector and a microfocus sealed X-ray tube (Cu K α radiation, $\lambda = 1.54184$ Å). Data were collected by performing ω -scans at a number of different κ and ϕ positions.

Data Integration, Structure Solution, and Refinement. Data were integrated using CrysAlisPro 1.171.40.74a software. A twin matrix corresponding to a 180° rotation along the reciprocal direction [0.45, 0, 0.90] was used to integrate both domains twinned by nonmerohedry. Outlier rejection and reflection averaging was performed according to Laue class $2/m$ (b^* unique). Empirical absorption correction using spherical harmonics, implemented in SCALE3 ABSPACK scaling algorithm was used. Relevant data are listed in Table 1.

Structure solutions and refinements were performed with the software JANA2006.⁴⁰ Initially, the HKL4 file containing untwinned data from a single twin domain was used for a crude structure solution exploiting the Superflip algorithm.⁴¹ The structure model was then refined against the data from the HKLS file refining also the twin volume fractions.

Due to disorder there is (statistical) inversion symmetry present in the crystal structure of thioxanthone. It gives rise to the symmetry corresponding to $P2_1/c$ space group. For the solid solution structure it is not entirely true and therefore the structure is described in $P2_1$. However, for each of the atoms related by the pseudo-inversion center (e.g., $a1$ and $a2$) the following constraints of the atomic positions and the ADP parameters were used: $x_{a2} = -x_{a1}$, $y_{a2} = -y_{a1}$, $z_{a2} = -z_{a1}$, $U11_{a2} = U11_{a1}$, $U22_{a2} = U22_{a1}$, $U33_{a2} = U33_{a1}$, $U12_{a2} = U12_{a1}$, $U13_{a2} = U13_{a1}$, $U23_{a2} = U23_{a1}$. Meanwhile, the atom occupancies (when

Table 1. Summary of the X-ray Diffraction Data Acquisition

	thioxanthone	thioxanthone:xanthone [75:25 mol %]
temperature/K	301	301
radiation type	Cu K α , $\lambda = 1.54184$ Å	
No. of refl. (cell meas.)	1250	1567
θ range/deg (cell meas.)	11.49 to 74.59	6.94 to 73.95
crystal size/mm ³	0.30 × 0.05 × 0.02	0.35 × 0.03 × 0.03
T_{min} T_{max}	0.744, 1	0.706, 1
no. of meas., unique, obs. [$I > 3\sigma(I)$] refl.	2455, 1818, 1219	1907, 1755, 939
R_{int} (obs.), R_{int} (unique)	0.0292, 0.0294	0.0192, 0.0193
θ range/deg	5.71 to 75.87	5.73 to 76.10
Index ranges	-9 ← h ← 9 -4 ← k ← 4 -19 ← l ← 19	-8 ← h ← 9 -5 ← k ← 5 -14 ← l ← 19

different from 1) were refined individually, i.e. not considering the inversion symmetry.

RESULTS AND DISCUSSION

Binary Melt Phase Diagram. Chemical schemes of xanthone and its sulfur analogue thioxanthone are depicted in Figure 1. The molecules are rigid, aromatic and differ only

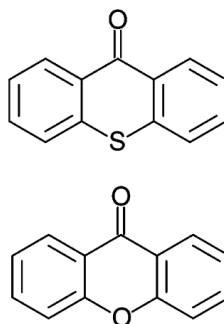


Figure 1. Chemical schemes of thioxanthone (top) and xanthone (bottom).

by S/O atoms. Besides, they lack hydrogen bond donors. Such conditions are favorable for the respective crystal structures to be isostructural as shown in a study of saccharin/thiosaccharin.⁴² This would imply complete miscibility in the solid state.

Binary melt phase diagram was constructed to explore how well both highly similar molecules are discriminated in the solid state. It was revealed that there is no single continuous solid solution, but two solid solutions form instead, i.e., near pure xanthone and near pure thioxanthone region (see Figure 2). This is an indication that both highly similar molecules pack differently in the solid state.

As can be seen in the phase diagram, xanthone dissolves in thioxanthone forming a solid solution (α) in a large composition range. Crystallizing thioxanthone–xanthone mixtures with xanthone content >0–80 mol % single phases were obtained. The DSC measurements showed a single endothermic signal for each measured composition (see Figure 3).

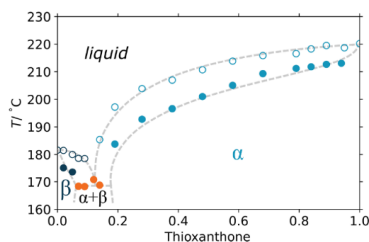


Figure 2. Melt phase diagram of xanthone–thioxanthone binary system (lines are guides for the eyes).

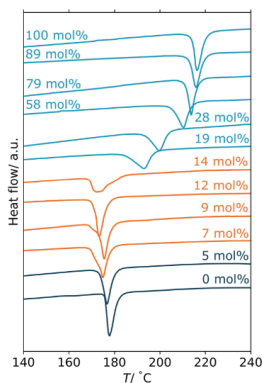


Figure 3. DSC curves of selected xanthone–thioxanthone compositions used for melt phase diagram construction (the indicated percentage refers to thioxanthone content).

Furthermore, PXRD patterns of the mixtures in the said composition range are very similar to that of pure thioxanthone and do not contain the characteristic peaks of pure xanthone phase (see Figure 4). The slight peak shifts and relative intensity variations are typical for solid solutions.

The DSC measurements suggest that a small amount of thioxanthone can be dissolved in xanthone, i.e. another solid solution (β) exists for this binary system. For example, a mixture containing 5 mol % thioxanthone melts exhibiting a single endothermic signal (see Figure 3) and only contains the diffraction peaks characteristic to xanthone (see Figure 4).

There is a relatively narrow biphasic region in the phase diagram where physical (different ratio) mixtures of both limiting-composition solid solutions α and β are present. This is associated with an additional endothermic signal in the DSC curves indicating for the eutectic melting. In this case, the eutectic melting signals can be observed as small but pronounced shoulders with an onset of around 169 K (see Figure 3). Mixture of two phases can also be noted in the PXRD patterns (see Figure 4).

The narrow biphasic region indicates that both molecules are discriminated in the solid state rather poorly. In composition ranges >0 –7 mol % and 20 – <100 mol % (thioxanthone), both kinds of molecules are incorporated in a single phase rather than a physical mixture of separate xanthone

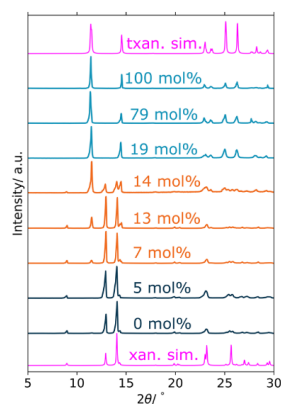


Figure 4. PXRD patterns of selected xanthone–thioxanthone compositions used for melt phase diagram construction (the indicated percentage refers to thioxanthone content). From structure simulated patterns shown in magenta (thioxanthone at top and xanthone at bottom).

and thioxanthone phases forms. The large miscibility range difference between solid solutions α and β could be explained by the different sizes of S and O atoms. In solid solution α , it is apparently much more feasible to substitute the thioxanthone molecules by xanthone molecules because the O atom is considerably smaller than the S atom. However, for solid solution β , an ever-increasing fraction of xanthone molecules need to be replaced by the large S atom-containing thioxanthone molecules to extend the composition range.

Observed behavior indicates that even though both studied molecules are highly similar and a large part of the composition range corresponds to solid solutions; at some limiting compositions, the molecules are discriminated in the solid state as different building blocks.

Structures of Xanthone, Thioxanthone, and the Corresponding Solid Solution. The structure of xanthone has been reported in numerous studies, where mostly the compound has been shown to crystallize in the orthorhombic space group $P2_12_12_1$.^{43–47} Recently, another polymorph in the monoclinic space group $P2_1$ has also been reported.⁴⁸ The PXRD patterns of the xanthone phases obtained in this study corresponds to the $P2_12_12_1$ polymorph.

Both xanthone polymorphs are very similar (see Figure 5). The $P2_12_12_1$ polymorph crystallizes with a single molecule in

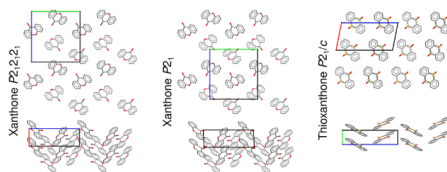


Figure 5. Crystal structure representations of the two known polymorphs of xanthone^{47,48} and that of thioxanthone (this work).

the asymmetric unit ($Z' = 1$). The second polymorph discovered recently⁴⁸ can be considered as a monoclinic distortion ($\beta \approx 93^\circ$) of the first one. It is described in a subgroup of $P2_12_12_1$, namely, $P2_1$ with $Z' = 2$ to compensate for the loss of the 2-fold screw axes.

Regarding thioxanthone, there are two entries given in the Cambridge Structural Database.⁴⁹ One of them solely contains the lattice parameters,⁵⁰ for the other one there are also atomic coordinates present.⁵ However, this structure is presented in an unnecessarily large unit cell. In this study, it was discovered that in the crystals of thioxanthone (and the corresponding solid solution) there is a special case of nonmerohedral twinning present. The lattices of the two twin domains are related by a 180° rotation along the reciprocal direction $[0.45, 0, 0.90]$. Furthermore, a following relationship holds: $la^* \approx 2l c^*$. Thus, there are two kinds of reflections present—the ones with a nearly exact overlap ($hkl: l = 2n$) and the ones without an overlap ($hkl: l = 2n + 1$). A section ($h - 1l$) of the reciprocal space reconstruction showing the relation of the twin lattices is given in Figure 6.

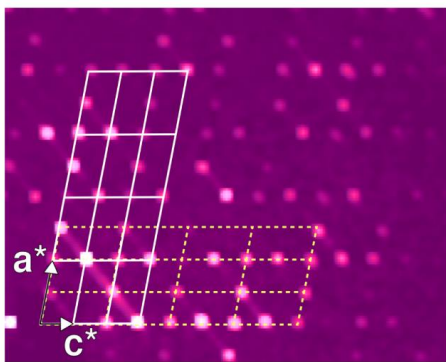


Figure 6. Section ($h - 1l$) of the reciprocal space reconstruction showing the relation of the twin lattices (solid lines, component #1; dashed lines, component #2). Note that due to $la^* \approx 2lc^*$ reflections $hkl, l = 2n$, have virtually an exact overlap while reflections $hkl, l = 2n + 1$, do not overlap.

This is indeed a tricky case of nonmerohedral twinning as the diffraction peaks from both domains can be indexed with a single orientation matrix if la^* is halved. This of course leads to a strange set of systematically absent reflections and it was the first indication for twinning when processing this data. Nevertheless, even performing the indexing wrongly it is possible to get a reasonable structure solution (with $a = 2a_{\text{true}}$). This example demonstrates the necessity to explore the synthetic precession images as highlighted also in the recent paper by Linden.⁵¹

Crystallographic data of the thioxanthone crystal and the crystal representing the solid solution (75 mol % thioxanthone) are given in Table 2.

The structure of thioxanthone has been solved and refined in the monoclinic space group $P2_1/c$. For this structure disorder is present and thus a statistical inversion center is created (see Figure 7). The structure of the solid solution phase could be better described in $P2_1$. Nevertheless, the symmetry constraints

Table 2. Crystallographic Data of the Structure Refinements (Observed Reflections: $[F^2 > 3\sigma(F^2)]$)

	thioxanthone	thioxanthone:xanthone [75:25 mol %]
crystal data		
<i>T</i> /K	301	301
formula	$C_{13}H_8SO$	$0.75 C_{13}H_8SO \cdot 0.25 C_{13}H_8O_2$
formula weight	212.3	208.2
crystal system	monoclinic	monoclinic
space group	$P2_1/c$	$P2_1$
<i>a</i> /Å	7.8388(7)	7.8269(4)
<i>b</i> /Å	3.9891(2)	3.9933(2)
<i>c</i> /Å	15.8019(11)	15.7726(7)
β /deg	101.199(7)	101.535(4)
<i>V</i> /Å ³	484.71(6)	483.02(4)
<i>Z</i> , <i>Z'</i>	2, 0.5	2, 1
<i>F</i> (000)	220	217
<i>D_x</i> /g cm ⁻³	1.4544	1.4316
μ /mm ⁻¹	2.661	2.183
meas. refl.	2455	1907
$[\sin(\theta)/\lambda]_{\text{max}}$ /Å ⁻¹	0.63	0.63
unique refl.	1818	1755
obs. refl.	1219	939
<i>R</i> _{int}	0.0294	0.0193
refinement		
refinement method	full-matrix least-squares on <i>F</i>	
no. of parameters	83	89
<i>V</i> _{tw1} : <i>V</i> _{tw2}	0.73:0.27	0.89:0.11
<i>R</i> ₁ (obs.)	0.0413	0.0379
<i>wR</i> (all)	0.0513	0.0550
<i>S</i>	2.72	2.33
H atom treatment	constr.	constr.
weighting scheme	$w = 1/(\sigma^2(F) + 0.0001F^2)$	
$\Delta\rho_{\text{max}}$ /e Å ⁻³	0.30	0.11
$\Delta\rho_{\text{min}}$ /e Å ⁻³	-0.22	-0.16

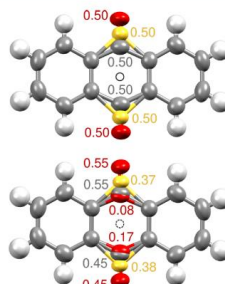
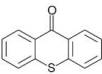
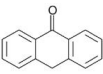
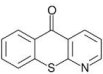
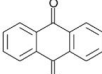
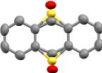
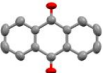
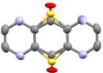
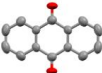


Figure 7. Molecular site representations of thioxanthone (top) and thioxanthone-xanthone [75:25 mol %] solid solution (bottom) crystal structures. The statistical (pseudo)inversion center is denoted with an open circle. Numbers represent symmetry imposed (top) and refined (bottom) occupancies of the disorder components.

for the atomic positions and the anisotropic displacement parameters corresponding to $P2_1/c$ were actually used. However, the occupancy for the inversely related disorder components was refined. It was found that a slight deviation from 0.5:0.5 occupancy ratio (and thus from the $P2_1/c$ symmetry) is, in fact, present. In particular, this concerns the

Table 3. Summary of Four Isostructural Structures Formed by Thioxanthone and Other Similar Molecules

	Thioxanthone	Anthrone	4-Azathioxanthone	Anthraquinone
Chemical scheme				
T/K	301	283 – 303	283 – 303	283 – 303
Space group	$P2_1/c$	$P2_1/c$	$P2_1/c$	$P2_1/c$
Molecular site				
$a/\text{\AA}$	7.8388(7)	7.8647(7)	7.7308(18)	7.8684(5)
$b/\text{\AA}$	3.9891(2)	3.9816(2)	3.8585(9)	3.9634(3)
$c/\text{\AA}$	15.8019(11)	15.813(1)	15.771(3)	15.7839(13)
$\beta/^\circ$	101.199(7)	101.786(4)	99.333(9)	102.687(6)
CCDC Refcode		ANTRON01	HODYUV	ANTQUO08
Reference	This work	52	53	54

minor solid solution component—the xanthone molecule (see Figure 7). The refined xanthone disorder component oxygen atom occupancies are 0.08 and 0.17 which is 1:2 as opposed to 1:1 that would be implied by the symmetry when choosing space group $P2_1/c$.

In spite of the great structural similarity of the xanthone and thioxanthone molecules, they pack differently in the crystalline state. This is in accordance with the obtained phase diagram. Were the structures of both components isostructural, a single continuous solid solution in the whole composition range would exist instead.

The molecular packing in the thioxanthone (and the solid solution) crystal structure can be regarded as a herringbone type with face-to-face overlap of the adjacent molecules (see Figure 5). This packing type is very favorable for the particular materials to be suitable for organic semiconductor use.⁶ Furthermore, room-temperature phosphorescence of thioxanthone and some of its halogenated derivatives have been recently confirmed,⁵ which is quite rare in all-organic solid state.

A survey in the Cambridge Structural Database⁴⁹ was performed to find that exactly the same packing as for thioxanthone is also present for compounds anthrone,⁵² 4-azathioxanthone (*5H*-1-benzothioopyrano(2,3-*b*)pyridin-5-one),⁵³ and anthraquinone.⁵⁴ All four structures are isostructural (see Table 3). Furthermore, they are all disordered in the same way (except for anthraquinone which molecule is itself centrosymmetric). For anthraquinone similar twinning has been described.⁵⁴ No details regarding possible twinning are given for the other two compounds.

Taking into account that the structures of thioxanthone, anthrone, 4-azathioxanthone, and anthraquinone are virtually identical, it is most likely that solid solutions for as large as (including xanthone) five-component system could be obtained. This is a matter for further research as the properties of these resulting solid solution phases could be finely tuned to obtain materials, for example, for the already mentioned semiconductor or room-temperature phosphorescence applications.

Why Is Xanthone an Outlier? Chemical intuition may lead one to believe that in terms of solid state packing the xanthone molecule is much more similar to the thioxanthone

one than, for example, anthraquinone is to thioxanthone. Yet, from Table 3 and Figure 5 it is clear that among five similar molecules only xanthone is found to organize differently in the solid state.

One reason for different packing could be existence of some efficient and thus crystal-packing-determining interactions that are not possible in other systems. For example, acridone is yet another similar compound (see Figure 8) that forms two

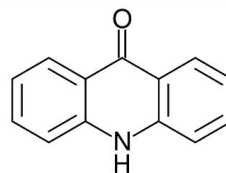


Figure 8. Chemical scheme of acridone.

polymorphs (HIBXOF⁵⁵ and HIBXOF01⁵⁶) with molecular packings very different from those already discussed. This is due to the formation of hydrogen bonds between the amino group hydrogen atoms and the oxygen atoms.

In this case, the xanthone molecule lacks a proper hydrogen bond donor and the only possible hydrogen-bond-like interactions would involve the phenyl group hydrogen atoms. In both xanthone polymorphs, such contact can be observed (see Figure 9). If xanthone were to pack the same way as molecules listed in Table 3 a similar close contact would be considerably longer and thus not as efficient. Nevertheless, the described interaction is not a classical hydrogen bond and it is not possible to directly evaluate the contribution of such contact to directing the molecular packing toward a certain outcome.

Another factor that might influence the observed differences in crystal packings is molecule geometry. The C–O–C bond lengths and the angle in xanthone molecule are considerably different from the corresponding parameters of the C–S–C moiety in the molecule of thioxanthone.

Finally, crystallization conditions (or phase stability/metastability) should be considered. All structures (except

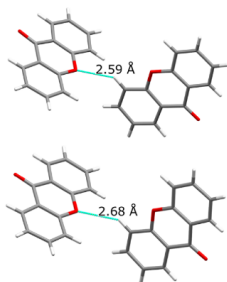


Figure 9. Representation of close contact formation between one of the oxygen and hydrogen atoms of xanthone molecule in the two highly similar polymorphs (top, $P2_1/c$; bottom, $P2_12_1$).

for xanthone $P2_1$ polymorph) discussed in this study are room temperature structures. Xanthone might as well crystallize similarly to thioxanthone, anthrone, 4-azathioxanthone, and anthraquinone (and *vice versa*) at different temperature or pressure.

CONCLUSIONS

Despite being highly similar, the molecules of xanthone and thioxanthone pack differently in the solid state. Nevertheless, up to 80 mol % of thioxanthone in the respective crystal structure can be substituted by xanthone. The crystals of pure thioxanthone and the respective solid solution are twinned by a special case of nonmerohedry. As a result an amiss structure of thioxanthone has been previously reported. There is evidence that another solid solution for xanthone–thioxanthone binary system exists, i.e., a small amount of xanthone can be substituted by thioxanthone in the corresponding xanthone parent structure. That means that both molecules in general are largely interchangeable in the solid state. The exact origin of the different crystal structure packings for pure xanthone and thioxanthone is not known. This demonstrates the complex nature of factors directing crystallization outcome. It is particularly intriguing for taking into account that at least three other compounds (anthrone, 4-azathioxanthone, and anthraquinone) do actually form isostructural structures with thioxanthone. Moreover, similar disorder features and even twinning behavior have been reported among the mentioned compounds. This demonstrates that within those four compounds the crystal packing and such fundamental features as disorder and twinning are not affected by the chemical differences of the molecules.

ASSOCIATED CONTENT

Accession Codes

CCDC 2030974–2030975 contain the supplementary crystallographic data for this paper. These data can be obtained free of charge via www.ccdc.cam.ac.uk/data_request/cif, or by emailing data_request@ccdc.cam.ac.uk, or by contacting The Cambridge Crystallographic Data Centre, 12 Union Road, Cambridge CB2 1EZ, UK; fax: +44 1223 336033.

AUTHOR INFORMATION

Corresponding Author

Toms Reķis – Faculty of Chemistry, University of Latvia, Riga, Latvia; orcid.org/0000-0001-5128-4611; Email: toms.rekis@lu.lv

Authors

Kristaps Saršūns – Faculty of Chemistry, University of Latvia, Riga, Latvia; orcid.org/0000-0002-8692-7768
 Agris Bērziņš – Faculty of Chemistry, University of Latvia, Riga, Latvia; orcid.org/0000-0002-4149-8971

Complete contact information is available at: <https://pubs.acs.org/10.1021/acs.cgd.0c01241>

Notes

The authors declare no competing financial interest.

ACKNOWLEDGMENTS

We thank Dr. A. Mishnov from the Latvian Institute of Organic Synthesis for the collection of the SCXRD data. Funding from the Latvian Council of Science, project “Crystal engineering of pharmaceutical multicomponent phases for more efficient crystalline phase design” (Project No. lzp-2018/1-0312), is acknowledged.

REFERENCES

- (1) Lusi, M. Engineering Crystal Properties through Solid Solutions. *Cryst. Growth Des.* **2018**, *18*, 3704–3712.
- (2) d’Agostino, S.; Fornasari, L.; Grepioni, F.; Braga, D.; Rossi, F.; Chierotti, M. R.; Gobetto, R. Precessional Motion in Crystalline Solid Solutions of Ionic Rotors. *Chem. - Eur. J.* **2018**, *24*, 15059–15066.
- (3) Wiscous, R. A.; Coropceanu, V.; Matzger, A. J. Quaternary Charge-Transfer Solid Solutions: Electronic Tunability through Stoichiometry. *Chem. Mater.* **2019**, *31*, 6598–6604.
- (4) Chung, H.; Chen, S.; Patel, B.; Garbay, G.; Geerts, Y. H.; Diao, Y. Understanding the Role of Bulky Side Chains on Polymorphism of BTBT-Based Organic Semiconductors. *Cryst. Growth Des.* **2020**, *20*, 1646–1654.
- (5) Wen, Y.; Liu, H.; Zhang, S.; Gao, Y.; Yan, Y.; Yang, B. One-dimensional – stacking induces highly efficient pure organic room-temperature phosphorescence and ternary-emission single-molecule white light. *J. Mater. Chem. C* **2019**, *7*, 12502–12508.
- (6) Chen, M.; Yan, L.; Zhao, Y.; Murtaza, I.; Meng, H.; Huang, W. Anthracene-based semiconductors for organic field-effect transistors. *J. Mater. Chem. C* **2018**, *6*, 7416–7444.
- (7) Bolton, O.; Lee, K.; Kim, H.; Lin, K. Y.; Kim, J. Activating efficient phosphorescence from purely organic materials by crystal design. *Nat. Chem.* **2011**, *3*, 205–210.
- (8) Kitaigorodskii, A. *Organic chemical crystallography*; Consultants Bureau: New York, 1961.
- (9) Kitaigorodskii, A. *Mixed Crystals*; Springer-Verlag: Berlin, 1984.
- (10) Reķis, T.; Bērziņš, A. On the structural aspects of solid solutions of enantiomers: an intriguing case study of enantiomer recognition in the solid state. *CrystEngComm* **2018**, *20*, 6909–6918.
- (11) Reķis, T.; Bērziņš, A.; Orola, L.; Holczbauer, T.; Actiņš, A.; Seidel-Morgenstern, A.; Lorenz, H. Single Enantiomer’s Urge to Crystallize in Centrosymmetric Space Groups: Solid Solutions of Phenylpiracetam. *Cryst. Growth Des.* **2017**, *17*, 1411–1418.
- (12) Reķis, T.; d’Agostino, S.; Braga, D.; Grepioni, F. Designing Solid Solutions of Enantiomers: Lack of Enantioselectivity of Chiral Naphthalimide Derivatives in the Solid State. *Cryst. Growth Des.* **2017**, *17*, 6477–6485.
- (13) Reķis, T. Crystallization of chiral molecular compounds: what can be learned from the Cambridge Structural Database? *Acta Crystallogr., Sect. B: Struct. Sci., Cryst. Eng. Mater.* **2020**, *76*, 307–315.

- (14) Brandel, C.; Amharal, Y.; Rollinger, J. M.; Griesser, U. J.; Cartigny, Y.; Petit, S.; Coquerel, G. Impact of Molecular Flexibility on Double Polymorphism, Solid Solutions and Chiral Discrimination during Crystallization of Diprophylline Enantiomers. *Mol. Pharmaceutics* **2013**, *10*, 3850–3861.
- (15) Huang, J.; Chen, S.; Guzei, I. A.; Yu, L. Discovery of a Solid Solution of Enantiomers in a Racemate-Forming System by Seeding. *J. Am. Chem. Soc.* **2006**, *128*, 11985–11992.
- (16) Kaemmerer, H.; Lorenz, H.; Black, S. N.; Seidel-Morgenstern, A. Study of System Thermodynamics and the Feasibility of Chiral Resolution of the Polymorphic System of Malic Acid Enantiomers and Its Partial Solid Solutions. *Cryst. Growth Des.* **2009**, *9*, 1851–1862.
- (17) Bredikhina, A. A.; Zakharychev, D. V.; Gubaidullin, A. T.; Fayzullin, R. R.; Pashagin, A. V.; Bredikhina, Z. A. Crystallization Features of the Chiral Drug Timolol Precursor: The Rare Case of Conglomerate with Partial Solid Solutions. *Cryst. Growth Des.* **2014**, *14*, 1676–1683.
- (18) Bialońska, A.; Ciunik, Z. Solid solutions of quasi-isomorphous diastereomeric salts - kinetics versus thermodynamics. *CrystEngComm* **2013**, *15*, 5681–5687.
- (19) Gervais, C.; Grimbergen, R. F. P.; Markovits, I.; Ariaans, G. J. A.; Kaptein, B.; Bruggink, A.; Broxterman, Q. B. Prediction of Solid Solution Formation in a Family of Diastereomeric Salts. A Molecular Modeling Study. *J. Am. Chem. Soc.* **2004**, *126*, 655–662.
- (20) Taratin, N.; Lorenz, H.; Binev, D.; Seidel-Morgenstern, A.; Kotelnikova, E. Solubility Equilibria and Crystallographic Characterization of the l-Threonine/l-Allo-Threonine System, Part 2: Crystallographic Characterization of Solid Solutions in the Threonine Diastereomeric System. *Cryst. Growth Des.* **2015**, *15*, 137–144.
- (21) Plutecka, A.; Rychlewski, U.; Prusniowska, N.; Gawroński, J. Solid solution of two diastereomers of [3a(R,S),7a(R,S)]-3-[(1'R)-1-phenylethyl]perhydro-1,3-benzothiazol-2-iminium chloride. *Acta Crystallogr., Sect. B: Struct. Sci.* **2010**, *66*, 678–686.
- (22) Oliveira, M. A.; Peterson, M. L.; Klein, D. Continuously Substituted Solid Solutions of Organic Co-Crystals. *Cryst. Growth Des.* **2008**, *8*, 4487–4493.
- (23) Sala, E.; Bērziņš, A.; Saršūns, K. Computational studies of droperidol/benperidol solid-solution phase formation. *Acta Crystallogr., Sect. A: Found. Adv.* **2018**, *74*, No. e348.
- (24) Vogt, F. G.; Vena, J. A.; Chavda, M.; Clawson, J. S.; Strohmaier, M.; Barnett, M. E. Structural analysis of 5-fluorouracil and thymine solid solutions. *J. Mol. Struct.* **2009**, *932*, 16–30.
- (25) Saršūns, K.; Bērziņš, A. Prediction of Solid Solution Formation among Chemically Similar Molecules Using Calculation of Lattice and Intermolecular Interaction Energy. *Key Eng. Mater.* **2020**, *850*, 54–59.
- (26) Dabros, M.; Emery, P.; Thalladi, V. A. Supramolecular Approach to Organic Alloys: Cocrystals and Three- and Four-Component Solid Solutions of 1,4-Diazabicyclo[2.2.2] octane and 4-X-Phenols (X = Cl, CH₃, Br). *Angew. Chem., Int. Ed.* **2007**, *46*, 4132–4135.
- (27) Theocharis, C. R.; Desiraju, G. R.; Jones, W. The use of mixed crystals for engineering organic solid-state reactions: application to benzylbenzylidencyclopentanones. *J. Am. Chem. Soc.* **1984**, *106*, 3606–3609.
- (28) Bučar, D.-K.; Sen, A.; Mariappan, S. V. S.; MacGillivray, L. R. A [2 + 2] cross-polydimerisation of photostable olefins via a three-component cocrystal solid solution. *Chem. Commun.* **2012**, *48*, 1790–1792.
- (29) Shemchuk, O.; Braga, D.; Grepioni, F. Alloying barbituric and thiobarbituric acids: from solid solutions to a highly stable keto-cocrystal form. *Chem. Commun.* **2016**, *52*, 11815–11818.
- (30) Omondi, B.; Lemmerer, A.; Fernandes, M. A.; Levendis, D. C.; Layh, M. Formation of isostructural solid solutions in 2,6-disubstituted N-phenylformamides and N-phenylthioamides. *Acta Crystallogr., Sect. B: Struct. Sci., Cryst. Eng. Mater.* **2014**, *70*, 106–114.
- (31) Chakraborty, S.; Desiraju, G. R. C-H...F Hydrogen Bonds in Solid Solutions of Benzoic Acid and 4-Fluorobenzoic acid. *Cryst. Growth Des.* **2018**, *18*, 3607–3615.
- (32) Lusi, M.; Vitorica-Yrezabal, I. J.; Zaworotko, M. J. Expanding the Scope of Molecular Mixed Crystals Enabled by Three Component Solid Solutions. *Cryst. Growth Des.* **2015**, *15*, 4098–4103.
- (33) Schur, E.; Nauha, E.; Lusi, M.; Bernstein, J. Kitaigorodsky Revisited: Polymorphism and Mixed Crystals of Acridine/Phenazine. *Chem. - Eur. J.* **2015**, *21*, 1735–1742.
- (34) Bouwstra, J. A.; Schouten, A.; Kroon, J.; Helmholdt, R. B. Structural studies of the system trans-stilbene/trans-azobenzene. III. The structures of three mixed crystals of trans-azobenzene/trans-stilbene; determinations by X-ray and neutron diffraction. *Acta Crystallogr., Sect. C: Cryst. Struct. Commun.* **1985**, *41*, 420–426.
- (35) Beuchel, A.; Goddard, R.; Imming, P.; Seidel, R. W. A solid solution of ethyl and d₃-methyl 2-[(4-methylpyridin-2-yl)amino]-4-(pyridin-2-yl)thiazole-5-carboxylate. *Acta Crystallographica Section E* **2020**, *76*, 1255–1259.
- (36) Corpinot, M. K.; Bučar, D.-K. A Practical Guide to the Design of Molecular Crystals. *Cryst. Growth Des.* **2019**, *19*, 1426–1453.
- (37) Slovokhotov, Y. Organic crystallography: three decades after Kitaigorodskii. *Struct. Chem.* **2019**, *30*, 551–558.
- (38) Cruz-Cabeza, A. J.; Lestari, M.; Lusi, M. Cocrystals Help Break the “Rules” of Isostructurality: Solid Solutions and Polymorphism in the Malic/Tartaric Acid System. *Cryst. Growth Des.* **2018**, *18*, 855–863.
- (39) Mazzeo, P. P.; Carraro, C.; Arns, A.; Pelagatti, P.; Bacchi, A. Diversity through Similarity: A World of Polymorphs, Solid Solutions, and Cocrystals in a Vial of 4,4'-Diazopyridine. *Cryst. Growth Des.* **2020**, *20*, 636–644.
- (40) Petříček, V.; Dušek, M.; Palatinus, L. Crystallographic Computing System JANA2006: General features. *Z. Kristallogr. - Cryst. Mater.* **2014**, *229*, 345–352.
- (41) Palatinus, L.; Chápuš, G. SUPERFLIP - a computer program for the solution of crystal structures by charge flipping in arbitrary dimensions. *J. Appl. Crystallogr.* **2007**, *40*, 786–790.
- (42) Corpinot, M. K.; Guo, R.; Tocher, D. A.; Buanz, A. B. M.; Gaisford, S.; Price, S. L.; Bučar, D.-K. Are Oxygen and Sulfur Atoms Structurally Equivalent in Organic Crystals? *Cryst. Growth Des.* **2017**, *17*, 827–833.
- (43) Toussaint, J. *Bull. Soc. Chim. Belg.* **1956**, *65*, 213.
- (44) Onuma, S.; Iijima, K.; Oonishi, I. Structure of xanthone. *Acta Crystallogr., Sect. C: Cryst. Struct. Commun.* **1990**, *46*, 1725–1727.
- (45) Biswas, S. C.; Sen, R. K. *Indian Journal of Pure and Applied Physics* **1982**, *20*, 414–415.
- (46) Jiang, N.; Li, S.-Y.; Xie, S.-S.; Yao, H.; Sun, H.; Wang, X.-B.; Kong, L.-Y. FeCl₃ and ether mediated direct intramolecular acylation of esters and their application in efficient preparation of xanthone and chromone derivatives. *RSC Adv.* **2014**, *4*, 63632–63641.
- (47) Tang, J.; Zhao, S.; Wei, Y.; Quan, Z.; Huo, C. CBr₄ promoted intramolecular aerobic oxidative dehydrogenative arylation of aldehydes: application in the synthesis of xanthenes and fluorenones. *Org. Biomol. Chem.* **2017**, *15*, 1589–1592.
- (48) Trapp, N.; Vastakaitė, G.; Wennemers, H. CCDC 1906607: *Experimental Crystal Structure Determination* **2019**, DOI: 10.5517/ccdc.csd.cc21zgzh.
- (49) Groom, C. R.; Bruno, I. J.; Lightfoot, M. P.; Ward, S. C. The Cambridge Structural Database. *Acta Crystallogr., Sect. B: Struct. Sci., Cryst. Eng. Mater.* **2016**, *72*, 171–179.
- (50) Toussaint, J. *Bulletin de la Societe Royale des Sciences de Liege* **1957**, *26*, 77.
- (51) Linden, A. Obtaining the best results: aspects of data collection, model finalization and interpretation of results in small-molecule crystal-structure determination. *Acta Crystallographica Section E* **2020**, *76*, 765–775.
- (52) Yap, G. P. A.; Wisner, J. A. CCDC 100187: *Experimental Crystal Structure Determination* **1997**, DOI: 10.5517/10.5517/cc3c7vj.
- (53) Khan, M. N.; Tahir, M. N.; Khan, M. A.; Khan, I. U.; Arshad, M. N. 5H-1-Benzothiopyrano[2,3-b] pyridin-5-one. *Acta Crystallogr., Sect. E: Struct. Rep. Online* **2008**, *64*, 01704.

(54) Fu, Y.; Brock, C. P. Temperature Dependence of the Rigid-Body Motion of Anthraquinone. *Acta Crystallogr., Sect. B: Struct. Sci.* **1998**, *54*, 308–315.

(55) Potts, G. D.; Jones, W. 9(10H)-Acridone. *Acta Crystallogr., Sect. C: Cryst. Struct. Commun.* **1995**, *51*, 267–268.

(56) Mei, X.; Wolf, C. Crystallization through Slow Acid-Controlled Hydrolytic Release of a Highly Polar Organic Compound: Formation of a Dipolar Acridone Polymorph. *Cryst. Growth Des.* **2005**, *5*, 1667–1670.



Saršūns, K., Ķemere, M., Karziņins, A., Kļimenkovs, I., Bērziņš, A.,
Šarakovskis, A., Reķis, T.

**FINE-TUNING SOLID STATE LUMINESCENCE
PROPERTIES OF ORGANIC CRYSTALS VIA SOLID
SOLUTION FORMATION: THE EXAMPLE OF 4-
IODOTHIOXANTHONE – 4-CHLOROTHIOXANTHONE
SYSTEM**

Crystal Growth & Design, **2022**, 22(8), 4838–4844

Reprinted with permission from American Chemical Society (ACS).

Copyright © 2022, American Chemical Society



Fine-Tuning Solid State Luminescence Properties of Organic Crystals via Solid Solution Formation: The Example of 4-Iodothioxanthone–4-Chlorothioxanthone System

Kristaps Sāršūns, Meldra Kemere, Aleksejs Karziņš, Igors Kļimenkovs, Agris Bērziņš, Anatolijs Sarakovskis, and Toms Reķis*

Cite This: *Cryst. Growth Des.* 2022, 22, 4838–4844

Read Online

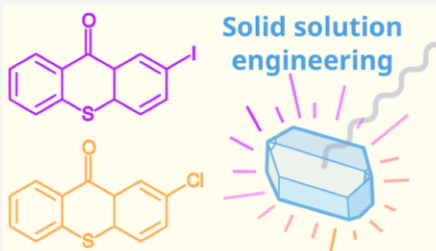
ACCESS |

Metrics & More

Article Recommendations

Supporting Information

ABSTRACT: Solid solutions with fine-tunable photoluminescence have been obtained in a 4-iodothioxanthone–4-chlorothioxanthone system. Both pure components are room-temperature luminophors demonstrating different luminescence properties. It was discovered that in the 4-chlorothioxanthone structure, up to half of the molecules can be replaced by the iodo analogue obtaining solid solutions in the respective composition range. Despite this solid solution existing in such a large composition range, the variation of the luminescence spectra is not substantial. In the 4-iodothioxanthone structure, only up to ~20% of the molecules can be replaced by the chloro analogue before the composition limit of this solid solution is reached. In contrast, there is a strong composition-dependent response of the luminescence. A considerable change in luminescence spectra is observed even if only a few mol % of the opposite component is added. The spectra of mechanical mixtures of pure components are different from those of the solid solutions, which demonstrates the unique behavior of the newly obtained solid phases. This study shows great potential to use solid solution engineering in the organic solid state to tune material properties in a continuum as opposed to other crystal engineering approaches, leading to property tunability in a stepwise fashion.



1. INTRODUCTION

Room temperature photoluminescence of purely organic crystals is a rare phenomenon. However, it has been recently increasingly explored due to technologically relevant applications of such materials.^{1–7} Phosphorescence of organic molecules in the crystalline state is mostly possible due to restricted molecular motions that otherwise annihilate triplet states via nonradiative rather than radiative relaxation.¹ The crystalline state can therefore be exploited to obtain novel materials with desired properties.

Luminescence properties of a phosphorescent crystal change by altering temperature.⁸ Furthermore, different emission spectra can be observed by changing the excitation wavelength.⁹ This is, however, not always enough for a reasonable material design. Current strategies for rationally tuning luminescence properties in the organic crystalline state can be divided into (1) the chemical approach and (2) the crystal engineering approach. The former aims to chemically alter molecules known to be solid state luminophors by changing substituents, e.g., halogen atoms,^{10,11} or alkyl chain lengths,^{12,13} or introducing other changes into the molecular structure.^{11,14,15}

The crystal engineering approach on the other hand focuses, e.g., on polymorphism, as different crystal packings of the same compound display different properties, including luminescence.^{16,17} Moreover, phase transitions between phosphorescent polymorphs can be induced *in situ* by changing temperature and applying pressure or mechanical force.^{18–21} In addition to polymorphism, cocrystallization or salt formation can be exploited, i.e., cocrystallizing a molecule with several different cofomers or changing the counterion of a molecular salt in order to obtain crystals with different luminescence properties.^{22–24}

All of the aforementioned strategies produce materials with their properties altered in a stepwise fashion. A neglected crystal engineering strategy that would allow tuning of any property of a crystalline material in a continuum is designed to

Received: March 12, 2022

Revised: June 28, 2022

Published: July 8, 2022



obtain solid solutions (*mixed crystals* or *alloys* are terms with the same meaning). Solid solutions of inorganic compounds have been rather extensively studied, including their varying composition effect on luminescence properties.^{25–28} For purely organic systems, the solid solution phenomenon has been explored not nearly as much. There are a small number of cases reported, where properties of molecular solid solutions have been studied related to semiconductor applications.^{29,30} The limited number of studies is mostly because the formation of molecular solid solutions is not so straightforward,³¹ and it is governed by complex molecular recognition processes in the solid state.³² In atomic lattices, it is relatively easy to exchange similar atomic species that eventually leads to alloys. For organic systems, it has been observed that even very similar molecular entities sometimes cannot be interchanged in the crystal lattice.³¹ To date, there are only some rough, empirical guidelines indicating what kind of binary systems would possibly show component miscibility in the solid state.^{31,33}

One type of binary system deemed to form solid solutions is a system constituting two molecules differing by the halogen atom type.^{31,34} Recently, halogenated thioxanthone derivatives were studied demonstrating a reasonable luminescence in the crystalline state.¹⁰ This prior knowledge allows us to explore solid solution formation in a selected halogenated thioxanthone system and study luminescence of the obtained materials.

The aim of this study was to obtain solid solutions of 4-iodothioxanthone and 4-chlorothioxanthone (I-TX and Cl-TX), to explore component miscibility limits, and to study the solid state luminescence property response to the variation of the solid solution composition.

2. EXPERIMENTAL SECTION

2.1. Materials. 2-Chlorothioxanthone (>98%) and acetonitrile (99.8%) were obtained from commercial sources. 2-Iodothioxanthone was synthesized by a cyclization reaction in concentrated sulfuric acid media according to a synthesis method available in the literature.¹⁰

2.2. Construction of Binary Melt Phase Diagram. Different compositions of Cl-TX and I-TX were prepared using an analytical balance, and the resulting mechanical mixtures were then completely dissolved in 10 to 25 mL of acetonitrile at 70°. The clear solutions were left to evaporate until dryness. The solid products were ground in a mortar to ensure complete homogenization. Samples of ~10 mg were loaded in closed-type aluminum pans for DSC analysis. The analysis was carried out on a DSC25 (TA Instruments) instrument using a heating rate of 10 K min⁻¹. For the construction of the solidus and liquidus lines the peak onset and offset temperatures were used, respectively.

2.3. Collection of PXRD Patterns. Samples of the prepared Cl-TX and I-TX compositions (see above) were measured on a D8 Advance (Bruker) instrument (Bragg–Brentano θ - θ geometry) equipped with a LynxEye position sensitive detector (Bruker). Copper radiation (Cu K α) at a wavelength of 1.541 80 Å was used.

2.4. Photoluminescence Measurements. Photoluminescence measurements were performed at room temperature using an FLS1000 spectrometer from Edinburgh Instruments equipped with a CW 450 W xenon lamp and a cooled red photomultiplier tube for detection. Emission maps were obtained by varying the excitation wavelength from 250 to 630 nm with a step of 2 nm. The absolute photoluminescence quantum yield (APLQY) measurements were performed with an Integrating Sphere Assembly N-M01, an accessory to Edinburgh Instruments luminescence spectrometer FLS1000. APLQY measurements of the samples in a form of solid tablets were done using direct excitation method. APLQY values were calculated using the software *Fluoracle* from Edinburgh Instruments.

2.5. Interaction Energy Calculations. The structures of Cl-TX and I-TX were retrieved from the Cambridge Structural Database.³⁵ First, relaxation of the unit cell atomic positions was performed in the program Quantum ESPRESSO³⁶ with ultrasoft pseudopotentials from the original library and a 130 Ry plane-wave cutoff energy using PBE functional with vdW interactions treated according to the D3 method of Grimme.³⁷ The unit cell volumes were fixed to the experimental values. Convergence thresholds were set to 1.0×10^{-3} and 1.0×10^{-2} for total energy and force, respectively.

Gaussian09³⁸ was used for interaction energy calculations. The calculations were performed using the MP2 functional and the DEF2-TZVP basis set. Basis set superposition error was corrected using the Counterpoise method.

3. RESULTS AND DISCUSSION

3.1. Engineering Novel Crystalline Phases of Cl-TX and I-TX. In spite of molecule similarity, Cl-TX and I-TX have different crystal packings (see Figure 1).¹⁰ Considering that

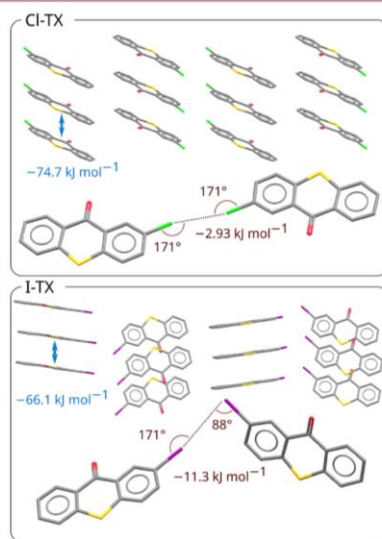


Figure 1. Representation of the crystal packings and respective halogen bonding in Cl-TX and I-TX. Interaction energies are given between pairs of π - π -stacked and halogen-bonded molecules. Atom colors: C (gray), O (red), S (yellow), Cl (green), I (violet). Hydrogen atoms omitted for clarity.

both molecules are aromatic and flat, there are π - π interactions present between the stacked molecules. Such interactions are known to facilitate luminescence, and those were attributed to the origin of an exceptionally efficient luminescence of crystalline Cl-TX.¹⁰ However, it is important to note that in both structures another energetically favorable interaction is also present, namely, the halogen bonding. Apart from being an important crystal-structure-stabilizing force, halogen bonding has been identified to have a crucial role in solid state luminescence.¹⁵ However, it is often neglected when analyzing molecular-level factors responsible for luminescence effects.³⁹ This type of interaction is highly directional, and both

packings display different geometry of halogen...halogen contacts corresponding to criteria for efficient interactions in each case⁴⁰ (see Figure 1). We calculated the interaction energy between the respective halogen-bonded molecules, and it is $-2.93 \text{ kJ mol}^{-1}$ and $-11.3 \text{ kJ mol}^{-1}$ for the Cl...Cl-bonded and I...I-bonded pairs, respectively. While the π - π interactions are very efficient in both cases, the halogen bonding can be considered an important contribution into stabilization of the crystal packing, especially for I-TX.

Empirical observations in crystal engineering hint that molecules differing merely by halogen substituents may form solid solutions.^{41–45} For a solid solution to exist in the whole composition range, it is mandatory for both pure components to have identical crystal packings. In that case, any component ratio in between can be accommodated in the respective structure. Although it is not the case for Cl-TX and I-TX, limited-solubility solid solutions may exist, as in each pure component structure, the opposite component molecules might be incorporated up to some limiting composition.

The most elegant way to explore possible solid solution formation is to construct a binary melt phase diagram of the desired system. Not only does such a phase diagram answer the question of whether solid solutions form, but it also summarizes thermodynamic miscibility limits and may indicate metastable solid solution phases.⁴⁶

Indeed, the construed melt phase diagram shows that solid state miscibility is present for this system; i.e., there are two limited-solubility solid solutions formed based on the structures of pure Cl-TX and I-TX phases, respectively (see Figure 2).

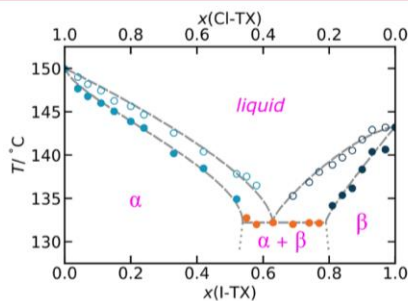


Figure 2. Melt phase diagram of Cl-TX-I-TX binary system (lines are guides for the eyes).

The structure of Cl-TX can accommodate up to $\sim 50 \text{ mol } \%$ of I-TX (solid solution α). Similarly, a solid solution that is based on the I-TX structure forms compositions with up to $\sim 20 \text{ mol } \%$ of Cl-TX (solid solution β). In the remaining composition range, the thermodynamically stable system is a physical mixture of both solid solutions α and β with the respective limiting compositions. In Figure S1, DSC curves on which the binary melt phase diagram was construed are depicted.

When the opposite component is introduced in the crystal structure of a pure compound, it intrinsically leads to a disordered phase (hence the name solid solution), and consequently some minor structural changes are induced, e.g., deviations of the lattice parameters. These effects are

reflected in the PXRD patterns (see Figure S2 for selected samples). Peak positions and intensities vary in different composition samples of the same solid solution. For the compositions covering the biphasic region, the characteristic peaks of both solid solutions can be observed. The PXRD results are consistent with the melt phase diagram shown above.

Both pure compounds exhibit technologically relevant luminescence properties. We studied this phenomenon for the newly obtained solid solutions to understand to what extent the luminescence properties are altered when the opposite component is introduced in the crystal structures.

3.2. Luminescence Properties of I-TX and Cl-TX Solid Solutions.

3.2.1. Solid Solution α . Solid solution α is based on the Cl-TX structure. The luminescence spectrum of pure Cl-TX represents a band with the maximum intensity of $\sim 600 \text{ nm}$. The excitation spectrum for this band contains three maxima at 330 nm , 420 nm , and 490 nm and a small shoulder at $\sim 390 \text{ nm}$ (see Figure 3, top).

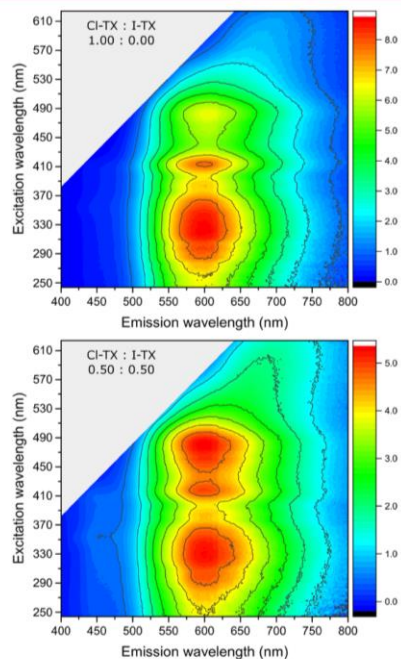


Figure 3. Room temperature excitation-emission luminescence maps of solid solution α at two compositions.

This is consistent with the reported results on the luminescence properties of Cl-TX powders. There, the main band was attributed to phosphorescence, while the weak intensity shoulder at $\sim 450 \text{ nm}$ was attributed to fluorescence.¹⁰

In solid solution α as many as around half of the Cl-TX molecules can be exchanged by I-TX. Although the accessible composition range is wide, the excitation-emission maps

change rather insignificantly. Nevertheless, in detailed comparison we see that for the luminescence band at 600 nm, there is a red-shifted shoulder present in the map of I-TX:Cl-TX composition of 0.50:0.50 (see Figure 3, bottom). Furthermore, the excitation maximum at 490 nm is equally intense to the maxima at 330 and 420 nm. Finally, the fluorescence band at 450 nm is notably more pronounced (see Figure 4). The data therefore show that in this particular case

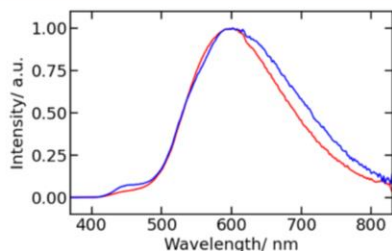


Figure 4. Room temperature photoluminescence spectra ($\lambda_{\text{ex}} = 330$ nm) of solid solution α at two Cl-TX:I-TX compositions: 1.0:0.0 (red); 0.5:0.5 (blue).

the halogen atom type has no major influence on the photoluminescence mechanism. The particularly efficient luminescence in Cl-TX in the previous study was associated with a favorable π - π stacking.¹⁰ Apparently, the minor difference in the electronic structure of both molecules and interplanar spacing variation in the crystalline state induced when part of the original Cl-TX molecules are exchanged by I-TX molecules does not result in a significant alteration of the luminescence spectral characteristics.

It is important to note that the solid solution spectra are significantly different from those of the physical mixtures of pure phases in the same ratios. For example, the photoluminescence spectrum of a 0.4:0.6 (I-TX:Cl-TX) mechanical mixture can be modeled as a linear combination of the distinct spectra of Cl-TX and I-TX with the coefficients corresponding to the compound fractions in the mixture. Meanwhile, the solid solution with the same component ratio displays a different spectrum (see Figure 5).

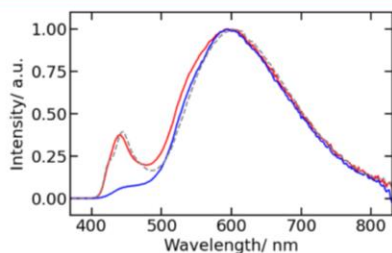


Figure 5. Room temperature photoluminescence spectra ($\lambda_{\text{ex}} = 330$ nm) of (1) 0.4:0.6 (I-TX:Cl-TX) mechanical mixture (red); (2) linear combination of I-TX and Cl-TX spectra scaled 0.4:0.6 (dashed gray); (3) 0.4:0.6 (I-TX:Cl-TX) solid solution (blue).

3.2.2. Solid Solution β . Solid solution β is based on I-TX structure, and it exists in a considerably narrower composition range than solid solution α . Only up to ~ 20 mol % of the 4-iodothioxanthone molecules can be exchanged by Cl-TX until the solubility limit is reached. However, in this case, even a few mol % of the opposite component has a major effect on the luminescence spectral properties. In Figure 6 (top), the excitation–emission luminescence map of pure I-TX in the powdered form is depicted. It features an intense band with the maximum at 445 nm that was attributed to fluorescence.¹⁰ The phosphorescence bands of pure I-TX are weak, but they change when Cl-TX molecules are introduced in the crystal structure. Only 2 mol % of Cl-TX significantly change the map characteristics (see Figure 6).

New emission bands are introduced with maxima at lower wavelengths. In the emission spectra at $\lambda_{\text{ex}} = 330$ nm given in Figure 7, this can be observed even more clearly. Further replacement of I-TX by Cl-TX induces changes in the relative intensity between the fluorescence and phosphorescence bands.

We believe that the pronounced phosphorescence effect caused by the increase of Cl-TX content in the I-TX matrix is related to the halogen bonding; i.e., this bonding is directly responsible for the phosphorescence mechanism in solid solution β . In pure I-TX, the halogen bonding interaction energy is -11.3 kJ mol⁻¹ (see Figure 1). When one or the other iodine atom is exchanged by chlorine, the interaction energy efficiency is reduced to -8.66 kJ mol⁻¹ and -5.06 kJ mol⁻¹. This indicates that efficient mixed halogen bonding interactions are maintained in the solid solutions. Such interactions are not present in mechanical mixtures of pure I-TX and Cl-TX.

Due to relative intensity changes of the spectral bands, there is a variation of the luminescence color. In Figure 8, a CIE chromaticity diagram is depicted for several solid solution β (and α) compositions.

For solid solution α there is almost no difference in the luminescence color even if half of the original Cl-TX molecules are exchanged by I-TX molecules in the crystal structure. Meanwhile, the color has a strong composition dependence in solid solution β . Within a 17 mol % of Cl-TX content, there is a large variation across the CIE space. The luminescence color can therefore be finely tuned by varying the solid solution composition.

The absolute photoluminescence quantum yield dependence on the solid solution composition is depicted in Figure S3. For pure Cl-TX, the quantum yield is 1.7%. It decreases to 0.88% as the 0.5:0.5 (I-TX:Cl-TX) composition is reached. For solid solution β , the quantum yield increases with increasing Cl-TX content from 0.37% to $\sim 0.8\%$.

4. CONCLUSIONS

We show that the solid solution approach can be used to fine-tune luminescence properties of organic crystalline materials. We anticipate that a strong luminescence property dependence on composition can be expected if the intermolecular interactions responsible for the luminescence are particularly affected by the formation of solid solutions. We have identified that in the studied solid solution β there are efficient halogen bonding interactions present that could be related with the luminescence mechanism. Accordingly, a significant variation of the luminescence spectra is observed. The demonstrated approach shows that as far as single-phase materials are

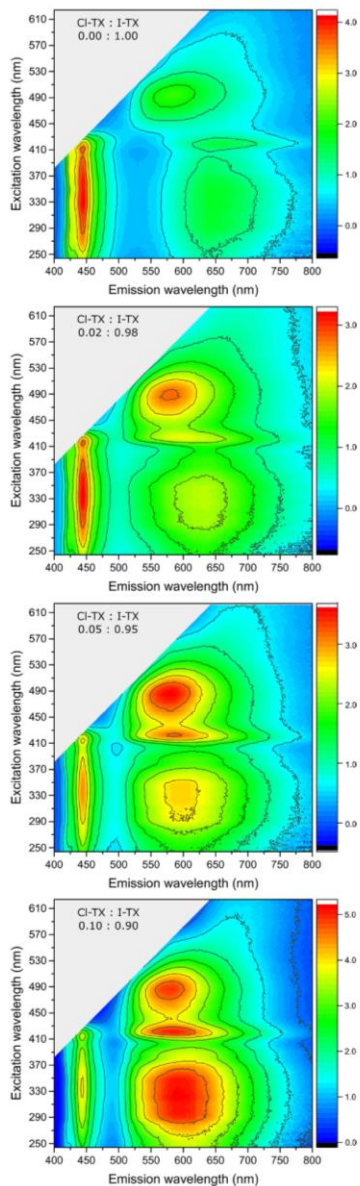


Figure 6. Room temperature excitation–emission luminescence maps of solid solution β at four compositions.

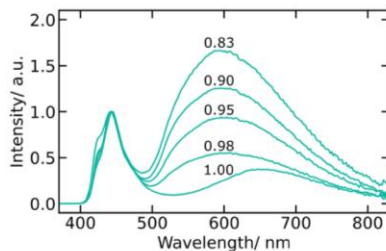


Figure 7. Room temperature photoluminescence spectra ($\lambda_{\text{ex}} = 330$ nm) of solid solution β at five Cl-TX:I-TX ratios. Compositions are given with respect to I-TX content.

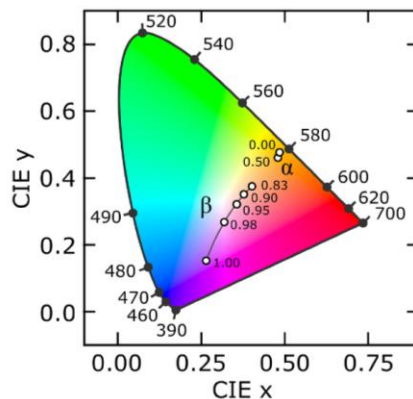


Figure 8. CIE chromaticity diagram (CIE 1931, standard observer) of several compositions of β and α solid solutions calculated from emission spectra excited at $\lambda_{\text{ex}} = 330$ nm (room temperature). Compositions given with respect to I-TX content.

considered, the properties can be tuned in a continuous fashion, which is not possible with chemically modifying the luminescent organic molecules or using other crystal engineering approaches.

■ ASSOCIATED CONTENT

Supporting Information

The Supporting Information is available free of charge at <https://pubs.acs.org/doi/10.1021/acs.cgd.2c00313>.

DSC curves, PXRD patterns, and absolute photoluminescence quantum yields of different composition solid solution samples (PDF)

■ AUTHOR INFORMATION

Corresponding Author

Toms Rekis – Faculty of Chemistry, University of Latvia, LV1004 Riga, Latvia; orcid.org/0000-0001-5128-4611; Email: toms.rekis@lu.lv

Authors

Kristaps Saršins – Faculty of Chemistry, University of Latvia, LV1004 Riga, Latvia

Meldra Kemere – Institute of Solid State Physics, University of Latvia, LV1063 Riga, Latvia

Aleksejs Karziņš – Faculty of Chemistry, University of Latvia, LV1004 Riga, Latvia

Igoris Kļimenkovs – Faculty of Chemistry, University of Latvia, LV1004 Riga, Latvia

Agris Bērziņš – Faculty of Chemistry, University of Latvia, LV1004 Riga, Latvia; orcid.org/0000-0002-4149-8971

Anatolijs Sarakovskis – Institute of Solid State Physics, University of Latvia, LV1063 Riga, Latvia

Complete contact information is available at:
<https://pubs.acs.org/10.1021/acs.cgd.2c00313>

Notes

The authors declare no competing financial interest.

ACKNOWLEDGMENTS

KS acknowledges funding from the European Social Fund project *Strengthening of the capacity of doctoral studies at the University of Latvia within the framework of the new doctoral model*, identification No. 8.2.2.0/20/1/006 and University of Latvia Foundation through a MikroTik Ltd. doctoral scholarship in the field of natural and medical sciences. This research was partly funded by the Latvian Council of Science, project *Crystal engineering of pharmaceutical multicomponent phases for more efficient crystalline phase design*, project No. lzp-2018/1-0312. Institute of Solid State Physics, University of Latvia as the Center of Excellence acknowledges funding from the European Union's Horizon 2020 Framework Programme H2020-WIDESPREAD-01-2016-2017-TeamingPhase2 under grant agreement No. 739508, project CAMART₂.

REFERENCES

- (1) Yuan, W. Z.; Shen, X. Y.; Zhao, H.; Lam, J. W. Y.; Tang, L.; Lu, P.; Wang, C.; Liu, Y.; Wang, Z.; Zheng, Q.; Sun, J. Z.; Ma, Y.; Tang, B. Z. Crystallization-Induced Phosphorescence of Pure Organic Luminescence at Room Temperature. *J. Phys. Chem. C* **2010**, *114*, 6090–6099.
- (2) Kenry; Chen, C.; Liu, B. Enhancing the performance of pure organic room-temperature phosphorescent luminophores. *Nat. Commun.* **2019**, *10*, 1–15.
- (3) Villa, M.; D'Agostino, S.; Sabatino, P.; Noel, R.; Busto, J.; Roy, M.; Gingras, M.; Ceroni, P. Pentasulfurated benzene-cored asterisks: relationship between crystal structure and luminescence properties. *New J. Chem.* **2020**, *44*, 3249–3254.
- (4) Zhao, Y.; Yang, H.; Ma, H.; Li, Y.; Qian, L.; Yu, T.; Su, W. Photo- and electro-luminescence properties of the organic bipolar molecules containing phenothiazine and phenanthroimidazole moieties. *Synth. Met.* **2020**, *265*, 116406.
- (5) Jia, W.; Wang, Q.; Shi, H.; An, Z.; Huang, W. Manipulating the Ultralong Organic Phosphorescence of Small Molecular Crystals. *Chemistry – A European Journal* **2020**, *26*, 4437–4448.
- (6) Zhuo, M.-P.; Su, Y.; Qu, Y.-K.; Chen, S.; He, G.-P.; Yuan, Y.; Liu, H.; Tao, Y.-C.; Wang, X.-D.; Liao, L.-S. Hierarchical Self-Assembly of Organic Core/Multi-Shell Microwires for Trichromatic White-Light Sources. *Adv. Mater.* **2021**, *33*, 2102719.
- (7) Wu, J.-J.; Zhuo, M.-P.; Lai, R.; Zou, S.-N.; Yan, C.-C.; Yuan, Y.; Yang, S.-Y.; Wei, G.-Q.; Wang, X.-D.; Liao, L.-S. Cascaded Excited-State Intramolecular Proton Transfer Towards Near-Infrared Organic Lasers Beyond 850 nm. *Angew. Chem., Int. Ed.* **2021**, *60*, 9114–9119.
- (8) Humayoun, U. B.; Tirunch, S. N.; Yoon, D.-H. On the crystal structure and luminescence characteristics of a novel deep red emitting SrLaScO₄:Mn⁴⁺. *Dyes Pigm.* **2018**, *152*, 127–130.
- (9) Wang, Y.; Tang, S.; Wen, Y.; Zheng, S.; Yang, B.; Yuan, W. Z. Nonconventional luminophores with unprecedented efficiencies and color-tunable afterglows. *Mater. Horiz.* **2020**, *7*, 2105–2112.
- (10) Wen, Y.; Liu, H.; Zhang, S.; Gao, Y.; Yan, Y.; Yang, B. One-dimensional – stacking induces highly efficient pure organic room-temperature phosphorescence and ternary-emission single-molecule white light. *J. Mater. Chem. C* **2019**, *7*, 12502–12508.
- (11) Hamzehpoor, E.; Perepichka, D. F. Crystal Engineering of Room Temperature Phosphorescence in Organic Solids. *Angew. Chem., Int. Ed.* **2020**, *59*, 9977–9981.
- (12) Xue, S.; Qiu, X.; Sun, Q.; Yang, W. Alkyl length effects on solid-state fluorescence and mechanochromic behavior of small organic luminophores. *J. Mater. Chem. C* **2016**, *4*, 1568–1578.
- (13) Davis, R.; Saleesh Kumar, N. S.; Abraham, S.; Suresh, C. H.; Rath, N. P.; Tamaoki, N.; Das, S. Molecular Packing and Solid-State Fluorescence of Alkoxy-Cyano Substituted Diphenylbutadienes: Structure of the Luminescent Aggregates. *J. Phys. Chem. C* **2008**, *112*, 2137–2146.
- (14) Shimizu, M.; Hiyaama, T. Organic Fluorophores Exhibiting Highly Efficient Photoluminescence in the Solid State. *Chemistry – An Asian Journal* **2010**, *5*, 1516–1531.
- (15) Yang, Z.; Xu, C.; Li, W.; Mao, Z.; Ge, X.; Huang, Q.; Deng, H.; Zhao, J.; Gu, F. L.; Zhang, Y.; Chi, Z. Boosting the Quantum Efficiency of Ultralong Organic Phosphorescence up to 52% via Intramolecular Halogen Bonding. *Angew. Chem., Int. Ed.* **2020**, *59*, 17451–17455.
- (16) Zheng, C.; Zang, Q.; Nie, H.; Huang, W.; Zhao, Z.; Qin, A.; Hu, R.; Tang, B. Z. Fluorescence visualization of crystal formation and transformation processes of organic luminogens with crystallization-induced emission characteristics. *Mater. Chem. Front.* **2018**, *2*, 180–188.
- (17) Fan, Y.; Zhao, Y.; Ye, L.; Li, B.; Yang, G.; Wang, Y. Polymorphs and Pseudopolymorphs of N,N-Di(n-butyl)Quinacridone: Structures and Solid-State Luminescence Properties. *Cryst. Growth Des.* **2009**, *9*, 1421–1430.
- (18) Anthony, S. P. Organic Solid-State Fluorescence: Strategies for Generating Switchable and Tunable Fluorescent Materials. *Chem-PlusChem.* **2012**, *77*, 518–531.
- (19) Guan, J.; Zhang, C.; Gao, D.; Tang, X.; Dong, X.; Lin, X.; Wang, Y.; Wang, X.; Wang, L.; Lee, H. H.; Xu, J.; Zheng, H.; Li, K.; Mao, H.-k. Drastic photoluminescence modulation of an organic molecular crystal with high pressure. *Mater. Chem. Front.* **2019**, *3*, 1510–1517.
- (20) Yuan, H.; Wang, K.; Yang, K.; Liu, B.; Zou, B. Luminescence Properties of Compressed Tetraphenylethene: The Role of Intermolecular Interactions. *J. Phys. Chem. Lett.* **2014**, *5*, 2968–2973.
- (21) Sagara, Y.; Kato, T. Mechanically induced luminescence changes in molecular assemblies. *Nat. Chem.* **2009**, *1*, 605–610.
- (22) Yan, D.; Delori, A.; Lloyd, G. O.; Friščić, T.; Day, G. M.; Jones, W.; Lu, J.; Wei, M.; Evans, D. G.; Duan, X. A Cocrystal Strategy to Tune the Luminescent Properties of Stilbene-Type Organic Solid-State Materials. *Angew. Chem., Int. Ed.* **2011**, *50*, 12483–12486.
- (23) d'Agostino, S.; Gregolini, F.; Braga, D.; Moreschi, D.; Fattori, V.; Delchiaro, F.; Di Motta, S.; Negri, F. Exciton coupling in molecular salts of 2-(1,8-naphthalimido)ethanoic acid and cyclic amines: modulation of the solid-state luminescence. *CrystEngComm* **2013**, *15*, 10470–10480.
- (24) Zhuo, M.-P.; Yuan, Y.; Su, Y.; Chen, S.; Chen, Y.-T.; Feng, Z.-Q.; Qu, Y.-K.; Li, M.-D.; Li, Y.; Hu, B.-W.; Wang, X.-D.; Liao, L.-S. Segregated Array Tailoring Charge-Transfer Degree of Organic Cocrystal for the Efficient Near-Infrared Emission beyond 760 nm. *Adv. Mater.* **2022**, *34*, 2107169.
- (25) Krishnan, R.; Swart, H. C. Luminescence properties of octahedrally and tetrahedrally coordinated Mo⁶⁺ in the solid solutions: Judd–Ofelt investigation. *J. Phys. Chem. Solids* **2020**, *144*, 109519.

- (26) Levushkina, V.; Spassky, D.; Tretyakova, M.; Zadneprovski, B.; Kamenskikh, I.; Vasil'ev, A.; Belsky, A. Luminescence properties of solid solutions $\text{LuY}_{1-x}\text{PO}_4:\text{Eu}^{3+}$. *Opt. Mater.* **2018**, *75*, 607–611.
- (27) Bayart, A.; Katelnikovas, A.; Blach, J.-F.; Rousseau, J.; Saitzek, S. Synthesis, structural and luminescence properties of $(\text{La}_{1-x}\text{Ln}_x)_2\text{Ti}_2\text{O}_7$ (Ln = lanthanides) solid solutions. *J. Alloys Compd.* **2016**, *683*, 634–646.
- (28) Dunce, M.; Birks, E.; Antonova, M.; Ignatans, R.; Nitiss, E.; Kundzinsh, M.; Grube, J.; Sarakovskis, A.; Sternberg, A. Photoluminescence in Er-doped $0.4\text{Na}_1/2\text{Bi}_{1/2}\text{TiO}_3\cdot(0.6-x)\text{SrTiO}_3\cdot x\text{PbTiO}_3$ solid solutions. *Ferroelectrics* **2020**, *567*, 150–159.
- (29) Fourmigué, M. Solid-solution (alloying) strategies in crystalline molecular conductors. *J. Mater. Chem. C* **2021**, *9*, 10557–10572.
- (30) Wiscons, R. A.; Coropceanu, V.; Matzger, A. J. Quaternary Charge-Transfer Solid Solutions: Electronic Tunability through Stoichiometry. *Chem. Mater.* **2019**, *31*, 6598–6604.
- (31) Corpinot, M. K.; Bučar, D.-K. A Practical Guide to the Design of Molecular Crystals. *Cryst. Growth Des.* **2019**, *19*, 1426–1453.
- (32) Rekis, T.; Bērziņš, A. On the structural aspects of solid solutions of enantiomers: an intriguing case study of enantiomer recognition in the solid state. *CrystEngComm* **2018**, *20*, 6909–6918.
- (33) Kitaigorodskii, A. *Mixed Crystals*; Springer-Verlag: Berlin, 1984.
- (34) Kitaigorodskii, A. *Organic chemical crystallography*; Consultants Bureau: New York, 1961.
- (35) Groom, C. R.; Bruno, I. J.; Lightfoot, M. P.; Ward, S. C. The Cambridge Structural Database. *Acta Crystallographica Section B* **2016**, *72*, 171–179.
- (36) Giannozzi, P.; et al. Advanced capabilities for materials modelling with QUANTUM ESPRESSO. *J. Phys.: Condens. Matter* **2017**, *29*, 465901.
- (37) Grimme, S.; Antony, J.; Ehrlich, S.; Krieg, H. A consistent and accurate ab initio parametrization of density functional dispersion correction (DFT-D) for the 94 elements H-Pu. *J. Chem. Phys.* **2010**, *132*, 154104.
- (38) Frisch, M. J. et al. *Gaussian 09*; Revision E.01; Gaussian Inc.: Wallingford, CT, 2009.
- (39) Wang, W.; Zhang, Y.; Jin, W. J. Halogen bonding in room-temperature phosphorescent materials. *Coord. Chem. Rev.* **2020**, *404*, 213107.
- (40) Bui, T.; Dahaoui, S.; Lecomte, C.; Desiraju, G.; Espinosa, E. The Nature of Halogen-Halogen Interactions: A Model Derived from Experimental Charge-Density Analysis. *Angew. Chem., Int. Ed.* **2009**, *48*, 3838–3841.
- (41) Vogt, F. G.; Vena, J. A.; Chavda, M.; Clawson, J. S.; Strohmeier, M.; Barnett, M. E. Structural analysis of 5-fluorouracil and thymine solid solutions. *J. Mol. Struct.* **2009**, *932*, 16–30.
- (42) Saršūns, K.; Bērziņš, A. Prediction of Solid Solution Formation among Chemically Similar Molecules Using Calculation of Lattice and Intermolecular Interaction Energy. *Materials Science and Applied Chemistry III* **2020**, 54–59.
- (43) Dabros, M.; Emery, P.; Thalladi, V. A Supramolecular Approach to Organic Alloys: Cocrystals and Three- and Four-Component Solid Solutions of 1,4-Diazabicyclo[2.2.2]octane and 4-X-Phenols (X = Cl, CH₃, Br). *Angew. Chem., Int. Ed.* **2007**, *46*, 4132–4135.
- (44) Theocharis, C. R.; Desiraju, G. R.; Jones, W. The use of mixed crystals for engineering organic solid-state reactions: application to benzylbenzylidencyclopentanones. *J. Am. Chem. Soc.* **1984**, *106*, 3606–3609.
- (45) Bučar, D.-K.; Sen, A.; Mariappan, S. V. S.; MacGillivray, L. R. A [2 + 2] cross-photodimerisation of photostable olefins via a three-component cocrystal solid solution. *Chem. Commun.* **2012**, *48*, 1790–1792.
- (46) Rekis, T.; Bērziņš, A.; Sarceviča, I.; Kons, A.; Balodis, M.; Orola, L.; Lorenz, H.; Actiņš, A. A Maze of Solid Solutions of Pimobendan Enantiomers: An Extraordinary Case of Polymorph and Solvate Diversity. *Cryst. Growth Des.* **2018**, *18*, 264–273.



Saršūns, K., Bērziņš, A.

**EXPERIMENTAL AND COMPUTATIONAL
INVESTIGATION OF BENPERIDOL AND DROPERIDOL
SOLID SOLUTIONS IN DIFFERENT CRYSTAL
STRUCTURES**

Crystal Growth & Design, **2023**, 23(2), 1133–1144

Reprinted with permission from American Chemical Society (ACS).

Copyright © 2023, American Chemical Society



Experimental and Computational Investigation of Benperidol and Droperidol Solid Solutions in Different Crystal Structures

Kristaps Saršūns and Agris Bērziņš*

Cite This: *Cryst. Growth Des.* 2023, 23, 1133–1144

Read Online

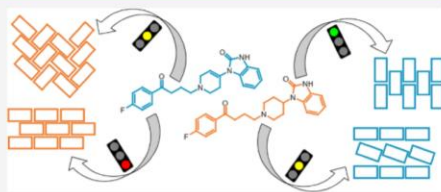
ACCESS |

Metrics & More

Article Recommendations

Supporting Information

ABSTRACT: We present an experimental and computational study of solid solution formation between structurally highly similar active pharmaceutical ingredients droperidol and benperidol in nonsolvates, dihydrates, and several solvates formed by these compounds. We demonstrate that the formation of solid solutions strongly depends on the crystal structure of the phase. In some of the structures, almost complete replacement of benperidol with droperidol can be achieved, whereas in other structures, the replacement is possible only up to a limited molar ratio. However, only limited replacement of droperidol with benperidol can be achieved and only in some of the structures. The solid solution formation is primarily determined by the change in intermolecular interaction energy resulting from the molecule replacement. Only structures where molecule replacement allows the formation of efficient intermolecular interactions can be obtained experimentally. The results indicate that the energy requirements of intermolecular interaction changes to obtain solid solutions in the nonsolvated phase are less strict than those for solvates.



1. INTRODUCTION

Crystal engineering includes developing approaches and tools allowing the use of already characterized crystals to predict the formation of unknown crystal structures and their properties.¹ Approaches allowing the prediction of formation of crystal structures of organic materials include evaluation of intermolecular interaction complementarity and preferences, most specifically hydrogen bonds^{2,3} and halogen bonds,^{4,5} and the use of knowledge-based approaches. Knowledge-based approaches are often based on data in the Cambridge Structure Database (CSD), such as hydrogen-bond propensity^{6–8} and nonbonded intermolecular interactions for a wide range of chemical groups available in the IsoStar database⁹ or mining the CSD for more specific information.^{10–13} Also, computational tools have been developed for predicting the formation of specific phases^{14–16} or crystal structures in general.^{17–19} Crystal engineering approaches have been used to design and tune important physical properties of crystals, such as solubility,^{20,21} optical²² and mechanical properties,²³ melting point,²⁴ etc.

Crystal engineering has been used to successfully design strong intermolecular interactions in the solid state,^{8,25,26} but a belief that crystal structures can now be easily designed is overly optimistic, as often only the dominant supramolecular synthons are designed and part of the success lies in the exploitation of the limited number of functional groups having notably different properties.^{26–28} For example, it has been shown^{29,30} that in the case of competing interactions, successful prediction is highly challenging or impossible. Moreover, weak intermolecular interactions, their contribution

to the stability of the crystal structure, and the effect of slight alteration of such interactions is even harder to be predicted and estimated.^{31–33} However, polymorph structures often are a result of an interplay of weak intermolecular interactions and conformation, while strong interactions could be unaltered.^{34–36} The rationalization of interactions in multicomponent phases is often even more challenging, and the propensity of a compound to form solvates and cocrystals in general cannot be reliably predicted. Nevertheless, factors responsible for solvate formation for specific compounds have been identified,^{37–41} and there are strategies for the prediction of formation of multicomponent phases for defined compounds.^{42–44}

Weak intermolecular interactions are very important in the formation of molecular solid solutions. The main requirement for the formation of solid solutions clearly is the miscibility of the components in the solid state.⁴⁵ This depends on two related concepts—structural mimicry^{46,47} and crystal isomorphism.^{48,49} It has long been demonstrated that primarily the size and shape of the entities have to be similar for a molecule replacement in the crystal lattice and formation of solid solution,^{50–52} provided the replacement does not break

Received: November 2, 2022

Revised: January 5, 2023

Published: January 17, 2023



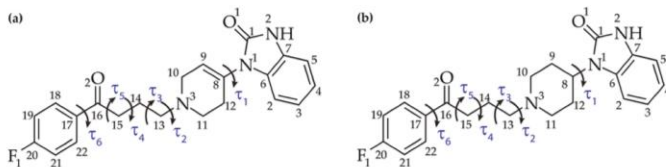


Figure 1. Molecular structure of (a) droperidol and (b) benperidol with the numbering of non-hydrogen atoms and labeling of flexible torsion angles.

the intermolecular hydrogen bonding network and limitations regarding the dipole moment are followed.⁵² The weak intermolecular interactions, however, are often weak enough so that their alteration will not exclusively prevent the formation of solid solutions but important enough to determine the replacement possibilities.⁵³ Nevertheless, it is reported that solid solutions between similar molecules can be obtained if the exchanged atoms or groups are not involved in energetically notable directional or electrostatic interactions.^{45,53–56} Overall, the studies of whether the replacement of relatively similar functional groups of organic molecules would allow the formation of either isostructural phases⁵⁷ or solid solutions⁵⁸ have gained increasing attention as a tool to develop or test the rules of crystal engineering.^{59,60} Moreover, solid solutions can be used to modify and fine-tune various properties of crystals,^{48,61} including solubility,^{62,63} optical properties,^{64,65} etc.

In this study, we explored the solid solution formation between two drug molecules: droperidol, 1-[1-[4-(4-fluorophenyl)-4-oxobutyl]-1,2,3,6-tetrahydro-4-pyridyl]-1,3-dihydro-2H-benzimidazol-2-one (Figure 1a), and benperidol, 1-[1-[4-(4-fluorophenyl)-4-oxobutyl]piperidin-4-yl]-1,3-dihydro-2H-benzimidazol-2-one (Figure 1b). The molecular structures of both compounds are very similar, and the difference is in the C8–C9 bond, which is saturated in benperidol and therefore is a part of a piperidine moiety, whereas it is unsaturated and a part of a 1,2,3,6-tetrahydropyridine moiety in droperidol.

The solid form landscapes of both compounds have been explored.^{66,67} Droperidol forms four polymorphs (in ambient crystallization, ^BI is obtained) and 11 solvates, including a set of isostructural solvates (methanol solvate ^DS_{MeOH}, ethanol solvate ^DS_{EtOH}, acetonitrile solvate ^DS_{ACN}) and nonstoichiometric hydrate ^DNSH, and a dihydrate ^DDH. Benperidol forms five polymorphs (in ambient crystallization, ^BI and ^BII are obtained) and 11 solvates, including two sets of isostructural solvates (type 1 solvates with methanol ^BS_{MeOH} and ethanol ^BS_{EtOH} and type 2 solvate with acetonitrile ^BS_{ACN}) and a dihydrate ^BDH.

A possibility for the formation of isostructural phases among these compounds has been studied by concluding that in conventional crystallization, no isostructural phase between both compounds is obtained, but some are accessible via cross-seeding.⁵⁷ Unique structures for each of the compounds are attributed to differences in the weak intermolecular interactions introduced by the molecular differences.

In this study, the formation of solid solutions between droperidol and benperidol has been explored by comparing the formation of solid solutions in nonsolvated forms as well as in several solvates of these compounds. Computational calculations were performed to get an insight into the factors responsible for the differences in droperidol and benperidol

solubility limits in several different phases formed by the other molecule and to evaluate the effects of intermolecular interactions, leading to the observed solubility differences.

2. EXPERIMENTAL SECTION

2.1. Materials. Benperidol polymorph ^BI (purity >99%) and droperidol polymorph ^DII (purity >99%) were obtained from JSC Grindeks (Riga, Latvia). Organic solvents of analytical grade were purchased from commercial sources and used without further purification.

2.2. Crystal Phase Preparation. Solid solution (SS) formation was tested by recrystallization of benperidol and droperidol mixtures (in different ratios from 5 to 95 mol % benperidol). Nonsolvated droperidol and benperidol phases were prepared by dissolving a mixture of droperidol and benperidol in isopropanol at 70 °C (obtaining a nearly saturated solution) and rapidly cooling the solution to –5 °C. Droperidol and benperidol dihydrate samples were obtained by dissolving a mixture of droperidol and benperidol in acetone at 50 °C (obtaining a nearly saturated solution), slowly adding a similar volume of water, and storing the resulting mixtures at 5 °C. Droperidol and benperidol ethanol, methanol, and acetonitrile solvate samples were obtained by dissolving a mixture of droperidol and benperidol in the respective solvent at 60–70 °C (obtaining a nearly saturated solution) and rapidly cooling the solution to –5 °C. More details of the crystallization experiments can be found in Table S1 in the Supporting Information.

The obtained solvated samples (containing either pure solid solution or a mixture of solid solutions in the case of limited solubility) were desolvated by heating at 80 °C (ethanol solvate and dihydrate samples) or 120 °C (methanol and acetonitrile solvate samples) to test the phase obtained after the desolvation.

2.3. Powder X-ray Diffraction (PXRD). All of the obtained crystallization products were characterized by PXRD. The PXRD patterns were measured at ambient temperature on a D8 Advance (Bruker) diffractometer using copper radiation (Cu K α) at a wavelength of 1.54180 Å, equipped with a LynxEye position-sensitive detector. The tube voltage and current were set to 40 kV and 40 mA. The divergence slit was set at 0.6 mm, and the antiscatter slit was set at 8.0 mm. The diffraction patterns were recorded using a 0.2 s/0.02° scanning speed from 3 to 35° on the 2 θ scale.

2.4. Differential Scanning Calorimetry/Thermogravimetry (DSC/TG). The differential scanning calorimetry/thermogravimetry (DSC/TG) analysis was performed with a TGA/DSC 2 (Mettler Toledo). Open 100 μ L aluminum pans were used. Heating of the samples from 25 to 240 °C was performed at a 10 °C min^{–1} heating rate. Samples of 5 to 10 mg mass were used, and the nitrogen flow rate was 100 \pm 10 mL min^{–1}.

2.5. Nuclear Magnetic Resonance (NMR) Spectroscopy. ¹H NMR spectra of pure benperidol and droperidol and most of the crystallization products dissolved in dimethyl sulfoxide (DMSO)-*d*₆ were recorded at a nominal temperature of 300 K with a Fourier 300 MHz (Bruker) spectrometer. Chemical shifts (δ) were found in parts per million (ppm) using the residual solvent peak as an internal reference. For quantitative determination of each compound in the mixture, the ¹H NMR area of peaks at 10.82 (1H, s), 1.56 (2H, q),

and 1.52 (2H, t) ppm were used for benperidol and at 10.90 (1H, s), 5.81 (1H, t), and 2.64 (2H, t) ppm for droperidol.

2.6. Theoretical Calculations. Theoretical calculations were performed for three sets of crystal structures as in our previous study.⁶⁸ The first set (original) comprised experimental crystal structures of droperidol and benperidol polymorphs and solvates and included droperidol polymorph ^BI GIXXOB,⁶⁹ dihydrate ^BDH DRPRDL,⁷⁰ and solvates ^DS_{EIOH} XOKKEP, ^DS_{MeOH} XOKLAM, and ^DS_{ACN} XOKJUE⁶⁶ as well as benperidol polymorph ^BII BENPRL02, dihydrate ^BDH DUJPAB, and solvates ^BS_{EIOH} DUJXAJ, ^BS_{MeOH} UHIZAO, and ^BS_{ACN} DUJXIR.⁶⁷ As the solvent molecules in ^BS_{EIOH} and ^DS_{MeOH} are disordered over two orientations related by inversion symmetry,⁶⁶ the starting geometries of ^DS_{EIOH} and ^DS_{MeOH} without disorder were prepared in P1 symmetry by discarding one of the solvent molecule's orientation. The second set (isostructural) comprised structures in which all of the molecules of the original compound (e.g., benperidol) were replaced with molecules of the other compound (e.g., droperidol) (see Figure 2). The third set

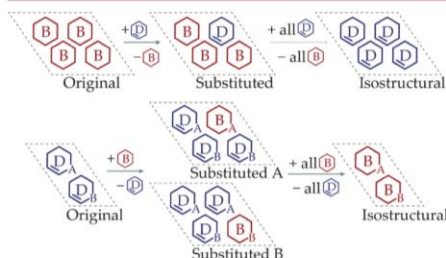


Figure 2. Schematic representation of the construction of substituted and isostructural structures from the original structures used for the calculations. The upper part shows the construction of substituted and isostructural structures from an original benperidol structure, and the lower part shows construction of the two different possible substituted structures A and B involving doubling the unit cell size and the isostructural structure from an original droperidol structure with $Z' = 2$.

(substituted) comprised structures for which symmetry was removed, unit cell size was set to $Z = 4$ ($Z = 6$ for ^BII), and one molecule of the original compound out of 4 (or out of 6 for ^BII) was exchanged to the molecule of the other compound (see Figure 2). For droperidol ^DS_{EIOH}, ^DS_{MeOH}, and ^DS_{ACN}, as well as benperidol ^BS_{ACN}, this meant doubling the unit cell volume, and for structures with $Z' = 2$ or 3, separate structures, designated with A, B, and C, were obtained by substitution of each of the symmetrically unique molecule. In preparation of isostructural and substituted structures, conversion of benperidol to droperidol always resulted in two sets of structures with different locations of the double bonded C8–C9. Among these two alternatives, only the structure with the lowest energy after the geometry optimization in Quantum ESPRESSO (see below) was considered and analyzed.

Calculation of total cell energy and total intermolecular interaction energy of all of the structures was performed using Quantum ESPRESSO⁷¹ after relaxation of positions of all atoms and the unit cell parameters, with ultrasoft pseudopotentials from the original pseudopotential library and a 44 Ry plane-wave cutoff energy using the Perdew–Burke–Ernzerhof (PBE) functional with van der Waals (vdW) interactions treated according to the D2 method of Grimme.⁷² The parameters of convergence, pseudopotentials, and the k -point grid were used as suggested for structure optimizations of pharmaceutical molecules.⁷³ The energy of isolated molecules for calculation of total intermolecular interaction was determined by extracting a single molecule from the optimized crystal structure and placing it inside a cubic unit cell with dimensions $40 \times 40 \times 40 \text{ \AA}^3$.

The total intermolecular interaction energy was calculated as the difference between the total cell energy and a sum of all of the energies of isolated molecules present in the unit cell.

Pairwise intermolecular interaction energy calculations for all of the structures were performed in CrystalExplorer 17.5 at the B3LYP/6-31G(d,p) level by calculating the pairwise interaction energies for molecules for which atoms are within 3.80 Å of the central molecule. Crystal structures were used after the geometry optimization in Quantum ESPRESSO.

The calculations of intramolecular energy were performed in Gaussian 09⁷⁴ at the M06-2X/6-31+G(d,p) level of theory. The potential energy surface (PES) scans of the flexible torsion angles⁵⁷ were used to determine the minimum potential energy conformations. These conformations were geometry optimized, and energy of the global minimum was found for both molecules. Further, benperidol and droperidol geometry was extracted from all of the considered structures (after geometry optimization in Quantum ESPRESSO), and constrained geometry optimization was performed using Gaussian 09 by freezing the torsion angles τ_1 , τ_2 , and τ_4 to the values as in the crystal structures. Intramolecular energy was calculated as the energy difference between the constrained and the global minimum geometry.

2.7. Crystal Structure Comparison and Analysis. Mercury 2020.2.0 software⁷⁵ was used for crystal structure visualization and analysis, including analysis and overlay of conformers present in the experimental and the modified crystal structures. Crystal structures after geometry optimization in Quantum ESPRESSO were used.

3. RESULTS AND DISCUSSION

As reported previously,^{57,66,67} the small differences in the molecular structure of benperidol and droperidol alter the possibility of the central ring to form weak intermolecular interactions, which is the reason why these two highly similar compounds form different crystal structures. Nevertheless, the formation of a droperidol solvate ^{D-iso-B}S_{EIOH} isostructural to the benperidol solvate as well as ^{D-iso-B}DH and ^{D-iso-B}II in the mixture with the original droperidol phases ^DDH or ^DII was observed in the performed cross-seeding experiments.⁵⁷ The formation of such phases confirms that droperidol can crystallize in structures originally observed for benperidol, which also suggests that the formation of solid solutions between these two compounds can be expected. Additionally, these results also suggest that the likelihood of the exchange of these molecules in the solid state depends on the crystal structure (exchange of benperidol with droperidol in the structure of ethanol solvate ^BS_{EIOH} is the easiest, and it is also possible in structures of ^BDH or ^BII, whereas the exchange of droperidol with benperidol was not observed).

In this study, we explore the formation of solid solution as a tool to understand how easily one compound can replace the other one in the solid state and use computational calculations to identify the reasons for the different replacement capabilities in different crystal structures.

3.1. Experimental Characterization of Solid Solution Formation in Different Phases. **3.1.1. Solid Solutions Obtained in Crystallization.** To evaluate the formation of solid solution between droperidol and benperidol in different phases, we initially crystallized mixtures of both compounds in different ratios from solution. We used several different crystallization conditions to obtain different solid phases—nonsolvated forms (in the selected conditions polymorphs ^BI or ^BII could be obtained for benperidol and polymorph ^DII for droperidol), dihydrates, and ethanol, methanol, and acetonitrile solvates. The crystallization conditions for the preparation of these phases were chosen based on the already reported

Table 1. Phases Obtained in Crystallization of a Mixture of Benperidol and Droperidol for Several Selected Molar Ratios under Conditions Producing Nonsolvents or the Selected Solvates^a

benperidol (mol %)	obtained phase				
	nonsolvate	ethanol solvate	methanol solvate	acetonitrile solvate	dihydrate
0	DII	^D S _{EtOH}	^D S _{MeOH}	^D S _{ACN}	^D DH
5	<i>DII + SS^DII</i>	<i>D</i> ^D S _{EtOH} + <i>SS^D</i> _{EtOH}	<i>SS^D</i> _{MeOH}	<i>SS^D</i> _{ACN}	<i>SS^D</i> _{DH}
10	SS^DII	<i>SS^D</i> _{EtOH}	<i>SS^D</i> _{MeOH}	<i>SS^D</i> _{ACN}	<i>SS^D</i> _{DH}
20	SS^DII	<i>SS^D</i> _{EtOH}	<i>SS^D</i> _{Me} + <i>SS^D</i> _{Me}	<i>SS^D</i> _{ACN}	<i>SS^D</i> _{DH} + <i>SS^D</i> _{DH}
30	SS^DII	<i>SS^D</i> _{EtOH}	<i>SS^D</i> _{Me} + <i>SS^D</i> _{Me}	<i>SS^D</i> _{ACN} + <i>SS^D</i> _{ACN}	<i>SS^D</i> _{DH} + <i>SS^D</i> _{DH}
40	SS^DII	<i>SS^D</i> _{EtOH}	<i>SS^D</i> _{Me} + <i>SS^D</i> _{Me}	<i>SS^D</i> _{ACN} + <i>SS^D</i> _{ACN}	<i>SS^D</i> _{DH} + <i>SS^D</i> _{DH}
50	SS^DII	<i>SS^D</i> _{EtOH}	<i>SS^D</i> _{MeOH}	<i>SS^D</i> _{ACN} + <i>SS^D</i> _{ACN}	<i>SS^D</i> _{DH} + <i>SS^D</i> _{DH}
60	SS^DII	<i>SS^D</i> _{EtOH}	<i>SS^D</i> _{MeOH}	<i>SS^D</i> _{ACN} + <i>SS^D</i> _{ACN}	<i>SS^D</i> _{DH} + <i>SS^D</i> _{DH}
70	SS^DII	<i>SS^D</i> _{EtOH}	<i>SS^D</i> _{MeOH}	<i>SS^D</i> _{ACN} + <i>SS^D</i> _{ACN}	<i>SS^D</i> _{DH}
80	SS^DII	<i>SS^D</i> _{EtOH}	<i>SS^D</i> _{MeOH}	<i>SS^D</i> _{ACN}	<i>SS^D</i> _{DH}
90	SS^DII	<i>SS^D</i> _{EtOH}	<i>SS^D</i> _{MeOH}	<i>SS^D</i> _{ACN}	<i>SS^D</i> _{DH}
100	BI	^B S _{EtOH}	^B S _{MeOH}	^B S _{ACN}	^B DH

^aSS designates solid solution with a crystal structure of the respective phase. Pure phases are in bold, and phase mixtures are in italic.

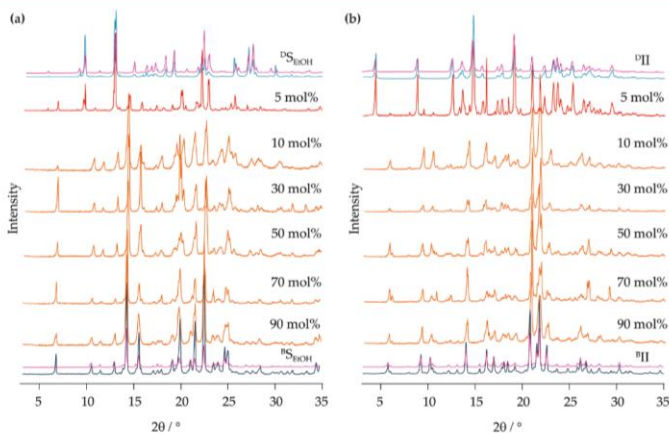


Figure 3. PXRD patterns of crystallization products when different ratios of benperidol and droperidol were crystallized from (a) ethanol by obtaining the ethanol solvate phase or phases and (b) isopropanol by obtaining nonsolvated phase or phases. Labels show the weighted molar fraction of benperidol used in the crystallization. PXRD patterns for additional compositions are given in the Supporting Information. Solid solutions are in orange, phase mixtures in red, pure benperidol and droperidol phases in blue, and patterns simulated from crystal structures in magenta.

procedures for obtaining the respective single-component phases and solvates of these compounds.⁵⁷

The solid products obtained in the crystallization were characterized by PXRD and DSC/TG. The phases present in the samples were identified based on the agreement with the PXRD patterns of droperidol and benperidol polymorphs and solvates reported previously^{66,67} and are given in Table 1. The employed crystallization procedure always resulted in the formation of the phase or phases with the desired composition, as the nonsolvated phase or phases (^BI, ^BII, and ^DII) were obtained from isopropanol, dihydrate or dihydrates (^DDH and ^BDH) from acetone/water and the respective solvate or solvates from the organic solvents (^BS_{EtOH} and ^DS_{EtOH} from ethanol, ^BS_{MeOH} and ^DS_{MeOH} from methanol, and ^BS_{ACN} and ^DS_{ACN} from acetonitrile). In most of the cases, crystallization of a mixture of droperidol and benperidol produced only a single

phase, meaning that a solid solution (designated by SS) containing both components in the respective crystal structure formed (see Table 1). The benperidol/droperidol ratio in the obtained products was confirmed by recording ¹H NMR spectra of selected samples and was always close to the weighted ratio (see Supporting Information).

The results presented in Table 1 clearly show that the ability to replace one molecule with the other strongly depends on the crystal structure, including even different capabilities to accommodate the other molecules by the isostructural solvate series ^DS_{EtOH}, ^DS_{MeOH}, and ^DS_{ACN} and by ^BS_{EtOH} and ^BS_{MeOH}. This appears both as a different limit up to which the replacement is possible as well as even a completely different ability of one molecule to replace the other. For example, no ability of benperidol to replace droperidol was detected in the nonsolvated phase ^DII and the ethanol solvate ^DS_{EtOH}, whereas

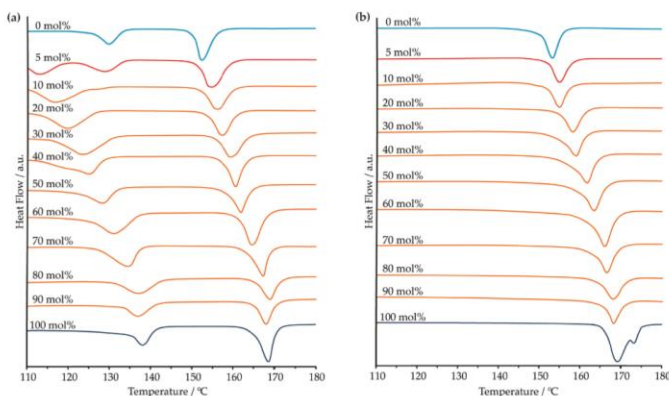


Figure 4. DSC curves for (a) the solvated solid solution SS^B_{EtOH} obtained in the crystallization from ethanol along with DSC curves of droperidol ethanol solvate $^D S_{EtOH}$ and benperidol ethanol solvate $^B S_{EtOH}$ and (b) the nonsolvated solid solution SS^B_{II} obtained in the crystallization from isopropanol, along with DSC curves of droperidol $^D II$ and benperidol $^B II$. The labels represent the benperidol content used in the crystallization. Solid solutions are in orange, phase mixtures in red, and pure benperidol and droperidol phases in blue.

the replacement of benperidol with droperidol in ethanol solvate $^B S_{EtOH}$ and nonsolvated phase $^B II$ was achieved even up to a state close to a complete substitution, as solid solutions where 90% of the benperidol molecules were replaced were obtained (see PXRD patterns in Figure 3). These solid solutions are designated as SS^B_{EtOH} and SS^B_{II} , respectively. These observations match well with the results of the cross-seeding experiments performed previously,⁵⁷ where a droperidol ethanol solvate $^{D-iso-B} S_{EtOH}$ isostructural to the benperidol ethanol solvate was obtained in a pure form and formation of $^{D-iso-B} II$ was also clearly observed. Therefore, it can be concluded that either a fully isostructural structure $^{D-iso-B} S_{EtOH}$ in which all of the benperidol molecules are replaced with droperidol exists and just was not obtained in the experimental conditions using 5 mol % benperidol, or instead of just seeding, a solid solution containing a small amount of benperidol was actually obtained in the previously performed experiments.⁵⁷

Crystallization of pure benperidol from isopropanol in our performed experiments produced pure benperidol polymorph $^B I$, even though a very similar approach has been used⁶⁷ to prepare polymorph $^B II$. However, when a small quantity of droperidol (5 mol %) was added, $^B I$ was still detected as the only crystallization product. $^1 H$ NMR measurements (see Supporting Information) indicated that droperidol was present only in trace amounts and therefore likely the obtained sample contained an impurity of the droperidol phase not detectable by the PXRD method (Figure S13). This suggests that droperidol apparently does not replace benperidol molecules in the structure of $^B I$ in contrast to the structure of $^B II$ where almost complete replacement was achieved.

A different outcome was observed for methanol and acetonitrile solvates and dihydrates. For these phases, droperidol was able to replace benperidol molecules in the original benperidol phases $^B S_{MeOH}$, $^B S_{ACN}$, and $^B DH$ in a limited range of up to 50 or 70 mol % of benperidol depending on the particular solvated phase. Moreover, in contrast to the ethanol solvate and nonsolvated phases, in this case, benperidol was able to replace droperidol molecules in the

original droperidol phases $^D S_{MeOH}$, $^D S_{ACN}$, and $^D DH$, although only for relatively small benperidol contents of up to 10 mol % for $^D S_{MeOH}$ and $^D DH$ and 20 mol % for $^D S_{ACN}$.

3.1.2. Characterization of the Obtained Solid Solutions.

All of the samples obtained in the crystallization were additionally characterized by DSC/TG analysis, and solvated phases were desolvated. The obtained desolvation products were characterized using PXRD for phase identification and DSC/TG analysis for thermal characterization. More details on the characterization of the crystallization products are provided in the Supporting Information.

In all of the DSC curves of nonsolvated solid solution SS^B_{II} samples, the melting endotherm is consistent with an essentially monophasic sample (see Figure 4). Across the composition range from 90 mol % down to 10 mol % benperidol, the onset and the peak temperature decrease monotonically as the amount of droperidol in the solid solution increase, consistent with the presence of a single solid solution phase in these samples, with the melting point being between that of benperidol polymorph $^B II$ ($T_{melt.} = 165$ °C) and droperidol polymorph $^D II$ ($T_{melt.} = 151$ °C) (see the phase diagram constructed from these data in Figure 5). A discontinuity in the melting behavior is observed for 5 mol % benperidol, as the sample contains a mixture of solid solution SS^B_{II} and droperidol phase $^D II$.

The DSC curves of the solvated solid solution SS^B_{EtOH} showed that a single desolvation peak is present across the composition range starting from pure benperidol to 10 mol % benperidol, and the desolvation temperature decreases monotonically as the amount of droperidol in the solid solution increases, consistent with the presence of a single solid solution phase in these samples. In contrast, two desolvation peaks are present for samples with 5 mol % benperidol, which agrees with the presence of two solvated phases. A similar monotonic decrease of the desolvation temperature by increasing the amount of droperidol in the solid solution was also observed for the solvated solid solution SS^B_{MeOH} and a tendency for the desolvation temperature to decrease by

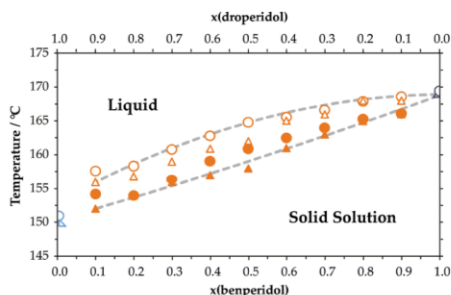


Figure 5. Part of a melt-phase diagram of the benperidol–droperidol binary system obtained from the DSC measurements. The circles correspond to data from samples obtained in the crystallization from isopropanol and were used to construct the phase diagram, in which the lines are guides for the eyes. The triangles correspond to the data measured for samples obtained in the desolvation of ethanol solvate samples and illustrate the agreement with the thermal characteristics of samples obtained in the crystallization.

increasing the amount of the compound replacing the original compound was also observed for other solvated solid solutions. In addition, the melting peak of the obtained desolvation product of SS^B_{EtOH} and in most cases that obtained from the other solvated samples also decreased monotonically over the whole composition range by increasing the amount of droperidol in the sample. To fully understand this monotonic decrease over the whole composition range, solvated samples obtained in the crystallization were desolvated and characterized.

By heating the solvated samples obtained in the crystallization experiments, a desolvated product always formed prior to the physical melting of the sample. Interestingly, we observed that the desolvation product is not dependent on the phase composition of the solvated sample being desolvated. The desolvation product of the only solvated solid solution existing in nearly the whole composition range, SS^B_{EtOH} was always the nonsolvated solid solution SS^B_{II} . This is consistent with the main desolvation product of pure benperidol ethanol solvate $^B_{EtOH}$ being polymorph $^B_{II}$.⁵⁷ Moreover, the nonsolvated solid solution SS^B_{II} was obtained as the only desolvation product also by desolvating almost all of the samples obtained from methanol, acetonitrile, and acetone/water regardless of whether the sample contained solid solution having a structure of the original benperidol solvate, solid solution having a structure of the original droperidol solvate, or even the mixture thereof. This was confirmed both by the PXRD patterns (see Figure 6 for PXRD patterns recorded for the desolvation products of dihydrate samples and Supporting Information) of the desolvated samples as well as by their DSC curves, in which the melting endotherm was consistent with an essentially monophasic sample with the melting onset and peak temperatures matching that of SS^B_{II} having an identical component composition (see Supporting Information). The formation of SS^B_{II} in the desolvation of phase mixture is also consistent with the already reported formation of phase isostructural to $^B_{II}$ in desolvation of a mixture of $^D_{DH}$ and $^{D-iso-B}_{DH}$ obtained in the cross-seeding experiments⁵⁷ and suggests that in those experiments $^{D-iso-B}_{DH}$

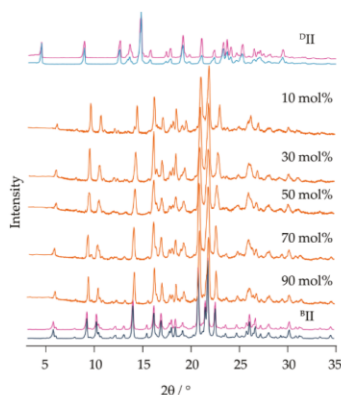


Figure 6. PXRD patterns of desolvation products of dihydrate samples obtained using different ratios of benperidol and droperidol in the crystallization. Labels show the weighted molar fraction of benperidol used in the crystallization. Solid solutions are in orange, pure benperidol and droperidol phases in blue, and patterns simulated from crystal structures in magenta.

must have actually been SS^B_{DH} containing some benperidol from the used seed material.

Considering the desolvation process, the desolvation of all of the solvates should be associated with recrystallization of the sample and is not a simple structure rearrangement after the solvent loss,^{76,77} which could not lead to the formation of a single solid solution phase SS^B_{II} regardless of the phase or phases present in the solvated sample.

In general, the formation of solid solution SS^B_{II} both in crystallization and desolvation experiments as the only nonsolvated crystal structure in cases when both benperidol and droperidol are present indicates its superior stability compared to any other nonsolvated binary phase or even a mixture of benperidol and droperidol single-component phases.

3.2. Structural and Computational Characterization of Solid Solutions. A detailed comparison of the crystal structures of benperidol and droperidol by focusing on the reasons for the formation of different crystal structures and comparison of the experimental structures with those of mostly hypothetical isostructural phases is already available.⁵⁷ In this study, however, we focus on the evaluation of structural and energy-related aspects for the formation of solid solutions by replacing part of the original molecules in the crystal structure with the molecules of the second compound. $^B_{I}$ was not considered as the solid solution formed in the benperidol structure $^B_{II}$ and part of the computational calculations was not possible for $^B_{I}$ because of the large size ($Z = 18$) of its unit cell.

3.2.1. Comparison of Molecular Conformation. A comparison of the crystal structures of benperidol and droperidol nonsolvates and solvates shows that only for a pair of nonsolvates $^B_{II}$ – $^D_{II}$ and acetonitrile solvates, the same hydrogen bonding motif is present, whereas in all of the other cases (most pairs of identical solvates, including dihydrates, where chains are formed by different hydrogen bonds), it is

Table 2. Basic Crystal Structure Information of Selected Benperidol and Droperidol Phases, by Comparing Structures of Benperidol and Droperidol Nonsolvates and Solvates Containing the Same Solvent in Pairs^a

structure	space group	Z/Z'	hydrogen bonding	τ_1 (deg)	τ_2 (deg)	RMSD (Å)
^B II	$\bar{P}1$	6/3	R_2^2 (8) dimers	48.6	-78.7	0.936/1.061/0.846 ^b
				31.1	-168.5	
				59.5	-80.2	
^D II	$P2_1/c$	4/1	R_2^2 (8) dimers	-130.8	-165.2	0.614
^B DH	$P2_1/n$	4/1	chains with water ^c	-109.3	-58.5	
^D DH	$P2_1/n$	4/1	chains with water ^c	-129.3	-54.1	
^B S _B OH	$P2_1/c$	4/1	C_2^2 (10) w/s	-109.9	-70.4	
^D S _B OH	$\bar{P}1$	2/1	R_2^2 (8) dimers + D w/s ^d	-125.3	-65.1	
^B S _M OH	$P2_1/c$	4/1	C_2^2 (10) w/s	126.7 ^e	64.9 ^e	0.658/0.662 ^f
^D S _M OH	$\bar{P}1$	2/1	R_2^2 (8) dimers + D w/s ^d	-108.5	-71.4	
^B S _{ACN}	$\bar{P}1$	2/1	R_2^2 (8) dimers	-123.3	-65.9	0.831/0.829
				125.2 ^e	67.0 ^e	
				-113.9	-71.9	
^D S _{ACN}	$P1$	2/2	R_2^2 (8) dimers	-126.9	-63.6	0.831/0.829
				126.0	64.1	

^aThe values of torsion angles τ_1 and τ_2 introducing the largest structure diversity are given after geometry optimization in Quantum ESPRESSO. ^bRoot-mean-square deviation (RMSD) value for non-hydrogen atom positions for each symmetry-independent benperidol molecule. ^cChains are formed by different hydrogen bonds (see Figure S19). ^dw/s = with solvent. ^eThe value for the second symmetry-independent molecule in the $P1$ space group as modeled in Quantum ESPRESSO is given in italic.

Table 3. Intramolecular Energy of Benperidol and Droperidol in Original Structures and Energy Penalty (in kJ mol^{-1}) Associated with Replacement of One and All Molecules in the Unit Cell

structure	^B II (A)	^B II (B)	^B II (C)	^B S _B OH	^B S _M OH	^B S _{ACN}	^B DH	
original	+9.8	+8.3	+7.1	+1.6	+1.9	+1.6	+2.1	
								Conformation Energy of Benperidol (kJ mol^{-1})
substituted	-5.0	+4.2	+3.8	+7.1	+6.7	+6.8	+5.9	
								Energy Penalty for Replacement of Benperidol with Droperidol (kJ mol^{-1})
isostructural	-0.4	+5.6	+5.4	+6.5	+6.1	+6.6	+0.8	
structure	^D II	^D S _B OH (A)	^D S _B OH (B)	^D S _M OH (A)	^D S _M OH (B)	^D S _{ACN} (A)	^D S _{ACN} (B)	^D DH
original	+2.3	+0.3	+0.3	+0.6	+0.6	+0.2	+0.2	+1.0
substituted	+9.6	+9.7	+9.8	+9.6	+8.9	+10.0	+9.9	+8.7
isostructural	+2.4	+8.9	+8.9	+9.0	+8.9	+9.0	+8.6	+1.7

different (see Table 2). A comparison of droperidol and benperidol conformation showed that the conformation in nonsolvates is notably different (with benperidol ^BII having the most distinct conformation), whereas the conformation in the studied solvates is similar. Even though this analysis shows that the replacement of molecules in nonsolvates would require notable adaptation of conformation, the resulting conformation still would correspond to the low-energy region of the PES.⁵⁷

As the overall shape of the molecule is affected not only by the torsion angles τ_1 and τ_2 characterizing the arrangement of benzimidazol-2-one ring and 4-fluorophenyl-4-oxobutyl chain with respect to the central piperidine/1,2,3,6-tetrahydropyridine ring but also by the different geometry of the central ring and differences in other torsion angles, whole molecules were overlaid (see Table S12) and the RMSD of non-hydrogen atoms was calculated (see Table 2). Although this comparison confirmed the nonsolvate pair ^BII–^DII to be the most different, the solvate pairs were also notably different, with dihydrates being the most similar pair.

To obtain more quantitative information on the energy penalty associated with the adaption of the conformation by the replaced molecule, conformation energy with respect to the

global energy minimum was calculated using Gaussian 09 for molecules in the original structures, for the replaced molecule in the substituted structures, and for the molecule in the isostructural structures (see Figure 2). These calculations showed that in all of the original structures except for the ^BII, the conformation energy is close to that of the global energy minimum (see Table 3). In contrast, in most cases, replacement of one or all of the molecules resulted in the adoption of energetically inefficient conformation by the replaced molecule, as could be predicted by the large RMSD values between molecules in all of the structure pairs. The smallest energy penalty was observed for replacement of benperidol with droperidol in ^BII because the original structure already has high conformation energy, and replacement of one of the molecules was even associated with energy lowering. Overall, the energy penalty for replacement of droperidol with benperidol is close to 10 kJ mol^{-1} in all of the structures, whereas replacement of benperidol with droperidol in general is associated with a lower energy increase. We also observed that in some of the structures (^BDH, ^DDH, and ^DII), there is a notable energy penalty for replacement of 1 of the 4 molecules in the unit cell, whereas a structure where all of the molecules

are replaced could adopt and only a minor increase in the conformation energy is present (Table 3).

3.2.2. Comparison of Intermolecular Interaction Energy. We also evaluated the changes in the intermolecular interaction energy introduced by the replacement of the molecules. Intermolecular interaction energy for all three sets of structures was calculated using Quantum ESPRESSO. The obtained data are presented in Table 4. Overall, replacement of

Table 4. Intermolecular Interaction Energy in Original Benperidol and Droperidol Crystal Structures (in kJ mol^{-1} of Benperidol or Droperidol) and Energy Change When One or All Molecules in the Unit Cell Are Replaced^a

structure	^B II	^B S _{EtOH}	^B S _{MeOH}	^B S _{ACN}	^B DH
<i>E</i> _{inter} of Benperidol Structures (kJ mol^{-1})					
original	-244.7	-331.6	-318.2	-288.4	-404.7
Change in <i>E</i> _{inter} by Insertion of Droperidol (kJ mol^{-1})					
substituted	+2.9	+3.6	+3.0	+5.2	+7.8
isostructural	-0.7	-5.4	-1.8	-3.6	+5.4
structure	^D II	^D S _{EtOH}	^D S _{MeOH}	^D S _{ACN}	^D DH
<i>E</i> _{inter} of Droperidol Structures (kJ mol^{-1})					
original	-237.3	-284.4	-281.0	-275.3	-403.5
Change in <i>E</i> _{inter} by Insertion of Benperidol (kJ mol^{-1})					
substituted	+5.4	+5.5	+6.3	+4.4	+4.2
isostructural	+5.3	+7.4	+8.0	+7.6	+9.6

^aFor structures with $Z' > 1$, the change in *E*_{inter} in substituted structures is the average value from structures where molecules of different symmetry were replaced.

one of the molecules is always associated with energy increase, which is the smallest for ^BII, ^BS_{MeOH}, and ^BS_{EtOH}. However, full replacement of all of the benperidol molecules with droperidol results in more efficient interactions in most of the structures, with the highest decrease of interaction energy calculated for ^BS_{EtOH}. In contrast, replacement of droperidol molecules with benperidol always results in less-efficient interactions. These results confirm that the interaction energy is an important factor in determining the molecule replacement capability in different structures. The obtained results allowed to predict the formation of solid solution in the ^BS_{EtOH} structure. However, the facile formation of ^BII and the relatively narrow concentration range for ^BS_{ACN} could not be predicted by these results.

To identify the cause of the observed change in intermolecular interaction energy by molecule replacement, we also calculated pairwise intermolecular interaction energies for the closest molecules for all three sets of structures in CrystalExplorer. First, we evaluated the effect of molecule replacement on the hydrogen bond interaction strength (see Table S23). Overall, we see that the hydrogen bond interactions do not restrict the formation of solid solutions, as for the nonsolvate and solvate structures with *R*₂² (8) dimers, mostly no noticeable changes are introduced by the molecule replacement. The largest changes for dimers (+2 to +3 kJ mol^{-1}) were introduced by inserting the benperidol molecule in ^DII, which nevertheless agrees with solid solution never observed in this structure. Generally, larger changes were introduced for hydrogen bonds formed with solvent molecules, with changes up to +3 to +5 kJ mol^{-1} for ^DS_{EtOH}, ^DS_{MeOH}, and ^DDH and up to +2 to +3 kJ mol^{-1} for benperidol solvates. In benperidol solvates, however, no correlation with the ability of the structure to form solid solution was observed.

Second, we evaluated the effect of molecule replacement on the interaction energy for molecule pairs forming the strongest dispersion interactions (for molecule pairs with *E*_{disp} < -45 kJ mol^{-1} , corresponding to 3–6 interactions for each benperidol/droperidol molecule depending on the structure) (see Tables 5

Table 5. Relative Average Intermolecular Interaction Energy (in kJ mol^{-1}) with Respect to That in the Original Structures for Molecule Pairs Forming the Strongest Dispersion Interactions

structure	^B II	^B S _{EtOH}	^B S _{MeOH}	^B S _{ACN}	^B DH
substituted	+0.6	-0.7	+0.6	+0.4	+2.1
isostructural	-0.2	-1.0	-0.1	-0.6	+3.6
structure	^D II	^D S _{EtOH}	^D S _{MeOH}	^D S _{ACN}	^D DH
substituted	+1.5	+0.5	+0.8	+0.4	-0.1
isostructural	+2.6	+1.9	+1.8	+2.0	0.0

and S24). Although overall no critical differences in such interactions were introduced by molecule replacement, the average interaction energy for such pairs became less efficient by $\sim 2 \text{ kJ mol}^{-1}$ for droperidol solvates ^DS_{EtOH}, ^DS_{MeOH}, and ^DS_{ACN} and by 3–4 kJ mol^{-1} for ^DII and ^DDH. In contrast, the average interaction energy for such pairs almost did not change for ^DDH, ^BII, and ^BS_{MeOH} and became more efficient by $\sim 1 \text{ kJ mol}^{-1}$ for benperidol solvates ^BS_{EtOH} and ^BS_{ACN}. We note that for more than half of the analyzed structures, the energy change appearing in the substituted structure was magnified in the isostructural structure. In contrast, the total intermolecular interaction energy values (Table 4) in the substituted structures were always calculated to be less efficient than that in the original structures.

We see that overall there is a correlation between the ability of a structure to form a solid solution and the total interaction energy of the structure as well as the interaction energy for molecule pairs forming the strongest dispersion interactions. In contrast, analysis of just hydrogen bond interactions does not provide information on the ability of structures to form solid solutions. The interaction energy analysis, however, does not explain the rather poor solid solution formation in ^BS_{ACN} structures, the average solid solution formation in ^BDH structures, and the very good solid solution formation of ^BII.

Third, we present a more comprehensive view on the energy differences by analyzing the interaction energy for all molecule pairs formed by molecules for which atoms within 3.80 Å radius from the central molecule are present (Tables S13–S22). Using these values, we calculated cumulative interaction energy from the molecule pairs with increasing distance between molecular centroids and plotted the difference between this energy in substituted and isostructural structures and that in the original structure. Selected plots are given in Figure 7, and the remaining plots in Figure S23.

From these plots, it can clearly be seen that the only structure with more efficient cumulative interaction energy from all such molecule pairs in both substituted and isostructural structures is ^BS_{EtOH}, easily forming solid solution. Although the cumulative energy for isostructural structures was also favorable for ^BS_{MeOH} and ^BS_{ACN}, the limited solid solution formation by these structures could be explained by the inefficient energy for substituted structures. Likewise, similar trends for the cumulative energy were also present for ^BII, confirming that the overall formation of solid solutions in this structure is highly likely. Generally, molecule replacement

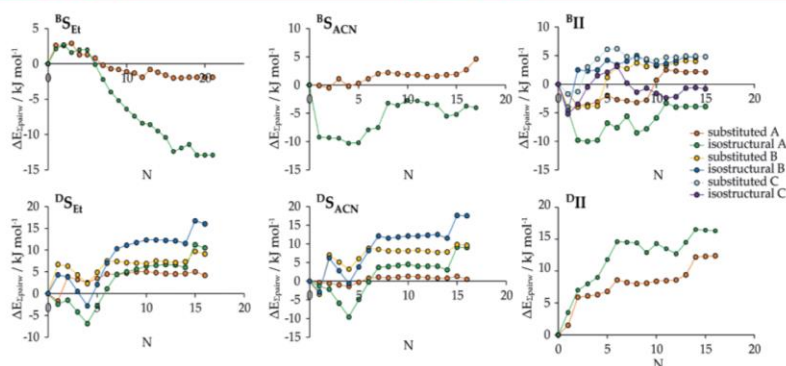


Figure 7. Difference in the cumulative interaction energy from the molecule pairs with increasing distance between molecular centroids between substituted and isostructural structures and that of the original structure plotted by increasing distance (N = molecule number).

reduced the efficiency of interactions in droperidol solvates D^S_{EtOH} , D^S_{MeOH} , and D^S_{ACN} , whereas no significant effect on D^S_{DH} was introduced. Clearly, in D^S_{II} , the interactions experience the most notable efficiency loss, which is consistent with this structure never being experimentally observed. Molecule replacement also significantly reduced the efficiency of interactions in D^S_{DH} , with notable energy loss observed for two identical molecule pairs, where oppositely oriented piperidin-dihydrobenzimidazolone rings interacted (also being the main contribution in increasing the average interaction energy for molecule pairs forming the strongest dispersion interactions, Table 5). Nevertheless, we believe that this could as well be caused by some problems in modelling structures of D^S_{DH} , as solid solution in this structure formed as good as in D^S_{ACN} and better than in D^S_{DH} .

This analysis also clearly shows that interactions with the closest molecules are not the ones determining the molecule replacement ability. For example, contrary to the observed formation of solid solutions, considering only the closest four molecules, the replacement is inefficient in B^S_{EtOH} but efficient for the isostructural structure of D^S_{EtOH} . Note, however, that the closest molecules do not necessarily correspond to efficient intermolecular interactions, and the hydrogen-bonded molecules for hydrogen-bonded dimers are among the most distant molecules considered in this analysis.

Taking into account the differences in phase composition between the considered structures, the analysis of the intermolecular interaction energies suggests that in this system solid solutions are more easily formed in single-component phases, as solid solutions over a wide composition range can experimentally be obtained if the molecule replacement maintains the same interaction efficiency as in the original structure, whereas for solvated phases, the formation of solid solution over a wide composition range requires notably favorable interactions if compared to the original structure. Although this is contrary to the observation that a third component can allow the miscibility of two immiscible components in the solid state,⁷⁸ in the case of solvates the solvent could complicate the miscibility in the structure if it increases the number or importance of spatially oriented interactions. Another explanation for the observed different

solid solution formation behaviors of the structures having a similar low change in the intermolecular interaction energy by molecule replacement, however, could be the different penalty associated with the adaption of the conformation, which was lower for the B^S_{II} structure (only +1 kJ mol⁻¹ for substituted and +3.5 kJ mol⁻¹ for isostructural) if compared to that for B^S_{MeOH} and B^S_{ACN} (+7 kJ mol⁻¹ for substituted and +6.5 kJ mol⁻¹ for isostructural).

4. CONCLUSIONS

We show that in the benperidol–droperidol system, solid solutions in different crystal structures form notably differently, and the extent up to which a structure can accommodate the other molecule strongly depends on the crystal structure. There are structure pairs in which droperidol can dissolve in a benperidol crystal structure almost up to complete replacement (90% replacement was reached for B^S_{EtOH} and B^S_{II} structures) of benperidol molecules with droperidol molecules, whereas replacement of droperidol with benperidol in the corresponding droperidol phases was not observed. In contrast, in the other studied structure pairs (dihydrates and methanol and acetonitrile solvates), we observe a notably lower ability of droperidol to replace benperidol in benperidol structures, but in these pairs benperidol can replace droperidol in droperidol structures. Nevertheless, benperidol still cannot replace droperidol in droperidol structures up to such an extent as observed for the reverse replacement direction.

We also show that desolvation of all of the solvated crystallization products obtained by crystallizing benperidol and droperidol in any ratio results in the formation of pure solid solution in the B^S_{II} structure regardless of the initial solvated phase composition of the sample. This means that the solid solution in this structure has superior stability over other potential nonsolvated phases and the desolvation of all solvates occurs via recrystallization of the sample and is not a simple structure rearrangement after the solvent loss.

We demonstrate that the considered analysis of the interaction energy changes introduced by the replacement of molecules in each crystal structure in general allows rationalization of the solid solution formation ability by each structure. This analysis demonstrates that there is no one

particular interaction defining whether the molecule replacement in the structure will be possible, but consideration of all of the interaction energies of nearby molecules, particularly the dispersion-type interactions, allows prediction of the solid solution formation likelihood. This clearly allowed identification of ${}^{\text{B}}\text{S}_{\text{EtOH}}$ as a structure in which molecule replacement is the most energetically favored. Additionally, the results suggest that the formation of solid solutions in a wide concentration range in nonsolvated structures requires maintaining the interaction efficiency, whereas the formation of solid solutions in a wide concentration range in the studied solvates is more difficult and requires increased interaction efficiency.

■ ASSOCIATED CONTENT

Supporting Information

The Supporting Information is available free of charge at <https://pubs.acs.org/doi/10.1021/acs.cgd.2c01269>.

Additional data of crystallization experiments, solid form characterization, i.e., PXRD patterns, DSC curves, and ${}^1\text{H}$ NMR spectra of different composition samples, additional results and data from comparison of crystal structures, and calculation of pairwise intermolecular interaction energy (PDF)

■ AUTHOR INFORMATION

Corresponding Author

Agris Bērziņš – Faculty of Chemistry, University of Latvia, Rīga LV-1004, Latvia; orcid.org/0000-0002-4149-8971; Phone: +(371)-67033903; Email: agris.berzins@lu.lv

Author

Kristaps Saršūns – Faculty of Chemistry, University of Latvia, Rīga LV-1004, Latvia; orcid.org/0000-0002-8692-7768

Complete contact information is available at <https://pubs.acs.org/doi/10.1021/acs.cgd.2c01269>

Funding

This research was funded by the MikroTik Ltd. project “Development of integrated experimental and computer modeling research methodology for prediction of the properties and diversity of phases of active pharmaceutical solids” administrated by the University of Latvia Foundation, project No. AHL-2202, and Latvian Council of Science project “Crystal engineering of pharmaceutical multicomponent phases for more efficient crystalline phase design”, project No. lzp-2018/1-0312.

Notes

The authors declare no competing financial interest.

■ ACKNOWLEDGMENTS

K.S. acknowledges financial support from the European Social Fund project “Strengthening of the capacity of doctoral studies at the University of Latvia within the framework of the new doctoral model”, identification No. 8.2.2.0/20/1/006, and MikroTik Ltd. doctoral scholarship in the field of natural and medical sciences administrated by the University of Latvia Foundation. The authors thank Rihards Klūga (University of Latvia) for ${}^1\text{H}$ NMR spectra measurements.

■ REFERENCES

- (1) Aakeröy, C. B.; Sinha, A. S. In *Co-Crystals: Preparation, Characterization and Applications*; Aakeröy, C. B.; Sinha, A. S., Eds.; Royal Society of Chemistry: Cambridge, 2018; Vol. 24.
- (2) Aakeröy, C. B.; Seddon, K. R. The Hydrogen Bond and Crystal Engineering. *Chem. Soc. Rev.* **1993**, *22*, 397–407.
- (3) Wittenberg, J. B.; Isaacs, L. Complementarity and Preorganization. *Supramolecular Chemistry: From Molecules to Nanomaterials*; John Wiley & Sons, Inc., 2012.
- (4) Cavallo, G.; Metrangola, P.; Milani, R.; Pilati, T.; Priimagi, A.; Resnati, G.; Terraneo, G. The Halogen Bond. *Chem. Rev.* **2016**, *116*, 2478–2601.
- (5) Mukherjee, A.; Tothadi, S.; Desiraju, G. R. Halogen Bonds in Crystal Engineering: Like Hydrogen Bonds yet Different. *Acc. Chem. Res.* **2014**, *47*, 2514–2524.
- (6) Galek, P. T. A.; Fábian, L.; Motherwell, W. D. S.; Allen, F. H.; Feeder, N. Knowledge-Based Model of Hydrogen-Bonding Propensity in Organic Crystals. *Acta Crystallogr., Sect. B: Struct. Sci.* **2007**, *63*, 768–782.
- (7) Wood, P. A.; Feeder, N.; Furlow, M.; Galek, P. T. A.; Groom, C. R.; Pidcock, E. Knowledge-Based Approaches to Co-Crystal Design. *CrystEngComm* **2014**, *16*, 5839–5848.
- (8) Sarkar, N.; Sinha, A. S.; Aakeröy, C. B. Systematic Investigation of Hydrogen-Bond Propensities for Informing Co-Crystal Design and Assembly. *CrystEngComm* **2019**, *21*, 6048–6055.
- (9) Wood, P. A.; Olsson, T. S. G.; Cole, J. C.; Cottrell, S. J.; Feeder, N.; Galek, P. T. A.; Groom, C. R.; Pidcock, E. Evaluation of Molecular Crystal Structures Using Full Interaction Maps. *CrystEngComm* **2013**, *15*, 65–72.
- (10) Devogelaer, J. J.; Meeke, H.; Vlieg, E.; de Gelder, R. Cocrytals in the Cambridge Structural Database: A Network Approach. *Acta Crystallogr., Sect. B: Struct. Sci., Cryst. Eng. Mater.* **2019**, *75*, 371–383.
- (11) Takiyeddin, K.; Khimyak, Y. Z.; Fábian, L. Prediction of Hydrate and Solvate Formation Using Statistical Models. *Cryst. Growth Des.* **2016**, *16*, 70–81.
- (12) Xin, D.; Gonnella, N. C.; He, X.; Horspool, K. Solvate Prediction for Pharmaceutical Organic Molecules with Machine Learning. *Cryst. Growth Des.* **2019**, *19*, 1903–1911.
- (13) Vriza, A.; Sovago, I.; Widdowson, D.; Kurlin, V.; Wood, P. A.; Dyer, M. S. Molecular Set Transformer: Attending to the Co-Crystals in the Cambridge Structural Database. *Digital Discovery* **2022**, *1*, 834.
- (14) Musumeci, D.; Hunter, C. A.; Prohens, R.; Scuderi, S.; McCabe, J. F. Virtual Cocrytal Screening. *Chem. Sci.* **2011**, *2*, 883–890.
- (15) Chan, H. C. S.; Kendrick, J.; Neumann, M. A.; Leusen, F. J. J. Towards Ab Initio Screening of Co-Crystal Formation through Lattice Energy Calculations and Crystal Structure Prediction of Nicotinamide, Isonicotinamide, Picolinamide and Paracetamol Multi-Component Crystals. *CrystEngComm* **2013**, *15*, 3799–3807.
- (16) Shishkin, O. V.; Zubatyuk, R. I.; Shishkina, S. V.; Dyakonov, V. V.; Medvediev, V. V. Role of Supramolecular Synthons in the Formation of the Supramolecular Architecture of Molecular Crystals Revisited from an Energetic Viewpoint. *Phys. Chem. Chem. Phys.* **2014**, *16*, 6773.
- (17) Price, S. L. Control and Prediction of the Organic Solid State: A Challenge to Theory and Experiment. *Proc. R. Soc. A* **2018**, *474*, No. 20180351.
- (18) Price, S. L.; Reutzel-Edens, S. M. The Potential of Computed Crystal Energy Landscapes to Aid Solid-Form Development. *Drug Discovery Today* **2016**, *21*, 912–923.
- (19) Nyman, J.; Reutzel-Edens, S. M. Crystal Structure Prediction Is Changing from Basic Science to Applied Technology. *Faraday Discuss.* **2018**, *211*, 459–476.
- (20) Blagden, N.; de Matas, M.; Gavan, P. T.; York, P. Crystal Engineering of Active Pharmaceutical Ingredients Intelligently to Improve Solubility and Dissolution Rates. *Adv. Drug Delivery Rev.* **2007**, *59*, 617–630.

- (21) Sandhu, B.; Sinha, A. S.; Desper, J.; Aakeröy, C. B. Modulating the Physical Properties of Solid Forms of Urea Using Co-Crystallization Technology. *Chem. Commun.* **2018**, *54*, 4657–4660.
- (22) Garain, S.; Ansari, S. N.; Kongasseri, A. A.; Chandra Garain, B.; Pati, S. K.; George, S. J. Room Temperature Charge-Transfer Phosphorescence from Organic Donor-Acceptor Co-Crystals. *Chem. Sci.* **2022**, *13*, 10011–10019.
- (23) Saha, S.; Mishra, M. K.; Reddy, C. M.; Desiraju, G. R. From Molecules to Interactions to Crystal Engineering: Mechanical Properties of Organic Solids. *Acc. Chem. Res.* **2018**, *51*, 2957–2967.
- (24) Perlovich, G. Melting Points of One- and Two-Component Molecular Crystals as Effective Characteristics for Rational Design of Pharmaceutical Systems. *Acta Crystallogr., Sect. B: Struct. Sci., Cryst. Eng. Mater.* **2020**, *76*, 696–706.
- (25) Krueger, E. L.; Sinha, A. S.; Desper, J.; Aakeröy, C. B. Exploring Binding Preferences in Co-Crystals of Conformationally Flexible Multitopic Ligands. *CrystEngComm* **2017**, *19*, 4605–4614.
- (26) Aitipamula, S.; Mapp, L. K.; Wong, A. B. H.; Chow, P. S.; Tan, R. B. H. Novel Pharmaceutical Cocrystals of Triflusal: Crystal Engineering and Physicochemical Characterization. *CrystEngComm* **2015**, *17*, 9323–9335.
- (27) Gunawardana, C. A.; Aakeröy, C. B. Co-Crystal Synthesis: Fact, Fancy, and Great Expectations. *Chem. Commun.* **2018**, *54*, 14047–14060.
- (28) Aakeröy, C. B.; Wijethunga, T. K.; Desper, J. Molecular Electrostatic Potential Dependent Selectivity of Hydrogen Bonding. *New J. Chem.* **2015**, *39*, 822–828.
- (29) Corpinot, M. K.; Bučar, D.-K. A Practical Guide to the Design of Molecular Crystals. *Cryst. Growth Des.* **2019**, *19*, 1426–1453.
- (30) Corpinot, M. K.; Stratford, S. A.; Arhangelskis, M.; Anka-Lufford, J.; Halasz, I.; Judaš, N.; Jones, W.; Bučar, D. K. On the Predictability of Supramolecular Interactions in Molecular Cocrystals: The View from the Bench. *CrystEngComm* **2016**, *18*, 5434–5439.
- (31) Desiraju, G. R. The C-H...O Hydrogen Bond: Structural Implications and Supramolecular Design. *Acc. Chem. Res.* **1996**, *29*, 441–449.
- (32) Taylor, R. It Isn't, It Is: The C-H...X (X = O, N, F, Cl) Interaction Really Is Significant in Crystal Packing. *Cryst. Growth Des.* **2016**, *16*, 4165–4168.
- (33) Gavezotti, A.; Presti, L. L. Building Blocks of Crystal Engineering: A Large-Database Study of the Intermolecular Approach between C-H Donor Groups and O, N, Cl, or F Acceptors in Organic Crystals. *Cryst. Growth Des.* **2016**, *16*, 2952–2962.
- (34) Yu, L.; Stephenson, G. A.; Mitchell, C. A.; Bunnell, C. A.; Snorek, S. V.; Bowyer, J. J.; Borchardt, T. B.; Stowell, J. G.; Byrn, S. R. Thermochemistry and Conformational Polymorphism of a Hexamorphic Crystal System. *J. Am. Chem. Soc.* **2000**, *122*, 585–591.
- (35) López-Mejías, V.; Kampf, J. W.; Matzger, A. J. Nonamorphism in Flufenamic Acid and a New Record for a Polymorphic Compound with Solved Structures. *J. Am. Chem. Soc.* **2012**, *134*, 9872–9875.
- (36) Bhowal, R.; Chopra, D. Investigating the Role of Weak Interactions to Explore the Polymorphic Diversity in Difluorinated Isomeric N-Phenylcinnamamides. *Cryst. Growth Des.* **2021**, *21*, 4162–4177.
- (37) Bērziņš, A.; Zvaniņa, D.; Trimdale, A. Detailed Analysis of Packing Efficiency Allows Rationalization of Solvate Formation Propensity for Selected Structurally Similar Organic Molecules. *Cryst. Growth Des.* **2018**, *18*, 2040–2045.
- (38) Bērziņš, A.; Kōns, A.; Saršūns, K.; Belyakov, S.; Actiņš, A. On the Rationalization of Formation of Solvates: Experimental and Computational Study of Solid Forms of Several Nitrobenzoic Acid Derivatives. *Cryst. Growth Des.* **2020**, *20*, 5767–5784.
- (39) Trimdale, A.; Mishnev, A.; Bērziņš, A. Combined Use of Structure Analysis, Studies of Molecular Association in Solution, and Molecular Modelling to Understand the Different Propensities of Dihydroxybenzoic Acids to Form Solid Phases. *Pharmaceutics* **2021**, *13*, No. 734.
- (40) Price, C. P.; Glick, G. D.; Matzger, A. J. Dissecting the Behavior of a Promiscuous Solvate Former. *Angew. Chem., Int. Ed.* **2006**, *45*, 2062–2066.
- (41) Boothroyd, S.; Kerridge, A.; Broo, A.; Buttar, D.; Anwar, J. Why Do Some Molecules Form Hydrates or Solvates. *Cryst. Growth Des.* **2018**, *18*, 1903–1908.
- (42) Braun, D. E.; Karamertzanis, P. G.; Price, S. L. Which, If Any, Hydrates Will Crystallise? Predicting Hydrate Formation of Two Dihydroxybenzoic Acids. *Chem. Commun.* **2011**, *47*, 5443–5445.
- (43) Braun, D. E.; Bhardwaj, R. M.; Florence, A. J.; Tocher, D. A.; Price, S. L. Complex Polymorphic System of Gallic Acid-Five Monohydrates, Three Anhydrides, and over 20 Solvates. *Cryst. Growth Des.* **2013**, *13*, 19–23.
- (44) Braun, D. E. Experimental and Computational Approaches to Rationalise Multicomponent Supramolecular Assemblies: Dapsone Monosolvates. *Phys. Chem. Chem. Phys.* **2019**, *21*, 17288–17305.
- (45) Lusi, M. A Rough Guide to Molecular Solid Solutions: Design, Synthesis and Characterization of Mixed Crystals. *CrystEngComm* **2018**, *20*, 7042–7052.
- (46) Braga, D.; Desiraju, G. R.; Miller, J. S.; Orpen, A. G.; Price, S. L. Innovation in Crystal Engineering. *CrystEngComm* **2002**, *4*, 500–509.
- (47) Sacconi, L.; Ciampolini, M.; Speroni, G. P. Structure Mimicry in Solid Solutions of 3d Metal Complexes with N-Methylsilyldiamine (Msal-Me). *J. Am. Chem. Soc.* **1965**, *87*, 3102–3106.
- (48) Romasanta, A. K. S.; Braga, D.; Duarte, M. T.; Grepioni, F. How Similar Is Similar? Exploring the Binary and Ternary Solid Solution Landscapes of p-Methyl/Chloro/Bromo-Benzyl Alcohols. *CrystEngComm* **2017**, *19*, 653–660.
- (49) Braga, D.; Grepioni, F.; Maini, L.; Polito, M.; Rubini, K.; Chierotti, M. R.; Gobetto, R. Hetero-Seeding and Solid Mixture to Obtain New Crystalline Forms. *Chem.—Eur. J.* **2009**, *15*, 1508–1515.
- (50) Jones, W.; Theocharis, C. R.; Thomas, J. M.; Desiraju, G. R. Structural Mimicry and the Photoreactivity of Organic Solids. *J. Chem. Soc., Chem. Commun.* **1983**, *23*, 1443.
- (51) Kitaigorodskii, A. I. *Molecular Crystals and Molecules*; Academic Press: New York, 1973; p 570.
- (52) Kitaigorodskii, A. I. Conditions of Formation of Substitutional Organic Solid Solutions. *Mixed Crystals*; Springer-Verlag: Berlin, 1984; pp 200–216.
- (53) Corpinot, M. K.; Guo, R.; Tocher, D. A.; Buanz, A. B. M.; Gaisford, S.; Price, S. L.; Bučar, D. K. Are Oxygen and Sulfur Atoms Structurally Equivalent in Organic Crystals? *Cryst. Growth Des.* **2017**, *17*, 827–833.
- (54) Desiraju, G. R.; Sarma, J. A. R. P. The Chloro-Methyl Exchange Rule and Its Violations in the Packing of Organic Molecular Solids. *J. Chem. Sci.* **1986**, *96*, 599–605.
- (55) Saršūns, K.; Bērziņš, A.; Reķis, T. Solid Solutions in the Xanthone–Thioxanthone Binary System: How Well Are Similar Molecules Discriminated in the Solid State? *Cryst. Growth Des.* **2020**, *20*, 7997–8004.
- (56) Mazzeo, P. P.; Carraro, C.; Arns, A.; Pelagatti, P.; Bacchi, A. Diversity through Similarity: A World of Polymorphs, Solid Solutions, and Cocrystals in a Vial of 4,4'-Diazopyridine. *Cryst. Growth Des.* **2020**, *20*, 636–644.
- (57) Bērziņš, A.; Actiņš, A. Why Do Chemically Similar Pharmaceutical Molecules Crystallize in Different Structures: A Case of Droperidol and Benperidol. *Cryst. Growth Des.* **2016**, *16*, 1643–1653.
- (58) Fonseca, J. D. C.; Tenorio Clavijo, J. C.; Alvarez, N.; Ellena, J.; Ayala, A. P. Novel Solid Solution of the Antiretroviral Drugs Lamivudine and Emtricitabine. *Cryst. Growth Des.* **2018**, *18*, 3441–3448.
- (59) Case, D. H.; Srirambhatla, V. K.; Guo, R.; Watson, R. E.; Price, L. S.; Polyzois, H.; Cockcroft, J. K.; Florence, A. J.; Tocher, D. A.; Price, S. L. Successful Computationally Directed Templating of Metastable Pharmaceutical Polymorphs. *Cryst. Growth Des.* **2018**, *18*, 5322–5331.
- (60) Braga, D. Crystal Engineering, Where from? Where To? *Chem. Commun.* **2003**, *3*, 2751–2754.

- (61) Lusi, M. Engineering Crystal Properties through Solid Solutions. *Cryst. Growth Des.* **2018**, *18*, 3704–3712.
- (62) Goldberg, A. H.; Gibaldi, M.; Kanig, J. L. Increasing Dissolution Rates and Gastrointestinal Absorption of Drugs via Solid Solutions and Eutectic Mixtures III: Experimental Evaluation of Griseofulvin-Succinic Acid Solid Solution. *J. Pharm. Sci.* **1966**, *55*, 487–492.
- (63) Trotta, J. T.; Zeidan, T. A.; Tilak, P. A.; Foxman, B. M.; Almarsson, Ö.; Oliveira, M. A.; Chiarella, R. A.; Hickey, M. B.; Remenar, J. F. Aripiprazole and Dehydro-Aripiprazole Solid Solutions: Crystalline Combinations of Drug and Active Metabolite in Tailored Compositions. *Cryst. Growth Des.* **2020**, *20*, 3944–3956.
- (64) Saršūns, K.; Kemere, M.; Karziņš, A.; Kļimenkovs, I.; Bērziņš, A.; Sarakovskis, A.; Reķis, T. Fine-Tuning Solid State Luminescence Properties of Organic Crystals via Solid Solution Formation: The Example of 4-Iodothioxanthone-4-Chlorothioxanthone System. *Cryst. Growth Des.* **2022**, *22*, 4838–4844.
- (65) Weerasekara, R. K.; Uekusa, H.; Hettiarachchi, C. V. Multicolor Photochromism of Fulgide Mixed Crystals with Enhanced Fatigue Resistance. *Cryst. Growth Des.* **2017**, *17*, 3040–3047.
- (66) Bērziņš, A.; Skarbulis, E.; Reķis, T.; Actiņš, A. On the Formation of Droperidol Solvates: Characterization of Structure and Properties. *Cryst. Growth Des.* **2014**, *14*, 2654–2664.
- (67) Bērziņš, A.; Skarbulis, E.; Actiņš, A. Structural Characterization and Rationalization of Formation, Stability, and Transformations of Benperidol Solvates. *Cryst. Growth Des.* **2015**, *15*, 2337–2351.
- (68) Saršūns, K.; Bērziņš, A. Prediction of Solid Solution Formation among Chemically Similar Molecules Using Calculation of Lattice and Intermolecular Interaction Energy. *Key Eng. Mater.* **2020**, *850*, 54–59.
- (69) Actins, A.; Arajs, R.; Belakovs, S.; Orola, L.; Veidis, M. V. The Crystal and Molecular Structure of a Polymorph and a Pseudo-Polymorph of Droperidol. *J. Chem. Crystallogr.* **2008**, *38*, 169–174.
- (70) Blaton, N. M.; Peeters, O. M.; De Ranter, C. J. 1-[4-(4-Fluorophenyl)-4-Oxobutyl]-1,2,3,6-Tetrahydro-4-Pyridyl]-1,3-Dihydro-2 H -Benzimidazol-2-One Dihydrate (Dehydrobenzperidol). *Acta Crystallogr., Sect. B: Struct. Crystallogr. Cryst. Chem.* **1980**, *36*, 2828–2830.
- (71) Giannozzi, P.; Baroni, S.; Bonini, N.; Calandra, M.; Car, R.; Cavazzoni, C.; Ceresoli, D.; Chiarotti, G. L.; Cococcioni, M.; Dabo, I.; Dal Corso, A.; De Gironcoli, S.; Fabris, S.; Fratesi, G.; Gebauer, R.; Gerstmann, U.; Gougousis, C.; Kokalj, A.; Lazzeri, M.; Martin-Samos, L.; Marzari, N.; Mauri, F.; Mazzarello, R.; Paolini, S.; Pasquarello, A.; Paulatto, L.; Sbraccia, C.; Scandolo, S.; Sclauzero, G.; Seitsonen, A. P.; Smogunov, A.; Umari, P.; Wentzcovitch, R. M. QUANTUM ESPRESSO: A Modular and Open-Source Software Project for Quantum Simulations of Materials. *J. Phys.: Condens. Matter* **2009**, *21*, No. 395502.
- (72) Grimme, S. Semiempirical GGA-Type Density Functional Constructed with a Long-Range Dispersion Correction. *J. Comput. Chem.* **2006**, *27*, 1787–1799.
- (73) Lund, A. M.; Orendt, A. M.; Pagola, G. L.; Ferraro, M. B.; Facelli, J. C. Optimization of Crystal Structures of Archetypical Pharmaceutical Compounds: A Plane-Wave DFT-D Study Using Quantum Espresso. *Cryst. Growth Des.* **2013**, *13*, 2181–2189.
- (74) Frisch, M. J.; Trucks, G. W.; Schlegel, H. B.; Scuseria, G. E.; Robb, M. A.; Cheeseman, J. R.; Scalmani, G.; Barone, V.; Mennucci, B.; Petersson, G. A.; Nakatsuji, H.; Caricato, M.; Li, X.; Hratchian, H. P.; Izmaylov, A. F.; Bloino, J.; Zheng, G.; Sonnenberg, J. L.; Hada, M.; Ehara, M.; Toyota, K.; Fukuda, R.; Hasegawa, J.; Ishida, M.; Nakajima, T.; Honda, Y.; Kitao, O. N.; Nakai, H.; Vreven, T.; Montgomery, J. A. J.; Peralta, J. E.; Ogliaro, F.; Bearpark, M.; Heyd, J. J.; Brothers, E.; Kudin, K. N.; Staroverov, V. N.; Kobayashi, R.; Normand, J.; Raghavachari, K.; Rendell, A.; Burant, J. C.; Iyengar, S. S.; Tomasi, J.; Cossi, M.; Rega, N.; Millam, J. M.; Klene, M.; Knox, J. E.; Cross, J. B.; Bakken, V.; Adamo, C.; Jaramillo, J.; Gomperts, R. S.; Stratmann, R. E.; Yazyev, O.; Austin, A. J.; Cammi, R.; Pomelli, C.; Ochterski, J. W.; Martin, R. L.; Morokuma, K.; Zakrzewski, V. G.; Voth, G. A.; Salvador, P.; Dannenberg, J. J.; Dapprich, S.; Daniels, A. D.; Farkas, O.; Foresman, J. B.; Ortiz, J. V.; Cioslowski, J.; Fox, D. J. *Gaussian 09*, revision D.01; Gaussian, Inc.: Wallingford, CT, 2009.
- (75) MacRae, C. F.; Sovago, I.; Cottrell, S. J.; Galek, P. T. A.; McCabe, P.; Pidcock, E.; Platings, M.; Shields, G. P.; Stevens, J. S.; Towler, M.; Wood, P. A. Mercury 4.0: From Visualization to Analysis, Design and Prediction. *J. Appl. Crystallogr.* **2020**, *53*, 226–235.
- (76) Petit, S.; Coquerel, G. Mechanism of Several Solid-Solid Transformations between Dihydrated and Anhydrous Copper(II) 8-Hydroxyquinolates. Proposition for a Unified Model for the Dehydration of Molecular Crystals. *Chem. Mater.* **1996**, *8*, 2247–2258.
- (77) Galwey, A. K. Structure and Order in Thermal Dehydrations of Crystalline Solids. *Thermochim. Acta* **2000**, *355*, 181–238.
- (78) Lusi, M.; Vitorica-Yrezabal, I. J.; Zaworotko, M. J. Expanding the Scope of Molecular Mixed Crystals Enabled by Three Component Solid Solutions. *Cryst. Growth Des.* **2015**, *15*, 4098–4103.

IV

Saršūns, K., Kons, A., Rekis, T., Bērziņš, A.

EXPERIMENTAL AND COMPUTATIONAL STUDY OF SOLID SOLUTION FORMED BETWEEN SUBSTITUTED NITROBENZOIC ACIDS

Crystal Growth & Design, **2023**, 23(9), 6609–6622

Reprinted with permission from American Chemical Society (ACS).

Copyright © 2023, American Chemical Society



Experimental and Computational Study of Solid Solutions Formed between Substituted Nitrobenzoic Acids

Kristaps Sarsūns, Artis Kons, Toms Rekis, and Agris Bērziņš*

Cite This: *Cryst. Growth Des.* 2023, 23, 6609–6622

Read Online

ACCESS |

Metrics & More

Article Recommendations

Supporting Information

ABSTRACT: We present an experimental and computational study of the formation of solid solutions in binary systems of substituted nitrobenzoic acids. Different isomers with a methyl group, hydroxyl group, and chlorine substituents are studied. We show that the solid solution formation likelihood evaluated based on the observed solubility limit is notably affected by both the exchanged functional groups and the location of the substituents in the molecular structure. This demonstrates that the component solubility limit strongly depends on the intermolecular interactions present in the crystal structure and is altered by the molecule replacement. Solid solutions form in all of the studied crystalline phases. Component solubility limits from ~5% up to 50% were observed. The obtained results indicated that the calculated intermolecular interaction energy change by the functional group replacement does not allow rationalization of the experimentally observed solubilities, considering neither the molecules adjacent to the replace group nor all the molecules within a 15 Å radius. The relative energy of the experimental structures and isostructural phases obtained from the computationally generated structure landscapes calculated at the level providing accurate energy ranking was found to be mostly consistent with the experimentally observed component solubilities.



1. INTRODUCTION

Solid solutions (or mixed crystals) are phases consisting of at least two components arbitrarily located at equivalent sites in the crystal structure. The composition of such phases can be varied continuously over a certain range.¹ Solid solutions of inorganic compounds are long known as metal alloys, and many of the minerals are solid solutions. Furthermore, it has been demonstrated that such phases enable fine-tuning of material structure and properties.^{2,3} Properties and rules of the formation of solid solutions in organic compound systems, however, are notably less explored.⁴ Nevertheless, in the past decades, the number of publications on molecular solid solutions has increased significantly. For example, such systems have gained increased attention as a promising tool to develop or test the rules of crystal engineering.^{5,6} Solid solutions also offer a promising approach for tuning properties of materials, such as optical and mechanical properties, in a continuous and smooth fashion by varying the component ratio.⁷ However, solid solutions are useful and effective only if the response of the desired property to varying component ratio is sensitive enough.⁸

It has long been demonstrated that similarities of molecule size and shape plays a significant role in determining the likelihood of solid solution formation between particular components.⁹ It has been shown that this depends on two related concepts—structural mimicry^{10,11} and crystal isomorphism.¹² However, in multiple cases, the weak intermo-

lecular forces represent a very important factor controlling the crystal structure stability and therefore the formation of molecular solid solutions.^{13–15} For example, it has been demonstrated that minor changes to the molecular structures (e.g., halogen atom exchange) usually significantly and unpredictably alter the crystal packing,^{16,17} while more pronounced changes (e.g., addition of groups with hydrogen bond formation ability) usually affect the supramolecular solid-state structures.¹⁸ However, according to Kitaigorodskii's principles of close packing, not always the change of hydrogen bonding groups or halogen atom exchange leads to significant structural changes.⁹ Molecules with chlorine atoms and methyl groups in equivalent sites are often interchangeable in the crystal structures,^{19,20} i.e., the overall structure is not significantly altered.²¹

Solid solutions have been discovered and their properties and formation explored between structurally highly similar compounds: molecules differing by halogen (and halogen/methyl) substituents;^{22,23} molecules differing by S/O

Received: April 29, 2023

Revised: July 17, 2023

Published: August 17, 2023





Figure 1. Molecular structures of (a) 2-substituted-4-nitrobenzoic acids, (b) 2-substituted-5-nitrobenzoic acids, (c) 4-substituted-3-nitrobenzoic acids, and (d) 5-substituted-2-nitrobenzoic acids, with the numbering of non-hydrogen atoms. Labels of carbon are given in black, oxygen in red, nitrogen in blue.

atoms;^{24,25} molecules differing by single/double bonds in the carbon atom framework;^{26,27} and molecules differing by F/H atoms.^{28,29} However, it has been observed that, in some cases, even very similar molecules are immiscible or only mix in limited composition ranges in the solid state.³⁰ Therefore, individual case studies on the miscibility of similar organic compounds in the solid state are necessary to uncover the general aspects governing solid solution formation.

In this study, we explored the formation of solid solutions between several substituted nitrobenzoic acids: 2-substituted-4-nitrobenzoic acids 2Cl4NBA, 2Me4NBA, and 2OH4NBA (Figure 1a), 2-substituted-5-nitrobenzoic acids 2Cl5NBA, 2Me5NBA, and 2OH5NBA (Figure 1b), 4-substituted-3-nitrobenzoic acids 4Cl3NBA, 4Me3NBA, and 4OH3NBA (Figure 1c), and 5-substituted-2-nitrobenzoic acids 5Cl2NBA, 5Me2NBA, and 5OH2NBA (Figure 1d). A methyl group (Me), a hydroxyl group (OH), and a chlorine atom (Cl) were chosen as substituents (R). The scaffolds of the nitrobenzoic acids were chosen so that the dominant intermolecular interactions, i.e., the hydrogen bonds formed by the carboxylic group, as well as part of the weak intermolecular interactions formed by the nitro group, would be maintained in the potential solid-solution phases. In addition to solid-solution screening, computational calculations were used to identify possible factors that lead to different solubility limits observed in different pairs of these chemically similar molecules.

The solid form landscapes for part of the studied compounds have already been explored, namely crystal forms obtained by crystallization of 2Me4NBA, 2Cl4NBA, 2OH4NBA, 2Cl5NBA, 4Cl3NBA, and 5Cl2NBA from common organic solvents have been reported.^{31–33} For 2Me5NBA,³⁴ 2OH5NBA,³⁵ and 4Me3NBA,³⁶ only crystal structures of nonsolvated phases have been reported. To the best of our knowledge, there is no information on solid forms or any crystal structures of 4OH3NBA, 5Me2NBA and 5OH2NBA. Therefore, as part of this study, limited solid form screening was performed and crystal structures of the discovered nonsolvated forms were determined and reported.

2. EXPERIMENTAL SECTION

2.1. Materials. 2Me4NBA (purity 97%), 2Me5NBA (95%), 4Me3NBA (95%), 5Me2NBA (95%), 2OH5NBA (97%), 4OH3NBA (95%), and 5OH2NBA (97%) were obtained from Fluorochem; 2Cl4NBA (98%) was received from Alfa Aesar, 2OH4NBA (97%) and 4Cl3NBA (98%) were obtained from Acros Organics, and 2Cl5NBA (97%) and 5Cl2NBA (99%) were received from Sigma–Aldrich. Ethanol (96%) and acetonitrile (99.8%) were obtained from commercial sources. All of the chemicals were used as received without further purification.

2.2. Solid-Solution Screening. Binary mixtures of nitrobenzoic acid derivatives in selected molar ratios with a total mass of 0.100 g were prepared by using an analytical balance. The mixtures were

completely dissolved in ~0.5 mL of ethanol (for mixtures containing 5OH2NBA, acetonitrile was used) at 70 °C. The obtained clear solutions were cooled, and the solvent was allowed to evaporate completely under ambient conditions. Pure nitrobenzoic acid derivatives were also crystallized using an identical approach. The obtained solid products were ground in a mortar to ensure complete homogenization and characterized using PXRD and DSC. More details of the crystallization experiments are given in Table S1 in the Supporting Information.

2.3. Characterization of the Obtained Crystallization Products. Powder X-ray diffraction (PXRD) patterns of all of the obtained crystallization products were recorded at ambient temperature on a D8 Advance (Bruker) diffractometer using copper radiation (Cu K α) at a wavelength of 1.54180 Å, equipped with a LynxEye position-sensitive detector. The tube voltage and current were set to 40 kV and 40 mA. The divergence slit was set at 0.6 mm, and the antiscattering slit was set at 8.0 mm. The diffraction patterns were recorded using a 0.2 s/0.02° scanning speed from 3° to 35° on the 2 θ scale.

Differential scanning calorimetry (DSC) curves were recorded on a DSC 25 (TA Instruments) calorimeter at the heating rate of 2 °C min⁻¹ from 25 °C to 140/250 °C (depending to the melting temperature of pure components), and the nitrogen flow rate was 50 ± 10 mL min⁻¹. Approximately 1.2 mg of each sample was weighed in a 70 μ L aluminum crucible, and the crucible was crimped.

The recorded DSC curves were used for the construction of binary melt phase diagrams. The solidus lines were constructed using the onset temperature of the respective DSC peaks, and the liquidus lines were constructed using the peak temperatures. More details on the thermal analysis are given in Table S2 in the Supporting Information.

¹H NMR spectra of most of the crystallization products and pure nitrobenzoic acid derivatives were recorded in a dimethyl sulfoxide (DMSO)-*d*₆ solution at a nominal temperature of 300 K with a Fourier 300 MHz (Bruker) spectrometer. Chemical shifts (δ) were found in parts per million (ppm) using the residual solvent peak as an internal reference. A characteristic peak was selected for each compound (see the Supporting Information), and its area was used for determination of the compound ratio in the obtained crystallization products.

2.4. Crystal Structure Determination. Single crystals of 5OH2NBA polymorph II (CCDC Deposition No. 2257122) and hydrate (2257119), and selected solid solutions (2257680–2257681, 2257683–2257686) were investigated on a XtaLAB Synergy-S dualflex diffractometer (RIGAKU Oxford Diffraction) equipped with a HyPix6000 detector and microfocus sealed X-ray tube with Cu K α radiation ($\lambda = 1.54184$ Å). A single crystal with approximate dimensions of 0.08 mm × 0.08 mm × 0.06 mm was fixed with oil in a nylon loop of a magnetic CryoCap and set on a goniometer head. The samples were cooled to 150 K in an open-flow nitrogen cryostat. Data were integrated using CrysAlisPro 1.171.41.115a³⁷ software, and structure solutions and refinements were performed with the software JANA2006.³⁸ All non-hydrogen atoms were refined anisotropically; H atoms were added in calculated positions and refined riding on their respective carbon or oxygen atoms.

Crystal structures of 4OH3NBA (2257118), 5Me2NBA (2257121), and 5OH2NBA polymorph I (2257120) were determined

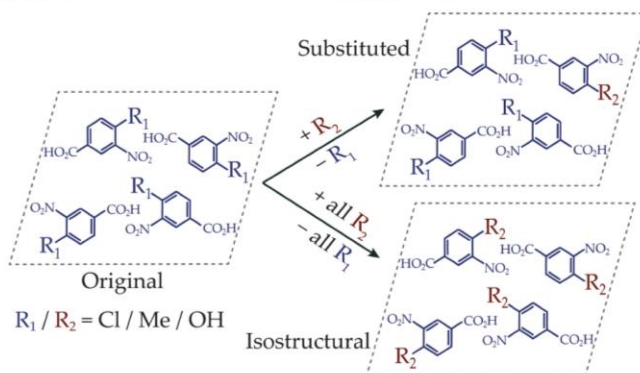


Figure 2. Schematic representation of the construction of substituted and isostructural structures from the original structures used for the calculations in the example of 4-substituted-3-nitrobenzoic acids.

from PXRD data. For this, PXRD patterns were measured on a D8 Discover (Bruker) diffractometer using copper radiation ($\text{Cu } K\alpha = 1.54180 \text{ \AA}$) in transmission mode and a LynxEye (1D) detector. The tube was employed with voltage and current settings of 40 kV and 40 mA. The sample was loaded into borosilicate glass capillaries of 0.5 mm outer diameter (Hilgenberg glass No. 10). A capillary spinner (60 rpm) and upper and lower knife edges were used. The diffractometer incident beam path was equipped with a Göbel Mirror, a Soller slit, and a 0.6 mm divergence slit, while the diffracted beam path was equipped only with a Soller slit. The diffraction patterns were recorded on the 2θ scale from 4° to 70° at a 0.01° step size using a scan speed of 36 s per step. Identical procedure as in our previous studies were used for the structure determination^{32,39} (see the Supporting Information).

2.5. Theoretical Calculations. Theoretical calculations were performed for three general sets of crystal structures as in our previous studies.^{27,40} The first set (original) consisted of experimental crystal structures of nitrobenzoic acid derivatives: 2Cl4NBA (polymorph I, CSD refcode VOLZEC³¹), 2OH4NBA (polymorph I, QUPSEC³²), 2Me4NBA (polymorph I, QUPRO101³³), 2Cl3NBA (polymorph I, CLNBZA01³²), 2OH3NBA (polymorph I, GUTNIS02³⁵), 2Me3NBA (polymorph I, GOJROM02³⁴), 4Cl3NBA (polymorph I, ZZZMVY01³³), 4OH3NBA (polymorph I, 2257118), 4Me3NBA (polymorph I, MATBIV01³⁶), 5Cl2NBA (polymorph I, QUPSUS³²), 5OH2NBA (polymorph I, 2257120), and 5Me2NBA (polymorph I, 2257121). The second set (isostructural) was structures in which the functional group or the halogen atom of the original molecules was fully replaced by one of the alternative studied functional groups or the halogen atom (see Figure 2). The third set (substituted) consisted of structures for which symmetry was removed, and the functional group or the halogen atom was replaced for one of the four molecules (out of 2 for 2OH3NBA, and 8 for 4Me3NBA and 5OH2NBA) in the unit cell (see Figure 2).

All three sets of crystal structures were initially geometry optimized in Quantum ESPRESSO⁴¹ by relaxing positions of all atoms and the unit-cell parameters (*vc-relax*), with ultrasoft pseudopotentials⁴² from the original pseudopotential library and a 130 Ry plane-wave cutoff energy using the Perdew–Burke–Ernzerhof (PBE)⁴³ functional with van der Waals (vdW) interactions treated according to the D3 method of Grimme.⁴⁴ The parameters of convergence, pseudopotentials, and the k -point grid were used as suggested for structure optimizations of pharmaceutical molecules.⁴⁵ For the substituted structures formed from $Z' = 2$ structures, both alternative structures were considered, and the lowest energy structure was selected and used for further calculations. Then pairwise intermolecular interaction energy calculations for all of the structures were performed in

CrystalExplorer 21.5⁴⁶ at the B3LYP/6-31G(d,p) level by calculating the pairwise interaction energies for molecules for which atoms are within a 15 Å of the central molecule. For the substituted structures, the interaction energies were calculated using the replaced molecule as the central molecule.

2.6. Crystal Structure Comparison and Analysis. Mercury 2022.3.0 software⁴⁷ was used for crystal structure visualization and analysis, including analysis of the intermolecular interactions and overlay of the experimental solid solution structures with the structure of pure compounds.

2.7. Location of Crystal Structures in Computationally Generated Structure Landscapes. A possibility to form isostructural or highly similar crystal structures among the 2-substituted-4-nitrobenzoic acids with replaced substituents was evaluated by using crystal structure landscapes obtained in a crystal structure prediction (CSP) study. Crystal structures generated using CrystalPredictor 2.2⁴⁸ and optimized with CrystalOptimizer 2.4.7⁴⁹ from an already published CSP study³² were used. The dataset consisted of 642 2Cl4NBA, 625 2Me4NBA, and 314 2OH4NBA lowest energy unique $Z' = 1$ structures. For identification of isostructural or highly similar crystal structures, initial structures with replaced substituents were prepared from the experimental structures of 2Cl4NBA, 2Me4NBA, and 2OH4NBA (see construction of isostructural structures in Figure 2). The obtained initial structures were optimized in CrystalOptimizer using an identical procedure as used in the CSP study.³² The obtained optimized structures were then compared with the computationally generated structures by assessing structural similarity in a cluster of molecules taken from each structure using the COMPACT tool.⁵⁰

The geometry optimization by relaxing lattice parameters and atomic positions (with Tkatchenko–Scheffler (TS)⁵¹ dispersion correction scheme and plane-wave cutoff energy of 570 eV) and single-point energy calculation (with many-body dispersion (MBD)⁵² correction scheme and plane-wave cutoff energy of 1000 eV) of the experimental structures and isostructural structures was performed in the CASTEP⁵³ plane-wave code using the PBE exchange-correlation density functional and on-the-fly generated ultrasoft pseudopotentials. This was used to improve the energy rankings of these structures.

3. RESULTS AND DISCUSSION

In this study, we explored the formation of solid solutions in binary systems formed by two nitrobenzoic acid derivatives of identical scaffold differing only by the substituent (methyl group, hydroxyl group, or chlorine atom (Figure 1)). The

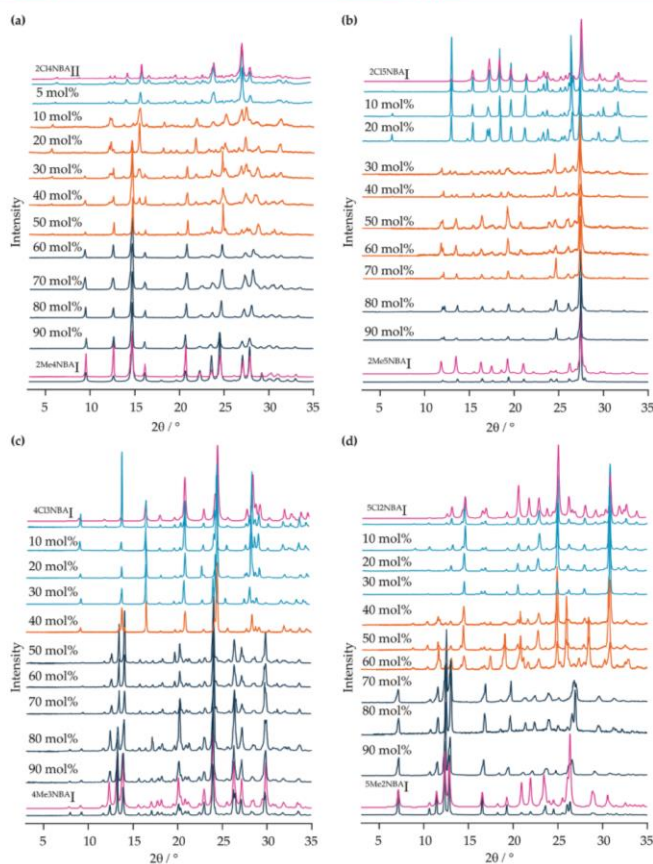


Figure 3. PXRD patterns of crystallization products obtained in crystallization of different ratios of methyl and chloronitrobenzoic acid isomers: (a) 2Me4NBA–2Cl4NBA, (b) 2Me5NBA–2Cl5NBA, (c) 4Me3NBA–4Cl3NBA, and (d) 5Me2NBA–5Cl2NBA from ethanol. Labels show the molar fraction of methyl nitrobenzoic acid used in the crystallization. PXRD patterns of solid solutions and the corresponding single-component phases are in identical shades of blue, phase mixtures are in orange, and patterns simulated from crystal structures of pure components are in magenta. Respective polymorphs are indicated by Roman numerals.

formation of solid solutions, i.e., the ability of compounds to replace each other in their pure-state crystal structures, was explored in all of the possible 12 binary systems (three for each nitrobenzoic acid isomer). Binary mixtures containing different amounts of the selected compounds were crystallized, and the solid solution formation was assessed by measuring the phase composition of the crystallization products using PXRD and constructing the two component phase diagrams based on DSC measurements. If available, crystallization conditions were chosen based on the published information for obtaining a single-component phases of the respective compounds. The phases present in the samples were identified based on the agreement with the PXRD patterns of the studied substituted nitrobenzoic acids reported previously^{31–36} or for 4OH3NBA, 5Me2NBA, and 5OH2NBA recorded in a limited solid form

screening performed as a part of this study. For selected systems, the formation of solid solutions was additionally confirmed by crystal structure analysis. Besides this, we also investigated the capability of computational calculations and crystal structure analysis to rationalize and predict the solid-solution formation in the respective systems.

3.1. Experimental Characterization of Solid-Solution Formation. **3.1.1. Solid Solutions Formed between Methyl nitrobenzoic Acids and Chloronitrobenzoic Acids.** The molecular structure differences introduced by replacing the methyl group with chlorine atom in all of the considered nitrobenzoic acid isomers lead to formation of different crystal structures; i.e., no isostructurality is observed. To evaluate the formation of partial solid solution between methyl nitrobenzoic acids and chloronitrobenzoic acids, binary mixtures of these

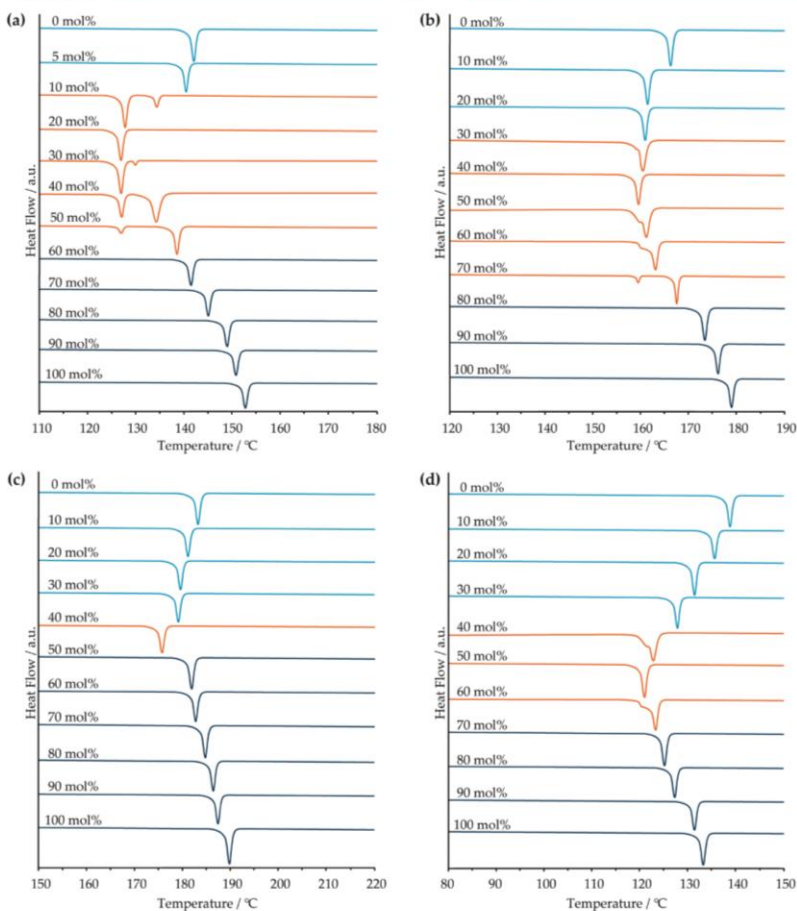


Figure 4. DSC curves of the crystallization products of the binary systems: (a) 2Me4NBA–2Cl4NBA, (b) 2Me5NBA–2Cl5NBA, (c) 4Me3NBA–4Cl3NBA, and (d) 5Me2NBA–5Cl2NBA. Labels represent the molar fraction of methyl nitrobenzoic acid used in the crystallization. Differential scanning calorimetry (DSC) curves of the solid solutions and the corresponding single-component phases are shown in an identical shade of blue, and phase mixtures are shown in orange.

compounds (2Me4NBA–2Cl4NBA, 2Me5NBA–2Cl5NBA, 4Me3NBA–4Cl3NBA, and 5Me2NBA–5Cl2NBA) with different compositions were crystallized from ethanol.

The PXRD patterns in Figure 3 show that only the characteristic peaks of the pure component phases are present in the crystallized mixtures. No formation of stoichiometric binary phases (cocrystals) were observed. For many binary compositions, only peaks corresponding to the respective major component phase are present. The presence of both compounds in these crystallization products was confirmed by recording ^1H NMR spectra. The determined compound ratio in all cases was close to the ratio used in the crystallization (see the Supporting Information). The obtained results clearly

show that partial solid solutions form in all four binary systems. The formation of solid solutions was further corroborated by studying the lattice parameters of the single-phase binary mixtures. The parameters are linearly dependent on the mixture composition, which is in agreement with Vegard's law^{54,55} (see Figure S50 in the Supporting Information).

Solid-solution composition ranges in each system are different. In the 2Me4NBA–2Cl4NBA system, up to ~5 mol % of the methylated derivative can be hosted in the chlorine-substituted nitrobenzoic acid, while up to ~40 mol % of 2Cl4NBA can be incorporated in the structure of 2Me4NBA. For 2Me5NBA–2Cl5NBA, up to ~20 mol % of the opposite component can be hosted in either of the pure

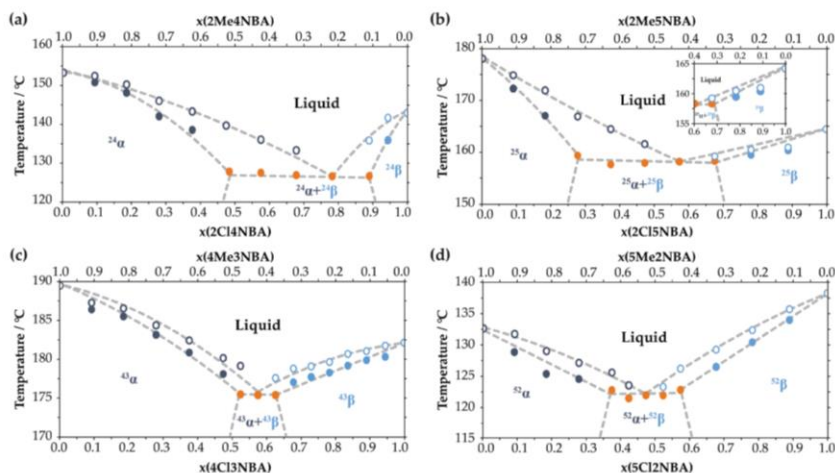


Figure 5. Melt phase diagrams of the binary systems (a) 2Me4NBA–2Cl4NBA, (b) 2Me5NBA–2Cl5NBA, (c) 4Me3NBA–4Cl3NBA, and (d) 5Me2NBA–5Cl2NBA. The color coding is identical to that used in Figures 3 and 4 (closed points represent solidus/eutectic; open symbols indicate liquidus; lines are present as guides for the eyes).

component structures. For 4Me3NBA–4Cl3NBA, up to ~30 mol % of 4Me3NBA can be incorporated in the structure of 4Cl3NBA and up to around 50 mol % of 4Cl3NBA can be incorporated in the structure of 4Me3NBA. Finally, in the 5Me2NBA–5Cl2NBA system, up to ~30 mol % of each opposite component can be incorporated in either of the pure component structures.

The DSC curves recorded for the crystallization products in which only a single phase was detected and thus identified as a solid solution are consistent with an essentially monophasic sample (see Figure 4). In these DSC curves, only a single melting endotherm was detected, with the melting point slightly lower than that of the respective single-component phase. In the DSC curves of the crystallization products containing a phase mixture, an endothermic signal corresponding to the eutectic melting was present followed by another endotherm. The second endotherm corresponds to the dissolution of the remaining phase in the eutectic melt. This is consistent with the most simple eutectic binary systems. The eutectic melting signal was observed as a separate peak or a small but pronounced shoulder with a constant onset temperature of ~126 °C for 2Me4NBA–2Cl4NBA (Figure 4a), 158 °C for 2Me5NBA–2Cl5NBA (Figure 4b), 175 °C for 4Me3NBA–4Cl3NBA (Figure 4c; to clearly see the eutectic melting formation, see Figure S21 in the Supporting Information), and 122 °C for 5Me2NBA–5Cl2NBA (Figure 4d).

The recorded DSC curves were used to construct the binary melt phase diagrams. As concluded from the PXRD and DSC analysis, partial solid solutions based on each component form in all four binary systems (Figure 5). Therefore, to some extent, all the methylchlorobenzoic acids dissolve in chloronitrobenzoic acids and vice versa. These solid solutions are designated as α (methylchlorobenzoic acids with dissolved chloronitrobenzoic acids) and β (chloronitrobenzoic acids with

dissolved methylchlorobenzoic acids), with indices in superscripts indicating the position of the methyl/chloro and nitro group. In all of the phase diagrams, there is a biphasic region where physical mixtures of both solid solutions with limiting compositions are present.

As already mentioned, the composition ranges in which the solid solutions form are different in each pair of nitrobenzoic acid isomers. The highest solubility of up to ~50 mol % is observed for 4Cl3NBA in 4Me3NBA, whereas the lowest solubility (<10 mol %) is observed for 2Me4NBA in 2Cl4NBA. The most likely cause for the different solubilities is a notable influence of the guest molecule on the host structure stability. The exchanged functional groups form different intermolecular interactions in each single-component structure. The molecule replacement by the opposite component has significant influence on the intermolecular interaction energy, as will be demonstrated further. In two of the systems (2Me4NBA–2Cl4NBA and 4Me3NBA–4Cl3NBA), the solubility of the Cl-containing compound in the methyl group-containing compound is notably better.

3.1.2. Summary of Solid Solutions Formed between the Studied Substituted Nitrobenzoic Acids. Identically, we also determined the solid-solution formation capability between hydroxynitrobenzoic acids and methylchlorobenzoic acids in pairs 2OH4NBA–2Me4NBA, 2OH5NBA–2Me5NBA, 4OH3NBA–4Me3NBA, and 5OH2NBA–5Me2NBA, as well as between hydroxynitrobenzoic acids and chloronitrobenzoic acids in pairs 2OH4NBA–2Cl4NBA, 2OH5NBA–2Cl5NBA, 4OH3NBA–4Cl3NBA, and 5OH2NBA–5Cl2NBA. The solid solution formation was evaluated based on the PXRD and DSC results. Melt phase diagrams were constructed (see Supporting Information for the PXRD patterns, DSC curves, and melt phase diagrams for these two-component systems). ^1H NMR spectra were recorded to confirm the compound ratio in the crystallization products. Slow evaporation of

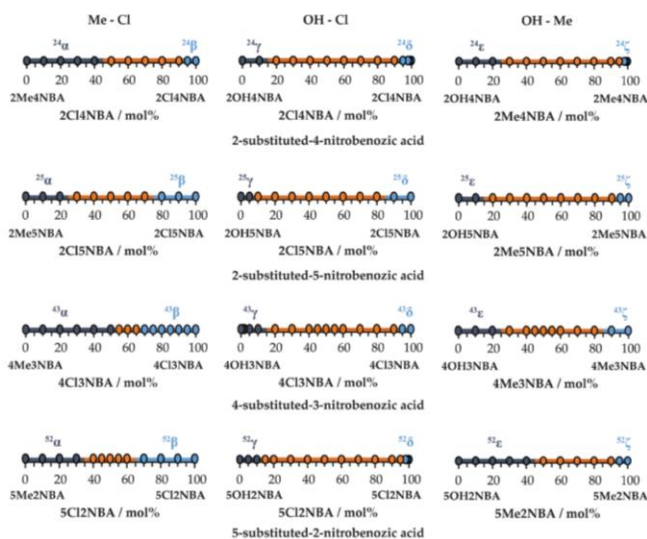


Figure 6. Schematic representation of the phases obtained in the crystallization of binary mixtures of various substituted nitrobenzoic acids for several tested molar ratios based on the recorded PXRD patterns and DSC curves. Solid solutions and the corresponding single-component phases are in identical shade of blue and phase mixtures in orange.

ethanol solutions resulted in a phase or phases with PXRD patterns corresponding to that or those of pure nonsolvated phases. For 2Me4NBA, this was polymorph I; for 2Cl4NBA, this was polymorph I; and for 5OH2NBA, this was polymorph I. Systems containing 5OH2NBA, however, were crystallized from acetonitrile to avoid the formation of a 5OH2NBA hydrate.

A summary of the solid solution composition limits for all 12 binary systems is given in Figure 6. Solid solutions were obtained in all of the explored binary systems. The obtained solid solutions are designated as γ (hydroxynitrobenzoic acids with dissolved chloronitrobenzoic acids), δ (chloronitrobenzoic acids with dissolved hydroxynitrobenzoic acids), ϵ (hydroxynitrobenzoic acids with dissolved methylnitrobenzoic acids), and ζ (methylnitrobenzoic acids with dissolved hydroxynitrobenzoic acids), with indices in superscript indicating position of methyl/chloro/hydroxyl and nitro group. Also, in these binary systems, no formation of stoichiometric phases (cocrystals) were observed.

The results show that the solid solution composition limits are rather different in each system. It demonstrates that not all of the functional groups can be equally easily replaced in the solid state. From Figure 6, it can be concluded that replacing methyl group-containing molecules by Cl-containing molecules (and vice versa) can be done to approximately the same extent as replacing hydroxyl group-containing molecules by the methyl group-containing molecules (from ~10 mol % to 40 mol %). Replacing hydroxyl group-containing molecules by the respective methyl group-containing molecules is only achievable up to ~10 mol %. The same holds for the binary systems with Cl-containing and hydroxyl group-containing molecules where no more than 10 mol % of the opposite component can

be incorporated in any of the eight partial solid solutions. The comparison of the functional groups and their properties shows that this is not surprising, as the replacement of hydroxyl/methyl groups and Cl/hydroxyl group are associated with a larger change in the molecule size, as well as larger differences in the intermolecular interactions possibly formed by the molecules, if compared to changes introduced by the replacement of methyl group and Cl. It is somewhat not obvious that the solubility of methyl group-containing molecules in hydroxyl group-containing molecules would be high in all of the systems. However, this could be because the methyl group can act as a donor of weak hydrogen bonds, and this could allow one to avoid a steep energy increase of the crystal structure by replacing these functional groups.

3.2. Identification of the Link between Crystal Structures and Solid-Solution Formation. As demonstrated above, the capability of the studied molecules to form binary solid solutions is partly dependent on the functional groups being exchanged, as molecules with exchanged Cl and methyl group showed the highest relative solubility (in most of the cases, up to 20–40 mol %), whereas molecules with exchanged Cl and hydroxyl group the lowest (not exceeding 5–10 mol %). The solubility in each pair of molecules, however, still could be notably different, which is expected to be associated with the respective crystal structures. Therefore, we investigated the crystal structures and tried to find whether crystallographic analysis and computational analysis of the energy associated with the molecule replacement could provide rationalization of the solid solution formation and could be used to predict the solid solution formation capability in each different case.

3.2.1. Comparison of Intermolecular Interactions and Their Energy. Intermolecular interactions and their energy in the experimental crystal structures and the structures modeling solid solution (substituted) and fully isostructural phase with complete molecule replacement (isostructural) were analyzed. In crystal structures of all the used nitrobenzoic acids, the carboxyl groups were hydrogen-bonded by forming $R_2^2(8)$ homodimers and this interaction was not notably altered in any of the modeled structures of solid solutions or isostructural phases (see Tables S7–S18 in the Supporting Information). In a few cases, the energy of this interaction was lowered by up to 5 kJ mol^{-1} , but among these, only in $2\text{Me}_{1-x}\text{OH}_x\text{4NBA}$ (x is the mole fraction from 0.0 to 1.0) the less-efficient energy in the isostructural structure correlated with low solubility observed in the experiments. Moreover, the experimental crystal structures of solid solutions $2\text{OH}_{0.10}\text{Cl}_{0.90}\text{5NBA}$, $4\text{Me}_{0.20}\text{Cl}_{0.80}\text{3NBA}$, $4\text{Me}_{0.25}\text{Cl}_{0.75}\text{3NBA}$, $4\text{Me}_{0.30}\text{Cl}_{0.70}\text{3NBA}$, $4\text{Me}_{0.50}\text{Cl}_{0.50}\text{3NBA}$ and $4\text{OH}_{0.05}\text{Cl}_{0.95}\text{3NBA}$, also confirmed that these interactions are not notably affected (as presented in Table S39 in the Supporting Information).

Evaluation of the weak intermolecular interactions formed by the group being replaced and the changes introduced by the replacement in substituted and isostructural structures (summarized in Tables S20–S23 in the Supporting Information) clearly demonstrated that, in each crystal structure, the interactions formed and the changes occurring by the functional group replacement are different. Overall, the replacement of the functional group could alter the weak interactions formed by the replaced functional group (for example, $\text{Cl}\cdots\text{H}-\text{O}2$ in $2\text{Cl}4\text{NBA}$ with $\text{C}8-\text{H}\cdots\text{O}2$ in $2\text{Cl}_0\text{Me}_1\text{4NBA}$) or introduce major change to those interactions (for example, $\text{C}8-\text{H}\cdots\text{O}1$ and $\text{C}8-\text{H}\cdots\text{O}_3\text{N}$ in $2\text{Me}5\text{NBA}$ with $\text{O}5\cdots\text{H}-\text{C}2$ and $\text{O}5\cdots\text{H}-\text{C}4$ in $2\text{Me}_0\text{OH}_1\text{5NBA}$). In the case of such change, the interactions can be of highly similar energy; for example, the interaction energy between molecules linked by $\text{O}5\cdots\text{H}-\text{O}2$ in $2\text{OH}5\text{NBA}$ is $-13.1 \text{ kJ mol}^{-1}$ and changing the linkage to $\text{Cl}\cdots\text{H}-\text{O}2$ in $2\text{OH}_{0.75}\text{Cl}_{0.25}\text{5NBA}$ and $2\text{OH}_0\text{Cl}_1\text{5NBA}$ changes the energy to $-14.0 \text{ kJ mol}^{-1}$ and $-12.2 \text{ kJ mol}^{-1}$, respectively. However, it can also either become notably less-efficient, for example, the interaction energy between molecules linked by $\text{O}5\cdots\text{H}-\text{C}3$ in $2\text{OH}5\text{NBA}$ is $-14.1 \text{ kJ mol}^{-1}$, and changing the linkage to $\text{Cl}\cdots\text{H}-\text{C}3$ in $2\text{OH}_{0.75}\text{Cl}_{0.25}\text{5NBA}$ and $2\text{OH}_0\text{Cl}_1\text{5NBA}$ changes the energy to -7.4 kJ mol^{-1} and -6.2 kJ mol^{-1} , respectively, or notably more efficient, for example, the interaction energy between molecules linked by $\text{Cl}\cdots\text{H}-\text{C}2$ in $4\text{Cl}3\text{NBA}$ is -3.9 kJ mol^{-1} , and changing the linkage to $\text{O}5\cdots\text{H}-\text{C}2$ in $4\text{Cl}_{0.75}\text{OH}_{0.25}\text{3NBA}$ and $4\text{Cl}_0\text{OH}_1\text{3NBA}$ change the energy to $-10.8 \text{ kJ mol}^{-1}$ and $-16.3 \text{ kJ mol}^{-1}$, respectively. Moreover, the replacement could also change the efficiency of the aromatic interactions between the closest molecules (for example, the $\pi\cdots\pi$ interaction becomes notably more efficient in $5\text{Cl}_2\text{Me}_2\text{NBA}$ and notably less-efficient in $2\text{Me}_0\text{Cl}_1\text{5NBA}$) and alter the energy between molecules linked by other weak intermolecular interactions; for example, the interaction energy between molecules linked by $\text{NO}_2\cdots\text{C}3-\text{H}$ in $2\text{Me}4\text{NBA}$ is $-16.0 \text{ kJ mol}^{-1}$, and changes to $-11.3 \text{ kJ mol}^{-1}$ and -5.2 kJ mol^{-1} in $2\text{Me}_{0.75}\text{OH}_{0.25}\text{4NBA}$ and $2\text{Me}_0\text{OH}_1\text{4NBA}$, respectively.

Nevertheless, the change in the sum of the pairwise interaction energy with molecules adjacent to the replaced functional group given in Table 1 could not be directly linked to the experimentally determined solubility limit in the

Table 1. Change of the Sum of Pairwise Intermolecular Interaction Energy Calculated in CrystalExplorer by the Replacement of the Functional Group for the Closest Molecules (3.80 Å) to the Replaced Functional Group and for the Molecule Pairs for Which There Are Atoms within a 15 Å Radius from the Central Molecule

structure	2OH4NBA		2Cl4NBA		2Me4NBA	
	–Cl	–CH ₃	–OH	–CH ₃	–OH	–Cl
Change of the sum of E_{inter} for the closest molecules (kJ mol^{-1})						
substituted	+31.4	+16.9	+6.2	+1.9	–2.7	–3.5
isostructural	+18.3	+2.1	+7.2	+4.3	+12.9	+10.6
Change of the sum of E_{inter} for the molecules within a 15 Å radius (kJ mol^{-1})						
substituted	+11.4	+2.9	+4.6	–5.0	+0.9	–0.9
isostructural	+15.1	+0.9	+0.5	–7.6	–0.4	+0.6
structure	2OH5NBA		2Cl5NBA		2Me5NBA	
	–Cl	–CH ₃	–OH	–CH ₃	–OH	–Cl
Change of the sum of E_{inter} for the closest molecules (kJ mol^{-1})						
substituted	+9.4	+11.0	+8.5	+1.1	+15.4	+12.0
isostructural	+5.4	+9.1	+11.3	+3.6	+14.4	+17.8
Change of the sum of E_{inter} for the molecules within a 15 Å radius (kJ mol^{-1})						
substituted	+12.4	+11.4	+8.8	–2.1	+7.9	+7.6
isostructural	+13.7	+10.9	+5.3	–2.2	+8.2	+13.0
structure	4OH3NBA		4Cl3NBA		4Me3NBA	
	–Cl	–CH ₃	–OH	–CH ₃	–OH	–Cl
Change of the sum of E_{inter} for the closest molecules (kJ mol^{-1})						
substituted	+14.8	+9.4	–10.0	–9.2	+6.4	+6.1
isostructural	+18.6	+6.9	–12.8	–19.5	+6.6	+4.4
Change of the sum of E_{inter} for the molecules within a 15 Å radius (kJ mol^{-1})						
substituted	+1.3	–1.1	–6.1	–4.4	–1.3	+3.4
isostructural	+1.8	–0.7	–23.5	–6.1	–11.8	+6.4
structure	5OH2NBA		5Cl2NBA		5Me2NBA	
	–Cl	–CH ₃	–OH	–CH ₃	–OH	–Cl
Change of the sum of E_{inter} for the closest molecules (kJ mol^{-1})						
substituted	+2.6	+0.6	–6.1	–4.4	+6.0	+23.9
isostructural	+0.5	+4.7	–25.6	–14.9	+3.2	+15.7
Change of the sum of E_{inter} for the molecules within a 15 Å radius (kJ mol^{-1})						
substituted	+14.9	+3.0	–5.0	–4.8	+8.2	+19.0
isostructural	+20.2	+1.9	–21.1	–7.6	–6.7	+34.4

respective molecule pair. There were cases where the energy became more efficient, but the solid solution formed in a very narrow concentration range as for $4\text{Cl}_{1-x}\text{OH}_x\text{3NBA}$ with an energy change of -10.0 and $-12.8 \text{ kJ mol}^{-1}$ in substituted and isostructural structures but determined solubility limit of only 5 mol %, and cases where the energy change was notably inefficient, but the solid solution formed in a wide concentration range as for $5\text{Me}_{1-x}\text{Cl}_x\text{2NBA}$ with energy changes of $+23.9$ and $+15.7 \text{ kJ mol}^{-1}$ in substituted and isostructural structures but determined solubility limit of up to 30 mol %.

Overall, a similar conclusion was also obtained from the comparison of the sum of the pairwise intermolecular interaction energies for the molecules within a 15 Å radius from the central molecule (for original and isostructural structures being an approximation of lattice energy); see Table 1. For example, despite the solubility of chloro-containing molecules in methyl-containing molecules overall being the

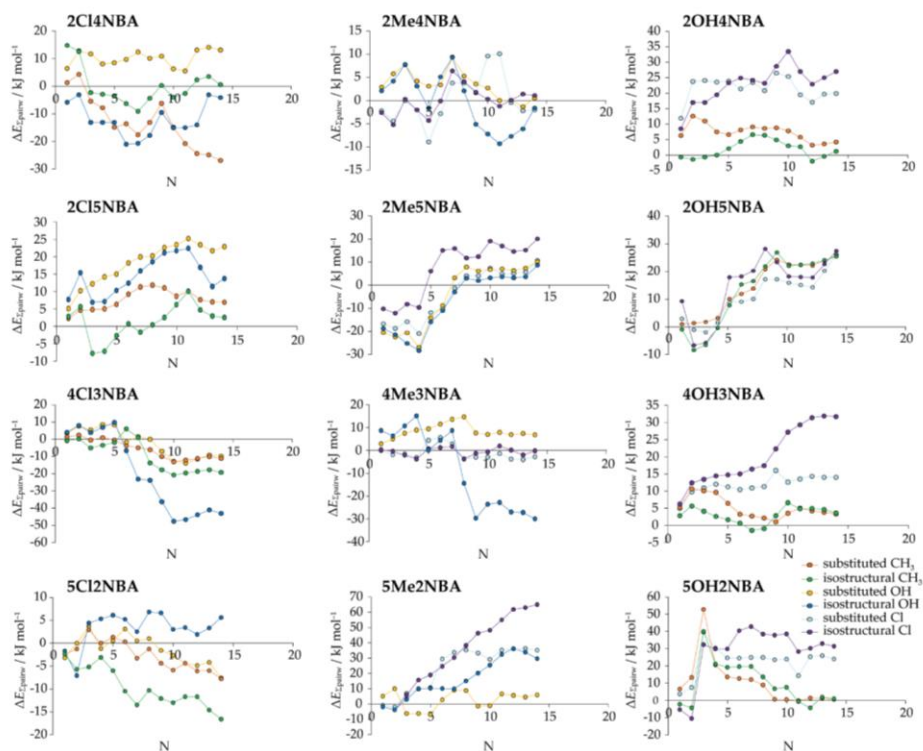


Figure 7. Difference in the cumulative interaction energy from the molecule pairs with increasing distance between the molecular centroids between substituted and isostructural structures and that of the original structure plotted by increasing distance (N = molecule number).

highest, only in some cases the energy change was calculated to be efficient. In contrast, despite the very low solubility of hydroxyl containing molecules in chloro-containing molecules, the energy change in most of the cases were calculated to be notably efficient or only slightly inefficient.

A potential explanation for the lack of correlation between the energy change and solid-solution formation is that the difference of interaction energy for the structure with replaced functional group and the structure with original functional group is not a correct criterion for comparison of structures with the introduced notable structure differences. Instead, to obtain reliable conclusions, the energy should be compared to the alternative states available to the system of the given composition and could also require evaluation of the thermal and entropy effects. In general, this is well-demonstrated by comparing the energy change associated with the replacement of selected functional groups in all of the isomers, as the replacement of methyl group with Cl, which, in the crystallization experiments, allowed to obtain solid solutions with the highest achieved dissolution, in almost all the cases is calculated to be associated with an energy increase, although no one particular cause for this increase could be identified in the analyses of the intermolecular interactions of these

structures. Likewise, the replacement of the methyl group with Cl in all of the cases was calculated to be associated with an increase of the total intermolecular interaction energy. Although such a replacement was associated with rather good solid solution formation, there is no strong correlation between the solubility limit and energy change. Moreover, the replacement of Cl with a hydroxyl group in 4Cl3NBA and 5Cl2NBA was calculated to be highly efficient, but experimentally these were among systems with the lowest determined dissolution limit.

In contrast, our previous study²⁷ shows that, in the case of notably smaller change of the molecular structure, as replacement of benperidol and droperidol molecules, the energy change can be used as a criterion for the prediction of solid solution formation.

Also, additional views on the energy differences were obtained by analyzing the interaction energy for molecule pairs for which there are atoms within a 3.80 Å radius from the central molecule given in Tables S7–S18 in the Supporting Information. The plots of the difference of the cumulative interaction energy from these molecule pairs with increasing distance between the molecular centroids in substituted and

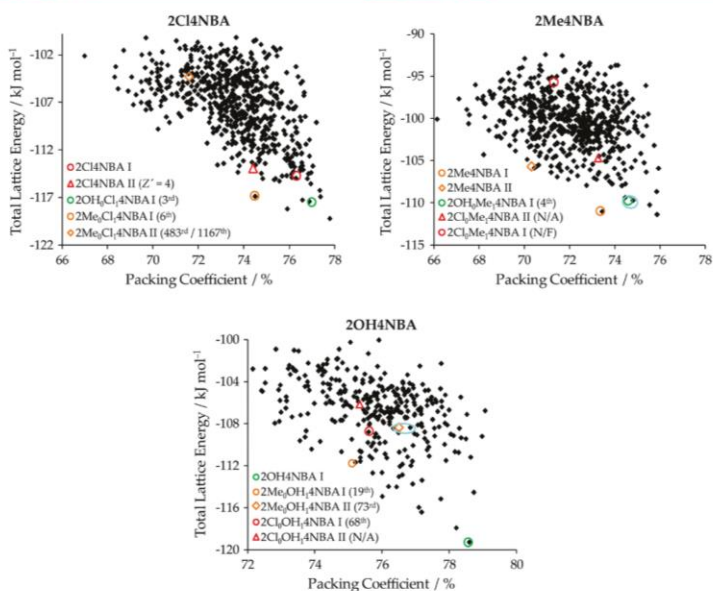


Figure 8. Crystal structure landscapes of 2Cl₄NBA, 2Me₄NBA, and 2OH₄NBA, where each black dot represents a stable lattice energy minimum, generated in the CSP study. Open shapes are either experimental structures or isostructural structures obtained by substituent replacement. CSP generated structures are linked to the experimental structure by a larger ellipse, if not falling within the symbol. Labels of isostructural structures contain a number corresponding to the energy ranking of the respective structure.

isostructural structures and that in the original structure are given in Figure 7.

These plots demonstrate that, in some of the cases, the analysis of only the closest molecule pairs can provide an incorrect picture of the effect of the substitution, as, for example, in the structure 2Me_{1-x}OH_xNBA the closest interactions are more efficient, whereas including molecule pairs with larger distance, the energy becomes inefficient, or, in contrast, in the structure 4Cl_{1-x}OH_x3NBA, the closest interactions are less-efficient, whereas including molecule pairs with larger distance, the energy becomes more efficient. Overall, by increasing the number of molecule pairs considered, the energy tends to converge to the result representing the total energy of all molecule pairs for which there are atoms within a 15 Å radius from the central molecule, as shown in Table 1, although for some of the structures a larger number of molecules appeared to be necessary to be included in the summation to approach this value.

3.2.2. Analysis of Computationally Generated Structure Landscapes. As an alternative tool for explanation of the solid solution formation likelihood, we considered the location of isostructural or highly similar structures in computationally generated structures obtained in CSP study, similarly as demonstrated for other compounds.⁵⁶ This tool was evaluated for 2-substituted-4-nitrobenzoic acids by comparing the computationally generated 2Cl₄NBA, 2Me₄NBA, and 2OH₄NBA structures obtained in our previous study³² and isostructural structures obtained from the experimental non-solvents of these compounds with replaced substituents after

the geometry optimization. This comparison in general showed that among the predicted structures there are such isostructural structures, and moreover, some of them are energetically competitive with the experimental crystal structures of the respective compound; see Figure 8 (and Table S24 in the Supporting Information).

2Cl₄NBA and 2Me₄NBA structures, which are isostructural to the experimental structure of 2OH₄NBA, appear as energetically very competitive in the landscapes of 2Cl₄NBA and 2Me₄NBA and are ranked as the third lowest energy structure for 2Cl₄NBA and fourth lowest for 2Me₄NBA. Similarly, structures isostructural to 2Me₄NBA polymorph I appear in the landscapes of 2Cl₄NBA and 2OH₄NBA and are ranked as the sixth lowest energy structure for 2Cl₄NBA and 19th lowest for 2OH₄NBA. Although structures isostructural to 2Me₄NBA, polymorph II can also be located in the landscapes of 2Cl₄NBA and 2OH₄NBA, these are energetically notably less competitive.

Structures isostructural to 2Cl₄NBA polymorph I appear in the landscape of 2OH₄NBA as the 68th lowest energy structure (having 11 kJ mol⁻¹ higher lattice energy), whereas the Z' = 4 structure obtained from polymorph II is energetically slightly less-efficient. Structure isostructural to 2Cl₄NBA I is not present in the landscape of 2Me₄NBA, as the lattice energy of such structure was calculated to be at least 12 kJ mol⁻¹ above the lowest energy experimental polymorph. In contrast, the structure isostructural to 2Cl₄NBA II was calculated to be only 6 kJ mol⁻¹ above the lowest energy experimental polymorph.

Table 2. Relative Energy of the Experimental and in the CSP Generated Isostructural Structures as Calculated in CASTEP after Geometry Optimization Using TS Dispersion Correction and Single Point Energy Calculation Using the MBD* Dispersion Correction Scheme

structure	ΔE (kJ mol ⁻¹)		structure	ΔE (kJ mol ⁻¹)		structure	ΔE (kJ mol ⁻¹)	
	TS	MBD*		TS	MBD*		TS	MBD*
2Cl4NBA I	2.0	2.9	2Me4NBA I	0.0	0.0	2OH4NBA I	0.0	0.0
2Cl4NBA II	0.3	0.1	2Me4NBA II	2.2	3.4	-	-	-
2Me ₀ Cl ₁ 4NBA I	0.0	0.0	2Cl ₀ Me ₁ 4NBA I	6.7	5.3	2Me ₀ OH ₁ 4NBA I	5.0	3.1
2Me ₀ Cl ₁ 4NBA II	1.4	2.7	2Cl ₀ Me ₁ 4NBA II	4.6	4.6	2Me ₀ OH ₁ 4NBA II	12.7	11.6
2OH ₀ Cl ₁ 4NBA I	1.4	3.7	2OH ₀ Me ₁ 4NBA I	2.6	4.5	2Cl ₀ OH ₁ 4NBA I	7.0	7.0

In general, the existence of mutually isostructural low-energy structures indicates that the formation of solid solutions is possible, as the respective structure is efficient for both compounds, and it has been demonstrated that this could even indicate on the possibility to obtain isostructural single component phases.^{56–58} The conclusions obtained from the structure landscape analysis, however, are only partly consistent with the experimental observations. The best solubility was observed for 2Cl4NBA in 2Me4NBA polymorph I which is consistent with the low energy of a 2Cl4NBA structure isostructural to 2Me4NBA I. In contrast, despite the structure isostructural to 2OH4NBA is among the lowest energy structures of 2Cl4NBA and 2Me4NBA, the solubility of 2Me4NBA in 2OH4NBA is only ~20 mol % and that of 2Cl4NBA only ~10 mol %. The low solubility of 2OH4NBA in 2Cl4NBA and in 2Me4NBA and low solubility of 2Me4NBA in 2Cl4NBA in general is consistent with the relatively high (>5 kJ mol⁻¹) energy for the respective isostructural phases.

Since the CrystalOptimizer only provides approximate energy ranking of the structures, we additionally performed geometry optimization of the experimental and in the CSP generated isostructural structures in CASTEP using TS dispersion correction and calculated their relative energy using the MBD* dispersion correction scheme. The obtained energy differences given in Table 2 show that the CrystalOptimizer energy ranking presented in Figure 8 overall provide a useful picture on the energy ranking of the experimental and isostructural structures, with relative energy usually altered by no more than ~3 kJ mol⁻¹ (see Table S24 in the Supporting Information), although the energy of 2Me₀Cl₁4NBA polymorph II and 2Cl₀Me₁4NBA polymorph I was notably lowered with this energy calculation approach. Nevertheless, the energy differences calculated by CASTEP provide notably better agreement with the experimentally observed solubility limits in the solid solutions, as the 2Me₀Cl₁4NBA polymorph I was calculated as the most efficient among the isostructural structures and the energy of 2OH₀Cl₁4NBA and 2OH₀Me₁4NBA was increased if compared to the relative energy provided by the CrystalOptimizer. However, full rationalization of the solid solution formation likelihood still could not be achieved by this approach, as better solubility of 2OH4NBA in 2Me4NBA was predicted by the obtained results.

4. CONCLUSIONS

This study of the solid-solution formation between different substituted nitrobenzoic acids clearly demonstrates that solid solutions in different crystal structures form notably differently, and the extent up to which a structure can accommodate the other molecule is strongly dependent on the intermolecular interactions present in the crystal structure and altered by

molecule replacement. There are structure pairs in which replacement of up to 40 mol % can be reached, as observed for chloronitrobenzoic acid in methylnitrobenzoic acid in pairs 2Me4NBA–2Cl4NBA and 4Me3NBA–4Cl3NBA and methylnitrobenzoic acid in hydroxynitrobenzoic acid in the pair 5OH2NBA–5Me2NBA. In contrast, in other studied structure pairs (mostly between hydroxyl-chloro and hydroxyl-methylnitrobenzoic acids), we observe notably lower solubility. For example, only up to 5 mol % of hydroxynitrobenzoic acid could be dissolved in chloronitrobenzoic acid in pairs 2OH4NBA–2Cl4NBA, 4OH3NBA–4Cl3NBA and 5OH2NBA–5Cl2NBA, and in methylnitrobenzoic acid in pairs 2OH4NBA–2Me4NBA, 2OH5NBA–2Me5NBA, and 5OH2NBA–5Me2NBA.

In general, however, the solubility of the molecules, to some extent, is determined by the properties and characteristics of the functional groups being exchanged. Overall, the best solubility therefore was observed for molecule pairs in which Cl substituent and methyl group were exchanged, as these groups are of similar size and properties, and has been shown to be often exchangeable in the solid state.^{19,20} In contrast, exchange of hydroxyl and methyl groups or Cl and hydroxyl groups having more different size and intermolecular interaction characteristics is disfavored and leads to a reduced solid-state solubility. The solubility of methylnitrobenzoic acids in hydroxynitrobenzoic acids, however, is rather high, regardless of the substituent arrangement, possibly due to the ability of the methyl group to act as a weak hydrogen bond donor, which, to some extent, can replace the properties of a hydroxyl group.

The effect of the functional group replacement on the intermolecular interactions and their energy in all of the considered crystal structures was also evaluated by searching for a tool allowing prediction of the solid solution formation likelihood. It was observed that in all of the structures the functional group replacement was associated with a change of the intermolecular interactions and to some extent also their energies. However, the quantitative evaluation of the intermolecular interaction energy change by the functional group replacement for neither the molecules close to the replace group nor the molecules within a 15 Å radius did not allow rationalization of the experimentally observed solubilities in each molecule pair. This suggests that the difference in interaction energy between the structures with replaced and original functional groups is not an adequate criterion for comparing structures in which such significant differences are introduced by molecule replacement. Instead, the energy should be compared with other states available for the given composition and may require an assessment of thermal and entropy effects. A better tool for the rationalization of the observed solid solution formation likelihood was the

identification of the low-energy isostructural phases in computationally generated structure landscapes, which was tested for 2-substituted-4-nitrobenzoic acids. In general, good agreement with the experimentally observed solubility limits was achieved by using energy ranking after structure optimization and energy calculation in CASTEP, although also this approach still did not allow rationalization of the relative solubility observed in all of the structures.

■ ASSOCIATED CONTENT

Supporting Information

The Supporting Information is available free of charge at <https://pubs.acs.org/doi/10.1021/acs.cgd.3c00529>.

Additional details and results of the crystallization experiments, results from characterization of the crystallization products of all the explored systems using PXRD patterns, DSC curves, and ^1H NMR spectra, additional results, and data from comparison of crystal structures, crystal structure determination, lattice parameters of solid solutions, and calculation of pairwise and cumulative intermolecular interaction energy (PDF)

Accession Codes

CCDC 2257118–2257122, 2257680–2257681, and 2257683–2257686 contain the supplementary crystallographic data for this paper. These data can be obtained free of charge via www.ccdc.cam.ac.uk/data_request/cif, or by emailing data_request@ccdc.cam.ac.uk, or by contacting The Cambridge Crystallographic Data Centre, 12 Union Road, Cambridge CB2 1EZ, UK; fax: +44 1223 336033.

■ AUTHOR INFORMATION

Corresponding Author

Agris Berziņš – Faculty of Chemistry, University of Latvia, Rīga LV-1004, Latvia; orcid.org/0000-0002-4149-8971; Phone: +(371)-67033903; Email: agris.berzins@lu.lv

Authors

Kristaps Saršūns – Faculty of Chemistry, University of Latvia, Rīga LV-1004, Latvia; orcid.org/0000-0002-8692-7768
Artis Kōns – Faculty of Chemistry, University of Latvia, Rīga LV-1004, Latvia; orcid.org/0000-0002-4055-8442
Toms Reķis – Faculty of Chemistry, University of Latvia, Rīga LV-1004, Latvia; orcid.org/0000-0001-5128-4611

Complete contact information is available at: <https://pubs.acs.org/doi/10.1021/acs.cgd.3c00529>

Funding

This research was funded by the Latvian Council of Science project, “Crystal Engineering of Pharmaceutical Multicomponent Phases for More Efficient Crystalline Phase Design” (Project No. lzp-2018/1–0312).

Notes

The authors declare no competing financial interest.

■ ACKNOWLEDGMENTS

K.S. acknowledges financial support from the European Social Fund project “Strengthening of the Capacity of Doctoral Studies at the University of Latvia within the Framework of the New Doctoral Model”, identification No. 8.2.2.0/20/I/006, and MikroTik Ltd. doctoral scholarship in the field of natural and medical sciences administrated by the University of Latvia

Foundation. The authors thank Rihards Klūga (University of Latvia) for ^1H NMR spectra measurements, and Kristīne Krūkle-Bērziņa (Latvian Institute of Organic Synthesis) for collection of SCXRD data.

■ REFERENCES

- (1) Barbour, L. J.; Das, D.; Jacobs, T.; Lloyd, G. O.; Smith, V. J. *Concepts and Nomenclature in Chemical Crystallography* **2012**, DOI: 10.1002/9780470661345.smc108.
- (2) Vujovic, D.; Raubenheimer, H. G.; Nassimbeni, L. R. One-Dimensional CdII Coordination Polymers: Solid Solutions with NiII, Thermal Stabilities and Structures. *Eur. J. Inorg. Chem.* **2004**, 2004 (14), 2943–2949.
- (3) Krishnan, R.; Swart, H. C. Luminescence Properties of Octahedrally and Tetrahedrally Coordinated Mo6+ in the Solid Solutions: Judd–Ofelt Investigation. *J. Phys. Chem. Solids* **2020**, 144, 109519.
- (4) Lusi, M. A Rough Guide to Molecular Solid Solutions: Design, Synthesis and Characterization of Mixed Crystals. *CrystEngComm* **2018**, 20 (44), 7042–7052.
- (5) Lusi, M. Engineering Crystal Properties through Solid Solutions. *Cryst. Growth Des.* **2018**, 18 (6), 3704–3712.
- (6) Braga, D. Crystal Engineering, Where from? Where To? *Chem. Commun.* **2003**, 3 (22), 2751–2754.
- (7) D’Agostino, S.; Fornasari, L.; Grepioni, F.; Braga, D.; Rossi, F.; Chierotti, M. R.; Gobetto, R. Precessional Motion in Crystalline Solid Solutions of Ionic Rotors. *Chem. - A Eur. J.* **2018**, 24 (56), 15059–15066.
- (8) Lusi, M.; Vitorica-Yrezabal, I. J.; Zaworotko, M. J. Expanding the Scope of Molecular Mixed Crystals Enabled by Three Component Solid Solutions. *Cryst. Growth Des.* **2015**, 15 (8), 4098–4103.
- (9) Molecular crystals and molecules: A. I. Kitaigorodsky. Volume 29 of Physical Chemistry, Edited by Ernest M. Loebel. Pp. 553. Academic Press, New York, 1973. Price: \$44.00. *Mater. Res. Bull.* **1974**, 9 (2), 199–200
- (10) Sacconi, L.; Ciampolini, M.; Speroni, G. P. Structure Mimicry in Solid Solutions of 3d Metal Complexes with N-Methylsalicylaldimine (Msal-Me). *J. Am. Chem. Soc.* **1965**, 87 (14), 3102–3106.
- (11) Jones, W.; Theocharis, C. R.; Thomas, J. M.; Desiraju, G. R. Structural Mimicry and the Photoreactivity of Organic Solids. *J. Chem. Soc. Chem. Commun.* **1983**, 23, 1443.
- (12) Braga, D.; Grepioni, F.; Maini, L.; Polito, M.; Rubini, K.; Chierotti, M. R.; Gobetto, R. Hetero-Seeding and Solid Mixture to Obtain New Crystalline Forms. *Chem. - A Eur. J.* **2009**, 15 (6), 1508–1515.
- (13) Taylor, R. Which Intermolecular Interactions Have a Significant Influence on Crystal Packing? *CrystEngComm* **2014**, 16 (30), 6852–6865.
- (14) Taylor, R. It Isn’t, It Is: The C–H...X (X = O, N, F, Cl) Interaction Really Is Significant in Crystal Packing. *Cryst. Growth Des.* **2016**, 16 (8), 4165–4168.
- (15) Gavezotti, A.; Presti, L. Lo. Building Blocks of Crystal Engineering: A Large-Database Study of the Intermolecular Approach between C–H Donor Groups and O, N, Cl, or F Acceptors in Organic Crystals. *Cryst. Growth Des.* **2016**, 16 (5), 2952–2962.
- (16) Corpinot, M. K.; Stratford, S. A.; Arhangelskis, M.; Anka-Lufford, J.; Halasz, I.; Judaš, N.; Jones, W.; Bučar, D. K. On the Predictability of Supramolecular Interactions in Molecular Cocrystals—the View from the Bench. *CrystEngComm* **2016**, 18 (29), 5434–5439.
- (17) Dubey, R.; Pavan, M. S.; Desiraju, G. R. Structural Landscape of Benzoic Acid: Using Experimental Crystal Structures of Fluorobenzoic Acids as a Probe. *Chem. Commun.* **2012**, 48 (72), 9020–9022.
- (18) Bučar, D.-K.; Henry, R. F.; Zhang, G. G. Z.; MacGillivray, L. R. Synthons Hierarchies in Crystal Forms Composed of Theophylline and Hydroxybenzoic Acids: Cocrystal Screening via Solution-Mediated Phase Transformation. *Cryst. Growth Des.* **2014**, 14 (10), 5318–5328.

- (19) Desiraju, G. R.; Sarma, J. A. R. P. The Chloro-Methyl Exchange Rule and Its Violations in the Packing of Organic Molecular Solids. *J. Chem. Sci.* **1986**, *96* (6), 599–605.
- (20) Omondi, B.; Fernandes, M. A.; Layh, M.; Levendis, D. C.; Look, J. L.; Mkwizu, T. S. P. Polymorphism and Phase Transformations in 2,6-Disubstituted N-Phenylformamides: The Influence of Hydrogen Bonding, Chloro-Methyl Exchange, Intermolecular Interactions and Disorder. *CrystEngComm* **2005**, *7* (114), 690–700.
- (21) Desiraju, G. R. *Crystal as a Supramolecular Entity*; **2007**; Vol. 2. DOI: 10.1002/9780470511459.
- (22) Romasanta, A. K. S.; Braga, D.; Duarte, M. T.; Grepioni, F. How Similar Is Similar? Exploring the Binary and Ternary Solid Solution Landscapes of p-Methyl/Chloro-Bromo-Benzyl Alcohols. *CrystEngComm* **2017**, *19* (4), 653–660.
- (23) Saršūns, K.; Kemere, M.; Karziņš, A.; Kļimenkovs, I.; Bērziņš, A.; Sarakovskis, A.; Reķis, T. Fine-Tuning Solid State Luminescence Properties of Organic Crystals via Solid Solution Formation: The Example of 4-Iodothioxanthone-4-Chlorothioxanthone System. *Cryst. Growth Des.* **2022**, *22* (8), 4838–4844.
- (24) Saršūns, K.; Bērziņš, A.; Reķis, T. Solid Solutions in the Xanthone–Thioxanthone Binary System: How Well Are Similar Molecules Discriminated in the Solid State? *Cryst. Growth Des.* **2020**, *20* (12), 7997–8004.
- (25) Shemchuk, O.; Braga, D.; Grepioni, F. Alloying Barbituric and Thiobarbituric Acids: From Solid Solutions to a Highly Stable Keto Co-Crystal Form. *Chem. Commun.* **2016**, *52* (79), 11815–11818.
- (26) Oliveira, M. A.; Peterson, M. L.; Klein, D. Continuously Substituted Solid Solutions of Organic Co-Crystals. *Cryst. Growth Des.* **2008**, *8* (12), 4487–4493.
- (27) Saršūns, K.; Bērziņš, A. Experimental and Computational Investigation of Benperidol and Propriolol Solid Solutions in Different Crystal Structures. *Cryst. Growth Des.* **2023**, *23* (2), 1133–1144.
- (28) Braun, D. E.; Griesser, U. J. Prediction and Experimental Validation of Solid Solutions and Isopolymorphs of Cytosine/5-Fluorocytosine. *CrystEngComm* **2017**, *19* (26), 3566–3572.
- (29) Fonseca, J. D. C.; Tenorio Clavijo, J. C.; Alvarez, N.; Ellena, J.; Ayala, A. P. Novel Solid Solution of the Antiretroviral Drugs Lamivudine and Emtricitabine. *Cryst. Growth Des.* **2018**, *18* (6), 3441–3448.
- (30) Corpinot, M. K.; Bučar, D.-K. A Practical Guide to the Design of Molecular Crystals. *Cryst. Growth Des.* **2019**, *19* (2), 1426–1453.
- (31) Barsky, I.; Bernstein, J.; Stephens, P. W.; Stone, K. H. The Study of the Polymorphic System of 2-Chloro-4-Nitrobenzoic Acid. *New J. Chem.* **2008**, *32* (10), 1747–1753.
- (32) Bērziņš, A.; Kōns, A.; Saršūns, K.; Belyakov, S.; Actiņš, A. On the Rationalization of Formation of Solvates: Experimental and Computational Study of Solid Forms of Several Nitrobenzoic Acid Derivatives. *Cryst. Growth Des.* **2020**, *20* (9), 5767–5784.
- (33) Pramanik, S.; Dey, T.; Mukherjee, A. K. Five Benzoic Acid Derivatives: Crystallographic Study Using X-Ray Powder Diffraction, Electronic Structure and Molecular Electrostatic Potential Calculation. *J. Mol. Struct.* **2019**, *1175*, 185–194.
- (34) Mir, S. H.; Takasaki, Y.; Engel, E. R.; Takamizawa, S. Enhancement of Dissipated Energy by Large Bending of an Organic Single Crystal Undergoing Twinning Deformation. *RSC Adv.* **2018**, *8* (39), 21933–21936.
- (35) Montis, R.; Hursthouse, M. B. Surprisingly Complex Supramolecular Behaviour in the Crystal Structures of a Family of Mono-substituted Salicylic Acids. *CrystEngComm* **2012**, *14* (16), 5242–5254.
- (36) Bharathi, M. D.; Ahila, G.; Mohana, J.; Chakkaravarthi, G.; Anbalagan, G. Structural, Optical, Thermal and Mechanical Characterization of an Organic Nonlinear Optical Material: 4-Methyl-3-Nitrobenzoic Acid Single Crystal. *J. Phys. Chem. Solids* **2016**, *98*, 290–297.
- (37) Agilent Technologies UK. CrysAlisPRO Software. Yarnton, Engl. 2014.
- (38) Petricek, V.; Dušek, M.; Palatinus, L. Crystallographic Computing System JANA2006: General Features. *Z. Kristallogr.* **2014**, *229* (5), 345–352.
- (39) Kōns, A.; Bērziņš, A.; Actiņš, A.; Reķis, T.; Van Smaalen, S.; Mishnev, A. Polymorphism of R-Encenicline Hydrochloride: Access to the Highest Number of Structurally Characterized Polymorphs Using Desolvation of Various Solvates. *Cryst. Growth Des.* **2019**, *19* (8), 4765–4773.
- (40) Saršūns, K.; Bērziņš, A. Prediction of Solid Solution Formation among Chemically Similar Molecules Using Calculation of Lattice and Intermolecular Interaction Energy. *Key Eng. Mater.* **2020**, *850*, 54–59.
- (41) Giannozzi, P.; Baroni, S.; Bonini, N.; Calandra, M.; Car, R.; Cavazzoni, C.; Ceresoli, D.; Chiarotti, G. L.; Cococcioni, M.; Dabo, I.; Dal Corso, A.; De Gironcoli, S.; Fabris, S.; Fratesi, G.; Gebauer, R.; Gerstmann, U.; Gougousis, C.; Kokalj, A.; Lazzeri, M.; Martin-Samos, L.; Marzari, N.; Mauri, F.; Mazzarello, R.; Paolini, S.; Pasquarello, A.; Paulatto, L.; Sbraccia, C.; Scandolo, S.; Sclauzero, G.; Seitsonen, A. P.; Smogunov, A.; Umari, P.; Wentzcovitch, R. M. QUANTUM ESPRESSO: A Modular and Open-Source Software Project for Quantum Simulations of Materials. *J. Phys.: Condens. Matter* **2009**, *21* (39), 395502.
- (42) Vanderbilt, D. Soft Self-Consistent Pseudopotentials in a Generalized Eigenvalue Formalism. *Phys. Rev. B* **1990**, *41* (11), 7892–7895.
- (43) Perdew, J. P.; Burke, K.; Ernzerhof, M. Generalized Gradient Approximation Made Simple. *Phys. Rev. Lett.* **1996**, *77* (18), 3865–3868.
- (44) Grimme, S.; Antony, J.; Ehrlich, S.; Krieg, H. A Consistent and Accurate Ab Initio Parametrization of Density Functional Dispersion Correction (DFT-D) for the 94 Elements H-Pu. *J. Chem. Phys.* **2010**, *132* (15). DOI: 10.1063/1.3382344.
- (45) Lund, A. M.; Orendt, A. M.; Pagola, G. I.; Ferraro, M. B.; Facelli, J. C. Optimization of Crystal Structures of Archetypical Pharmaceutical Compounds: A Plane-Wave DFT-D Study Using Quantum Espresso. *Cryst. Growth Des.* **2013**, *13* (5), 2181–2189.
- (46) Spackman, P. R.; Turner, M. J.; McKinnon, J. J.; Wolff, S. K.; Grimwood, D. J.; Jayatilaka, D.; Spackman, M. A. CrystalExplorer: A Program for Hirshfeld Surface Analysis, Visualization and Quantitative Analysis of Molecular Crystals. *J. Appl. Crystallogr.* **2021**, *54* (3), 1006–1011.
- (47) MacRae, C. F.; Sovago, I.; Cottrell, S. J.; Galek, P. T. A.; McCabe, P.; Pidcock, E.; Platings, M.; Shields, G. P.; Stevens, J. S.; Towler, M.; Wood, P. A. Mercury 4.0: From Visualization to Analysis, Design and Prediction. *J. Appl. Crystallogr.* **2020**, *53*, 226–235.
- (48) Karamertzanis, P. G.; Pantelides, C. C. Ab Initio Crystal Structure Prediction. II. Flexible Molecules. *Mol. Phys.* **2007**, *105* (2–3), 273–291.
- (49) Kazantsev, A. V.; Karamertzanis, P. G.; Adjiman, C. S.; Pantelides, C. C. Efficient Handling of Molecular Flexibility in Lattice Energy Minimization of Organic Crystals. *J. Chem. Theory Comput.* **2011**, *7* (6), 1998–2016.
- (50) Chisholm, J. A.; Motherwell, S. COMPACK: A Program for Identifying Crystal Structure Similarity Using Distances. *J. Appl. Crystallogr.* **2005**, *38* (1A), 228–231.
- (51) Tkatchenko, A.; Scheffler, M. Accurate Molecular Van Der Waals Interactions from Ground-State Electron Density and Free-Atom Reference Data. *Phys. Rev. Lett.* **2009**, *102* (7), 073005.
- (52) Tkatchenko, A.; DiStasio, R. A.; Car, R.; Scheffler, M. Accurate and Efficient Method for Many-Body van Der Waals Interactions. *Phys. Rev. Lett.* **2012**, *108* (23), 236402.
- (53) Clark, S. J.; Segall, M. D.; Pickard, C. J.; Hasnip, P. J.; Probert, M. I. J.; Refson, K.; Payne, M. C. First Principles Methods Using CASTEP. *Zeitschrift für Krist. - Cryst. Mater.* **2005**, *220* (5–6), 567–570.
- (54) Vegard, L.; Schjelderup, H. Die Konstitution Der Mischkristalle. *Phys. Z.* **1917**, *18*, 93–96.
- (55) Vegard, L. Die Konstitution Der Mischkristalle Und Die Raumfüllung Der Atome. *Zeitschrift für Phys.* **1921**, *5* (1), 17–26.

(56) Case, D. H.; Srirambhatla, V. K.; Guo, R.; Watson, R. E.; Price, L. S.; Polyzois, H.; Cockcroft, J. K.; Florence, A. J.; Tocher, D. A.; Price, S. L. Successful Computationally Directed Templating of Metastable Pharmaceutical Polymorphs. *Cryst. Growth Des.* **2018**, *18* (9), 5322–5331.

(57) Srirambhatla, V. K.; Guo, R.; Price, S. L.; Florence, A. J. Isomorphous Template Induced Crystallisation: A Robust Method for the Targeted Crystallisation of Computationally Predicted Metastable Polymorphs. *Chem. Commun.* **2016**, *52* (46), 7384–7386.

(58) Arlin, J. B.; Price, L. S.; Price, S. L.; Florence, A. J. A Strategy for Producing Predicted Polymorphs: Catemeric Carbamazepine Form V. *Chem. Commun.* **2011**, *47* (25), 7074–7076.

V

Saršūns, K., Kons, A., Leduskrasts, K., Kļimenkovs, I., Bērziņš, A.,
Rekis, T.

MODULATION OF PHYSICO-CHEMICAL PROPERTIES VIA SOLID SOLUTION FORMATION OF THIOXANTHONE DERIVATIVES

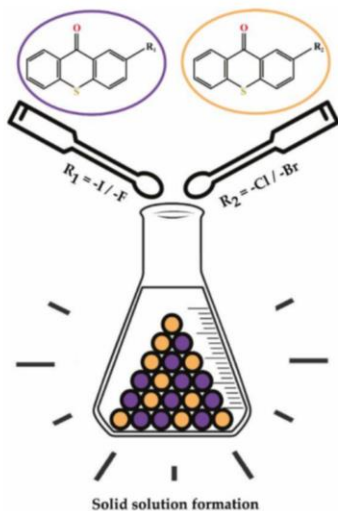
Manuscript in process of development

Modulation of physico-chemical properties *via* solid solution formation of thioxanthone derivatives

Kristaps Saršūns¹, Artis Kons¹, Kaspars Leduskrasts², Igors Kļimenkovs¹, Agris Bērziņš¹, Toms Reķis^{1*}

¹Faculty of Chemistry, University of Latvia, Riga, Latvia

²Latvian Institute of Organic Synthesis, Riga, Latvia



1. INTRODUCTION

The occurrence of photoluminescence in purely organic crystals at room temperature is uncommon, but it has become more extensively researched recently because of the practical applications of these materials¹⁻⁴.

By adjusting the temperature of a phosphorescent crystal, its luminescence characteristics can be modified⁵. Additionally, altering the excitation wavelength can result in diverse emission spectra⁶. Despite this, these factors alone may not be sufficient for creating a well-designed material. Current approaches to optimizing luminescence properties in organic crystals can be divided into two main categories: the chemical approach and the crystal engineering approach. The chemical approach involves modifying the molecular structure of known solid state luminophores by altering substituents, such as halogen atoms^{7,8}, alkyl chain lengths^{9,10} or introducing other changes to the molecule's configuration^{11,12}. The crystal engineering approach, on the other hand, focuses on manipulating the crystal lattice to influence the luminescence properties. Despite these strategies, it is important to note that simply employing them may not always result in a successful material design.

The concept of solid solutions has long been recognized as an effective crystal engineering strategy for tuning the properties of inorganic compounds^{13,14}. By altering the composition of solid solutions, researchers have been able

ABSTRACT: We present an experimental study of solid solution formation between structurally highly similar model compounds thioxanthone derivatives: 2-iodothioxanthone, 2-chlorothioxanthone, 2-bromothioxanthone and 2-fluorothioxanthone. All of named components are room-temperature luminophores. In some of binary system mixtures, almost complete replacement of both compounds can be achieved, whereas in other cases, the replacement is possible only up to a limited molar ratio. The obtained crystalline phases were characterized using powder X-ray diffraction (PXRD) and differential scanning calorimetry (DSC) methods in order to construct respective binary phase diagrams. Furthermore, photoluminescence spectra of all crystalline phases in powder form were recorded to see how they change with respect to those of the pure substances known from the literature. This study proves great potential to use solid solution engineering in the organic solid state to tune material properties in a continuum.

to modify a wide range of properties, including non-linear optical¹⁵, solubility and melting point^{16,17}, and mechanical properties¹⁸. However, when it comes to purely organic systems, the solid solution phenomenon is still relatively unexplored.

One of the main reasons for this is that the formation of molecular solid solutions is not as straightforward as inorganic solid solutions. The design and synthesis of organic solid solutions with desired properties is a significant challenge in crystal engineering, requiring a deep understanding of the molecular intermolecular interactions and the resulting crystal structures¹⁹. Instead, it is governed by complex molecular recognition processes in the solid state. Molecular recognition refers to the ability of molecules to interact with each other in specific ways, forming stable structures that are held together by intermolecular forces^{20,21}. In the case of solid solutions, this means that two or more molecular entities must be able to interact in such a way that they can be incorporated into the same crystal lattice. Despite these challenges, researchers have found that by carefully selecting the molecular components, it is possible to create solid solutions that exhibit desirable properties^{22,23}.

However, the number of reported cases of molecular solid solutions is still relatively small, and there are few clear guidelines for predicting which binary systems will exhibit component miscibility in the solid state^{24,25}. This makes the exploration of organic solid solutions an exciting area of research with significant potential for discovery and innovation. By expanding our understanding of molecular recognition and crystal engineering, we may be able to unlock new possibilities for designing materials with fine-tuned properties.

* Corresponding Author: toms.rekis@lu.lv

In this study we explored the solid solution formation between four organic luminophore molecules: 2-iodothioxanthone, 2-iodo-9H-thioxanthen-9-one (Figure 1a), 2-chlorothioxanthone, 2-chloro-9H-thioxanthen-9-one (Figure 1b), 2-bromothioxanthone, 2-bromo-9H-thioxanthen-9-one (Figure 1c) and 2-fluorothioxanthone, 2-fluoro-9H-thioxanthen-9-one (Figure 1d). The compounds have been selected based on reported room-temperature solid-state luminescence phenomena²⁶ and differ only by halogen atoms (-I, -Cl, -Br and -F) - may not significantly affect the dominant intermolecular interactions.

Only the crystal structure of I-TXANT, Cl-TXANT and Br-TXANT non-solvated phases have been reported²⁶, whereas to the best of our knowledge there is no information on any crystal structures of F-TXANT, but during the research work, solid form landscape were studied and

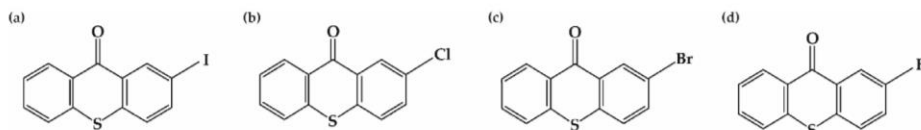


Figure 1: Molecular structures of 2-iodothioxanthone (a), 2-chlorothioxanthone (b), 2-bromothioxanthone (c) and 2-fluorothioxanthone (d).

2. EXPERIMENTAL SECTION

2.1. Materials.

2-chlorothioxanthone (purity >98%), and acetonitrile (99.8%) were obtained from commercial sources and used without further purification. Thioxanthone derivatives (-I, -Br and -F) were synthesized¹ by a cyclization reaction in concentrated sulfuric acid media, all the reagents and solvents used for the synthesis were purchased from commercial sources and used without further purification.

2.2. Solid solution screening.

Binary mixtures of thioxanthone derivatives in selected molar ratios with a mass of 0.1500 g were prepared using an analytical balance ($d = 0.1$ mg). The mechanical mixtures of the solids were then completely dissolved in 12 mL to 15 mL of acetonitrile at 70°C. The obtained clear solutions were cooled, and the solvent was allowed to evaporate completely in ambient conditions. The obtained solid products were ground in a mortar to ensure complete homogenization and characterized using PXRD and DSC. More details of the crystallization experiments are given in Table S1, Supporting Information.

2.3. Characterization of the obtained crystallization products.

Powder X-ray diffraction (PXRD) patterns of all the obtained crystallization products were recorded at ambient temperature on a *D8 Advance (Bruker)* diffractometer using copper radiation ($\text{Cu K}\alpha$) at a wavelength of 1.54180 Å, equipped with a *LynxEye* position-sensitive detector. The tube voltage and current were set to 40 kV and 40 mA. The divergence slit was set at 0.6 mm, and the antiscattering slit was set at 8.0 mm. The diffraction patterns were recorded using a 0.2 s/0.02° scanning speed from 3 to 35° on the 2 θ scale.

crystal structures of discovered non-solvated forms were determined.

In this study the formation of solid solutions between binary systems of various thioxanthone derivatives has been explored by comparing the formation of solid solutions in non-solvated forms. Crystallization experiments were performed to determine the information about formation of solid solutions, also photoluminescence spectra of all crystalline phases in powder form were recorded to see how they change with respect to those of the pure substances known from the literature²⁶, as a result, this confirmed that fine-tuning solid state luminescence properties of molecular crystals can be modulated via solid solution formation.

Differential scanning calorimetry (DSC) curves were recorded on a *DSC 25 (TA Instruments)* calorimeter at the heating rate of 2 °C min⁻¹ from 25 to 150 / 180 °C (depending to the melting temperature of pure components) and the nitrogen flow rate was 50 ± 10 mL min⁻¹. Approximately a 1.2 mg of each sample was weighed in a 70 μL aluminium crucible and the crucible was crimped.

The recorded DSC curves were used for construction of binary melt phase diagrams. The solidus lines were constructed using the onset temperatures of the respective DSC peaks and the liquidus lines were constructed using the peak temperatures of the melting peaks. More details on the thermal analysis are given in Table S2, Supporting Information.

Photoluminescence measurements were performed at room temperature using an *FS5 spectrometer* (Edinburgh Instruments) equipped with a 150 W CW xenon lamp and single-photon counting detector.

¹H NMR spectra of most of the crystallization products and pure nitrobenzoic acid derivatives were recorded in dimethyl sulfoxide (DMSO)-d₆ solution at a nominal temperature of 300 K with a *Fourier 300 MHz (Bruker)* spectrometer. Chemical shifts (δ) were found in parts per million (ppm) using the residual solvent peak as an internal reference. A characteristic peak was selected for each compound (see Supporting Information) and its area was used for determination of the compound ratio in the obtained crystallization products.

2.4. Crystal structure determination.

Single crystals of 2-fluorothioxanthone polymorph I, II and III and selected solid solutions were investigated on:

- *XtaLAB Synergy-S dualflex* diffractometer (*Rigaku Oxford Diffraction*) equipped with a *HyPix6000* detector and microfocus sealed X-ray tube with $\text{CuK}\alpha$ radiation ($\lambda = 1.54184$ Å) at ambient temperature;

- *Huber 4 circle kappa* diffractometer equipped with a Dectris CdTe 1M detector and an X-ray tube with synchrotron radiation - $\lambda = 0.61992 \text{ \AA}$ (P24, PETRA III, Deutsches Elektronen-Synchrotron DESY, Germany);
- *MD3 Microdiffractometer* equipped with Eiger 16M Hybrid-pixel detector and an X-ray tube with synchrotron radiation - $\lambda = 0.68879 \text{ \AA}$ (BioMax, MAX IV Synchrotron, Sweden).

Data were integrated using *CrysAlisPro 1.171.41.115a*²⁷ software, structure solutions and refinements were performed with the software *JANA2006*²⁸. All non-hydrogen atoms were refined anisotropically; H atoms were added in calculated positions and refined riding on their respective carbon or oxygen atoms.

Crystal structure of 2-chlorothioxanthone polymorph II were determined from PXRD data. this, PXRD patterns were measured on a *D8 Discover (Bruker)* diffractometer using copper radiation ($\text{Cu K}\alpha = 1.54180 \text{ \AA}$) in transmission mode and a *LynxEye* (1D) detector. The tube was employed with voltage and current settings of 40 kV and 40 mA. The sample was loaded into a borosilicate glass capillaries of 0.5 mm outer diameter (Hilgenberg glass No. 10). A capillary spinner (60 rpm) and upper and lower knife edges were used. The diffractometer incident beam path was equipped with a Göbel Mirror, Soller slit, and a 0.6 mm divergence slit, while the diffracted beam path was equipped only with a Soller slit. The diffraction patterns were recorded on the 2θ scale from 4 to 70° at a 0.01° step size using a scan speed of 36 s per step. Identical procedure as in our previous studied were

used for the structure determination^{29,30} (see the Supporting Information).

2.5. Determination of lattice parameters of solid solutions

The lattice parameters of pure thioxanthone derivatives and the obtained solid solutions were determined using Pawley refinement of the ambient temperature PXRD patterns recorded for the crystallization products (see Table S4 and S5). The Pawley refinement was performed in *TOPAS5* by relaxing the lattice parameters, crystallite size parameter, peak shape, and background parameters. In case the lattice parameters of pure single component phases were not a suitable initial guess for the refinement, LP-Search algorithm in *TOPAS5* was used for finding a suitable values.

2.6. Solid form landscapes of F-TXANT and Cl-TXANT

Solid forms of F-TXANT and Cl-TXANT were screened using solvent evaporation, recrystallization from melt, slurrying in ACN and antisolvent addition experiments (Figure 2a). These experiments resulted in a total of 6 crystal forms: 3 neat polymorphs (I–III) for F-TXANT and 3 neat polymorphs (I–III) for Cl-TXANT. All of the obtained polymorphs were characterized by PXRD and DSC methods. Figure 2b shows the PXRD patterns of the F-TXANT and Cl-TXANT polymorphs. All of the crystal forms give characteristic PXRD patterns and therefore are easily distinguishable. DSC investigations of F-TXANT and Cl-TXANT polymorphs shown in Figure 2c.

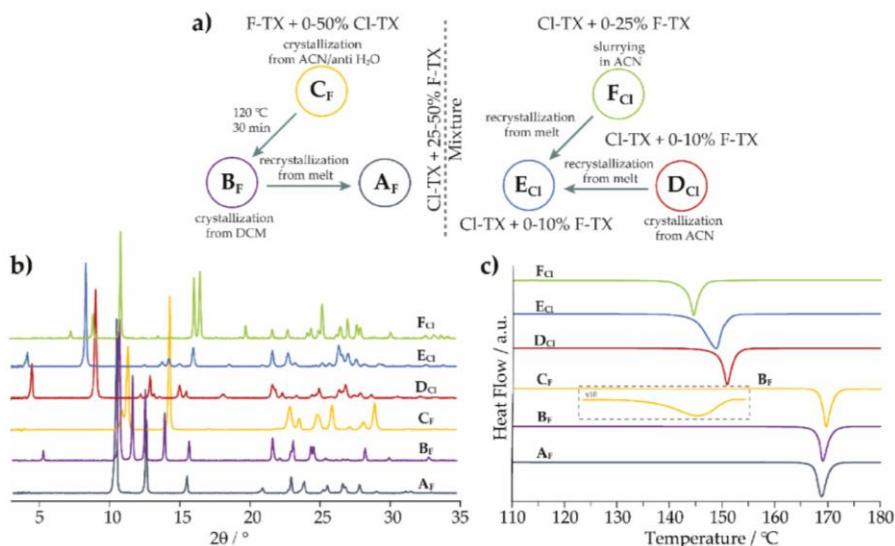


Figure 2. (a) Preparation and transition pathways of the F-TXANT and Cl-TXANT solid forms. (b) PXRD patterns of F-TXANT and Cl-TXANT neat crystalline forms. (c) DSC curves of F-TXANT and Cl-TXANT neat polymorphs.

2.7. Theoretical Values (Schröder–Van Laar equation).

The eutectic behavior determined by DSC was compared with the predicted melting point (T_m) values calculated from the simplified version of the Schröder–Van Laar Equation (eq 1), which is based on the ideal mixing theory^{31,32}.

$$\ln(x) = \frac{\Delta H_{\text{fusion}}}{R} \left(\frac{1}{T} - \frac{1}{T_M} \right) \quad (1)$$

where ΔH_{fusion} represents the heat of fusion (J mol⁻¹) and T represents the melting point (in Kelvin) of one of the pure drugs in the mixture. T_M is the melting point of the binary mixture at a specific mole fraction (x), and R is the universal gas constant (8.31451 J K⁻¹ mol⁻¹).

3. RESULTS AND DISCUSSION

As reported previously²³, where solid solutions with fine-tunable photoluminescence have been obtained in a 2-iodothioxanthone–2-chlorothioxanthone system, we wanted to prove that other thioxanthone derivatives, *i.e.*, both named compounds with 2-bromothioxanthone and 2-fluorothioxanthone, can also form solid solutions with fine-tunable properties. In this study we explore the formation of solid solution in six different binary systems and that fine-tune photoluminescence can be reached between various thioxanthone derivatives.

3.1 Experimental characterization of solid solution formation.

Solid solutions obtained in crystallization

For evaluation of the formation of solid solution between different thioxanthone derivatives in non-solvated phases by thus checking how easily one compound can replace the second one in its crystal structure, crystallization from solution of a mixture of compounds was selected. The preparation of the solid solutions of 2-iodothioxanthone, 2-chlorothioxanthone, 2-bromothioxanthone and 2-fluorothioxanthone were based on slow evaporation crystallization experiments.

The solid mixtures were characterized by DSC and X-ray powder diffraction. The small differences of molecular structure of experimentally used thioxanthone derivatives altered the possibility of the crystal structure to form weak intermolecular interaction which led to formation of different crystal structures. Melting together two different thioxanthone derivatives, in various stoichiometric ratios yields solid solutions, as confirmed by PXRD and DSC. A comparison of the experimental X-ray powder diffraction patterns measured at room temperature on various solid solutions is shown in Figure 3. The formation of solid solutions was also confirmed by the lattice parameters of the single phase containing crystallization products, which were linearly dependent on the composition of the mixture used in the crystallization in agreement with the Vegard's law^{31,32}, see Figure S10, Supporting Information.

Characterization of the obtained solid solutions

All of the samples obtained in the crystallization were additionally characterized by DSC analysis.

In all the DSC curves of non-solvated solid solutions samples the melting endotherm is consistent with an essentially monophasic sample (see Figure S1-S3 and Table S2). There is a relatively narrow biphasic region in the phase diagram where physical (different ratio) mixtures of both limiting-composition solid solutions are present. This is associated with an additional endothermic signal in the DSC curves indicating for the eutectic melting. The eutectic melting signal is observed as small but pronounced shoulder with an onset temperature of around 132°C for I-TXANT-Cl-TXANT, around 144°C for I-TXANT-Br-TXANT, around 131°C for F-TXANT-Br-TXANT and around 114°C for I-TXANT-F-TXANT. Mixture of two phases can also be noted in the PXRD patterns (see Figure 3).

Binary melt phase diagram was constructed to explore how well highly similar molecules are discriminated in the solid state. As concluded from the PXRD analysis, the Br-TXANT (I form) molecule is isostructural with Cl-TXANT (I form) and their crystals are isomorphous, a continuous solid solution in all the composition range, form in between those molecules, but in other cases two different solid solutions close to the pure component region form instead (see Figure 4). This is an indication that both highly similar molecules pack differently in the solid state. These solid solutions are designated as 2-fluorothioxanthone I ($P2_1/a$) **A_F**, II ($P2_12_12_1$) **B_F** and III (P_c or $P2_1/c$) **C_F**, 2-chlorothioxanthone I ($P-1$) **D_{Cl}**, II ($P2_12_12_1$) **E_{Cl}** and III ($Pna2_1$) **F_{Cl}**, 2-bromothioxanthone I ($P-1$) **D_{Br}** and 2-iodothioxanthone I ($P2_12_12_1$) **E_I**. The narrow biphasic region indicates that both molecules are discriminated in the solid state rather poorly – figure 4a, in composition ranges >0–20 mol % and 50–<100 mol % (2-chlorothioxanthone), figure 4b, in composition ranges >0–50 mol % and 80–<100 mol % (2-bromothioxanthone), figure 4c, in composition ranges >0–10 mol % and 90–<100 mol % (2-bromothioxanthone), figure 4d, in composition ranges 0–5 mol % and 98–<100 mol % (2-fluorothioxanthone) and figure 4e, in whole composition range (0–100 mol %). In all the phase diagrams there is also a relatively narrow biphasic region where physical mixtures of both solid solutions with limiting-composition are present.

It can clearly be seen that the composition range in which these solid solutions can be obtained are different in each pair of thioxanthone derivatives. The highest solubility up to more than 50 mol% was observed for Cl-TXANT in I-TXANT and I-TXANT in Br-TXANT, whereas the lowest (less than 5 mol%) for F-TXANT in Br-TXANT.

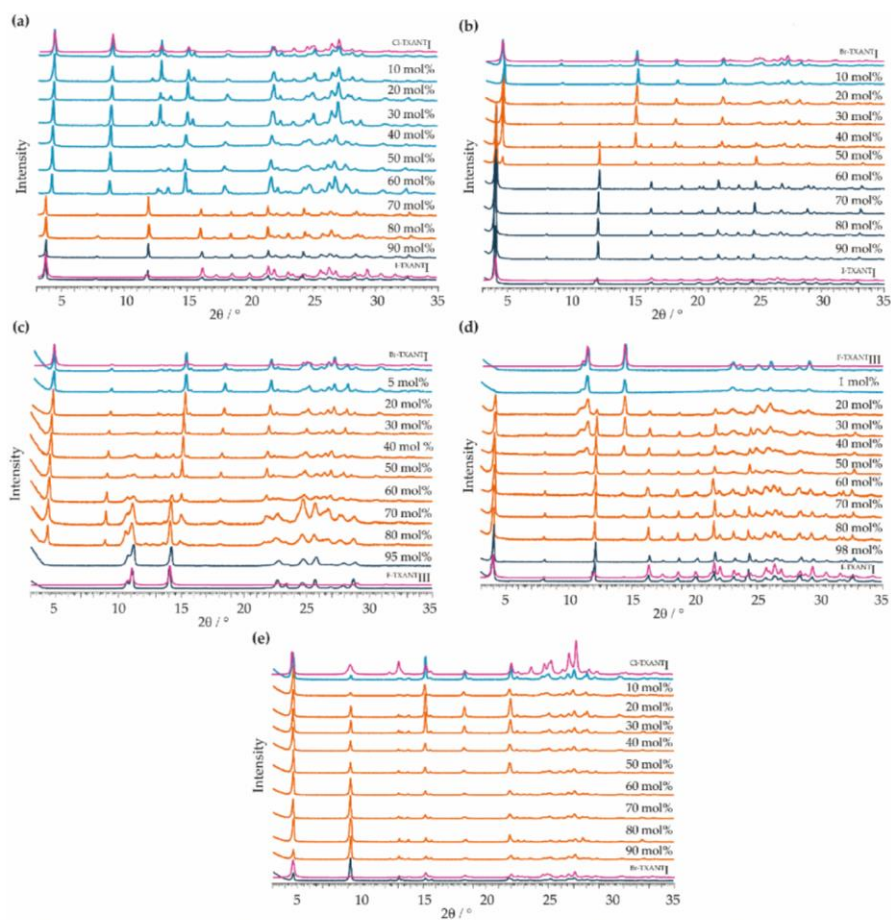


Figure 3: PXRD patterns of crystallization products obtained in crystallization of different ratios of thioxanthone derivatives: a) I-TXANT-Cl-TXANT, b) I-TXANT-Br-TXANT, c) F-TXANT-Br-TXANT, d) I-TXANT-F-TXANT and e) Br-TXANT-Cl-TXANT from acetonitrile. PXRD patterns of solid solutions and the corresponding single component phases are in identical shade of blue, phase mixtures are in orange, and patterns simulated from crystal structures are in magenta.

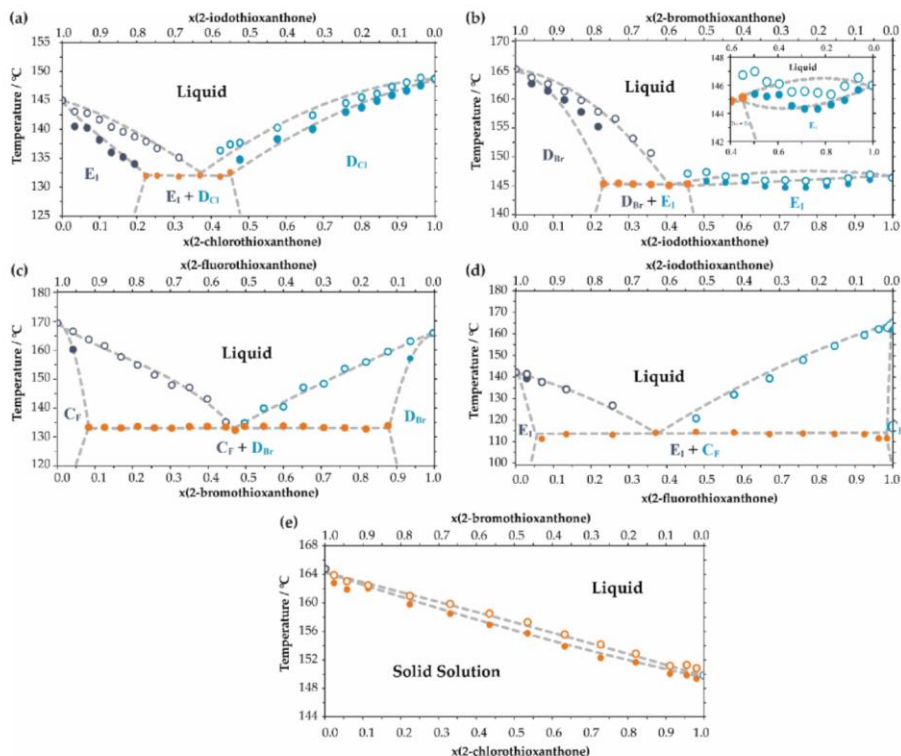


Figure 4: Melt phase diagrams of binary systems (a) I-TXANT-Cl-TXANT, (b) I-TXANT-Br-TXANT, (c) F-TXANT-Br-TXANT, (d) I-TXANT-F-TXANT and (e) Br-TXANT-Cl-TXANT. Lines are guides for the eyes, the colour coding is identical to that used in Figures 2.

Predicted phase diagram using Schröder–Van Laar (SVL) model vs. experimentally obtained data

The experimentally determined solidus and liquidus temperatures were plotted against the concentration to construct the phase diagrams. In addition, theoretical values, based on the Schröder–Van Laar equation (see section Theoretical values), few examples were added and are shown in Figure 5 (detailed information see in Supporting

information). The figures are typical of eutectic systems and show the liquidus and solidus curves and the experimental and theoretical points at which these curves meet, *i.e.*, the eutectic points^{33,34}. The eutectic ratios and their corresponding temperatures (T_e), both experimentally and theoretically determined for all analyzed nitrobenzoic acid derivative and their isomer mixtures, are shown in Table 1. The theoretical eutectic points did not differ by more than 10% from the experimentally determined values.

Table 1. Experimental and theoretical eutectic point and T_e values for various thioxanthone derivative mixtures.

Eutectic point and T_e	I-TXANT-Cl-TXANT	I-TXANT-Br-TXANT	I-TXANT-F-TXANT	F-TXANT-Br-TXANT
Experimental eutectic point mixture / mol	0.63 : 0.37	0.41 : 0.59	0.63 : 0.37	0.53 : 0.47
Experimental T_e / °C	132.2	144.5	116.0	129.4
Theoretical eutectic point mixture / mol	0.42 : 0.58	0.56 : 0.44	0.63 : 0.37	0.53 : 0.47
Theoretical T_e / °C	112.2	114.4	117.3	127.7

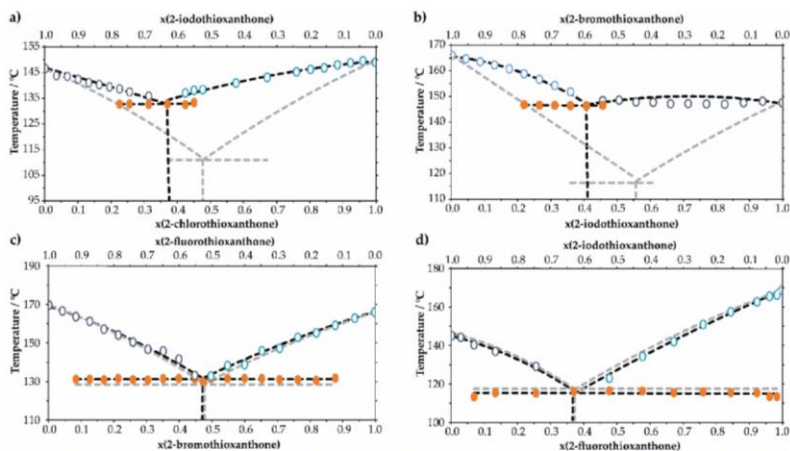


Figure 5: Phase diagrams of (a) I-TXANT-Cl-TXANT, (b) I-TXANT-Br-TXANT, (c) F-TXANT-Br-TXANT and (d) I-TXANT-F-TXANT, samples using experimentally determined data (colored circles) and theoretical data using the Schröder–Van Laar equation (grey dotted line).

3.2 Materials with modulated properties via solid solution formation.

Due to relative intensity changes of the spectral bands (see Supporting Information Figure S13, there is a variation of

the luminescence color. In Figure 6, a CIE chromaticity diagram is depicted for several solid solutions compositions.

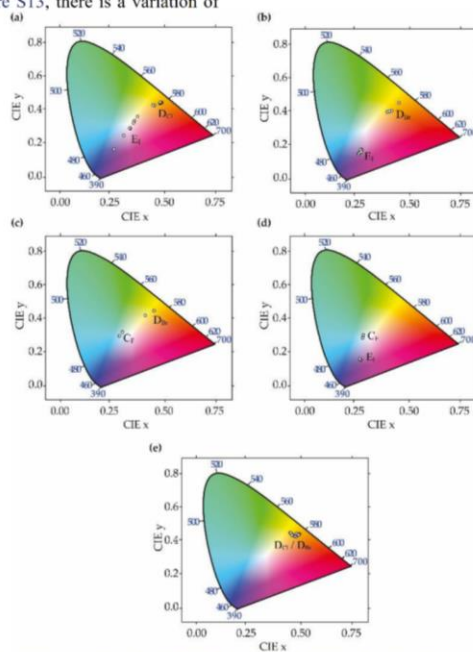


Figure 6: CIE chromaticity diagrams (CIE 1931, standard observer) of several compositions of solid solutions from emission spectra excited at $\lambda_{exc} = 330$ nm (room temperature): (a) I-TXANT-Cl-TXANT²³, (b) I-TXANT-Br-TXANT, (c) F-TXANT-Cl-TXANT, (d) F-TXANT-Br-TXANT, (e) I-TXANT-F-TXANT and (f) Br-TXANT-Cl-TXANT.

3.3 Ternary solid solutions: I-TXANT_{1-x-y}Br-TXANT_xCl-TXANT_y solid solutions.

As a natural extension of our study on two-component solid solutions of various thioxanthone derivatives, the propensity of these systems to form three-component solid solutions was also investigated. The ternary 1 : 1 : 1 solid solution prepared, as in the case of the binary solid solutions, by slow evaporation crystallization experiments showed distinct peaks in the PXRD pattern (Figure 7), which could be attributed to the formation of the ternary phase, isomorphous with the parent ones. DSC measurements were instrumental in confirming the formation of the ternary solution, as only one peak was observed, at a different temperature with respect to the previously analysed solid solutions. Solid solutions of I-TXANT/Br-TXANT/Cl-TXANT were also prepared at various stoichiometric ratios. DSC measurements of the solid solutions at various ratios revealed only one phase for each composition. Varying the concentration of one component while leaving the two other components to be equimolar resulted in slight changes in the corresponding PXRD patterns (see Supporting Information Figure S9).

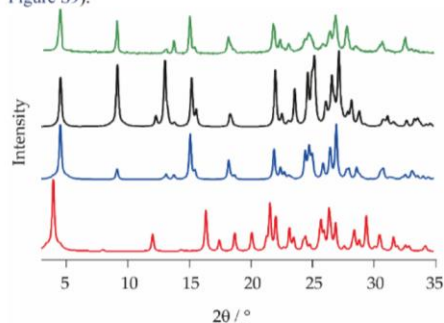


Figure 7: Comparison between the experimental PXRD pattern for the I-TXANT_{0.33}Br-TXANT_{0.33}Cl-TXANT_{0.33} ternary solid solution (upper line) and the RT calculated ones (from top to bottom) of the pure iodide, bromine and chlorine derivatives (patterns simulated from crystal structures - I-TXANT (KOPZEX), Br-TXANT (KOPZAT), Cl-TXANT (CLTXAN01))²⁶.

In order to investigate the melting point behaviour of the ternary system, a large number of DSC measurements were carried out (see the Supporting information). Figure 8 provides a visual representation of the results. Generally, the melting points of the solid solutions were lower than those of the pure compounds; the lowest melting points for the ternary solid solutions were found at excess I-TXANT, with the I-TXANT_{80mol%}Br-TXANT_{10mol%}Cl-TXANT_{10mol%} solid solution showing the lowest one.

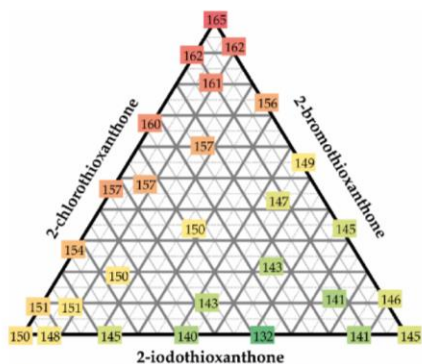


Figure 8: 3D Ternary diagrams showing (left) compositions of the I-TXANT_{1-x-y}Br-TXANT_xCl-TXANT_y solid solutions and (right) the corresponding melting points (°C, peak temperatures from DSC). Red and green colours (yellow in between) mark high and low melting points, respectively.

3.4 Solid solution polymorphism in case of F-TXANT – Cl-TXANT system.

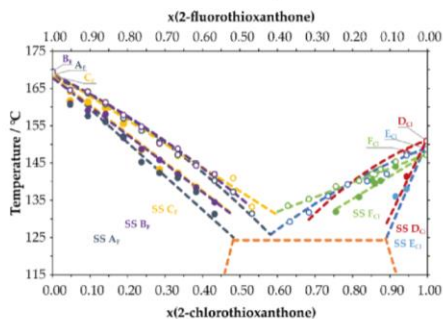


Figure 9: Melt phase diagrams of various binary systems of F-TXANT – Cl-TXANT.

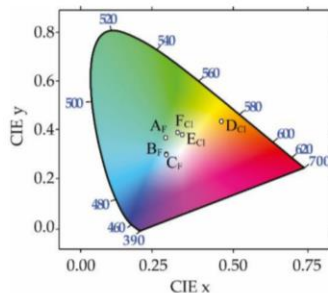


Figure 10: CIE chromaticity diagram (CIE 1931, standard observer) of pure 2-fluorothioxanthone and 2-chlorothioxanthone polymorphs from emission spectra excited at $\lambda_{exc} = 330$ nm (room temperature).

4. CONCLUSIONS

In this paper we have extended our previous work²³ on solid solutions of I-TXANT and Cl-TXANT to the bromine Br-TXANT and fluorine F-TXANT analogue, obtaining new binary solid solutions in various systems, i.e., I-TXANT-Br-TXANT, F-TXANT-Cl-TXANT, F-TXANT-Br-TXANT, I-TXANT-F-TXANT and Br-TXANT-Cl-TXANT. Our study indicates that the technique of solid solution can be employed to adjust the luminescence characteristics of organic crystalline materials. This leads to a substantial alteration in the luminescence spectra. Our findings demonstrate that when dealing with single-phase materials, it is possible to fine-tune their properties continuously using this approach, which cannot be achieved by chemically altering the luminescent organic molecules.

ASSOCIATED CONTENT

Supporting Information

The Supporting Information is available free of charge on the ACS Publications website at DOI: https://pubs.acs.org/doi/10.1021/acs.cgd._____.

Additional details and results of the crystallization experiments, results from characterization of the crystallization products of all the explored systems using PXRD patterns, DSC curves and ¹H NMR spectra, additional results and data from comparison of crystal structures, crystal structure determination and lattice parameters of solid solutions (PDF).

Accession Codes

CCDC _____ and _____ contain the supplementary crystallographic data for this paper. These data can be obtained free of charge via www.ccdc.cam.ac.uk/data_request/cif, or by emailing data_request@ccdc.cam.ac.uk, or by contacting The Cambridge Crystallographic Data Centre, 12 Union Road, Cambridge CB2 1EZ, UK; fax: +44 1223 336033.

AUTHOR INFORMATION

Corresponding Author

Toms Rekis – Faculty of Chemistry, University of Latvia, LV-1004 Riga, Latvia; orcid.org/0000-0001-5128-4611;

Email: toms.rekis@lu.lv

Author

Kristaps Saršūns – Faculty of Chemistry, University of Latvia, LV-1004 Riga, Latvia; orcid.org/0000-0002-8692-7768

Artis Kons – Faculty of Chemistry, University of Latvia, LV-1004 Riga, Latvia; orcid.org/0000-0002-4055-8442

Kaspars Leduskrasts – Latvian Institute of Organic Synthesis, LV-1006 Riga, Latvia; orcid.org/0000-0002-4055-8442

Igors Klīmenkovs – Faculty of Chemistry, University of Latvia, LV-1004 Riga, Latvia

Agris Bērziņš – Faculty of Chemistry, University of Latvia, LV-1004 Riga, Latvia; orcid.org/0000-0002-4149-8971

Complete contact information is available at: https://pubs.acs.org/doi/10.1021/acs.cgd._____

Funding

This research was funded by the Latvian Council of Science project *Crystal engineering of pharmaceutical multicomponent phases for more efficient crystalline phase design*, project No. lzp-2018/1-0312.

Notes

The authors declare no competing financial interest.

ACKNOWLEDGEMENTS

K.S. acknowledges financial support from the European Social Fund project *Strengthening of the capacity of doctoral studies at the University of Latvia within the framework of the new doctoral model*, identification No. 8.2.2.0/20/1/006 and University of Latvia Foundation through a MikroTik Ltd. doctoral scholarship in the field of natural and medical sciences. The authors thank Rihards Klūga (University of Latvia) for ¹H NMR spectra measurements and Kristīne Krūkle-Bērziņa (Latvian Institute of Organic Synthesis) for collection of SCXRD data.

REFERENCES

- (1) Zheng, C.; Zang, Q.; Nie, H.; Huang, W.; Zhao, Z.; Qin, A.; Hu, R.; Tang, B. Z. Fluorescence Visualization of Crystal Formation and Transformation Processes of Organic Luminogens with Crystallization-Induced Emission Characteristics. *Mater. Chem. Front.* **2018**, *2* (1), 180–188. <https://doi.org/10.1039/c7qm00435d>.
- (2) Yun, S. S.; Kim, J. K.; Jung, J. S.; Park, C.; Kang, J. G.; Smyth, D. R.; Tickink, E. R. T. Pseudo-Polymorphism in the Tri(o-Tolyl)Phosphinegold(I) 2-Mercaptobenzoates: Crystallographic, Thermal Decomposition, and Luminescence Studies. *Cryst. Growth Des.* **2006**, *6* (4), 899–909. <https://doi.org/10.1021/cg0504206>.
- (3) Guan, J.; Zhang, C.; Gao, D.; Tang, X.; Dong, X.; Lin, X.; Wang, Y.; Wang, X.; Wang, L.; Lee, H. H.; Xu, J.; Zheng, H.; Li, K.; Mao, H. K. Drastic Photoluminescence Modulation of an Organic Molecular Crystal with High Pressure. *Mater. Chem. Front.* **2019**, *3* (8), 1510–1517. <https://doi.org/10.1039/c9qm00082h>.
- (4) Singh, R.; Gupta, A. K.; Pradeep, C. P. Synthesis of a New Series of Organic Solid-State Near-Infrared Emitters: The Role of Crystal Packing and Weak Intermolecular Interactions and Application in Latent Fingerprint Detection. *Cryst. Growth Des.* **2021**, *21* (2), 1062–1076. <https://doi.org/10.1021/acs.cgd.0c01392>.
- (5) Zhang, J.; Li, N.; Wang, T.; Wu, J.; Yu, S.; Fan, J.; Zhang, S.; Zhang, M.; Zhao, L.; Chen, W.; Bai, J. Temperature-Dependent Long Persistent Luminescence Properties and Trap Distributions in Sr₂MgAl₁₂O₃₆: Eu²⁺. *J. Alloys Compd.* **2022**, *900*, 163482. <https://doi.org/https://doi.org/10.1016/j.jal>

- lcom.2021.163482.
- (6) Man, Z.; Lv, Z.; Xu, Z.; Liu, M.; He, J.; Liao, Q.; Yao, J.; Peng, Q.; Fu, H. Excitation-Wavelength-Dependent Organic Long-Persistent Luminescence Originating from Excited-State Long-Range Proton Transfer. *J. Am. Chem. Soc.* **2022**, *144* (28), 12652–12660. <https://doi.org/10.1021/jacs.2c01248>.
 - (7) Sharber, S. A.; Mullin, W. J.; Thomas, S. W. Bridging the Void: Halogen Bonding and Aromatic Interactions to Program Luminescence and Electronic Properties of π -Conjugated Materials in the Solid State. *Chem. Mater.* **2021**, *33* (17), 6640–6661. <https://doi.org/10.1021/acs.chemmater.1c01969>.
 - (8) Morita, M.; Yamada, S.; Konno, T. Halogen Atom Effect of Fluorinated Tolanes on Their Luminescence Characteristics. *New J. Chem.* **2022**, *46* (10), 4562–4569. <https://doi.org/10.1039/D1NJ05539A>.
 - (9) Alam, P.; Leung, N. L. C.; Liu, J.; Cheung, T. S.; Zhang, X.; He, Z.; Kwok, R. T. K.; Lam, J. W. Y.; Sung, H. H. Y.; Williams, I. D.; Chan, C. C. S.; Wong, K. S.; Peng, Q.; Tang, B. Z. Two Are Better Than One: A Design Principle for Ultralong-Persistent Luminescence of Pure Organics. *Adv. Mater.* **2020**, *32* (22), 1–7. <https://doi.org/10.1002/adma.202001026>.
 - (10) Han, Y.; Cao, H.-T.; Sun, H.-Z.; Wu, Y.; Shan, G.-G.; Su, Z.-M.; Hou, X.-G.; Liao, Y. Effect of Alkyl Chain Length on Piezochromic Luminescence of Iridium(III)-Based Phosphors Adopting 2-Phenyl-1H-Benzoimidazole Type Ligands. *J. Mater. Chem. C* **2014**, *2* (36), 7648–7655. <https://doi.org/10.1039/C4TC00993B>.
 - (11) Tu, D.; Leong, P.; Guo, S.; Yan, H.; Lu, C.; Zhao, Q. Highly Emissive Organic Single-Molecule White Emitters by Engineering o-Carborane-Based Luminophores. *Angew. Chemie - Int. Ed.* **2017**, *56* (38), 11370–11374. <https://doi.org/10.1002/anie.201703862>.
 - (12) Ito, S.; Nagai, S.; Ubukata, T.; Ueno, T.; Uekusa, H. Relationship between Crystal Structure, Crystal Morphology, and Mechanochromic Luminescence of Triphenylimidazolylbenzothiadiazole Derivatives. *Cryst. Growth Des.* **2020**, *20* (7), 4443–4453. <https://doi.org/10.1021/acs.cgd.0c00253>.
 - (13) Vujovic, D.; Raubenheimer, H. G.; Nassimbeni, L. R. One-Dimensional CdII Coordination Polymers: Solid Solutions with NiII, Thermal Stabilities and Structures. *Eur. J. Inorg. Chem.* **2004**, *2004* (14), 2943–2949. <https://doi.org/https://doi.org/10.1002/ejic.200300794>.
 - (14) Krishnan, R.; Swart, H. C. Luminescence Properties of Octahedrally and Tetrahedrally Coordinated Mo6+ in the Solid Solutions: Judd–Ofelt Investigation. *J. Phys. Chem. Solids* **2020**, *144* (March), 109519. <https://doi.org/10.1016/j.jpcs.2020.109519>.
 - (15) Shao, Y.; Yang, Y. Organic Solid Solutions: Formation and Applications in Organic Light-Emitting Diodes. *Adv. Funct. Mater.* **2005**, *15* (11), 1781–1786. <https://doi.org/10.1002/adfm.200500032>.
 - (16) Saršūns, K.; Bērziņš, A. Experimental and Computational Investigation of Benperidol and Droperidol Solid Solutions in Different Crystal Structures. *Cryst. Growth Des.* **2023**, *23* (2), 1133–1144. <https://doi.org/10.1021/acs.cgd.2c01269>.
 - (17) Trotta, J. T.; Zeidan, T. A.; Tilak, P. A.; Foxman, B. M.; Almarsson, Ö.; Oliveira, M. A.; Chiarella, R. A.; Hickey, M. B.; Remenar, J. F. Aripiprazole and Dehydro-Aripiprazole Solid Solutions: Crystalline Combinations of Drug and Active Metabolite in Tailored Compositions. *Cryst. Growth Des.* **2020**, *20* (6), 3944–3956. <https://doi.org/10.1021/acs.cgd.0c00263>.
 - (18) D'Agostino, S.; Fornasari, L.; Grepioni, F.; Braga, D.; Rossi, F.; Chierotti, M. R.; Gobetto, R. Precessional Motion in Crystalline Solid Solutions of Ionic Rotors. *Chem. - A Eur. J.* **2018**, *24* (56), 15059–15066. <https://doi.org/10.1002/chem.201803071>.
 - (19) Lusi, M. A Rough Guide to Molecular Solid Solutions: Design, Synthesis and Characterization of Mixed Crystals. *CrystEngComm* **2018**, *20* (44), 7042–7052. <https://doi.org/10.1039/C8CE000691A>.
 - (20) Aakeröy, C. B.; Seddon, K. R. The Hydrogen Bond and Crystal Engineering. *Chem. Soc. Rev.* **1993**, *22* (6), 397–407. <https://doi.org/10.1039/CS9932200397>.
 - (21) Wittenberg, J. B.; Isaacs, L. Complementarity and Preorganization. *Supramol. Chem.* **2012**. <https://doi.org/10.1002/9780470661345.smc004>.
 - (22) Wiscons, R. A.; Coropceanu, V.; Matzger, A. J. Quaternary Charge-Transfer Solid Solutions: Electronic Tunability through Stoichiometry. *Chem. Mater.* **2019**, *31* (17), 6598–6604. <https://doi.org/10.1021/acs.chemmater.9b00502>.
 - (23) Saršūns, K.; Kemere, M.; Karziņš, A.; Kļimenkovs, I.; Bērziņš, A.; Sarakovskis, A.; Rekis, T. Fine-Tuning Solid State Luminescence Properties of Organic Crystals via Solid Solution Formation: The Example of 4-Iodothioxanthone-4-Chlorothioxanthone System. *Cryst. Growth Des.* **2022**, *22* (8), 4838–4844. <https://doi.org/10.1021/acs.cgd.2c00313>.
 - (24) Corpinot, M. K.; Bučar, D.-K. A Practical Guide to the Design of Molecular Crystals. *Cryst. Growth Des.* **2019**, *19* (2), 1426–1453. <https://doi.org/10.1021/acs.cgd.8b00972>.
 - (25) Cuevas-Diarte, M. A.; Oonk, H. A. J. *Molecular Mixed Crystals*; Cuevas-Diarte, M. À., Oonk, H. A. J., Eds.; Physical Chemistry in Action; Springer International Publishing: Cham, 2021. <https://doi.org/10.1007/978-3-030-68727-4>.
 - (26) Wen, Y.; Liu, H.; Zhang, S.; Gao, Y.; Yan, Y.; Yang, B. One-Dimensional π - π Stacking Induces Highly Efficient Pure Organic Room-Temperature Phosphorescence and Ternary-Emission Single-Molecule White Light. *J. Mater. Chem. C* **2019**, *7* (40), 12502–12508. <https://doi.org/10.1039/C9TC04580E>.
 - (27) Agilent Technologies UK. CrysAlisPRO Software. *Yarnton, Engl.* **2014**.

- (28) Petricek, V.; Dušek, M.; Palatinus, L. Crystallographic Computing System JANA2006: General Features. *Zeitschrift für Krist.* **2014**, *229* (5), 345–352. <https://doi.org/10.1515/zkri-2014-1737>.
- (29) Bērziņš, A.; Kons, A.; Saršūns, K.; Belyakov, S.; Actiņš, A. On the Rationalization of Formation of Solvates: Experimental and Computational Study of Solid Forms of Several Nitrobenzoic Acid Derivatives. *Cryst. Growth Des.* **2020**, *20* (9), 5767–5784. <https://doi.org/10.1021/acs.cgd.0c00331>.
- (30) Trimdale-Deksne, A.; Kons, A.; Orola, L.; Mishnev, A.; Stepanovs, D.; Mazur, L.; Skiba, M.; K. Dudek, M.; Fantozzi, N.; Virieux, D.; Colacino, E.; Bērziņš, A. Crystallographic and Computational Analysis of the Solid-Form Landscape of Three Structurally Related Imidazolidine-2,4-Dione Active Pharmaceutical Ingredients: Nitrofurantoin, Furazidin, and Dantrolene. *Cryst. Growth & Des.* **2023**, *23* (2), 930–945. <https://doi.org/10.1021/acs.cgd.2c01142>.
- (31) Bi, M.; Hwang, S. J.; Morris, K. R. Mechanism of Eutectic Formation upon Compaction and Its Effects on Tablet Properties. *Thermochim. Acta* **2003**, *404* (1–2), 213–226. [https://doi.org/10.1016/S0040-6031\(03\)00185-0](https://doi.org/10.1016/S0040-6031(03)00185-0).
- (32) Javadian, S.; Dalir, N.; Gilani, A. G.; Kakemam, J.; Yousefi, A. A New Approach to Study Interaction Parameters in Cyanobiphenyl Liquid Crystal Binary Systems. *J. Chem. Thermodyn.* **2015**, *80*, 22–29. <https://doi.org/10.1016/j.jct.2014.08.010>.
- (33) Vegard, L.; Schjelderup, H. Die Konstitution Der Mischkristalle. *Phys. Z* **1917**, *18*, 93–96.
- (34) Vegard, L. Die Konstitution Der Mischkristalle Und Die Raumbfüllung Der Atome. *Zeitschrift für Phys.* **1921**, *5* (1), 17–26. <https://doi.org/10.1007/BF01349680>.
- (35) Cherukuvada, S.; Nangia, A. Eutectics as Improved Pharmaceutical Materials: Design, Properties and Characterization. *Chem. Commun.* **2014**, *50* (8), 906–923. <https://doi.org/10.1039/c3cc47521b>.
- (36) Abbott, A. P.; Ahmed, E. I.; Prasad, K.; Qader, I. B.; Ryder, K. S. Liquid Pharmaceuticals Formulation by Eutectic Formation. *Fluid Phase Equilib.* **2017**, *448*, 2–8. <https://doi.org/10.1016/j.fluid.2017.05.009>.